

POLITECNICO DI TORINO

Master of Science in Biomedical Engineering

**Synthesis and characterization of electrospun
composite fibers containing bioactive glass
powders**



Supervisor

prof. Enrica Verné

Co-supervisors

prof. Marta Miola

Internship tutor

Prof. Aldo R. Boccaccini

Candidate

Elisa Piatti

July 2019

Abstract

Electrospinning is a well-established technique widely used for the fabrication of micro- and nanofibrous mats for numerous applications, including for the biomedical field, e.g. drug delivery and tissue engineering scaffolds. Bioactive glasses (BGs) are non crystalline materials that are able to bond with living tissue and stimulate new tissue growth. Because of their high biomineralization ability, biodegradability, osteogenic and angiogenic potential, BGs are promising candidates for tissue-engineering applications. The aim of this master thesis project is the fabrication and characterization of composite electrospun fibers containing bioactive glass particles. Bioactive glass containing boron and copper have been prepared via sol-gel process and characterized using SEM, EDS, BET, XRD and bioactivity analysis; this part of the master thesis was performed at Politecnico di Torino (Turin, Italy). After that, at University Friedrich-Alexander of Erlangen (Germany), composite fibers were prepared using the electrospinning technique. For the preparation of these fibers, the following materials have been used: poly(ϵ -caprolactone), benign solvents and sol-gel bioactive glasses. The processing parameters have been optimized, in order to enhance the potential of these composite materials for tissue application. Fibers have been characterized by means of SEM, EDS, FTIR, water contact angle measurements, mechanical tensile test, bioactivity analysis, degradation test and biological assay.

Acknowledgements

I would like to thank my supervisor Enrica Verné for this thesis opportunity and for never stopped supporting me and to express my deepest gratitude to my co-supervisor Marta Miola, who helped me to carry out my experimental work and to write this master thesis, with great patience.

I would also thank professor Boccaccini, for hosting me in the Institute of Biomaterials at the Friedrich Alexander Universität Erlangen-Nürnberg (Germany), giving me the opportunity to live an interesting experience abroad and to work in a talented and international research group, whose members were very kind and helpful with me. Therefore, I would like to thank them, in particular Liliana Liverani for her kindness und help during this phase of my experimental work.

Although they do not want to be thanked, I need to write a sincere and lovely thanks to my family and my boyfriend Lorenzo. During all this academic years, they always believe in me and encourage me to follow my dreams, despite all difficulties. There is no word to express how I love them all and how I am grateful.

Finally, but not least, I would like to thank all my friends.

Contents

| | |
|--|-----|
| Abstract..... | ii |
| Acknowledgements..... | iii |
| List of Figures..... | vi |
| List of Tables..... | xi |
| 1 Introduction..... | 1 |
| 1.1 Tissue engineering and composite scaffolds..... | 2 |
| 1.1.1 A brief introduction to scaffolds..... | 2 |
| 1.1.2 Main features of a composite material..... | 3 |
| 1.1.3 Polymers used in the fabrication of composite materials..... | 5 |
| 1.2 Bioactive glasses..... | 7 |
| 1.2.1 Glasses..... | 7 |
| 1.2.2 Bioactivity..... | 7 |
| 1.2.3 Bioactive glasses..... | 8 |
| 1.2.4 Preparation methods..... | 17 |
| 1.3 Electrospinning..... | 24 |
| 1.3.1 Advantages..... | 25 |
| 1.3.2 Mechanismus and apparatus..... | 26 |
| 1.3.3 Parameters..... | 28 |
| 1.3.4 Use of benign solvents..... | 34 |
| 1.3.5 Addition of glass nanoparticles..... | 35 |
| 2 Aim of work..... | 36 |
| 3 Materials and methods..... | 37 |
| 3.1 Materials..... | 37 |
| 3.2 Synthesis of the glasses..... | 38 |
| 3.3 Characterization of the glasses..... | 43 |
| 3.3.1 Morphological characterization..... | 43 |
| 3.3.2 Compositional characterization..... | 44 |
| 3.3.3 X-ray diffraction analysis..... | 44 |
| 3.3.4 BET analysis..... | 44 |
| 3.3.5 Acellular bioactivity test..... | 45 |
| 3.4 Preparation of the solution for electrospinning..... | 47 |
| 3.5 Electrospinning process..... | 48 |
| 3.6 Characterization of the fibers..... | 50 |
| 3.6.1 Morphological characterization..... | 50 |

| | | |
|-------|---|-----|
| 3.6.2 | Compositional characterization..... | 51 |
| 3.6.3 | FTIR analysis | 51 |
| 3.6.4 | Mechanical characterization | 51 |
| 3.6.5 | Water Contact-Angle measurements..... | 52 |
| 3.6.6 | Acellular bioactivity test | 53 |
| 3.6.7 | Degradation test | 55 |
| 3.6.8 | Biological assay | 55 |
| 3.6.9 | Stability test | 56 |
| 4 | Results and discussion | 57 |
| 4.1 | Features of prepared glasses | 57 |
| 4.1.1 | Morphological characterization | 57 |
| 4.1.2 | Compositional characterization..... | 64 |
| 4.1.3 | X-ray diffraction analysis..... | 66 |
| 4.1.4 | BET analysis | 71 |
| 4.1.5 | Acellular bioactivity test | 72 |
| 4.2 | Optimization of electrospinning solution..... | 90 |
| 4.2.1 | Fiber morphology observations | 90 |
| 4.3 | Features of the final mats | 101 |
| 4.3.1 | Morphological characterization | 101 |
| 4.3.2 | Compositional characterization..... | 103 |
| 4.3.3 | Physical-chemical characterization..... | 104 |
| 4.3.4 | Water-Contact-Angle measurements | 105 |
| 4.3.5 | Acellular bioactivity test | 107 |
| 4.3.6 | Degradation test | 119 |
| 4.3.7 | Mechanical test | 126 |
| 4.3.8 | Stability test | 128 |
| 4.3.9 | Biological assay | 146 |
| 5 | Conclusion and future works | 148 |
| 6 | Bibliography | 151 |

List of Figures

| | |
|---|----|
| Figure 1.1: Sol-gel process | 19 |
| Figure 1.2: Electrospinning technique | 26 |
| Figure 3.1: Schematic representation of sol-gel methods | 42 |
| Figure 3.2: FESEM Gemini (a) and samples (b) | 43 |
| Figure 3.3: BET analyser | 44 |
| Figure 3.4: Example of samples for BET analysis:..... | 45 |
| Figure 3.5: Chemical reagents for preparation of SBF solution | 46 |
| Figure 3.6: Glass samples for bioactivity test..... | 47 |
| Figure 3.7: Electrospinning solution preparation..... | 48 |
| Figure 3.8: Electrospinning set-up..... | 49 |
| Figure 3.9: Preparation of fiber samples for SEM (and EDS) analysis | 50 |
| Figure 3.10: Example of fiber samples for SEM analysis | 51 |
| Figure 3.11: Preparation of sample for mechanical test..... | 52 |
| Figure 3.12: Mechanical test – a) testing machine b) detail of broken sample..... | 52 |
| Figure 3.13: Contact angle measurements set-up | 53 |
| Figure 3.14: Set-up for preparation of SBF solution..... | 54 |
| Figure 3.15: Preparation of sample for acellular bioactivity test | 54 |
| Figure 3.16: Glasses soaked in acetic acid..... | 56 |
| Figure 4.1: SEM micrographs at 10K X of S1 (a) and S2 (b)..... | 57 |
| Figure 4.2: SEM micrographs at 30K X of S1 (a) and S2 (b)..... | 57 |
| Figure 4.3: SEM micrographs at 50K X of S1 (a) and S2 (b)..... | 57 |
| Figure 4.4: SEM micrographs at 10K X of SB1 (a) and SB2 (b) | 58 |
| Figure 4.5: SEM micrographs at 30K X of SB1 (a) and SB2 (b) | 58 |
| Figure 4.6: SEM micrographs at 10K X of SBCu1 (a) and SBCu2 (b) | 58 |
| Figure 4.7: SEM micrographs at 30K X of SBCu1 (a) and SBCu2 (b) | 58 |
| Figure 4.8: SEM micrograph at 100K X of S1 | 59 |
| Figure 4.9: SEM micrograph at 50K X of S2 | 59 |
| Figure 4.10: SEM micrographs at 100K X of SB1 | 60 |
| Figure 4.11: SEM micrographs at 150K X of SB1 | 60 |
| Figure 4.12: SEM micrographs at 100K X of SB2 | 61 |
| Figure 4.13: SEM micrograph at 100K X of SBCu1 | 61 |
| Figure 4.14: SEM micrograph at 100K X of SBCu2 | 62 |
| Figure 4.15: SEM micrograph at 100K X of SBCu2 | 62 |

| | |
|---|----|
| Figure 4.16: EDS spectra of S1 (a) and S2 (b) | 65 |
| Figure 4.17: EDS spectra of SB1 (a) and SB2 (b) | 65 |
| Figure 4.18: EDS spectra of SBCu1 (a) and SBCu2 (b)..... | 66 |
| Figure 4.19: XRD spectrum of S1 as example..... | 67 |
| Figure 4.20: XRD spectra comparison of glasses S1 (a), S2 (b), SB1 (c), SB2 (d), SBCu1 (e) and SBCu2 (f)..... | 67 |
| Figure 4.21: trend of peaks in the XRD spectrum of SB1 | 68 |
| Figure 4.22: peaks of Ca_2SiO_4 in SB1 | 69 |
| Figure 4.23: peaks of B_2O_3 in SB1..... | 70 |
| Figure 4.24: pH trend during acellular bioactivity test of glasses..... | 74 |
| Figure 4.25: EDS spectra of S glasses at different time points in SBF..... | 75 |
| Figure 4.26: EDS spectra of SB glasses at different time points in SBF | 76 |
| Figure 4.27: EDS spectra of SBCu glasses at different time points in SBF | 77 |
| Figure 4.28: P and Ca amounts during immersion of glasses in SBF..... | 78 |
| Figure 4.29: trend of P amount during immersion of glasses in SBF | 79 |
| Figure 4.30: trend of Ca amount during immersion of glasses in SBF..... | 79 |
| Figure 4.31: SBCu glasses after 1 day in SBF | 80 |
| Figure 4.32: SBCu glasses after 3 days (left) and 7 days (right) in SBF | 80 |
| Figure 4.33: SBCu glasses after 14 days in SBF | 80 |
| Figure 4.34: Change in Cu amount during immersion in SBF | 81 |
| Figure 4.35: Comparison of XRD spectra of S1 | 82 |
| Figure 4.36: Comparison of XRD spectra of S2 | 83 |
| Figure 4.37: Comparison of XRD spectra of SB1 | 83 |
| Figure 4.38: Comparison of XRD spectra of SB2 | 84 |
| Figure 4.39: Comparison of XRD spectra of SBCu1..... | 84 |
| Figure 4.40: Comparison of XRD spectra of SBCu2..... | 85 |
| Figure 4.41: Peaks of hydroxyapatite in SB1 1d | 85 |
| Figure 4.42: Peaks of hydroxyapatite in SB2 1d | 86 |
| Figure 4.43: Hydroxyapatite peaks vs peaks in a) SB1 1d and b) SB2 1d | 86 |
| Figure 4.44: Hydroxyapatite peaks vs peaks in a) SBCu1 1d and b) SBCu2 1d | 87 |
| Figure 4.45: Peaks of Ca_2SiO_4 in SBCu2 1d..... | 87 |
| Figure 4.46 XRD spectrum of SB1 14d..... | 88 |
| Figure 4.47: SEM micrograph of SB1 after 14 days in SBF (at 50K X) | 88 |
| Figure 4.48 SEM micrograph of SB1 after 14 days in SBF (at 50K X) | 89 |
| Figure 4.49: SEM micrograph of SB2 after 14 days in SBF (at 20K X) | 89 |

| | |
|--|-----|
| Figure 4.50 SEM micrograph of SBCu1 after 14 days in SBF (at 30K X)..... | 89 |
| Figure 4.51 SEM micrograph of SBCu2 after 14 days in SBF (at 40K X)..... | 90 |
| Figure 4.52: SEM micrographs of fibers containing 5% of S1 and S2..... | 91 |
| Figure 4.53: SEM micrographs of fibers containing 5% of SB1 and SB2..... | 92 |
| Figure 4.54: SEM micrographs of fibers containing 5% of SBCu1 and SBCu2 | 93 |
| Figure 4.55: PCL/AA/FA/S1(5%) SBF 1d where a) 1K X b) 10K X c) 45k X..... | 94 |
| Figure 4.56: PCL/AA/FA/S2(5%) SBF 1d where a) 1K X b) 10K X c) 45K X..... | 94 |
| Figure 4.57: PCL/AA/FA/SBCu1(5%) SBF 1d where a) 1K X b) 10K X c) 45K X | 94 |
| Figure 4.58: PCL/AA/FA/SBCu2(5%) SBF 1d where a) 1K X b) 10K X c) 45K X | 94 |
| Figure 4.59: Comparison between different methods of glass addition..... | 96 |
| Figure 4.60: Comparison between PCL/AA/FA and PCL/AA systems | 97 |
| Figure 4.61: Examples of glass incorporation in fibers | 98 |
| Figure 4.62: SEM micrographs of PCL/AA/FA/SBCu1(30%) at 500.00 K X (a) and at 10.00 K X (b)..... | 98 |
| Figure 4.63: Comparison of fibers containing different concentration of SBCu2 | 100 |
| Figure 4.64: SEM micrographs of PCL/AA/S2(20%) at 500 X (a), at 1K X (b) and at 20K X (c) and (d)..... | 101 |
| Figure 4.65: SEM micrographs of PCL/AA/SB2(0%) at 1K X (a), at 4K X (b), at 20K X (c) and (d)..... | 102 |
| Figure 4.66: SEM micrographs of PCL/AA/SBCu2(0%) at 1K X (a), at 5K X (b), at 10K X (c) and (d) and at 45K X (e)..... | 102 |
| Figure 4.67: SEM micrograph and EDS spectrum of an area of PCL/AA/S2(20%)..... | 103 |
| Figure 4.68: EDS map of PCL/AA/SB2(20%) at 1kX (a), 5.00 K X (b) and 10.00 K X (c) and spectrum (d) | 104 |
| Figure 4.69: SEM micrograph and EDS spectrum of an area of PCL/AA/SBCu2(20%)..... | 104 |
| Figure 4.70: FTIR spectra of neat and composite fibers..... | 105 |
| Figure 4.71: Contact angle values of the different electrospun fibers | 106 |
| Figure 4.72: pH value trends during acellular bioactivity test of fibers..... | 107 |
| Figure 4.73: SEM micrograph of PCL/AA/S2(20%) at different time points of immersion in SBF | 108 |
| Figure 4.74: SEM micrograph and EDS pattern of glass clusters in PCL/AA/S2(20%) SBF 1d | 109 |
| Figure 4.75: SEM micrograph of PCL/AA/S2(20%) SBF 3d(a), SBF 7d (b) and 14d (c) | 110 |
| Figure 4.76: SEM micrograph of PCL/AA/SB2(20%) SBF 1d..... | 111 |

| | |
|--|-----|
| Figure 4.77: SEM micrograph of PCL/AA/S2(20%) SBF 1d..... | 111 |
| Figure 4.78: SEM micrograph of PCL/AA/S2(20%) SBF 1d example 2 | 112 |
| Figure 4.79: SEM micrograph of PCL/AA/SB2(20%) SBF 3d (a), SBF 7d (b) and SBF 14d (c) | 112 |
| Figure 4.80: SEM micrograph of PCL/AA/SBCu2(20%) immersed in SBF | 113 |
| Figure 4.81: SEM micrograph and EDS pattern of PCL/AA/SBCu2(20%) SBF 1d..... | 114 |
| Figure 4.82: SEM micrograph and EDS pattern of PCL/AA/SBCu2(20%) SBF 3d..... | 115 |
| Figure 4.83: SEM micrograph and EDS pattern of PCL/AA/SBCu2(20%) SBF 7d..... | 115 |
| Figure 4.84: SEM micrograph and EDS spectra of PCL/AA/SBCu2(20%) SBF 14d.... | 116 |
| Figure 4.85: SEM micrograph and EDS spectra of PCL/AA/S2(20%) SBF 21d..... | 117 |
| Figure 4.86: SEM micrograph and EDS spectra of PCL/AA/SB2(20%) SBF 21d | 118 |
| Figure 4.87: SEM micrograph and EDS spectra of PCL/AA/SBCu2(20%) SBF 21d.... | 119 |
| Figure 4.88: PBS pH trend of both neat and composite electrospun mats..... | 120 |
| Figure 4.89: Comparison of FTIR results of PCL/AA/S2(20) 0d and 7d..... | 121 |
| Figure 4.90: Comparison of FTIR results of PCL/AA/SB2(20) 0d and 7d | 121 |
| Figure 4.91: Comparison of FTIR results of PCL/AA/S2(20) 0d and 7d..... | 122 |
| Figure 4.92: SEM micrographs of neat PCL fibers at different time point of immersion in PBS | 123 |
| Figure 4.93: SEM micrographs of PCL/AA/S2(20%) at different time point of immersion in PBS | 124 |
| Figure 4.94: SEM micrographs of PCL/AA/SB2(20%) at different time point of immersion in PBS | 125 |
| Figure 4.95: SEM micrographs of PCL/AA/SBCu2(20%) at different time point of immersion in PBS | 125 |
| Figure 4.96: Example of tensile stress – tensile stress curve | 127 |
| Figure 4.97: S2 (a), SB2 (b) and SBCu2 (c) after 1 hour of immersion in AA | 128 |
| Figure 4.98: SEM micrographs of glasses of synthesis 2 after immersion in AA | 129 |
| Figure 4.99: pH trend during acellular bioactivity test of all glasses soaked in AA..... | 130 |
| Figure 4.100: EDS spectra of S2 glasses at different time points in SBF..... | 131 |
| Figure 4.101: EDS spectra of SB2 glasses at different time points in SBF | 132 |
| Figure 4.102: EDS spectra of SBCu2 glasses at different time points in SBF | 133 |
| Figure 4.103: P amount in S2 and S2/AA after immersion in SBF | 134 |
| Figure 4.104: P amount in SB2 and SB2/AA after immersion in SBF..... | 134 |
| Figure 4.105: P amount in SB2 and SB2/AA after immersion in SBF..... | 135 |
| Figure 4.106: Ca amount in S2 and S2/AA after immersion in SBF | 135 |

| | |
|---|-----|
| Figure 4.107: Ca amount in SB2 and SB2/AA after immersion in SBF..... | 136 |
| Figure 4.108: Ca amount in SBCu2 and SBCu2/AA after immersion in SBF | 136 |
| Figure 4.109: XRD spectra of S2/AA before and after immersion in SBF | 138 |
| Figure 4.110: XRD spectrum of S2/AA after 14 days in SBF and related peaks lists.... | 139 |
| Figure 4.111: XRD spectra of SB2/AA before and after immersion in SBF..... | 140 |
| Figure 4.112: XRD spectrum of SB2/AA 14d and related peaks lists..... | 141 |
| Figure 4.113: XRD spectra of SBCu2/AA before and after immersion in SBF | 142 |
| Figure 4.114: XRD spectrum of SBCu2/AA SBF 1d with peaks of copper acetate..... | 143 |
| Figure 4.115 XRD spectrum of SBCu2/AA after 14 days in SBF and related peaks lists | 144 |
| Figure 4.116: SEM micrograph of S2/AA SBF 1d (at 4K X)..... | 145 |
| Figure 4.117: SEM micrograph of SBCu2/AA in SBF 14d at 30K X (a) and at 50.K X (b) | 145 |
| Figure 4.118: Biological assay results for both neat and composite electrospun mats... | 146 |
| Figure 4.119: Fluorescence microscopy images | 147 |

List of Tables

| | |
|---|-----|
| Table 1: Total amounts of synthesized glasses..... | 43 |
| Table 2: Comparison of atomic% between S1 and S2..... | 65 |
| Table 3: Comparison of atomic% between SB1 and SB2..... | 65 |
| Table 4: Comparison of atomic% between SBCu1 and SBCu2 | 66 |
| Table 5: Values of surface areas calculated by BET..... | 71 |
| Table 6: Ca/P ratio of glasses during acellular bioactivity test..... | 80 |
| Table 7: Mechanical properties of electrospun fibers | 126 |
| Table 8: Ca/P ratio of glasses immersed in AA during acellular bioactivity test | 137 |

1 Introduction

In order to solve the lack of autografts and immune and disease problems related to allografts, new strategies in the tissue engineering field have been developed. Among them, advanced composite scaffolds, whose components are polymers and bioactive glasses (BGs), are gaining a lot of attention. BGs have been investigated and applied for decades in bone regeneration, but recent studies have also shown the capacity of BGs to stimulate vascularization and to heal soft tissue wounds [1]. Therefore, the first subchapter of the introduction describes the main requisites of a tissue engineering (TE) scaffold and features and advantages of using a composite material for these applications, paying particular attention on the composites composed by polymers and bioactive glasses. A brief description of the polymer, poly-(caprolactone), which was used during this master thesis work, is also given in the same chapter.

The second introductory subchapter chapter is focused on bioactive glasses, which are a special subset of biocompatible glasses that can bond to hard and soft tissues and stimulate new tissue growth while dissolving over time [2]. During this experimental work, BG nanoparticles were produced using a sol-gel method. Therefore, the second subchapter of the introduction includes an explanation of historical background, different compositions, influence of ion incorporation (focusing on the effects of phosphorus, copper and boron) and different fabrication techniques (giving major attention to the sol-gel technique).

In the third introductory subchapter, the electrospinning technique is described, focusing on working principles, advantages and open issues, such as the optimal incorporation and dispersion of bioactive glass particles in the polymeric matrix.

The fourth chapter is based on the description of the analysis techniques, which have been used to characterize the bioactive glasses and the electrospun composite fibers.

The analysis results are reported and discussed in the fifth chapter.

Finally, in the sixth and last chapter the experimental work is shortly summarized and new future developments and applications are introduced.

1.1 Tissue engineering and composite scaffolds

Disease, injury and trauma can lead to damage and degeneration of tissues in the human body, which necessitate treatments to facilitate their repair, replacement or regeneration. Treatment typically focuses on transplanting tissue from one site to another in the same patient (an autograft) or from one individual to another (a transplant or allograft). Unfortunately, both these treatments have some drawbacks. Harvesting autografts is expensive, painful, constrained by anatomical limitations and associated with donorsite morbidity due to infection and hematoma. Similarly, allografts and transplants also have serious constraints due to problems with accessing enough tissue for all of the patients who require them and the fact that there are risks of rejection by the patient's immune system and the possibility of introducing infection or disease from the donor to the patient. Alternatively, in order to overcome barriers of current clinical treatments, the field of tissue engineering is emerging [3]. The definition of Tissue engineering (TE) was provided for the first time by Dr. Langer and Dr. Vacanti in 1993: "Tissue engineering is an interdisciplinary field which applies the principles of engineering and the life sciences toward the development of biological substitutes that restore, maintain or improve tissue function [4]. The major goal of TE is the regeneration of diseased or damaged tissues, instead of their replacement, restoring impaired function, using combinations of functional cells and scaffolds able to reproduce the in vivo microenvironment [5][6][7].

1.1.1 A brief introduction to scaffolds

Scaffolds are tridimensional structures that act as templates for tissue regeneration, guiding the growth of new tissue. Therefore, the scaffold role is to allow cells to attach, proliferate, differentiate and organize into normal, healthy tissue as the scaffold degrades [7].

Scaffolds for tissue engineering should possess the following requirements:

- structural and mechanical properties that match with of the host tissue;
- physically stability in the implanted site;
- biocompatibility;
- appropriate morphology to support cell integration, adhesion and growth;

- high porosity and interconnection to transmit regulatory chemical signals, nutrients, oxygen and metabolic wastes;
- *in vivo* degradation and resorption kinetics that physically support the regenerating tissues and allow cells to proliferate and secrete their own extracellular matrix, while the scaffold gradually vanishes, without producing toxic degradation products [5][6].

In the past few years, various biomaterials have been used to prepare scaffolds in tissue engineering, including natural materials, such as collagen, gelatin and elastin and synthetic materials, such as poly(ϵ -caprolactone)(PCL), poly(glycolic acid)(PGA), poly(lactic acid)(PLA), poly(hydroxy alkenoates) (PHAs) and their copolymers. However, many biomaterials are difficult to meet the mechanical properties of engineering scaffolds due to their own limitations [5]. Recent research results have shown that mechanical properties, such as elasticity, stiffness and strength, are essential factors that directly influence the ability of cell adhesion, proliferation and differentiation [5].

1.1.2 Main features of a composite material

A composite material consists of two or more type of materials (metallic, ceramic, or polymeric), that represent chemically distinct phases, separated by interface(s). The classification of engineering composite materials is based on the matrix materials (metals, ceramics, and polymers) or on the reinforcement dimensions/shapes (particulates, whiskers/short fibres, and continuous fibres) or on the bioactivity of composites (in case of biomedical composites where at least one of the constituent materials should be bioactive, which may render the composite bioactive) [8].

Using the matrix material as the basis for classification, there are three types of biomedical composites [8]:

- polymer matrix composites,
- metal matrix composites,
- ceramic matrix composites.

Using the bioactivity of composites as the basis for classification, there are also three types composites [8]:

- bioinert composites
- bioactive composites,
- bioresorbable composites.

A composite is designed to have a combination of the best characteristics of each of the component materials, maintaining their advantages and minimising their shortcomings, in order to suit better the mechanical and physiological demands of the host tissue [8].

Composites of polymers and bioactive glasses are being developed with the aim to improve the combined mechanical properties and tissue interaction [9][10][11][12], imparting strength and bioactivity by an inorganic bioactive filler while keeping the positive properties of the polymer, such as flexibility and capacity to deform under loads [13][14].

Polymers and ceramics (and glasses) that have the ability to degrade *in vivo* are ideal candidates for composite scaffolds which gradually degrade while new tissue is formed [15]. While massive release of acidic degradation products from polymers can cause a large decrease in the local pH and, consequently, inflammatory reactions that, in case of skin wounds lead to blisters, scar hyperplasia and severe wound contraction [1], the basic degradation of bioactive glasses could buffer the acidic products of polymers (thanks to rapid exchange of protons in water for alkali in the glass), thus contributing to avoid a local increase in acidity and subsequent formation of an unfavourable environment for cells due to low pH values [15][16].

Many factors (listed below) can affect properties of biomedical composites [16]:

- reinforcement shape, size, and size distribution;
- reinforcement properties and volume percentage;
- bioactivity and biostability of the reinforcement (or the matrix);
- matrix properties (molecular weight, grain size, etc.);
- distribution of the reinforcement in the matrix;
- strength of interfacial bond between component materials;
- reinforcement-matrix interfacial state.

Bioactive glasses can be added to different polymer matrices in the form of micron sized or nanoscale particles or fibres [13]. However, they have been

resulted to be particularly successful as an agent for loading and improved bioactivity in the form of nanoparticle dispersion (BGNP) [27]. The larger specific surface area of the nanoparticles should lead to increased interface effects, providing a greater transfer of load from the matrix to the reinforcing phase, and should contribute to improved bioactivity, when compared to standard (μm -sized) particles [13].

Polymer fibres may be used as the matrix material, which can provide a stronger and stiffer matrix than the isotropic polymer [3]. In particular, electrospun fiber mats are uniquely suitable for use as scaffolds because of their 3D structure with high porosity [7].

1.1.3 Polymers used in the fabrication of composite materials

Polymers used for the composites for tissue application are generally biodegradable, that means they have the potential to produce an implant that with time is substituted by living tissue [16]. Biodegradable polymers can be divided in two groups: natural and synthetic polymers. The use of natural biomaterials like proteins can be considered advantageous for TE applications due to their biochemical and structural similarity to the components of the native ECM. However, the residues from the degradation of synthetic polymers can decrease the local pH and can potentially cause cells and tissues necrosis, inflammatory and immune response in the body.

Synthetic polymers can be produced under controlled conditions and therefore exhibit in general predictable and reproducible mechanical and physical properties such as tensile strength, elastic modulus and degradation rate. A further advantage is the control of material impurities. Possible risks such as toxicity, immunogenicity and favoring of infections are lower for pure synthetic polymers with constituent monomeric units having a well-known and simple structure [11]. Among the important synthetic biopolymers, polyesters, such as poly(lactic acid) (PLA), poly(glycolic acid) (PGA), polycaprolactone (PCL) and polyhydroxybutyrate (PHB), poly(lactic-coglycolide) (PLGA) copolymers, play the most important role [11][16][17].

1.1.3.1 Polycaprolactone

Polycaprolactone (PCL) is a linear and aliphatic polyester, composed by nonpolar methylene groups and one semi-polar ester group. It was first synthesized in the 1930s and now is widely used for drug delivery and fabrication of 3D scaffolds for tissue engineering applications. Its advantages include biocompatibility, biodegradability, melting point ranging from 55°C to 60°C, very high drug permeability, strong solubility, relatively slow degradation rate, formation of less acid products when compared to other polyesters, and blend compatibility with other biomaterials [55]. Moreover, PCL is elastic in nature and can be used in various forms such as films, fibers, and microparticles [7]. Thanks to its semicrystalline and hydrophobic nature, PCL can take several years to degrade in vivo (from 2 to 4 years, depending on the starting molecular weight). It has been found that the degradation of PCL system with a high molecular weight (M_n of 50,000) requires 3 years for complete removal from the host body. Therefore, due to its slow degradation rate, PCL is a good candidate for bone scaffolding applications. The degradation of PCL and its copolymers proceeds in two stages: random hydrolytic ester cleavage that occurs by uptake of water followed by the hydrolysis of ester bonds (de-esterification) and weight loss through the diffusion of oligometric species from the bulk. Once degraded, the monomeric components of each polymer are removed by natural pathways. The body already contains highly regulated mechanisms for completely removing monomeric components of lactic and glycolic acids. Different factors affect the degradation kinetics, such as: chemical composition and configurational structure, processing history, molar mass (M_w), polydispersity (M_w/M_n), environmental conditions, stress and strain, crystallinity, device size, morphology (e.g. porosity) and chain orientation, distribution of chemically reactive compounds within the matrix, additives, presence of original monomers and overall hydrophilicity.

Although exhibiting these advantageous properties, PCL is not bioactive [18][18]. Many researchers have reported that incorporation of calcium carbonate (CaCO_3), calcium phosphate such as hydroxyapatite (HA) or bioactive glass (BG) particles helped to promote mineralization of the constructs and improve osteoblast

proliferation and differentiation [19], having a relevant effect on osteogenesis and angiogenesis processes [18][20].

Recently, composite scaffolds, obtained by electrospun polymeric fibers incorporating bioactive ceramics have been investigated [21]. These composites phases are favored for hard tissue applications, due to their mechanical and biological properties, which can be tuned appropriately for cellular functions and bone formation [22][23]. Besides, the use of inorganic nanoparticles (NP) has been shown to reduce the hydrophobic behavior of PCL and, consequently, to accelerate its degradation process which, as mentioned above, occurs via hydrolytic process [24].

1.2 Bioactive glasses

1.2.1 Glasses

Glass belongs to ceramic materials group and is typically produced freezing a liquid, which solidifies quickly, forming an amorphous structure. The solidification is so fast that the crystalline lattice has no enough time to form; thus, glass is an isotropic solid material that is characterized only by a short-range order. In the disorganized lattice of glass, composed by former ions, there are some interstices, in which contaminants can enter. Therefore, the structure of glass is composed of network formers, network modifiers and intermediate oxides. The network formers can form glasses alone without additional components; the network modifiers affect the glass structure by bonding to non-bridging oxygen atoms as Si-O-M^+ where M^+ is a modifier cation; the intermediate oxides can act either as network modifiers or enter the structure of glasses like network formers. Only materials with a slow crystallization velocity, such as SiO_2 , GeO_2 , B_2O_3 , P_2O_5 , can form glass [25].

1.2.2 Bioactivity

Bioactivity or bioreactivity refers to the capability of a material to affect its biological surroundings, inducing a physiological response that is supportive of the function and performance of the biomaterial. In bioactive glasses and bioactive ceramics, this term refers to the ability of implanted materials to interact

with surrounding living tissue, forming strong bonds to bone (and in some cases soft) tissue [13].

The first definition of bioactivity was formulated in 1974 and enunciated that a biomaterial was an inert substance, regarding both interaction with human organism and pharmacological response, designed in order to be implanted and incorporated in a living system.

When implanted, bioactive materials are partially reabsorb, guaranteeing the formation of strong chemical bonds with the surrounding damaged tissues, helping the growth of new tissue.

The bioactivity is evaluated using a parameter (IB) that links the bioactivity of the material to the time which is needed by the 50% of material to bond with the bone.

1.2.3 Bioactive glasses

Bioactive glasses caused a revolution in healthcare and paved the way for modern biomaterial-driven regenerative medicine.

Bioactive glasses (BGs) are synthetic biomaterials, which are able to induce a specific biological activity, that leads to formation of an apatite layer on their surface, when they are exposed to physiological fluid or simulated body fluid, avoiding the formation of an undesirable fibrous encapsulation [11][25][26][27]. This layer bonds strongly to both hard and soft tissues and releases ion products after its dissolution [27].

1.2.3.1 *Historical background*

Bioactive glasses were firstly developed in the late 1960s [25]. The discovery of bioactive glasses (BGs) is attributed to Larry Hench, a research professor in the Department of Materials Science and Engineering at the University of Florida and then director of the Bioglass Research Centre at the same University [28]. Talking with a U.S. Army colonel just returned from the Vietnam War about the rejection of polymeric and metal implants, due to fibrous capsule formation, Hench was fascinated by the question and started developing his so-called “hypothesis of bioactive glass”. This hypothesis was based on two pillars: (i) metals and synthetic polymers elicited a “foreign body reaction” because their components

were completely different from those that make up living tissues, and (ii) a material that was able to form a bone-like hydroxyapatite layer on its surface should not be rejected by the body, as hydroxyapatite is the main mineral phase of natural bone tissue. From 1969 to 1971, Hench and his coworkers designed and studied different glass formulations based on the $\text{SiO}_2\text{-Na}_2\text{O-CaO-P}_2\text{O}_5$ oxide system, and they finally selected the composition $45\text{SiO}_2\text{-}24.5\text{Na}_2\text{O-}24.5\text{CaO-}6\text{P}_2\text{O}_5$ (wt%), named as 45S5 Bioglass, that was found to be able to chemical bond with rat bone. The high amounts of Na_2O and CaO , as well as the relatively high $\text{CaO/P}_2\text{O}_5$ ratio of this glass make the glass surface very reactive in physiological environment [7].

It is worth noticing that the name Bioglass® was then trademarked by the University of Florida as the name for the original 45S5 composition and, therefore, it should be used only referring to that composition and not generally to indicate BGs.

Since the announcement of Hench's patented Bioglass, extensive studies by *in vitro* techniques have succeeded on various bioactive silicate glasses and glass-ceramics [29]. Over the last forty years, many new compositions and other types of BGs have been proposed for optimizing the body's response for specific clinical applications.

Because bioactivity and specific surface area intrinsically linked, the last decade has seen a focus on the development of highly porous and/or nano-sized materials [30]. Mesoporous bioactive glasses (MBGs) were developed first the first time in 2004 and have rapidly gained great interest thanks to their numerous beneficial properties [31]; owing to their high surface area and ordered structure, they are optimal candidates for controlled drug-delivery systems.

1.2.3.2 Main features and applications of bioactive glasses

Bioactive glasses are biocompatible, as a direct result of their chemical compositions, which contain ions commonly found in the physiological environment (such as Ca^{2+} , K^+ , Mg^{2+} , Na^+ , etc.) and eventually other ions showing very limited toxicity to body tissues (such as Al^{3+} and Ti^{2+}).

BGs have the capability to degrade with controllable degradation rate, once in contact with biological fluids, and to bond to both soft and hard tissues, without

fibrous encapsulation [7][30][32][33]. In fact, they dissolve to different extents under biological conditions, being osteoconductive, osteoinductive (or osteoproduktive) and even angiogenic in some compositions [25][34]. They are able to induce the precipitation of a biologically active, calcium-deficient, hydroxy carbonate apatite (HCA) surface layer at the interface between the bone and the implanted material, when in contact with relevant physiological fluid or during *in vivo* applications, thanks to the release of ions such as Na^+ , Si_4^+ and Ca^{2+} and the [26][35][36]. This HCA phase is chemically and structurally equivalent to the mineral phase in bone, providing the interfacial bonding and chemical bindings with bone that ensure the osteo-integration of the implant [37].

Moreover, it has been demonstrated that dissolution products from bioactive glasses upregulate the expression of genes that control osteogenesis and production of growth factor, and promote bone tissue regeneration, explaining the higher rate of bone formation in comparison to other inorganic ceramics such as hydroxyapatite [13][37]. Bioactive glasses have been found to support enzyme activity, vascularization, osteoblast adhesion/growth/differentiation and induce the differentiation of mesenchymal cells into osteoblasts [11][15].

Moreover, thanks to their degradation ability, there is no need for a second surgery to remove these glasses from body.

The high biomineralization ability of bioactive glasses is related to their composition but is also influenced by their physical properties, such as particle size, porosity, density, surface area, morphology and crystallinity [9][16]. Because bioactivity is directly related to the glass dissolution rate, it is obvious that it will also be dependent on its morphology. The higher the specific surface area, i.e., the contact surface between the material and the physiological fluid, the greater is the glass bioactivity. An increase in specific surface area and pore volume greatly accelerates the deposition of hydroxyapatite (HA) and therefore enhances the bioactivity [37][38][39].

Strategies to obtain a significant specific surface area imply an increase in the porosity and/or a decrease in the size of the materials synthesized. Therefore, the bioactive behavior increases with the decrease in the particle diameter.

Moreover, a smaller diameter increases protein adhesion, enhances osteoblast proliferation or differentiation, and engenders the anti-microbial and anti-inflammatory properties.

Thanks to these unique features, bioactive glasses are very promising materials for soft and hard tissue engineering (TE) [8][31][34]. Their tissue restoration potential has been demonstrated through both *in vivo* studies and clinical practice [34], in particular their ability to induce the formation of a hydroxyapatite layer on their surface after immersion in body fluid is essential for bone regeneration *in vivo* and makes them very useful in bone tissue applications (such as bone fractures, bone diseases and dental applications) [2][11][15][25][35][36][40], whereas their biological activity to promote angiogenesis and healing processes in soft tissue regeneration and wound healing allows their use for soft tissue repair applications [25]. Early applications of bioactive glasses were in the form of solid pieces for small bone replacement, i.e. in middle ear surgery. Later, other clinical applications of bioactive glasses were proposed, for example in periodontology, endodontology, or as coating on metallic orthopedic implants [7][13]. More recently, applications of bioactive glasses in tissue engineering and regenerative medicine are emerging [13].

Bioactive glass powders can be used as scaffolds materials, either as filler or coatings of polymer structures, or as porous materials themselves [11], sometimes also serving as vehicle for the local delivery of selected ions being able to control specific cell functions [7]. Among various morphologies of BGs, bioactive glass nanoparticles (BGNs) are attractive biomaterials for a large number of biomedical applications, due to their small size, large specific surface area, and their large surface to volume ratio that confer them special properties [25]. Owing to these attractive morphological characteristics, BGNs exhibit obvious advantages over their micron-sized counterparts in some applications such as TE composite scaffolds. Indeed, their morphological characteristics should facilitate their homogenous incorporation into polymer matrices for fabrication of composite scaffolds or bioactive coating on implants. The great potential of nanometric bioactive glass systems lies not only in the field of bone tissue engineering but

also in dentistry, for example in dentin regeneration and in the reconstruction of critical bone defects as well as in osteochondral and cartilage regeneration.

Finally, it is worth noting that their size also permits them to be internalized by different type of cells (macrophages, bone cells, cancer cells, etc.). If well controlled and oriented, this could be very interesting for drug delivery and cancer treatment, for example [41].

1.2.3.3 Formation of the HCA layer

Once a bioactive glass is implanted *in vivo* or immersed in an aqueous phosphate solutions similar to body fluid, generally named as simulated body fluid *in vitro* (e.g. in SBF), it dissolves gradually and the ions released promote the growth of a carbonated hydroxyapatite layer at its surface. This dissolution mechanism is enhanced by the low connectivity of the SiO₂ network, thanks to the presence of network modifiers, like sodium and calcium, leading to the formation of non-bridging silicon-oxygens bonds [30]. Thus, the bioreactivity of bioactive glasses leads to a cascade of reactions, which leads to formation of a hydroxyapatite-like layer. When this event is simulated *in vitro* a sequence of five consecutive steps take place:

- i. exchange of ions (Na⁺, Ca²⁺ and PO₄³⁻ if initially present) with H⁺ from the biological fluid, creating Si-OH bonds;
- ii. breaking of surface Si-O-Si bonds, promoted by the increase in local pH, and release of soluble silica,
- iii. condensation of some of the surface silanol groups that are formed in steps (i) and (ii) condense to form a hydrated silica-rich layer on the surface, depleted in modifier cations (Na⁺ and Ca²⁺ cations);
- iv. diffusion of Ca²⁺ and PO₄³⁻ through the surface silica gel layer in order to form a superficial amorphous calcium phosphate layer, which is rich of calcium and phosphorus;
- v. crystallization of the amorphous layer and formation of the hydroxyapatite layer. Sometimes this amorphous film incorporates additional carbonate ions from solution and crystallizes to hydroxycarbonate apatite.

1.2.3.4 BG compositions and the effect of different ions

The most investigated network formers in BGs are silica (SiO₂), phosphorus pentoxide (P₂O₅), and boron trioxide (B₂O₃). However, the most widely used in biomedical applications are silica bioactive glasses, incorporating sodium, calcium and phosphorus in different relative proportions, but also other additional elements (such as fluorine, magnesium, strontium, iron, silver, boron, potassium or zinc) can be incorporated in the silicate network in order to confer additional beneficial properties [13]. The effect of different ions incorporation into the composition of BGs has been evaluated. A complete explanation of effect of ion incorporation falls outside the final purpose of this master thesis work, therefore only the effects of the ions that are relevant for this experimental work will be briefly reviewed.

It is well known that single inorganic ions such as the ones contained in the glasses prepared during this master thesis work (silicon, phosphorous, calcium, boron and copper) play a physiological role in angiogenesis and growth and mineralization of bone tissue. These inorganic factors are particular interesting because of their low cost, high stability and potentially better clinical safety when compared to organic growth factors. For this reason, bioactive glasses containing traces of these elements have been developed and studied in the past years.

Since calcium (Ca) and phosphorous (P) are the main components of biological apatite, they obviously play an essential role in bone formation and resorption. However, this is not the only effect of these ions.

In addition to silicate glasses, **phosphate glasses**, exhibiting less pronounced bioactivity but high solubility in contact with biological fluids, have been developed.

Calcium is also an important factor in the wound healing of skin and is supposed to be required for the migration of epidermal cells [1][42]. Moreover, Ca²⁺ ions can realize a synergistic antimicrobial effect with Cu²⁺, whose effects will be explain later [43].

Boron is one of the trace elements in the human body which plays an important role in many life processes including embryogenesis, bone growth and maintenance, immune function and psychomotor skills [44][45]. It is well known

that boron stimulates wound healing and improves bone health [1][46]. Different compositions of bioactive glasses (BGs) containing boron, including boron-doped, borosilicate and borate glasses, are being investigated for bone and soft tissue engineering under the premise that these BGs are suitable carriers of boron. Being boron trivalent and silicon quadrivalent, it has been speculated that the incorporation of boron into MBG scaffolds by replacing parts of silicon can significantly influence the physiochemistry and biological property of MBG scaffolds. Therefore, *Wu et al.* [44] have developed boron-doped mesoporous bioactive scaffolds (B-MBG) by sol-gel method, substituting some of the silicon in the glass composition by boron, in order to investigate the effect of boron on their physiochemistry and osteoblast response. By controlling the contents of boron in the B-MBG scaffolds, it is possible to control release kinetics of boron ions. Moreover, low concentrations of released boron ions are safe to human and can significantly improve the proliferation and the gene expression of osteoblasts (Col I and Rux2). *Rezai Moonesi Rada et al.* [47] have synthesized amorphous and nano-sized BGs containing boron ions in various percentage (7%, 14% and 21%) in order to evaluate their effects on human dental pulp stem cells (hDPSCs) and have demonstrated that boron incorporation increase intracellular calcium amounts (in particular, the highest intracellular calcium amount was observed in glass nanoparticles with 21% of B_2O_3) and stimulate expression of DSPP, osteopontin and collagen type I. Moreover, other experimental studies have demonstrated that substitution of SiO_2 with B_2O_3 can lead to a more rapid conversion of the glass to HAp in SBF, hence to a higher bioactivity [42][45]. The effect of gradual addition of B_2O_3 replacing SiO_2 in commercial S53P4 glass composition on the apatite forming ability, cell proliferation and antibacterial properties was explored and discussed by *Sakthi Prasad et al.* [41]. Their results show that B_2O_3 substituted glasses exhibit improved antibacterial properties and better cell compatibility and proliferation, compared to base glass (BG0B). These glasses showed, in fact, possibility of bactericidal properties against *Escherichia Coli* bacteria compared to commercially available S53P4 glass which showed only bacterial inhibition.

Recently developed **borate glasses** have shown many advantages such as faster dissolution of ions, higher bioactivity, soft tissue repair, wound healing applications and blood vessel formation by release of vascular growth factors [48][49]. As example, it is possible to mention the boron based 45S5B bioglass successfully produced and characterized by *Roberto Gustavo Furlan et al.* [49] using a sol-gel process. According to their results, this glass is highly bioactive and safe for biological applications, showing the formation of large amounts of hydroxyapatite at the surface of the 45S5B bioglass after immersion in SBF and a cytotoxic effect similar to 45S5 under the tested conditions against eukaryotic OSTE01 cells *in vitro*. Moreover, antibacterial effects of some borate glasses were studied and inhibition against various Gram-positive and Gram-negative bacterial species was demonstrated where borate ions were playing major part in exhibiting antibacterial effects.

Copper (Cu) ions are considered as metallic angiogenic factors, due to their intensive involvement in blood vessel growth and endothelial cells proliferation [43][50][51][52]. The release of Cu^{2+} ions has been shown to enhance angiogenesis in both soft and hard tissue repair, by stabilizing the expression of hypoxia-inducible factor (HIF-1 α) and secretion of vascular endothelial growth factor (VEGF); in other words copper effect is to artificially mimic hypoxia, which plays a critical role in the recruitment and differentiation of cells and in blood vessel formation [1][53][54]. The release of Cu also enhances the stem cells differentiation towards the osteogenic lineage, stimulating osteogenesis in osseous defects *in vivo* [43][50][55]. Borate bioactive glass (13-93 B3) microfibers doped with varying amounts of Cu (0e3.0 wt.% CuO) were created and evaluated *in vitro* and *in vivo* by *Zhao et al* [1]. The ionic dissolution products of these Cu-doped glasses stimulated HUVEC migration, tubule formation and VEGF secretion, improved collagen deposition, maturity and orientation, and the expression levels of angiogenic-related genes of fibroblasts. It is also worth noticing that the expression degree of these genes increased with increasing Cu concentration in the microfibers. Therefore, these Cu-doped borate bioactive glass microfibers seem to be very promising candidates for use as wound dressings.

However, borate-based bioactive glasses are not currently approved by the US Food and Drug Administration for *in vivo* use. On the other hand, many silicate bioactive glasses such as 45S5 and 13–93 have been used in clinical applications for several years, but the effect of Cu doping on their ability to stimulate angiogenesis and osteogenesis has received little attention.

Scaffolds with a grid-like microstructure composed of silicate 13–93 BG doped with varying amounts of copper (0–2.0 wt.% CuO) have been fabricated and evaluated *in vitro* and *in vivo* by *Lin et al* [56]. Their results show that the highest concentration (2.0 wt.%) significantly enhanced blood vessel area in the new forming fibrous tissue that infiltrated the scaffolds.

Seza Özge Gönen et al. [57] have reported for the first time the successful incorporation of strontium or copper substituted bioactive glass particles into the gelatin/PCL nanocomposite scaffolds by means of electrospinning technique. These nanocomposite fiber mats combine the high bioactivity of bioactive glasses, the beneficial effects of therapeutic metallic ions on bone growth and an interconnected porous structure of electrospun nanofibers that may allow cell adhesion, cell invasion and vascularization. Researchers also have pointed out that the addition of more than 2 wt% SrO and CuO into bioactive glass composition may be better to improve the osteogenic, angiogenic, and antibacterial potential of the nanocomposite fiber mats as scaffolds for bone tissue engineering. Indeed, as mentioned above, incorporating copper ions (Cu^{2+}) into the glass system, it has been possible to develop bioactive glasses which exhibit an antibacterial and antimicrobial effect [43][58]. In general, the mechanisms for this strong bactericidal effect are not clear but it is accepted that Cu^{2+} ions are small enough to disrupt bacterial cell membranes producing further the disruptions of enzyme functions [58].

The above reported studies are only a small part of all experiments carried out in order to evaluate the therapeutic effect of these ions, but a complete review of these experimental results falls outside of this master thesis; indeed, the aim of this section was only to underline the evident and well-known effects of the above discussed ions and justify their selection for the glass compositions used in this experimental work.

1.2.4 Preparation methods

Controlled synthesis of BGs is critical to their effective use in biomedical applications since their characteristics (such as morphology and composition) depend on the synthesis process [25]. There are two general methods to synthesize the BGs: melt-quenching process and sol-gel technique [59][25][27][31][55].

1.2.4.1 *Melting technique*

The original bioactive glass developed by Hench was prepared through a conventional high-temperature melting process followed by a quenching step [30]. According to this technique, powders of inorganic precursors, such as metal oxides or carbides, are mixed together at more than 1300°C. Reaction conditions are relatively easy to achieve, but there are some drawbacks, which focus primarily on the inhomogeneity of the starting materials. In mixtures of two or more powders, complete conversion is limited by mass transport: initial reaction takes place at the edges of adjacent particles and, if reactant diffusion is blocked, areas of unreacted starting material are still present at the end of the process. Some of these issues can be overcome by ball-milling, reducing the particle size and increasing the sample surface area. However, extended heating or multiple treatments separated by successive sample milling steps may be required. Furthermore, it is often difficult to control particle morphology using solid state methods [60].

1.2.4.2 *Sol-Gel technique*

Sol-gel approaches are drawing widespread attention, considering the convenience and versatility of tuning the properties of BGs [15].

The fabrication of BGs using sol-gel technique was reported for the first time in 1991, but sol-gel science dates back over 150 years. Although in 1640 van Helmont discovered “water glass” by dissolving silicate materials in alkali and then precipitating silica gel under acidic conditions, true sol-gel experiments began only in 1846, when Ebelmen observed the formation of a transparent glass after the exposure to the atmosphere of a silane obtained from SiCl_4 and ethanol

and only in 1864 the term “sol–gel” was coined by Graham during his work on silica sols [27] [60][61][62].

The sol-gel method is a wet-chemistry process that leads to the production of an inorganic phase (composed by inorganic polymers or ceramics) from a solution through the transformation of liquid precursors initially to a sol and finally to gel, due to the polymerization reaction of a solution containing suitable precursors that are chosen in order to adapt the composition of the system to the final purpose [25][30][60][62].

A sol can be more generally defined as a colloidal suspension. The International Union of Pure and Applied Chemistry (IUPAC) define a colloidal system as a dispersion of one phase in another where, “the molecules or polymolecular particles dispersed in a medium have at least in one direction a dimension roughly between 1 nm and 1 mm” [60][63].

The gel state is, generally, defined as an inorganic non-fluid and highly interconnected tridimensional network characterized by the presence of sub-micrometric pores and polymeric continuous chains of micrometric length that extend through a secondary phase, which is usually a liquid phase [60][61][62].

According to the chosen precursors, sol-gel products can be obtained by [62][63][64]:

- i. gelation of a solution of colloidal powders;
- ii. hydrolysis and poly-condensation of alkoxide or nitrate precursors followed by hypercritical drying of the gel;
- iii. hydrolysis and polycondensation of alkoxide precursors followed by aging and drying under ambient atmosphere (this approach is the main one used for the production of biomedical bioactive sol-gel glasses).

In the sol-gel synthesis of biomedical glasses, precursors are mixed and react under liquid conditions in a controlled manner, following these main steps (as shown in Figure 1.1) [25][62]:

- (i) mix of the precursors (that leads to the formation of covalent linkages between the elements) and preparation of a sol, at room temperature;
- (ii) gelation of the sol, with progressive increase in sol viscosity;
- (iii) removal of the liquid phase

- a. aging,
- b. drying to form a dense ‘xerogel’ via collapse of the porous network or supercritical drying (thermal annealing) to form an aerogel;
- (iv) dehydration or stabilization;
- (v) densification.

Depending on the specific application, these stages can be extended, altered, or with the exception of solvation and gelation, removed entirely [61].

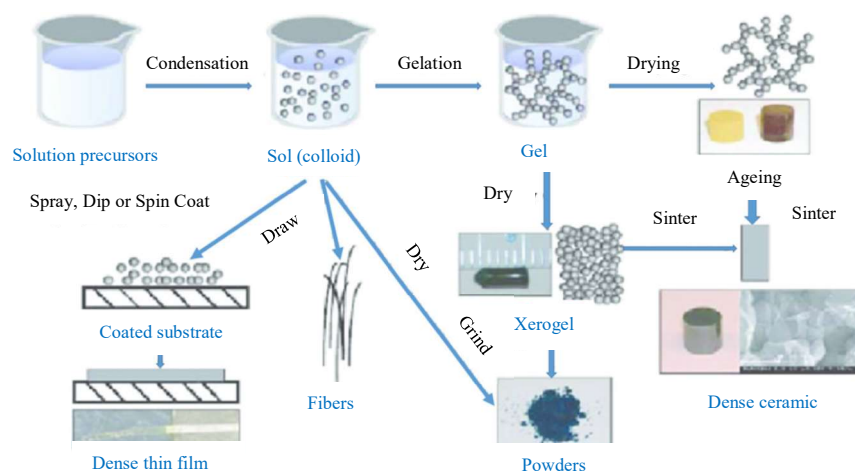


Figure 1.1: Sol-gel process

1.2.4.2.1 Reactions of sol-gel process

Sol-gel processes are driven by hydrolysis and polycondensation reactions, that generally occur simultaneously and compete against each other until complete homogenization of the solution under mild reaction conditions, since condensation begins before hydrolysis is completed [62][64].

The addition of water to the precursors leads to a hydrolysis reaction, during which the OR group is substituted by the OH as a consequence of a nucleophilic attack. This substitution is necessary to create reactive groups and then activate the process of sol formation at room temperature and ambient pressure [62]. In fact, after being hydrolysed, precursors can react with other precursors, both hydrolysed (condensation with formation of water) or not hydrolysed (condensation with formation of alcohols). In order to achieve dehydration, two HO– groups must take part in the formation of an Si–O–Si bond, whereas

dealcoholation results from the direct transfer of proton to the leaving group on a neighboring substrate. Thus, polycondensation takes place, leading to the formation of a solid 3D network, which corresponds at macroscopic level with the gelification [62][64]. During ageing, the polymerization of non-reacted Si-OR and Si-OH groups occurs and, as a consequence, there is a decrease in the porosity of the material and an increase in strength of gel thanks to the increased connection and densification of the matrix [62][64]; moreover, the densification of the network results in expulsion of solvent [62]. The residual liquid phase is removed from pores during the drying step.

To give a more detailed explanation of sol-gel reactions, the example of silica gel is illustrated. In case of silica gels, the following three reactions take place [62][64]:

- 1) $n \text{Si(OR)}_4 + 4n \text{H}_2\text{O} \rightarrow n \text{Si(OH)}_4 + 4n \text{ROH}$
- 2) $n \text{Si(OR)}_4 + n \text{Si(OH)}_4 \rightarrow 2n \text{SiO}_2 + 4n \text{ROH}$
- 3) $n \text{Si(OH)}_4 \rightarrow n \text{SiO}_2 + 2n \text{H}_2\text{O}$.

The sol-gel reactions can be summarized as follows: $n \text{Si(OR)}_4 + 4n \text{H}_2\text{O} \rightarrow n \text{SiO}_2 + 2n \text{H}_2\text{O}$.

1.2.4.2.2 Parameters of sol-gel process

Hydrolysis and polycondensation processes can be carefully tuned, for example through acid or base catalysis, to form very different structures [60], such as 3D gelled structures in case of acid conditions or individual particles in case of basic conditions if using silicon alkoxides as precursors [25]. The structure and size of the resulting gel is significantly different depending on the catalyst and this is due to the relative rates of the hydrolysis and condensation reactions [60][65].

Factors that determine the kinetic constant of the reactions are reported below (from the most relevant to the less influential) [62][64]:

- type and concentration of precursors;
- in case of alkoxides precursors, ratio 'r' of water to alkoxide, which is the H₂O:Si ratio in case of TEOS;
- type and concentration of solvent;

- type and concentration of the electrolyte (R-group) and, consequently, pH value;
- presence, type, concentration and force of catalyst;
- ionic force of electrolytes in solution;
- temperature;
- pressure.

In the final part of this paragraph, the effect of the main factors is explained, focusing on silicate glasses and alkoxides precursors. In fact, most of the BGs produced through sol-gel method are silicate glasses and the most used forming agents in sol-gel processes are tetra-functional alkoxide monomers where R of the formula $\text{Si}(\text{OR})_n$, is an alkyl group. Usually alkoxide-based sol-gel chemistry involves early transition group metals (e.g. Ti, Zr) or early p-block elements (e.g. Al, Si). Thus, the formation of the sol occurs through hydrolysis and partial condensation of metal alkoxide precursors that leads to the formation of metal-oxo-metal or metal-hydroxy-metal bonds [60]. Therefore the glass building blocks are the silicate tetrahedron and metallic ions [25]. The synthesis of specific silicate bioactive glasses by the sol-gel technique at low temperatures using metal alkoxides as precursors was shown in 1991 by Li et al. [13].

Many experimental studies show that high value of 'r' promote hydrolysis (which, in this case, occurs before last stages of condensation are reached), but if this value is high and constant during the reactions, the concentration of silicates decreases and, consequently, also the rate of hydrolysis and condensation decrease, leading to an increase of gelification time.

The sol-gel chemistry of silica is typically driven by either acid or base catalysts as the neutral reaction is very slow [64]. Both hydrolysis and condensation can be catalysed to lower their activation energy. Acid or basic condition are established according to the isoelectric point of silicon ($\text{pH} = 2.5$): if $\text{pH} < 2.5$ (situation that occurs when, for instance, one of the following catalysts is used: HF, HCl, HNO_3 , H_2SO_4), the catalysis is acid; if $\text{pH} > 2.5$ (when NH_4OH or HOAc is used), the catalysis is basic [62].

Reaction rates and colloidal stability in systems are directly related to the concentration and strength of the acid or the basis used, depending on solution pH

(therefore, from this point of view, both temperature and solvents used for the synthesis play a secondary role in the determination of the reaction kinetics): a decrease in pH induces protonation of leaving groups and promotes hydrolysis (therefore reducing the stability of the ligand in question), whereas an increase in pH induces deprotonation of -OH groups and promotes condensation [61][62]. Therefore, in acid conditions the rate of hydrolysis is more rapid than that of condensation, whereas condensation is faster if compared to hydrolysis in neutral or basic conditions (ranging from pH 7 to pH 9) [61]. However, OH⁻ is a highly efficient nucleophilic species and electron transfer from -OH groups can be facilitated by H⁺ in the immediate environment [61].

In conclusion, acid conditions allow formation of weakly branched sol and, after gelification process, weakly crosslinked linear polymers [63]; so, in this conditions it is possible to obtain mesoporous exagonal well-ordered structures [61]. On the other hand, basic conditions and high 'r' value lead to the formation of a very highly packed particulate sol and later to a gel-like structure, often without the formation of any mesopores [61]. In particular, hydrolysis of silicon alkoxide at appropriate pH with basic catalysts such as NH₃ enables to synthesize monodisperse highly purified silica particles [66]. This difference in cluster formation is due to the solubility of resultant metal oxides in reaction medium. The solubility of the silicon oxide is more in alkaline medium which favors the inter-linking of silica clusters than acidic medium [63].

1.2.4.2.3 Advantages of sol-gel process

Mixing precursors at molecular level, sol-gel method offers many advantages, such as [30][60][61]:

- ease of fabrication, including the possibility to produce complex inorganic materials such as ternary and quaternary oxides;
- low-temperature processing;
- possibility of produce highly homogeneous and chemically pure materials;
- precise microstructural and chemical control that leads to produce BGs with tunable properties.

Moreover, in the sol–gel process, a gel can be formed in different ways and, sometimes, the same precursors can result in very different structures with only small changes in conditions; for example, by simply changing the pH of the solvent, BGs with different morphologies can be achieved [25]. Therefore, it is easy to shape BGs to different morphologies, such as massive materials (such as 3D porous scaffolds), powders, micro- and nanoparticles, films, fibers or coatings [25][60][61].

Thanks to low processing temperatures, it is also possible to add biomolecules and polymers during the synthesis process, without causing their denaturation or decomposition [25].

The sol–gel derived glasses provide:

- higher pore volume and specific surface area (two orders of magnitude higher than the melt-derived ones), that lead to better bonding to living tissue, when use in TE implants, and allow to use them as carrier of absorbed drugs;
- good degree of biocompatibility, resulting in a good cellular response;
- higher bioactivity and higher degradation rate, with higher SiO₂ limits, beyond which the powders lose their bioactive properties (up to 90% of SiO₂ instead of 60% required in Bioglass): they resorb more quickly than melt derived glasses of similar composition, but also reducing the number of components gel glasses maintain their bioactivity [34], for example the simplified binary SiO₂–CaO system obtained by the sol–gel method can be as bioactive as the quaternary system of 45S5 Bioglass;
- an external surface that is rich of Si-OH groups, because the low elaboration temperature does not promote oxolation reactions, resulting in a lower connectivity of sol-gel glasses compared to melt-quenched ones. The presence of these superficial active sites allow easy functionalization by suitable biomolecules [25]. It appears that sol–gel methods hold the potential to apply an ever-increasing range of glass-based bioactive coating to materials, which have previously remained incompatible with alternative coating techniques [61][67].

1.2.4.2.4 Fabrication of bioactive glass nanoparticles

Monodispersed spherical silicate nanoparticles (SiO₂ NPs), with diameter size ranging from 500 nm to 2 μm, can be produced through a base-catalyzed sol-gel routine, carried out at room temperature and higher pH (~10), using tetraethyl orthosilicate (TEOS) as silicate precursor, water and/or ethanol as solvents and ammonia [25][68]. This method was developed by Stöber et al. in 1968 and, in fact, it is called the Stöber method.

The classical, Stöber process can be modified in order to introduce other metal ions, such as Ca²⁺ and PO₄³⁻ ions, into the silica network [30]. Metal ion precursors can be added during the hydrolysis and condensation of TEOS or after the formation of SiO₂ NPs [25]. The addition of these metal ion precursors impacts on the surface charge of the neat SiO₂ NPs and can cause nanoparticle aggregation or disturb the further growth of nanoparticles [25]. Therefore, the interactions between metal ion precursors and the colloidal SiO₂ NPs must be carefully controlled, controlling the addition of the metal ion precursors, in order to achieve monodispersed spherical BGN, avoiding irregular shapes, inhomogeneity in size and aggregation, typical problems that can occur after these syntheses [25][34][60].

1.3 Electrospinning

Electrostatic spinning or electrospinning (ES) technique is a one of the major method for the fabrication of micro- and nanofibrous mats [69]. Because of the inherently high aspect ratio and specific surface area, electrospun mats are potentially useful for numerous applications [59][70][71]. A large fraction of these applications is related to the biomedical field, e.g. tissue engineering (TE) scaffolds for drug delivery, vascular/cartilage/nerve/skin/bone bioengineering, and wound healing [6][70][72].

Electrospinning appeared for the first time in the literature more than a century ago. In 1902, Cooley [73] and Morton [74], separately, patented methods and apparatuses for electrically dispersing fluids, a concept later known as

electrospinning. However, it was not until the 1990s that electrospun polymer nanofibers became a topic of great research interest [69][75][76].

1.3.1 Advantages

The advantages of using electrospinning to fabricate fiber mats are here briefly summarized [17][20][70][71][75][77][78][79][80]:

1. It allows to produce extremely thin nonwoven continuous fibers with fibrillar structure and diameters in the range of sub micrometers down to nanometers (typically hundreds of nanometers in diameter). This ability is very important in TE applications, because such small-size fibers could physically mimic the native structure and function of the extracellular matrix (ECM) of a great variety of native tissues and organs, which are deposited and characterized by well-organized hierarchical fibrous structures realigning from nanometer to millimeter scale.
2. It allows controlling morphology, porosity and composition of the fibers, using relatively unsophisticated equipment. Therefore, electrospun scaffolds can be easily tailored in accordance with the purpose of their use.
3. It is very versatile, allowing to fabricate scaffolds from a variety of viscoelastic polymers, blends of different polymers, and inorganic materials.
4. Electrospun scaffolds provide highly porous microstructure with interconnected pores, adjustable pore size distribution and extremely large surface-area-to-volume ratio. The highly interconnected porous structure of nanofibrous scaffolds (and the consequent high surface-area-to-volume ratio) provides an appropriate substrate for cell attachment and nutrient transport and, therefore, is conducive to tissue growth.
5. It permits the easy incorporation of functional components (drugs, living cells, genes, enzymes, etc.), making electrospun scaffolds suitable candidates for tissue engineering.
6. It is simple, cost-effective and potential for production scale-up.

1.3.2 Mechanismus and apparatus

The basic electrospinning setup mainly comprised of four main parts: a glass syringe containing a polymer solution, a metallic needle, an adjustable high voltage power and a grounded or negatively charged collector (as shown in Figure 1.2) [77][80][81].

The principle at the basis of the electrospinning process is “electrostatic attraction” of charges, due to the application of a high voltage between two electrodes of opposite polarity, one of them located at the tip of a needle containing a polymer solution (or suspension or melt) and the second one on the collector, serving as a counterelectrode [20][76][81]. The solution has its own surface tension inside the syringe which can be charged outside by applying a high voltage power supply at the tip of the needle [76].

In the electrospinning technique, in order to form the jet, the conventional mechanical forces are replaced with electric forces; thus, this process is also known as electrohydrodynamic jetting [46].

Generally, two possible instrument configurations, such as vertical and horizontal, are in practice. In vertical type, the electric force is not the only one which acts on the polymeric jet, but fiber formation is also influenced by gravitational pull, whereas in the horizontal type the gravitational forces does not interfere in the process because the acceleration of the fiber formation is up to 600 m/s^2 , which is close to two orders of magnitude greater than the acceleration of gravitational forces. Because of this, it is possible to form fibers from top-down, bottom up or other types of arrangements [69].

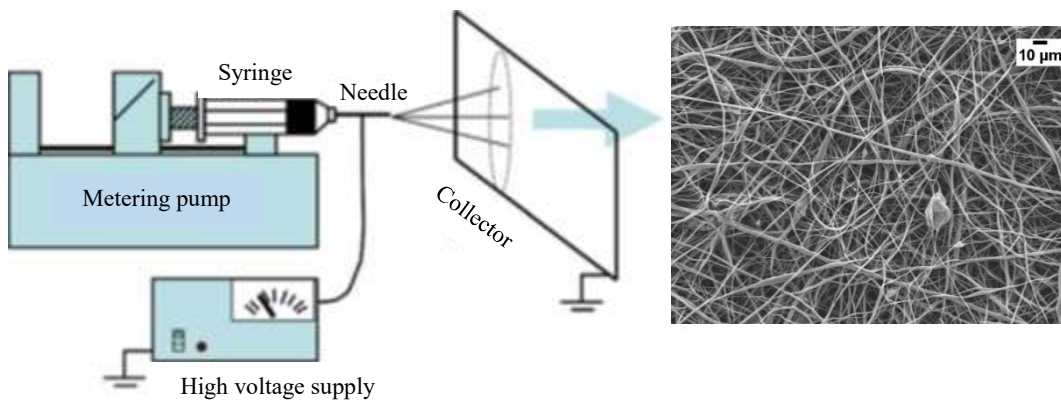


Figure 1.2: Electrospinning technique

There are two different types of electrospinning:

- solution electrospinning, in which a viscoelastic polymer is dissolved in an appropriate solvent;
- melt electrospinning, in which the polymer is melted using high temperature (the direct write or direct writing electrospinning is a type of melt electrospinning).

In both cases, a continuous filament is drawn between the collector and the needle tip through a spinneret (the needle) due to the existence of a high potential difference and later deposited on a conductive substrate (the collector). According to Reneker and Chun, this filamentous jet can be divided in four regions: the base, the jet, the splay and the collection, as follows [17][19][20][73][80][82]:

1. After the activation of the pump, the polymer solution or melt drops from the end of the capillary tube. At the beginning of the process, the drop is held at a needle tip by surface tension, but the application of an electric field causes the induction of charge within the polymer. Consequently, the coupling of the surface charge and the external electric field create a charge repulsion within the solution, resulting in a tangential stress, that cause a deformation of the droplet shape, which is altered from a circular to a conical one, called a Taylor cone (base region).
2. Increasing the electric field, when the applied electric force is able to overcome the surface tension forces of the polymer solution or melt, a jet originates from the Taylor cone and is ejected from the tip of the capillary tube. A stable charge jet can be formed only when the polymer solution has sufficient cohesive force.
3. This polymeric jet moves in the direction of the external electric field and elongates according to external and internal electrical forces: it travels in a direct route for few seconds, known as stable zone; after passing the stable zone, the electric forces accelerate and stretch the polymer jet and, consequently, the jet becomes thinner and unstable and undergoes a series of electrically driven bending and whipping instabilities, which are caused by mutually repulsive forces resulting from the electric charges of the jets

and the surface tension. The diameter of the jet decreases as its length increases, because of the elongation and solvent evaporation.

4. Finally, the jet gets deposited on the collector in the form of fibers. In the solution electrospinning, during the time of flight the solvent evaporates from the charged solution, so that solid fibers can be collected on the grounded target.

1.3.3 Parameters

Even if the set-up of the process is quite simple, the electrospinning process and the features of the obtained electrospun mats, such as fiber dimension and surface porosity, are affected by several parameters, making the process not easy as it could appear. Moreover these parameters need to be optimized in order to obtain the desired composite with a controlled fiber morphology and this optimization process is cumbersome and time consuming when compared to solvent casting or other fabrication techniques [17][83]. In the end, reproducibility is a well-known issue in research involving electrospun materials and one of the main obstacles preventing this processing technique to prevail into the industry. Therefore, in order to produce uniform and reproducible fibers, investigations on parameters involved in electrospinning process have been performed [84].

The processing parameters could be grouped in three categories [17][20][77]:

a) Solution parameters:

Before illustrating the different solution parameters and their effects, it is important to underline that the effects of the solution properties cannot easily isolate since the variation of just one solution parameter can generally affect the others (for example, changing the conductivity can also change the viscosity) [77].

a. **Solution viscosity**

The viscosity is one of the biggest determiners of fiber size and morphology. Solutions with optimum viscosity guarantee only formation of fibers with diameters in the micro to nano scale

dimensional range. On the other hand, solutions with both very low and very high viscosity lead to formation of beaded fibers [9].

As shown by numerous experimental results, an increase of the solution viscosity by increasing polymer concentration and/or adding glass nanoparticles, results in less defects, more uniformity and bigger diameter. This result is achieved because the jet stretching is opposed by viscous forces and surface tension, so that it is obvious that a higher viscosity causes a lower stretching rate and thicker fibers. Moreover, that increase in fiber diameter is correlated directly to a decrease in the surface area of electrospun mats. However, for solutions that were too viscous, the droplet dried out at the tip of the needle, preventing electrospinning process and consequently fiber formation.

b. Polymer concentration:

At low polymer concentrations, defects in the form of beads and droplets have been observed. Additionally, the presence of junctions and bundles have been seen, indicating that the fibers were still wet when reaching the collector.

c. Polymer molecular weight:

The influence of the molecular weight of the polymer is obviously related to the viscosity, surface tension and conductivity of the solution. Indeed, the higher the molecular weight, the higher the viscosity due to the higher number of the chain entanglements. Consequently, solution of polymers with high molecular weight result in thicker fibers. Hence, fibers with different diameter can be produced both by different or same polymers with different molecular weight.

Moreover, polymers with higher molecular weight are easier to electrospin since the numerous chain entanglements stabilize the polymeric jet.

d. Solvent:

The role of the solvent is extremely important because of its interaction with the polymer. Indeed, the solvent used has a significant influence on

the spinnability of the polymer solution, affecting polymer dissolution, solution surface tension and solvent evaporation rate:

- i. not all available solvents are able to completely dissolve the polymer, some of them only partially do it or cause the swelling of the polymer itself;
- ii. different solvents exert different surface tensions;
- iii. volatile solvents with high vapor pressures may begin to evaporate earlier, causing a decrease in jet diameter and velocity or an increase in superficial porosity and subsequently an increase in surface area [77].

Thus, the selection of a suitable solvent system is fundamental in order to improve the electrospinning ability of the solution [8][70][78].

e. **Surface tension:**

It depends on the solvent used. If surface tension is too high, the polymeric jet is unstable and generally fibers with defects (such as droplets and beads) are formed. Thus, reducing the surface tension of the solution without changing its concentration, it is possible to obtain smooth fibers [76].

f. **Solution conductivity:**

Conductivity of the solution plays a key role in fiber formation process. It depends on polymer, solvent and presence of salts. By adding salts such as NaCl, KCl and KBr, the solution conductivity can be increased; hence, the addition of bioactive glass nanoparticles leads to an increase in the conductivity. Generally, an increase in conductivity corresponds to an increase in charge density and, consequently, results in the formation of thinner fibers due to the decrease in total mass transported between the two electrodes (mass deposition rate) [9][85]. If solution conductivity is too low or too high, discontinuous fibers with defects are obtained. In case of high conductivity value, fibers show also irregular diameters, due to the high instability of polymeric jet.

g. **Charge density:**

Taylor cone formation is due to the accumulation of charge in the fluid and the resultant competition between surface tension and surface charge repulsion. Therefore, an increase in charge density in an electrospinning solution should influence the behavior of the fluid droplet: an increased charge density should result in a smaller radius of curvature of the tip of the Taylor cone, which in turn results in a concentration of electric stresses at the tip, a steeper cone, a narrower initial jet and a decrease in the mass deposition rate [85].

b) Processing parameters:

a. **Voltage:**

The electrical potential is also critical to the electrospinning process, because it must provide a suitable level of charge to the polymer solution. The applied voltage directly influences the available electric field which in turn influences the electrostatic forces that prevail on the surface tension of the polymer, causing the jet expulsion. A minimum voltage is required so that the polymer solution can be ejected from the tip of the Taylor cone. When the applied voltage is increased, the diameter of the fibers becomes smaller due to an increase in the jet length correlated with the stretching of the polymer solution caused by higher repulsive forces within the polymer jet. Anyway, a high electrical potential is not desired as it may lead to bead formation or defects in the nanofibers [8]. However, other researchers have reported an increase in fiber diameter at high voltage, because a greater quantity of polymeric solution is ejected. Therefore, there is a discrepancy trend in the experiments reported in literature, showing the ambiguity of the influence of the applied voltage on the fiber morphology.

b. **Flow rate:**

The value of the flow rate influences fiber formation, affecting fiber diameter distribution, size and initiating shape of the droplet, trajectory of the jet, maintenance of Taylor cone, areal density and nanofiber morphology, or even not allowing it [21]. Uniform beadless electrospun

nanofibers could be prepared via a critical flow rate that varies with the polymer system. In general, it was found that lower flow rates yielded fibers with smaller diameter, allowing complete solvent evaporation before the jet reaches the collector, whereas higher flow rates result in thicker fibers, because a higher amount of polymer solution is ejected in the same time interval. Moreover, increasing the flow rate could also lead to the formation of beads, ribbon-like defects, unspun droplet and pores: the larger volume of solution drawn from the needle tip needs a longer time to dry and the residual solvent might induce the fibers to merge together and make webs instead of fibers or could evaporate developing porosity. However, the formation of beads and ribbon-like structures with an increased flow rate was also attributed to the low stretching of the solution in the flight between the needle and metallic collector. In conclusion, lower flow rates are more desirable as the solvent will have sufficient time for evaporation.

c. **Working distance** (distance from the tip of the needle to collector):

This parameter influences mainly the solvent evaporation. In case of short distance, there is higher control on jet instability but the solvent has less time to evaporate and thick defective fibers might be formed. It is worth noticing that a minimum distance is necessary to guarantee fiber formation: if the working distance is lower than this minimum value, the solvent has no enough time to evaporate.

On the other hand, increasing the working distance, the diameter of the nanofiber decreased. Moreover, bigger distance leads also to discontinuity in the obtained fibers. Summarizing, a long working distance results in formation of discontinuous thin fibers.

In conclusion, by fixing other thing constant, variation in the distance between tip and collector can have a pronounced effect on the fibers morphology, because it depends on the deposition time, evaporation rate and whipping or instability interval, and in most cases a critical distance needs to be maintained to prepare smooth and uniform electrospun nanofibers.

c) Set-up parameters:

a. **Collector:**

The choice of a suitable collector depends mainly on the nature of application associated with the fabricated nanofibers. Different types of collector, such as drum collector, plate collector, parallel plate, disc collector etc, are available. The geometry and movements of the collector influence the arrangement and orientation of the fibers, which can be casually or orderly oriented [1][9]. For example, drum collectors are mostly used to get well aligned and nanosized fibers in laboratory level experiments. Moreover, in case of a moving collector, the collector velocity affects fiber morphology.

b. **Needle:**

Diameter and shape of the gauge changes the fibers diameter and morphology respectively. Increase in gauge size effects the fibers of micro scale diameter meanwhile change in the shape of gauge (sphere and elliptic) will affect the fibers morphology [9].

d) Environmental parameters:

Climate conditions have a strong influence on bead formation, fiber dimensions and surface textures.

a. **Temperature:**

It has been demonstrated that the surrounding temperature can leads to two different effect: the first one is related to the evaporation rate of the solvent, because at higher temperature the solvent evaporates faster; the second one is based on solution viscosity, which is lower at higher temperature due to the higher kinetic energy and resulting superior freedom of the polymer chains. Referring to the first mentioned effect, it has been observed that, increasing the temperature to the boiling point of the solvent used, pores were introduced on the nanofibers by the evaporation of the solvent molecules present on the fiber surface. If temperature was further increased, the solvent evaporation accelerated and a greater number of bigger pores was produced.

b. Humidity:

Several studies have been focused on the influence of relative humidity (RH) in the electrospinning process and nowadays it is confirmed that RH can affect the fiber morphology. The main effect is related to the dispersion of the charges in the water vapor molecules present in the surroundings atmosphere. While temperature changes have only a moderate effect on the resulting fibers, relative humidity cause changes in the nanofibers diameter by controlling the solidification process of the charged jet [18]. Setting the temperature at 23 °C, Liliana Liverani et al. [13] have tested different values of relative humidity, namely 25%, 30%, 40%, 50% and 60%, and have finally found out the optimized humidity value (40%) for processing neat PCL fibers. It was determined that in a quite wide range of RH values, between 30% and 50%, it was possible to obtain stability in terms of fiber distribution and process yield, whereas the lowest and highest RH values, namely 25% and 60%, introduced fiber branching and non-homogeneous fiber diameter distribution.

1.3.4 Use of benign solvents

Most of the solvents suitable for electrospinning are toxic and harmful and may cause adverse effects to cells if not removed completely and difficulty in controlling pore size and pore shape. Unfortunately, they are still used because of their better performance in the dissolution of polymer. Despite to this trend, to avoid the previous mentioned disadvantages of these solvents, the concept of “Green Electrospinning” has been developed: recently several research works have focused on the use of less toxic and harmful solvents for electrospinning, i.e. acetic acid, formic acid and acetone [20][86]. The use of benign solvents aims to avoid the presence of toxic solvent residuals inside the mats which could limit their applications in the biomedical field. Limiting the use of harsh solvents is also highly beneficial in terms of processing proteins, such as collagen and other sensitive biomolecules, preventing their denaturation. Moreover, using benign solvents also brings advantages in terms of lab worker safety and environmental

impact [2]. However, most of these harmful solvents are not directly suitable for electrospinning, requiring a longer and more accurate optimization of the process.

1.3.5 Addition of glass nanoparticles

One of the main challenges in preparing composite fibers containing nanoparticles is to achieve good dispersion of the individual nano-sized (primary) particles, which owing to their high surface area have a strong tendency to combine together forming strongly bonded aggregates, which may further unite to produce even larger structures, commonly named “agglomerates” [15][90]. Decreasing their size, the dispersion of nanoparticles becomes increasingly difficult and can thus pose a challenge [28].

Although the accepted definition of nanomaterials is that the material must have at least one dimension in the size range 1–100 nm, most of the reported BGN exhibit a size larger than 100 nm and they are actually in the submicron scale. Individual BGN smaller than 100 nm tend to agglomerate to larger clusters that are usually larger than 100 nm [24].

To form high quality and high performance composites, the particle agglomerates must be broken down during composite processing into primary particles (i.e., the smallest particulate pieces of the minor component existing in as-fabricated or as-received ceramic or glass powders), which must be sufficiently dispersed in the polymer matrix. Ideally, particles present in the composite should be in a dispersed state [8]. Characteristics of ceramic particles (i.e., particle morphology, size, etc.), interparticle attraction, particle surface treatment, and particle volume fraction in the composite can significantly affect particle dispersion and distribution in the composite [8]. Processing parameters, such as mixing mode and mixing time (stirring time), also affect the quality of composites produced [8][90].

2 Aim of work

The development of biomimetic materials mimicking the composition, structure, morphology, and bioactivity of natural tissues represents the main goal of tissue engineering. In this regard, the development of advanced composite nanofibrous scaffolds containing bioactive glasses able to enhance tissue regeneration is attracting significant research interest. In an effort to fabricate an innovative composite material, this master thesis project was focused on the fabrication and characterization of composite electrospun fibers containing bioactive glass particles incorporating boron and copper ions. For the preparation of these fibers, the following materials were used: poly(ϵ -caprolactone), benign solvents and sol-gel bioactive glasses.

3 Materials and methods

3.1 Materials

During this master thesis work the following materials were used:

- for the synthesis of the bioactive glasses
 - distilled water
 - ethanol (EtOH)
 - nitric acid (HNO₃) at 70%
 - tetraorthosilicate (TEOS) C₈H₂₀O₄Si at 99% (Sigma Aldrich)
 - triethyl phosphate (TEP) C₆H₁₅O₄P at 99% (Alfa Aesar)
 - calcium nitrate tetrahydrate Ca(NO₃)₂ · 4 H₂O
 - copper nitrate trihydrate Cu(NO₃)₂ · 3 H₂O (Fluka)
 - boric acid H₃BO₃ at 99% (Sigma Aldrich)
 - ammonia solution NH₄OH at 28-30% (Emsure)
- for the fabrication of the electrospun fibers
 - poly(ε-caprolactone) (PCL) with an average molar mass of 80 000 (Sigma Aldrich)
 - acetic acid at 98% (AA, VWR, Germany)
 - formic acid at 98% (AA, VWR, Germany)
 - bioactive glasses previously produced at the Department of Applied Science and Technology (DISAT) of Politecnico di Torino
 - pluronic F-127 (Sigma Aldrich, code P2443)
 - ethanol at 96% (EtOH, VWR, Germany)
- for the characterization of samples
 - SBF solution
 - PBS solution
 - gold and chromium for sputtering the samples before analysis with Field Emission Scanning Electronic Microscope (FE-SEM)
 - murine-derived stromal cells ST-2 (obtained from Leibniz-Institut DSMZ-Deutsche Sammlung von Mikroorganismen und Zellkulturen GmbH, Braunschweig, Germany)
 - trypsin (Sigma Aldrich, Munich, Germany)

- roswell Park Memorial Institute medium (RPMI 1640) (Gibco™, Thermo Fisher Scientific, Schwerte, Germany)
- WST-8 assay (Cell counting Kit-8, Sigma Aldrich, Munich, Germany)
- fixation solution containing 1,4-piperazinediethanesulfonic acid buffer, ethylene glycol tetraacetic acid, polyethylene glycol, paraformaldehyde, DPBS and sodium hydroxide (Sigma Aldrich, Munich, Germany);
- permeabilization buffer containing triton X, sucrose and PBS (Sigma Aldrich)
- rhodamine phalloidin (ThermoFisher Scientific, Schwerte, Germany)
- DAPI (ThermoFisher Scientific, Schwerte, Germany).

All materials were used as received without further purification.

3.2 Synthesis of the glasses

The first step of this work was the selection of suitable composition and synthesis route for the preparation of the bioactive glasses. Therefore, before starting any kind of experiments, a research in the literature about already experienced compositions and possible synthesis for bioactive glass nanoparticles was carried out, in order to synthesize bioactive glass particles with average size in the nanometric range and an innovative composition.

Silicate bioactive glasses, in particular in the ternary system $\text{SiO}_2\text{-CaO-P}_2\text{O}_5$, are widely investigated [25]. Therefore, in agreement with literature studies, the glass 77S was selected as starting composition and used as control. In an effort to confer angiogenic and antibacterial properties to the glasses, boron and copper were used as doping ions.

The selected compositions of the glasses are reported, as follows:

1. $\text{SiO}_2\text{-CaO-P}_2\text{O}_5$ (named S)

77 wt% SiO_2

14 wt% CaO

9 wt% P_2O_5

2. SiO₂-B₂O₃-CaO-P₂O₅ (named SB)
 - 62 wt% SiO₂
 - 15 wt% B₂O₃
 - 14 wt% CaO
 - 9 wt% P₂O₅
3. SiO₂-B₂O₃-CaO-P₂O₅-CuO (named SBCu)
 - 62 wt% SiO₂
 - 15 wt% B₂O₃
 - 9 wt% CaO
 - 9 wt% P₂O₅
 - 5 wt% CuO.

TEOS, TEP, calcium nitrate tetrahydrate, copper nitrate trihydrate and boric acid were used as precursors for silice, phosphors, calcium, copper and boron, respectively.

As TEOS is immiscible within water, a solvent (usually alcohol) is often added to the solution in order to avoid phase separation during hydrolysis and facilitate homogenization [62]; in this case ethyl alcohol was chosen.

In agreement with literature, the glasses were prepared through an acid/base co-catalyzed synthesis [3][87], following two different strategies [30], as shown in Figure 3.1. Both these synthesis methods differ from the original Stöber method, because there is an additional hydrolysis step of TEOS in acidic media (in particular in nitric acid) and the addition of concentrated ammonia solution (NH₄OH). Nitric acid (HNO₃) was used as hydrolysis catalyst, while the ammonia solution was added, in order to induce particle formation and decrease the gelation time (from several hours to several minutes), acting as a gelling agent and accelerating the condensation [65]. The first strategy involves the synthesis of silica nanoparticles in an acid media followed by pH increase thanks to addition of NH₄OH and adsorption of calcium, phosphate, boron and copper ions in a basic condition. The second one introduces calcium, phosphate, boron and copper ions along with the silica precursor prior to increase the pH in order to form gel and so the particles.

Initially, in both cases, a solution of 30 ml of EtOH, 7.2 ml of H₂O, 1.2 ml of HNO₃ 2M and 11.2 ml of TEOS was prepared and left under gentle and constant magnetic stirring for 1 h, in order to complete acid hydrolysis of TEOS.

At this point, the two synthesis strategies diverge: according to the first method (called synthesis 1), NH₄OH 2M was added to the initial solution (containing only the first precursors, in this case TEOS), which became a gel, whereas according to 2^o method (synthesis 2), NH₄OH 2M was added after the addition of all other precursors, so that gelification occurred only at the end of the process.

In both cases, NH₄OH 2M was added dropwise during vigorous magnetic stirring until a final pH of 8,3 – 9 was reached. Indeed, literature results have shown that the size of the bioactive glass particles could be controlled by adjusting the pH value of the sol using ammonia solution.

Each precursor was added at time interval of 30 min under gently magnetic stirring, following a fixed order. For S glasses, 11.20 ml TEOS, 0.84 ml TEP and 2.31 g Ca(NO₃)₂·4 H₂O. For SB glasses, 11.20 ml TEOS, 1.04 ml TEP, 2.87 g Ca(NO₃)₂·4 H₂O and 1.30 g H₃BO₃. For SBCu glasses, 11.20 ml TEOS, 1.04 ml TEP, 1.85 g Ca(NO₃)₂·4 H₂O, 0.74 g Cu(NO₃)₂·3 H₂O and 1.30 g H₃BO₃.

After addition of the last precursor (in case of synthesis 1) or of ammonia solution (in case of synthesis 2), the obtained gels were dried at 60 °C in a heater for 48 h and then calcinated at 700 °C in furnace for 2 h (annealing step). The thermal annealing is necessary to eliminate nitrate ions and to allow the diffusion of calcium/phosphorus/boron and copper ions inside the silica network.

Summarizing, six types of glasses with three different compositions and two methods of synthesis were prepared: S1, S2, SB1, SB2, SBCu1 and SBCu2, where 1 means “prepared using synthesis 1” and 2 “using synthesis 2”, as outlined in the following diagrams and shown in Figure 3.1.

Synthesis 1:

ethanol + H₂O + HNO₃ 2M

↓
add TEOS

↓
magnetic stirring for 1 h

↓
drop NH₄OH 2M

↓
formation of gel

↓
add TEP

↓
magnetic stirring for 30 min

↓
add Ca(NO₃)₂ · 4 H₂O

↓
magnetic stirring for 30 min

↓
add Cu(NO₃)₂ · 3 H₂O and magnetic stirring for other 30 min **ONLY if SBCu**

↓
add H₃BO₃ and magnetic stirring for 30 min **if SB and SBCu**

↓
dry at 60°C in heater (48 h)

↓
annealing a 700°C in furnace (2 h)

Synthesis 2:

ethanol + H₂O + HNO₃ 2M

↓
add TEOS

↓
magnetic stirring for 1 h

↓
add TEP

↓
magnetic stirring for 30 min

↓
add Ca(NO₃)₂ · 4 H₂O

↓
magnetic stirring for 30 min

↓
add Cu(NO₃)₂ · 3 H₂O and magnetic stirring for other 30 min **ONLY if SBCu**

↓
add H₃BO₃ and magnetic stirring for 30 min **if SB and SBCu**

↓
drop NH₄OH 2M

↓
formation of gel

↓
dry at 60°C in heater (48 h)

↓
annealing at 700°C in furnace (2 h).

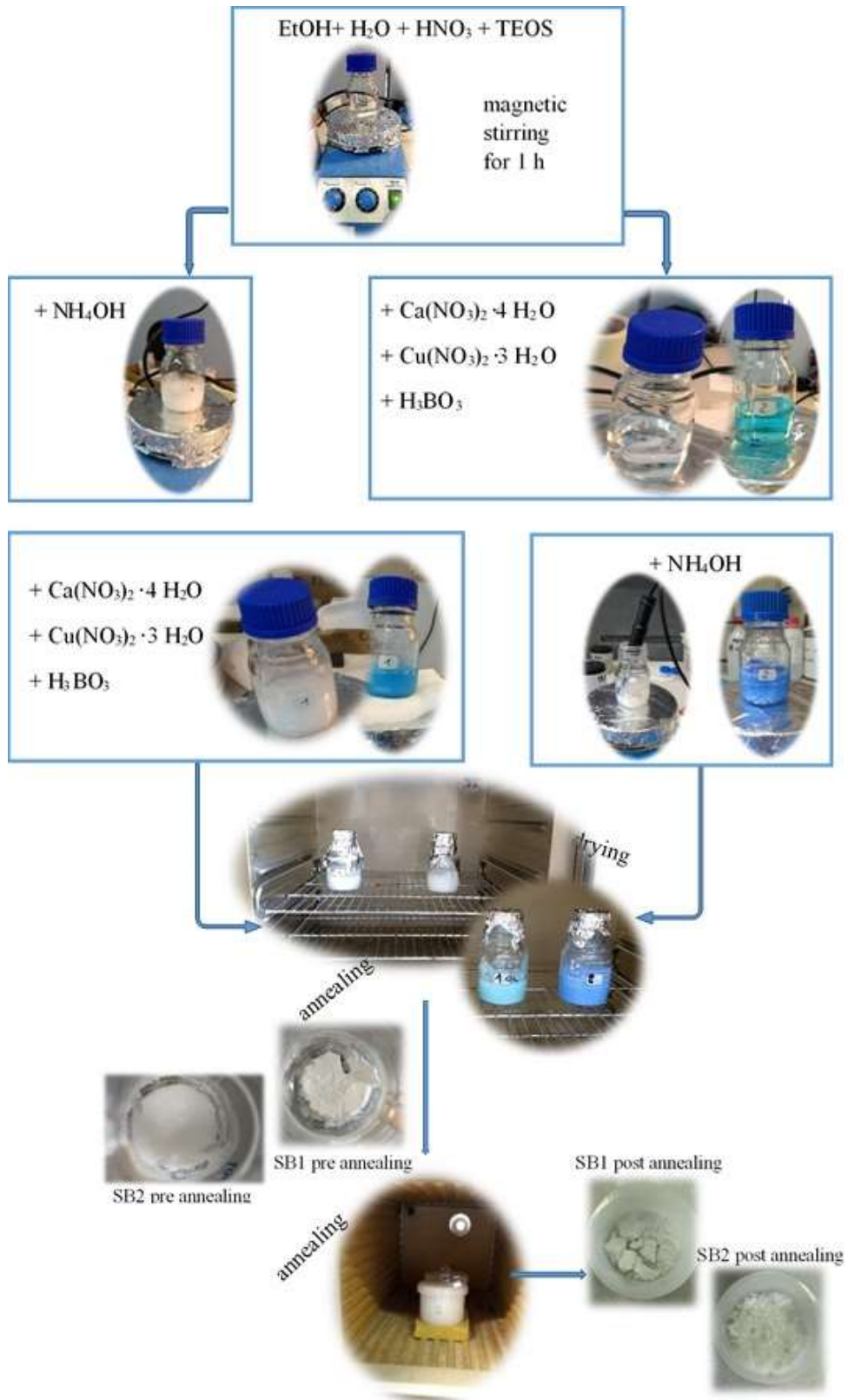


Figure 3.1: Schematic representation of sol-gel methods

Each synthesis was redone several times in order to produce around 11 g of each glass (as reported in Table 1).

Table 1: Total amounts of synthesized glasses

| Glasses [g] | |
|-------------|--------|
| S1 | 11.1 g |
| S2 | 11.8 g |
| SB1 | 11.4 g |
| SB2 | 11.3 g |
| SBCu1 | 11.1 g |
| SBCu2 | 11.8 g |

3.3 Characterization of the glasses

3.3.1 Morphological characterization

The morphology of glasses was observed using the Field Emission Scanning Electron Microscopy (FESEM) technique. The microscope FE-SEM Gemini SUPRATM 40 (Zeiss, Germany) was used (see Figure 3.2). The samples were prepared attaching a double-side carbon tape on a specific holder (aluminium stub) and putting the glass powders on the upper side of this tape (as shown in Figure 3.2), then they were sputtered with chromium.

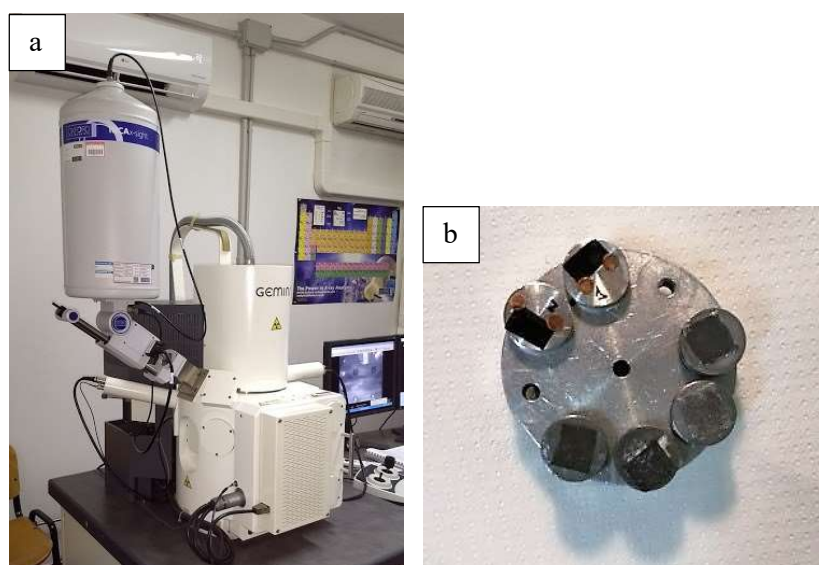


Figure 3.2: FESEM Gemini (a) and samples (b)

3.3.2 Compositional characterization

The glasses were characterized through the energy dispersive spectroscopy (EDS) using the same microscope and the same samples used for morphology assessment. An accelerating voltage of 20 kV was used.

3.3.3 X-ray diffraction analysis

X-ray diffraction (XRD) was used to verify the glasses structures. These tests were performed using the Bragg Brentano camera geometry and the Cu-K α incident radiation (source voltage and current set at 40 kV and 30 mA, incident wavelength $\lambda = 1.5405 \text{ \AA}$, step size $\Delta(2\theta) = 0.02^\circ$, fixed counting time of 1 s per step), $2\theta = 10^\circ$ to 70° .

3.3.4 BET analysis

Through the method developed by Brunauer, Emmett, Teller (BET method), it is possible to determine the specific surface area and the pore volume and pore surface distributions in the glasses [88]. The basic principle of this method is the physical adsorption of gases onto solid surfaces [89]. The N₂ adsorption and desorption measurements were performed using the analyzer shown in Figure 3.3. Prior to the analysis, the glass samples were degassed under vacuum conditions.



Figure 3.3: BET analyser

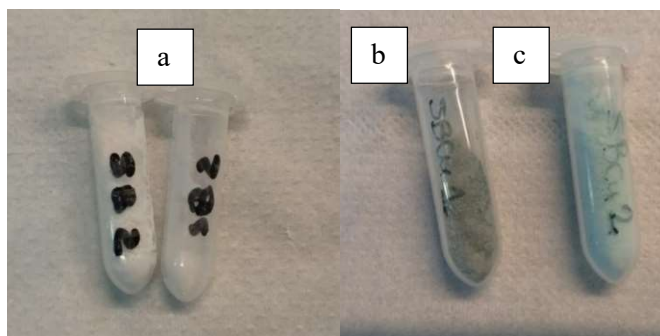


Figure 3.4: Example of samples for BET analysis:
 a) SB2 glass powders b) SBCu1 glass powders c) SBCu2 glass powders

3.3.5 Acellular bioactivity test

In order to examine *in vitro* their ability to mineralize, glasses were soaked in a solution which mimicks the human plasma. This solution, called simulated biologic fluid (SBF) is acellular aqueous solution, buffered at physiological pH, with an ionic composition and concentration similar to those of the inorganic part of human plasma. The SBF solution was prepared according to Kokubo protocol [90], by dissolving NaCl, KCl, $K_2HPO_4 \cdot 3H_2O$, $MgCl_2 \cdot 6H_2O$, $CaCl_2$, and Na_2SO_4 into distilled water and buffering at pH 7.4 with tris (hydroxymethyl) amminomethane $(HOCH_2)_3CNH_2$ (TRIS) and hydrochloric acid (HCl).

The protocol used for the preparation of 1 liter of SBF solution is briefly reported below:

- 700 ml of distilled water was poured in a plastic bottle and preheated in an incubator in order to optimize the time necessary to reach the temperature of $36.5 \pm 1.5^\circ C$;
- a pH-meter (Crison) was used to check temperature to be be sure that it is included in the range between 36-37 °C before adding reagents (shown in Figure 3.5):
 1. 8.035 g of NaCl at $\geq 99\%$
 2. 0.355 g of $NaHCO_3$ at $\geq 99.5\%$;
 3. 0.225 g of KCl at $\geq 99\%$;
 4. 0.231 of $K_2HPO_4 \cdot H_2O$ at 99.0%
 5. 0.311 g of $MgCl_2 \cdot 6H_2O$ at 99.99%
 6. 39 ml of 1M HCl
 7. 0.292 g of $CaCl_2 \cdot 2H_2O$ at 96.0%

8. 0.072 g of Na₂SO₄ at ≥99%;

- if the solution has smaller volume than 900 ml, water has to be added in order to reach that volume;
- if pH value is around 2.0±1.0, carefully keeping temperature at 36.5±1.5°C, some TRIS was slowly added until the pH of the solution reached 7.45±0.01;
- when this pH value was reached, 1M HCl was added dropwise in order to reduce the pH to 7.42±0.01 (it is important to notice that the minimum possible pH value is 7.40±0.01);
- when a pH value between 7.40±0.01 and 7.42±0.01 was reached, TRIS was added again until the pH was 7.45±0.01;
- at this point, 1M HCl was dropped again in the solution in order to lower the pH value and so on, continuing to add TRIS and 1M HCl until all TRIS (6.118 g at ≥99.8% purchased from Sigma Aldrich) was completely dissolved;
- if necessary, the pH could be adjusted at 7.40±0.01 at 36.5±0.1°C by adding 1M HCl;
- 100 ml of de-ionized water was added in order to reach a volume of 1 l.
- the prepared SBF solution was stored in the fridge.



Figure 3.5: Chemical reagents for preparation of SBF solution

The ratio between glass powders and SBF solution for samples soaking was 1:1, so 100 mg of glass were soaked in 100 ml of SBF.

The soaking periods were 1, 3, 7, and 14 days, without renovation of SBF solution along the assays. To reproduce the conditions of the living organisms, making them as close as possible to that surrounding the glass when implanted in animals or humans, the samples were kept in an orbital shaker with temperature fixed at

37 °C and shaking movement rate at 1000 rpm (as shown in Figure 3.6). After being soaked, the glass powders were removed from SBF solution and rinsed with deionized water as described below. As much as possible SBF solution was took away, deionized H₂O was added and powders+H₂O were poured in an eppendorf and centrifugated at 5000 rpm for 10 minutes. Finally, after centrifugation, water was removed and glass powders were dried in an incubator at 37 °C.

The *in vitro* bioactivity was evaluated through pH measurements, SEM-EDS and XRD analysis. The pH variations were monitored throughout the bioactivity assay, measuring the pH after 1, 3, 5, 7, 10, 12 and 14 days, using the same pH-meter used for preparation the solution. After immersion, the morphological changes on the surface were observed by SEM and XRD, whereas the chemical changes by EDS.



Figure 3.6: Glass samples for bioactivity test

3.4 Preparation of the solution for electrospinning

Considering the final aim of this project, the new concept of “Benign electrospinning” was adopted and benign solvents were used for preparing the electrospinning solution.

Moreover, due to the novelty of the combination of these glasses with PCL matrix, it was necessary to optimize the protocol for the glass addition. Different solvents and methods for addition of the glasses were tried. The first solvent choice was a mixture of formic acid (FA) and acetic acid (AA). Indeed, the use of the mixture of AA and FA for the successful electrospinning of poly(ϵ -caprolactone) (PCL) has already been reported by Liliana Liverani et al. [20]. According to these previous literature results, with the system PCL/AA/FA using 20 kV, 11 cm as working distance and a flow rate of 0.67 ml/h, it is possible to

obtain nanofibres with the typical continuous fibrous structure. So, because of the average size (50 nm) of the glass nanoparticles prepared at Politecnico di Torino, the system PCL/AA/FA was initially used. In details, PCL was dissolved at 15 w/v% in a mixture of AA and FA and stirred on a magnetic stirring plate at 100 rpm, until a transparent solution was obtained. In a second approach, already used in previous experimental works [91][18], PCL was added at 20 w/v% just in acetic acid, mixing overnight at 30°C until the solution became clear. Before use, this second solution was ultrasonicated for 1 h to ensure homogeneity. When the polymer solution was ready, glass powders were added, as shown in Figure 3.7.

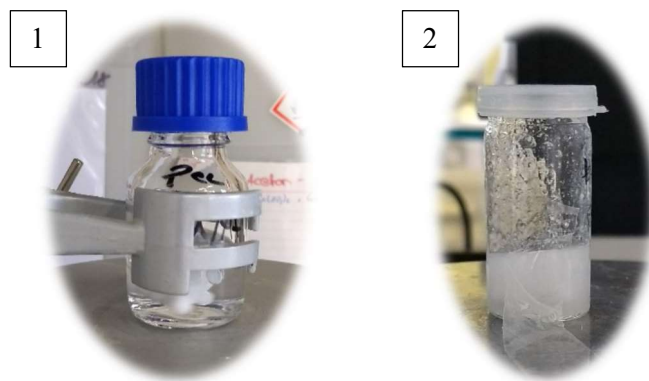


*Figure 3.7: Electrospinning solution preparation
1) PCL solution 2) addition of glass nanoparticles*

Different glass concentrations were used to investigate the electrospinnability of the glass/polymer dispersion and the bioactivity of the composite fibers. Considering the aggregation of the glass nanoparticles, in agreement with previous works [31], an initial glass concentration of 5%, related to polymer amount, was chosen and progressively increased up to 30%.

3.5 Electrospinning process

The electrospinning setup (Starter Kit 40 KV Web, Linari srl, Italy) used in this master thesis work is shown in Figure 3.8. The positive electrode of the high-voltage power supply was clamped directly to a needle, whereas the negative electrode was connected to a flat collector plate, which was wrapped with aluminum foil acting as the conducting material which collects the fibers.

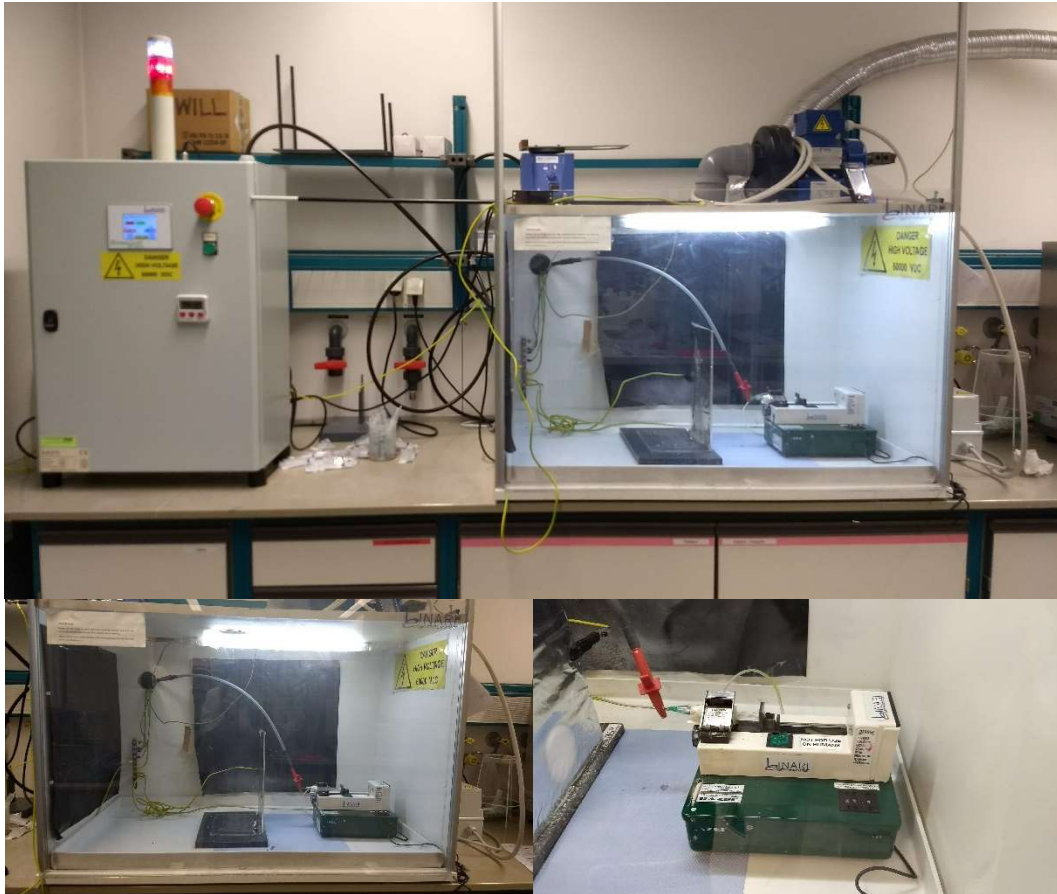


Figure 3.8: Electrospinning set-up

A BD plastic syringe of 3 ml with a cross-section of $0.589 \text{ sq} \cdot \text{cm}$ was used. As nozzle tip for the syringe were used two different types of needles, in particular two single-used cannulas with a diameter of 18 G x 7/8" and 21, respectively.

The syringe was filled with the solution and placed on the syringe pump.

The electrospinning solution was delivered via the syringe pump for controlling the mass flow rate during the electrospinning process. In particular, the pump used is the BSP-99M Razel and required the selection of the number selector switch, in order to set the desired flow rate according to the equation 2.1 (available in the operating manual of the instrument):

$$\text{Flow rate} = 0.23446 \cdot n^\circ \text{ of selector rate} \cdot \text{syringe cross section} \quad (2.1)$$

where

- the flow rate is expressed in cc/hr
- the number of selector rate is expressed in cm/hr
- the syringe cross section is expressed in sq.cm.

Adapting the electrospinning process conditions to the different kind of solvents and glasses and, consequently, to the different solutions, various combinations of process parameters (applied voltage, flow rate and working distance) were tried, in order to optimize the fabrication of the composite fibers. Flowrate for each solution was selected according to the behavior of the first solution drop coming out from the needle. The distance and applied voltage chosen were selected according to the previous work of the group of the department of Biomaterials of the University FAU on the electrospinning of PCL with benign solvents [20][91], but, if necessary, they were changed or optimized, after looking the glass distribution and fibers morphology with the use of the scanning electron microscope.

All electrospinning experiments were carried out at room temperature in air. Environmental parameters, such as temperature (T) and relative humidity (RH) were checked, but it was not possible to control them.

3.6 Characterization of the fibers

3.6.1 Morphological characterization

The morphology and diameter of the electrospun fibers were observed and determined with the use of a scanning electron microscope (FE-SEM Auriga, Carl-Zeiss, Germany, at University Friedrich-Alexander of Erlangen-Nürnberg; FE-SEM Jeol JCH-6000 plus at Politecnico di Torino). To carry out SEM analysis, a small section of the fibers was carefully sectioned and mounted onto a SEM holder (on which a carbon tape was previously fixed), as shown in Figure 3.9.

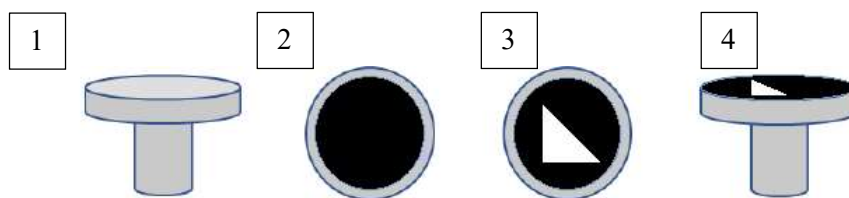


Figure 3.9: Preparation of fiber samples for SEM (and EDS) analysis

Before SEM analysis, the samples were sputtered with gold or with chromium at Politecnico di Torino (Figure 3.10).

Fiber average diameters were calculated by using the software ImageJ analysis software (NIH, USA) on SEM micrographs.

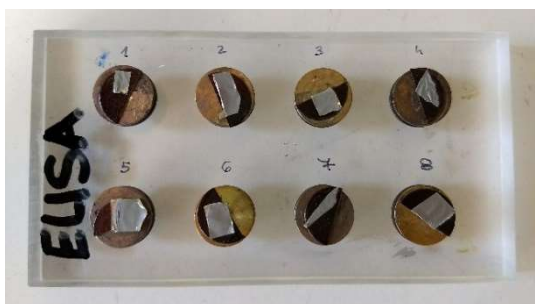


Figure 3.10: Example of fiber samples for SEM analysis

3.6.2 Compositional characterization

PCL and composite membranes were characterized by Energy dispersive spectroscopy (EDS), in order to evaluate glass incorporation and glass distribution inside the PCL matrix.

3.6.3 FTIR analysis

PCL and composite membranes were characterized by Fourier Transform Infrared (FTIR) spectroscopy, in order to obtain the spectra of the investigated samples. The FTIR spectrometer (Shimadzu IRAffinity-1S, Shimadzu Corp, Japan) was used in attenuated total reflectance (ATR), with a number of spectral scans selected of 40, a resolution of 40 cm^{-1} and a wavenumber range between 4000 and 400 cm^{-1} .

3.6.4 Mechanical characterization

Mechanical properties of electrospun fibrous mats were determined by a uniaxial tensile test, carried out with a uniaxial testing machine (INSTRON 5967) using a 50 N load cell under a cross-head speed of 10 mm/min at ambient conditions. All samples were prepared in the form of rectangular shape with dimensions of 3x10 mm from the electrospun fibrous membranes, cutting the mats e fixing them in a paper frame. The inner dimension of the frame is 10x10 mm while the external one is 20x20 mm (as shown in Figure 3.11). The thickness of the electrospun membranes was measured in 10 parts of each mat with a digital micrometer having a precision of $1\text{ }\mu\text{m}$ and then the measured values were averaged, but for

major accuracy this value was compared with the thickness of each sample, which was measured in triplicate with the same digital micrometer.

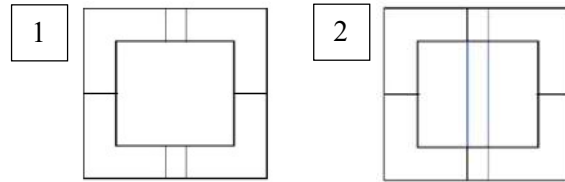


Figure 3.11: Preparation of sample for mechanical test

The main steps of this test can be summarized, as follows: firstly, the frame was fixed at the machine by means of two clamps, then the frame was cut with a scissor and, finally, the load was applied allowing the stretching of the sample until its failure (see Figure 3.12). Five samples were tested for each type of electrospun fibrous membranes.

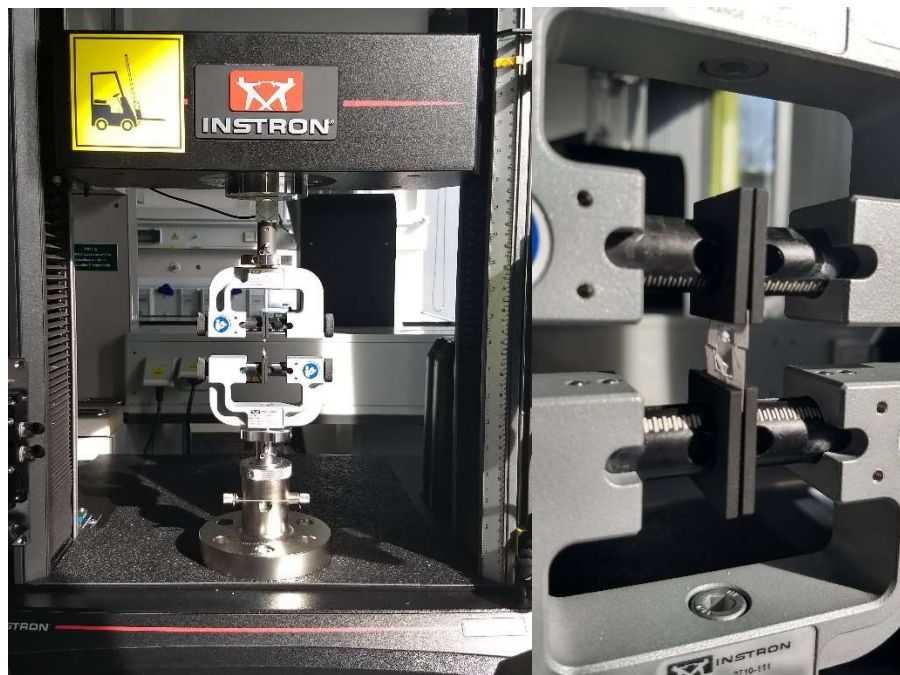


Figure 3.12: Mechanical test – a) testing machine b) detail of broken sample

3.6.5 Water Contact-Angle measurements

Wettability and hydrophilicity/hydrophobicity of the electrospun fibers was measured with the use of a contact angle measurement device, dropping 3 μ l of distilled water onto the fibrous membranes, as shown in Figure 3.13. In details, to carry out the contact angle measurements, a drop shape analyzer (Krüss DSA30,

Hamburg, Germany) was used. Indeed, the contact angle is the angle where a liquid–vapor interface meets a solid surface and indicates the wetting ability of the materials. A small piece of the fiber mat was cut and gently placed on a support. The contact angles of the mats were calculated automatically. At least three measurements were performed for each type of electrospun fibrous membranes, by evaluating the contact angle value for each second in a time frame of 10 seconds.



Figure 3.13: Contact angle measurements set-up

3.6.6 Acellular bioactivity test

The acellular bioactivity of the samples containing bioactive glasses was evaluated by immersing them into SBF solution, which was prepared following the Kokubo's protocol. Before immersion in SBF, the electrospun mats were fixed on cylindrical scaffold holders (called scaffoldex), which were printed using a 3D printer.

The protocol used for the preparation of 1 liter of SBF solution is analogous to the one used at Politecnico di Torino. In this case, the quantities and purities of the reagents used were: 8.0756 g of NaCl at 99.0%, 0.3532 g of NaHCO₃ at 100.0%, 0.2250 g of KCl at 99.5%, 0.2310 g of K₂HPO₄·H₂O at 99.0%, 0.3033 g of MgCl₂·6H₂O at 100.5%, 39 ml of 1M HCl, 0.3638 g of CaCl₂·2H₂O at 101.0%, 0.0716 g of Na₂SO₄ at 99.6% and 6.0568 g of TRIS at 100%.



Figure 3.14: Set-up for preparation of SBF solution

The volume of SBF solution employed for testing was calculated according to the following equation $V_s = S_{tot}/10$ where V_s denotes the volume of SBF in terms of ml and S_{tot} is the surface area in terms of square millimeter, calculated as $S_{tot} = 2S_i$ (S_i is the inner area of the holder, which represent the minimal useful area; that value was multiplied for 2 in order to consider both sides of the membrane).

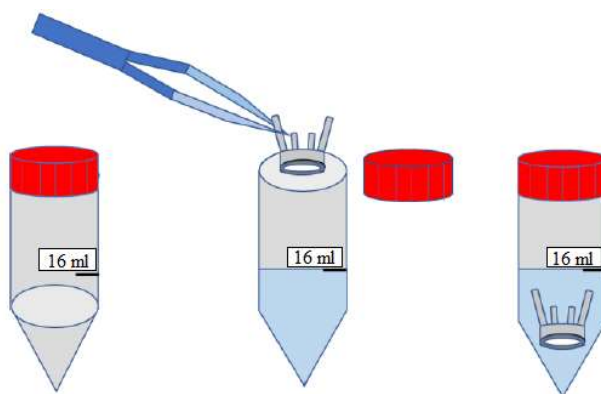


Figure 3.15: Preparation of sample for acellular bioactivity test

The samples were kept in a polypropylene falcon tube at 37 °C in an incubator on an oscillating tray for up to 21 days, without renewing the SBF solution. A falcon tube containing SBF solution was used as a control, in order to control over time the stability of the testing solution. After immersion in SBF, the samples were analyzed using SEM-EDS and FTIR. Before carrying out these analyses, the samples were gently rinsed three times with deionized water and dried under fumehood. The pH in the SBF solution was also investigated for each time point.

3.6.7 Degradation test

For evaluating the possible morphological modifications and degradation of the fabricated composites due to hydrolysis reaction, the electrospun mats were immersed in a phosphate buffered saline solution (PBS) up to 7 days. The PBS solution was prepared dissolving 1 specific commercial tablet in 100 ml of distilled water. For carrying out the experiment, a volume of PBS identical to the volume of SBF (used for the mineralization test) was used. The samples, fixed on cylindrical scaffold supports (analogously to the SBF test), were inserted in a polypropylene falkon tube, filled with PBS solution, and incubated in an orbital shaker at 37°C and at 90 rpm.

The experiment was carried out in triplicate and two time points were selected:

- 1 day
- 7 days.

At each time point, the pH was measured. A falcon tube containing only PBS solution was used as a reference for pH measurements.

After immersion in PBS, the samples were gently rinsed three times with deionized water and dried under fumehood and then analyzed using SEM and FTIR.

3.6.8 Biological assay

For the biological assay an adapted protocol from a previous work [91] was used. Bone murine stromal cells ST-2 cell line (Leibniz-Institut DSMZ – German Collection of Microorganisms and Cell Cultures GmbH, Germany) was used to assess cell viability and morphology on the electrospun mats. All the samples were cut and fixed on appropriate sample holders (Scaffdex) and put in 24-multiwell and disinfected by exposure to UV light for 1 hour. Neat PCL electrospun fibers were used as control.

ST-2 cells were cultured in RPMI 1640 medium (Thermo Fisher Scientific), supplemented with 10% fetal bovine serum (Lonza) and 1% penicillin/streptomycin (Lonza) and incubated at 37°C with 5% CO₂. The seeding on the electrospun mats was performed with drop seeding, in which a drop of 100

ul of cell suspension with inoculum ratio of $1.65 \cdot 10^5$ cells/mL was put in the center of the mats. 15 minutes after the deposition of the drop, 1 mL of RPMI medium was added to each well. To assess cell viability, WST-8 assay was performed 1 day and 7 days after the seeding ((2-(2-methoxy-4-nitrophenyl)-3-(4-nitrophenyl)-5-(2,4-disulfophenyl)-2H-tetrazolium, monosodium salt), Sigma).

Fluorescence microscopy was used to investigate the morphology of the cells adherent on the substrate. In particular, as dye rhodamine phalloidin and DAPI (ThermoFisher Scientific) were used for the staining of actin filament and cell nuclei, respectively. The protocol for the staining contains initial step of immersion of the samples in fixation solution (1,4-piperazinediethanesulfonic acid buffer, ethylene glycol tetraacetic acid, polyethylene glycol, paraformaldehyde, PBS and sodium hydroxide (Sigma)) and permeabilization buffer. Subsequently, rhodamine phalloidin and DAPI were added in the concentration of $8 \mu\text{L}/\text{mL}$ and $1 \mu\text{L}/\text{mL}$ to each well, respectively. Fluorescent microscope (Axio Scope A1, Zeiss) was used for the analysis.

3.6.9 Stability test

Glasses (S2, SB2 and SBCu2) were immersed up to 1 hour in AA in same ratio used for electrospinning solution (as shown in Figure 3.16) and then, after removing the acid, dried under fumehood for 48 hours. The morphology of the glasses immersed in AA was observed using FE-SEM. The mineralization ability of these glasses was also tested, immersing them in SBF solution up to 14 days. The pH of each sample was measured after 1, 3, 7, 10, 12 and 14 days. At each time point same samples were removed from SBF solution, rinsed with distilled water (centrifuging them for 10 min at 5000 rpm), dried in a heater at $37 \text{ }^\circ\text{C}$ and analysed with FE-SEM, FTIR and XRD.



Figure 3.16: Glasses soaked in acetic acid

4 Results and discussion

4.1 Features of prepared glasses

4.1.1 Morphological characterization

SEM images of all synthesized glasses are reported below (Figure 4.1, Figure 4.2, Figure 4.3, Figure 4.4, Figure 4.5, Figure 4.6, Figure 4.7, Figure 4.8, Figure 4.9, Figure 4.10, Figure 4.11, Figure 4.12, Figure 4.13, Figure 4.14, Figure 4.15).

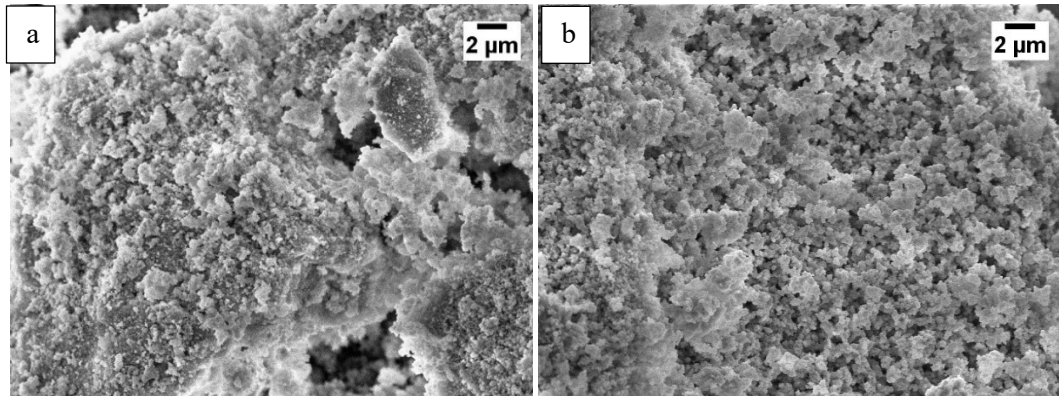


Figure 4.1: SEM micrographs at 10K X of S1 (a) and S2 (b)

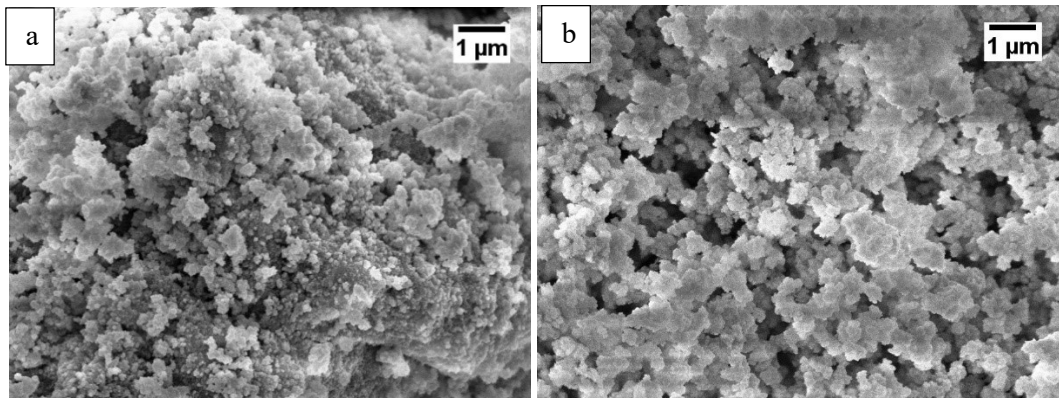


Figure 4.2: SEM micrographs at 30K X of S1 (a) and S2 (b)

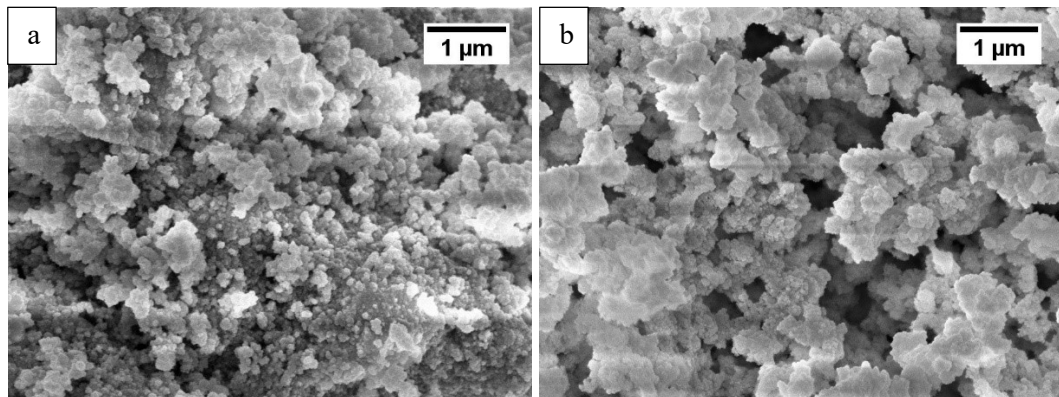


Figure 4.3: SEM micrographs at 50K X of S1 (a) and S2 (b)

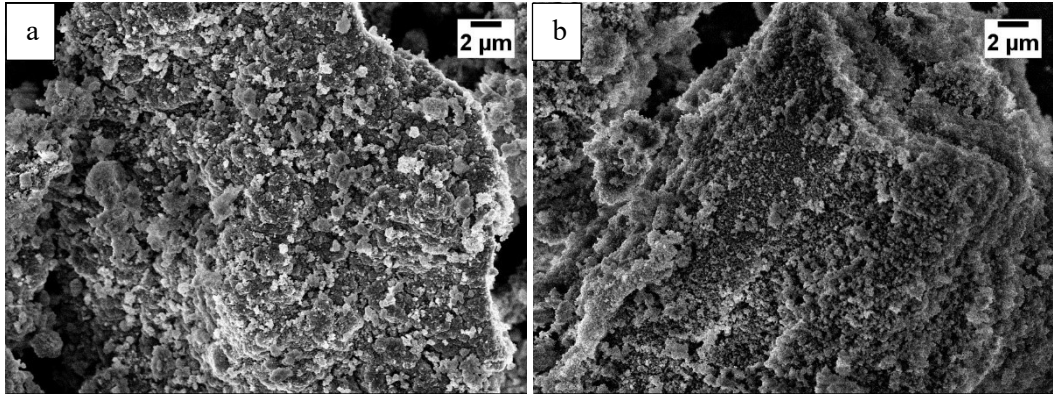


Figure 4.4: SEM micrographs at 10K X of *SBI* (a) and *SB2* (b)

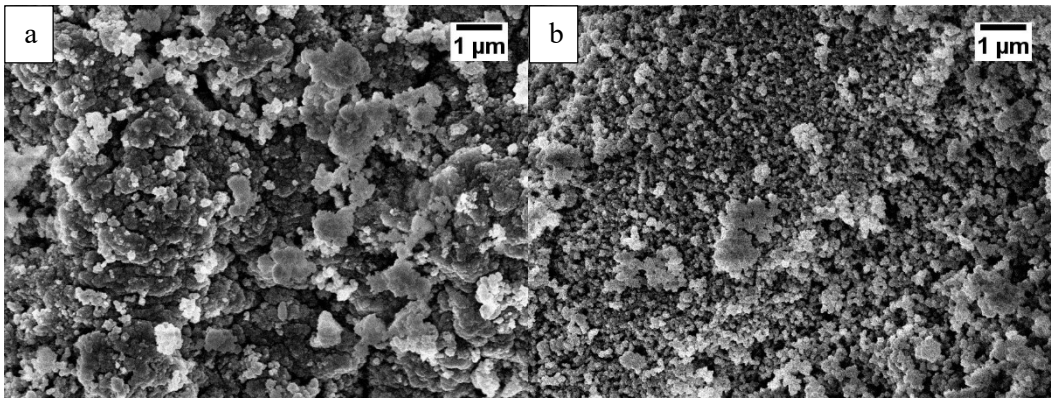


Figure 4.5: SEM micrographs at 30K X of *SBI* (a) and *SB2* (b)

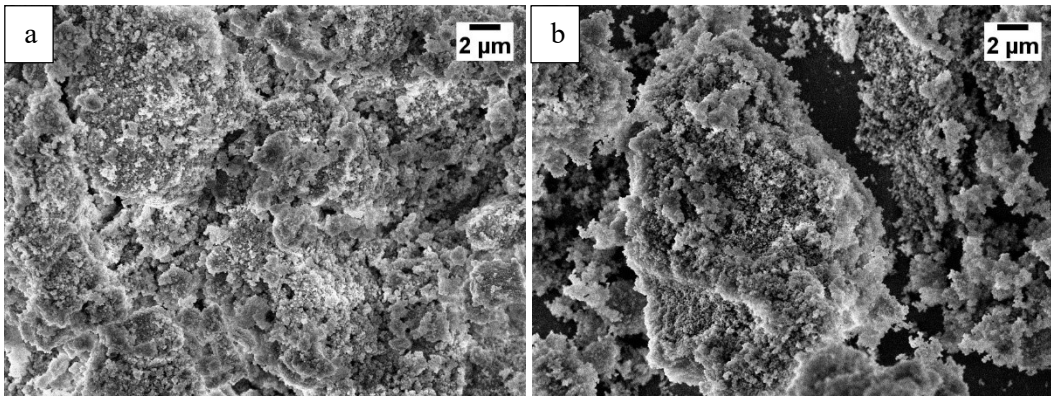


Figure 4.6: SEM micrographs at 10K X of *SBCu1* (a) and *SBCu2* (b)

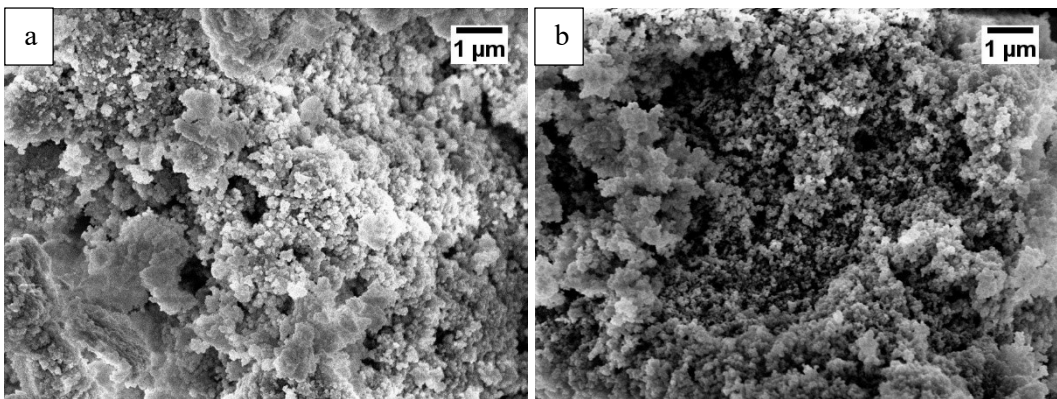


Figure 4.7: SEM micrographs at 30K X of *SBCu1* (a) and *SBCu2* (b)

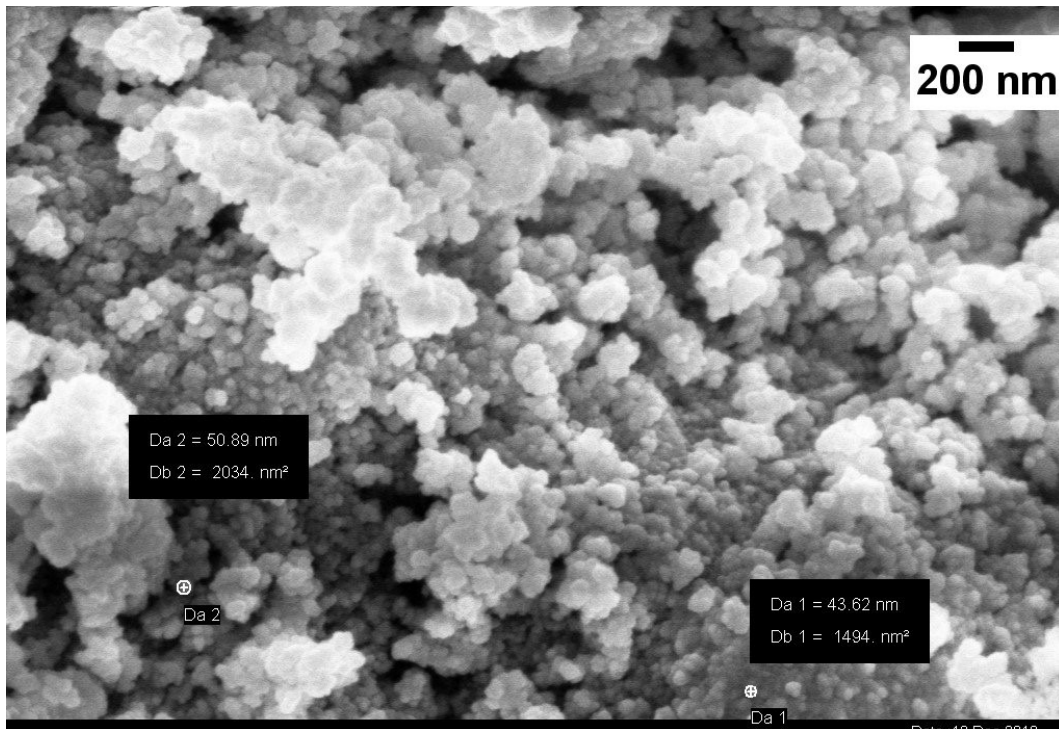


Figure 4.8: SEM micrograph at 100K X of S1

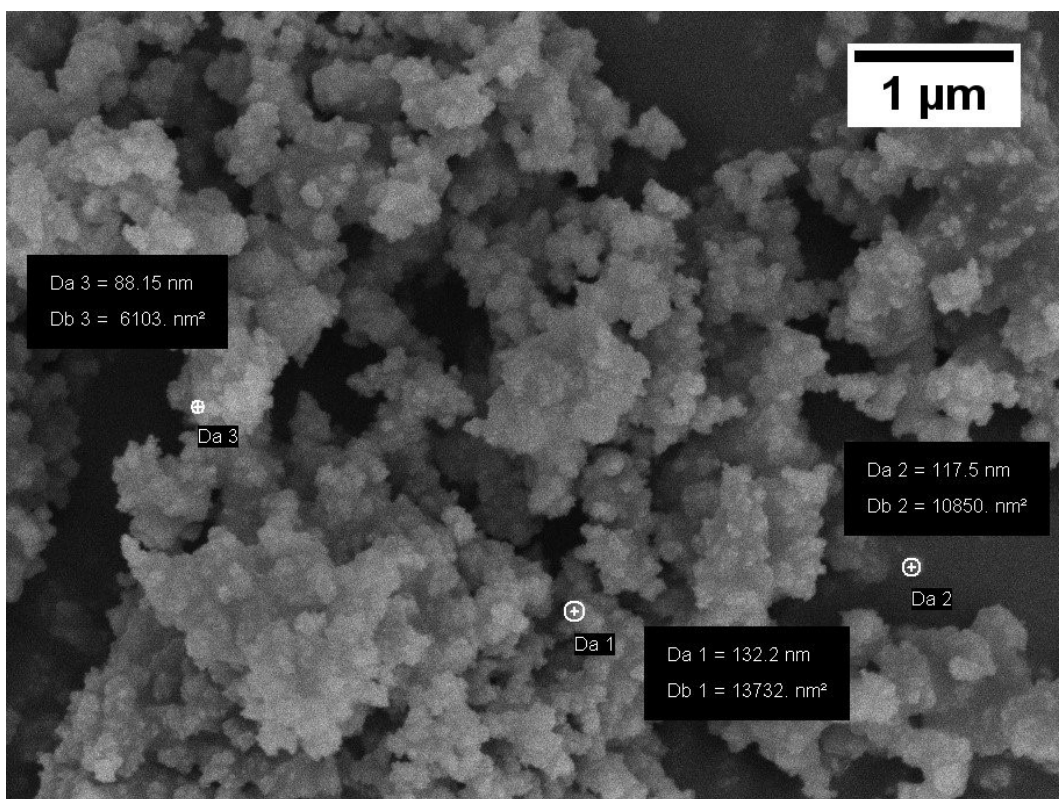


Figure 4.9: SEM micrograph at 50K X of S2

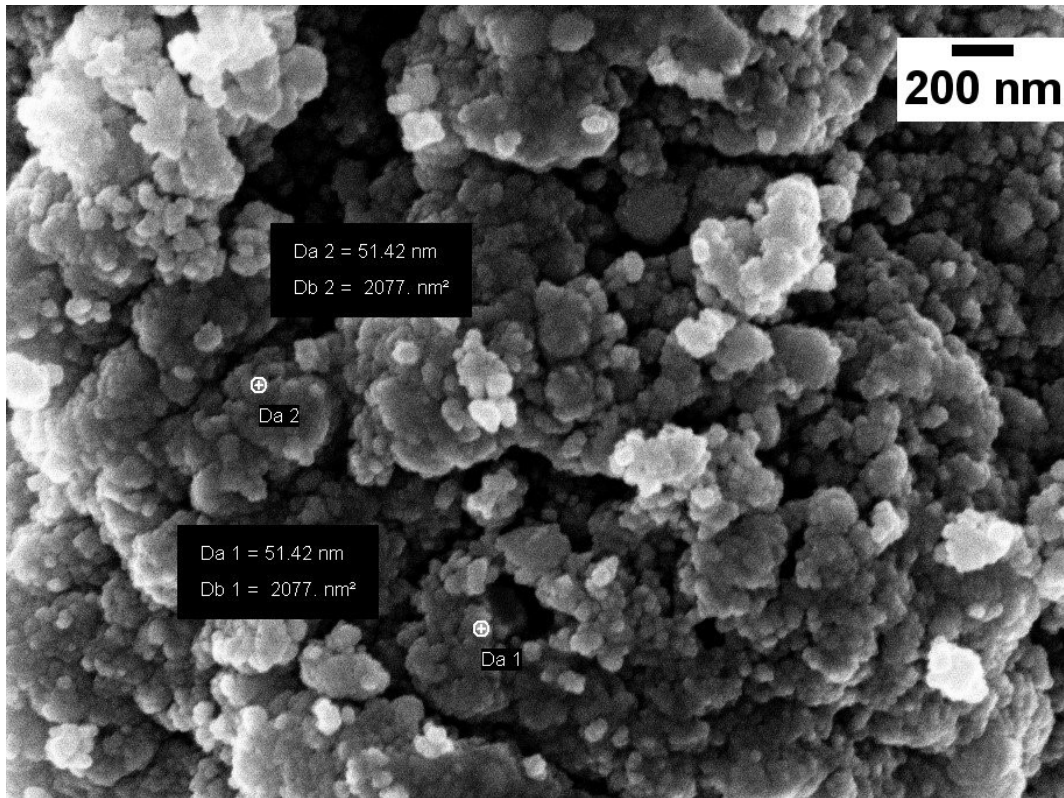


Figure 4.10: SEM micrographs at 100K X of SB1

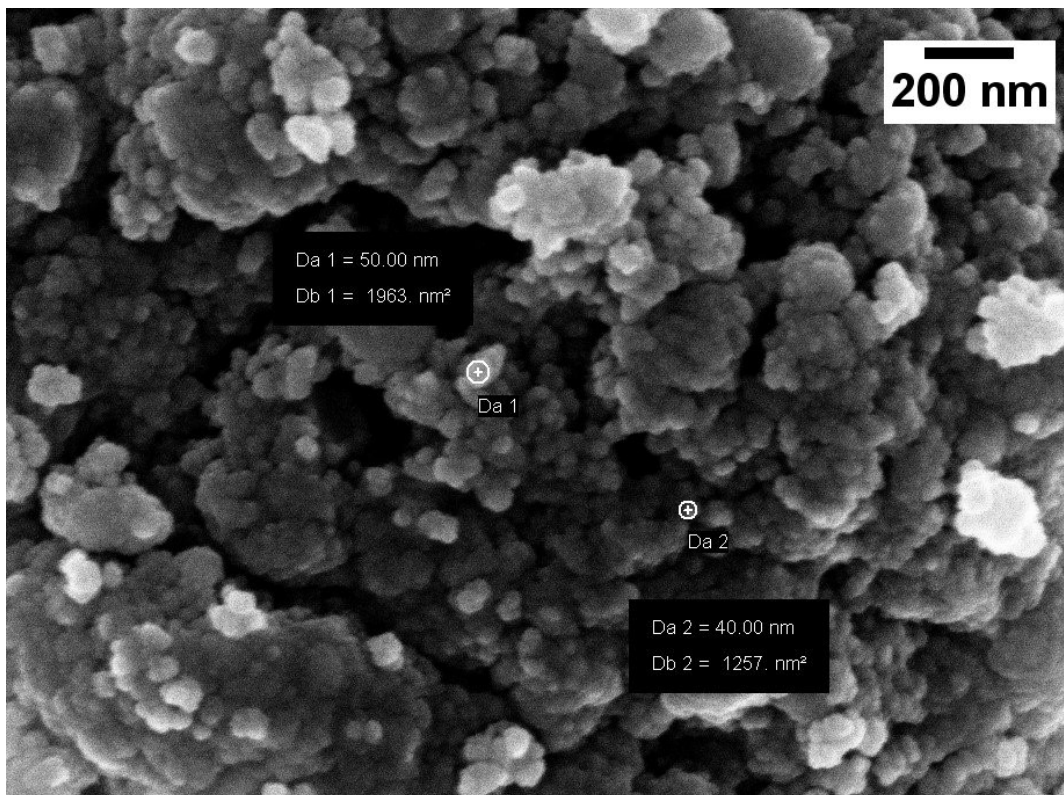


Figure 4.11: SEM micrographs at 150K X of SB1

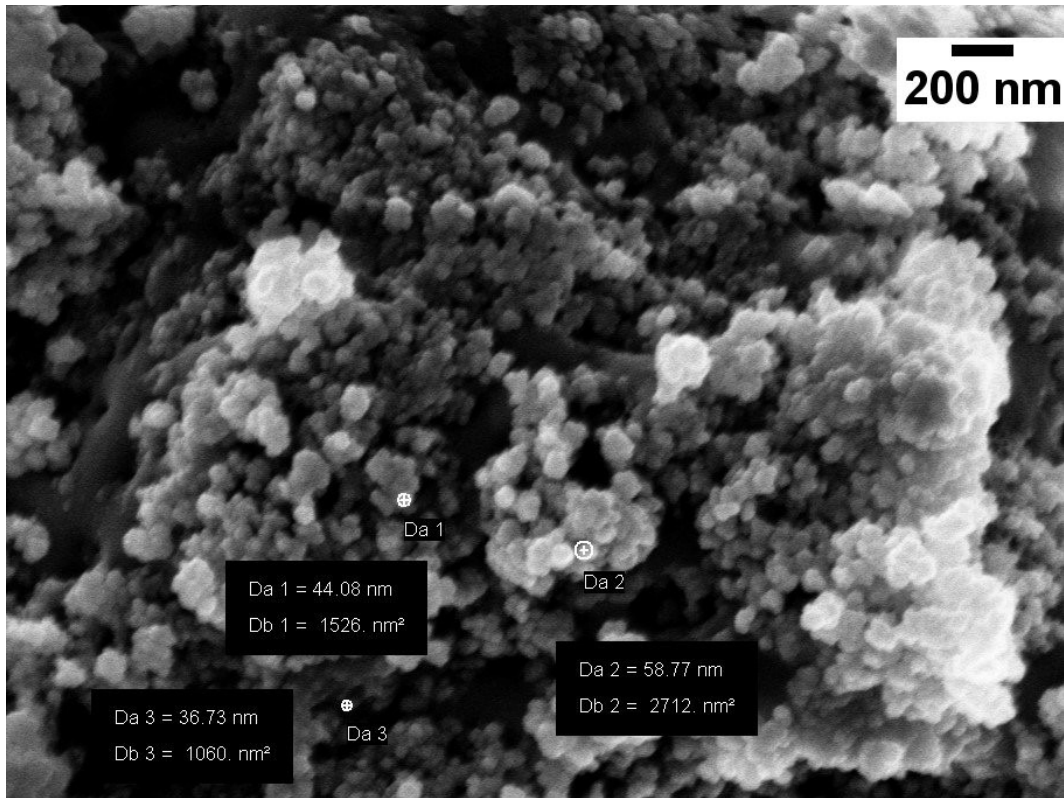


Figure 4.12: SEM micrographs at 100K X of SB2

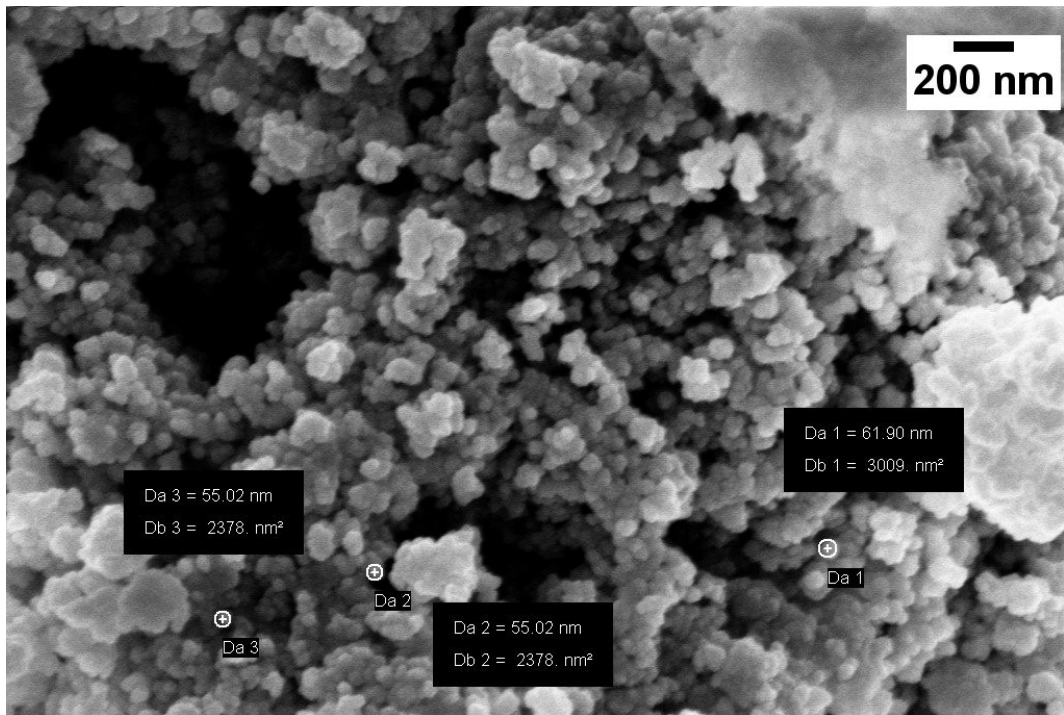


Figure 4.13: SEM micrograph at 100K X of SBCu1

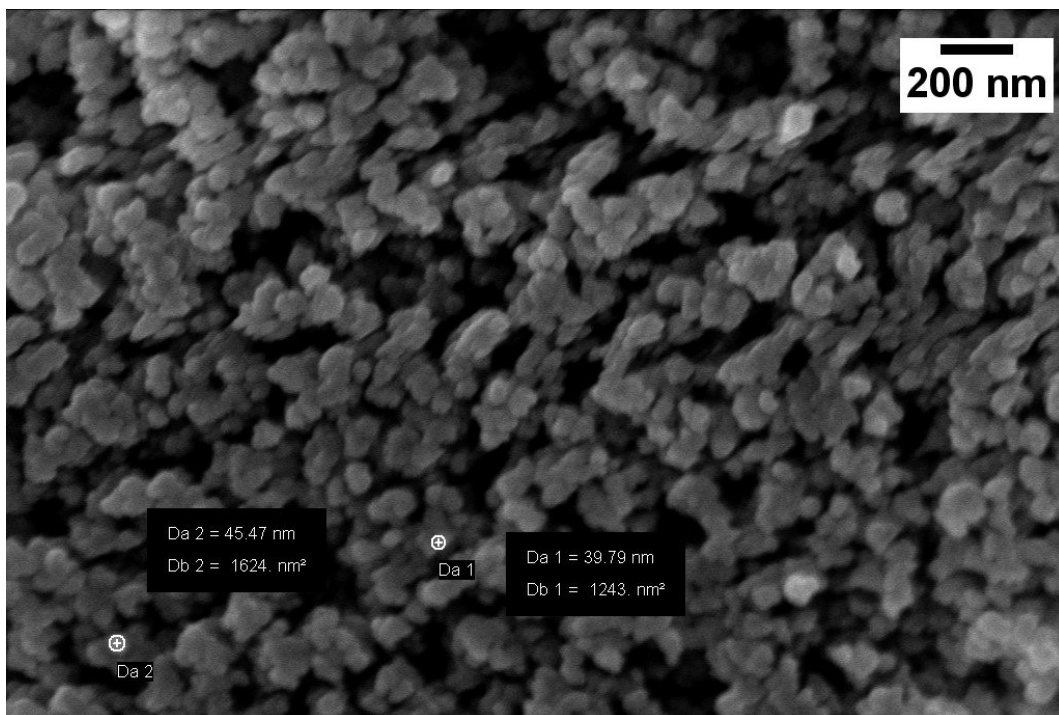


Figure 4.14: SEM micrograph at 100K X of *SBCu2*

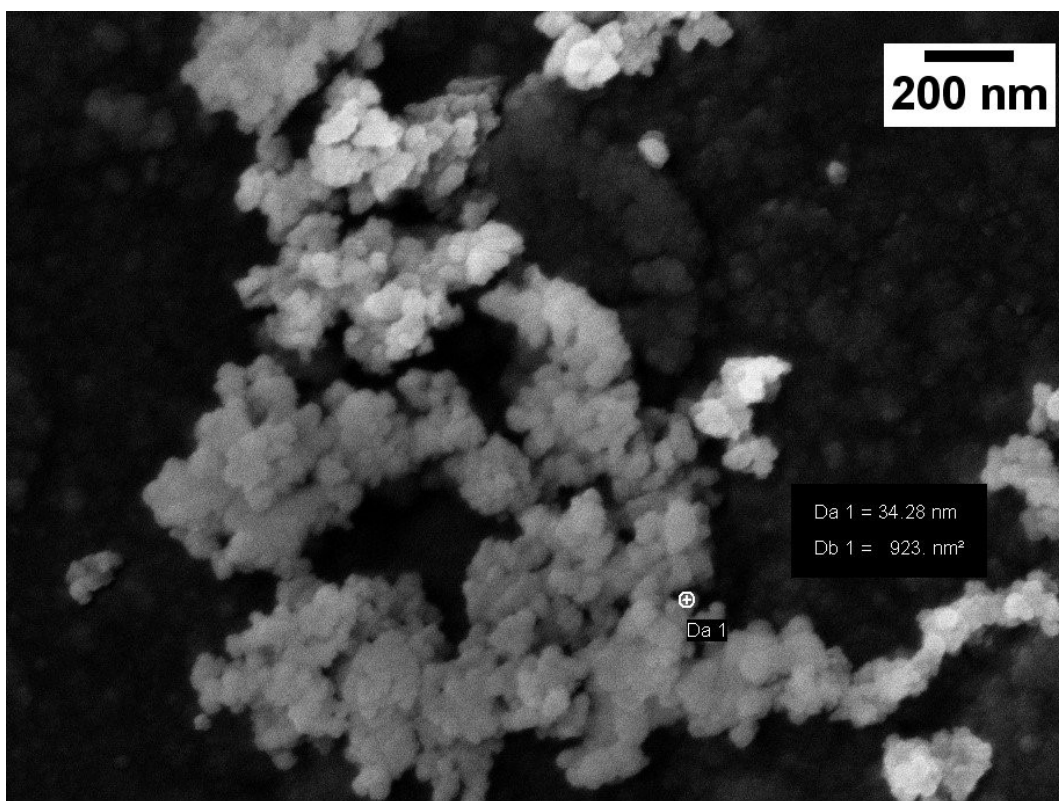


Figure 4.15: SEM micrograph at 100K X of *SBCu2*

As expected, nanosized round-shaped particles have been obtained for all syntheses and compositions. The morphology and particles size did not change significantly with the incorporation of boron and copper. In fact, according to *Labbaf et al.* spherical shape is in part due to the use of ammonium hydroxide as catalyst [92].

However, even though literature results show that, when using a base catalyst to control the condensation reaction, particles do not assemble, the nanoparticles are very aggregated. Indeed, nanosized particles with curvilinear edges and voids among them were observed. As previously proved by many literature results, it is very difficult to obtain disaggregated particles in the nanometric dimensional range, because particles size decrease is inversely proportional to their surface energy increases and, consequently, due to this increase in their surface energy, they tend to agglomerate.

The mean particle size of all glasses is smaller than 100 nm and the predominant diameter seems to be 50 nm, although it is difficult to measure the effective particle size due to particle agglomeration. In any case, this is a remarkable result if compared to literature. As comparative example, the following sol-gel synthesis experimental works are reported. In 2009, *Lei et al.* [93] have synthesized SiO₂-P₂O₅-CaO spherical mesoporous particles with a narrow size distribution of about 2–5 μm. In 2010, following a sol-gel route similar to the synthesis 2 carried out during this master thesis work, *El-Kady et al.* have obtained bioactive glass nanoparticles composed of 60% SiO₂, 36% CaO, 4% P₂O₅ (wt%) having most of their grains smaller than 100 nm [94]. In 2010, *Mozafari et al.* [95] prepared glass particles with a composition of 64% SiO₂, 5% P₂O₅, and 31% CaO (mol%) and grain size in the range of 100–200 nm. In the same year, through an acid-catalysed sol-gel synthesis, *Zhao et al.* [96] have obtained BG mesoporous microspheres with fixed calcium content (15 mol%) and different contents of SiO₂ (70 mol%, 75 mol% and 80 mol%) and P₂O₅ (5 mol%, 10 mol% and 15 mol%), that show diameters ranging from 4 μm to 5 μm (the lowest size was obtained for glasses with the highest content of phosphorus, demonstrating the inhibiting effect of P on the particle size). It is interesting to observe that these researchers have mixed glass precursors in a mixture of water, ethanol and nitric acid (used as catalyst),

analogously it has been done in this work, but they also adopted two surfactants (P123 and CTAB) to facilitate the formation of particles with spherical shape.

4.1.2 Compositional characterization

The elemental composition of pure and doped BG was confirmed by EDS analysis. Estimation of element concentration are reported in Table 2, Table 3 and Table 4 and related compositional spectra are shown in Figure 4.16, Figure 4.17 and Figure 4.18.

EDS patterns indicate that:

- both S glasses are chemically composed of Si, Ca, P and O;
- both SB glasses are chemically composed of Si, Ca, P, B and O;
- both SBCu glasses are chemically composed by Si, Ca, P, B, Cu and O.

Moreover, it is immediately possible to observe that no peaks correspond to any impurity element and higher is the element concentration, higher is the intensity of peaks assigned to the metals.

However, these results show that P content is underestimated, indicating that some of the phosphorus was not absorbed during the sol–gel reactions and remained in solution. This lower actual P content is particularly evident in case of doped BG, as previously observed in other experimental studies [97]. Moreover, glasses obtained through synthesis 1 contain less phosphorus, probably because, after gelification, there is much more competition between ions in order to enter the silica network.

A comparison between pure glasses (S glasses) and doped glasses (SB and SBCu glasses) also underlines a slight difference in the element distribution in the three different analysed domains of the samples: elements are more homogeneously distributed in case of glasses containing boron and copper. However, it is important to highlight that EDS analysis were not able to identify and quantify the boron amount.

Comparison of S glasses:

Table 2: Comparison of atomic% between S1 and S2

| S glasses | | | | | |
|-----------|------------|------------|------------|------------|------------|
| element | at% theor. | S1 | | S2 | |
| | | at% EDS | wt% EDS | at% EDS | wt% EDS |
| Si | 77.3 | 82.6 ± 1.2 | 78.0 ± 2.1 | 82.6 ± 1.6 | 78.0 ± 2.1 |
| P | 7.6 | 4.9 ± 0.6 | 5.1 ± 0.1 | 4.9 ± 0.1 | 5.1 ± 0.1 |
| Ca | 15.1 | 12.6 ± 0.9 | 16.9 ± 2.2 | 12.6 ± 1.7 | 16.9 ± 2.2 |

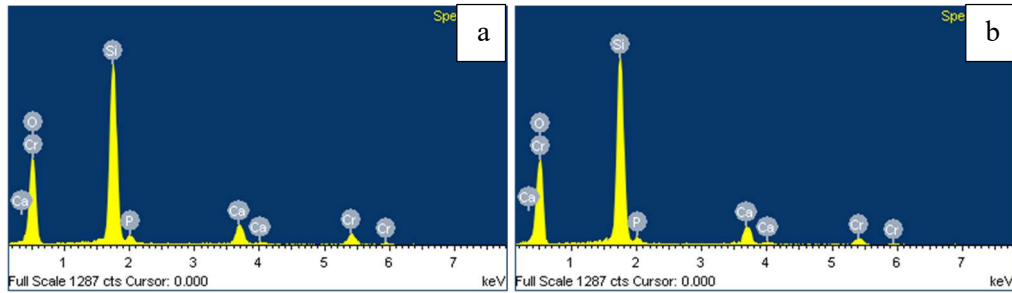


Figure 4.16: EDS spectra of S1 (a) and S2 (b)

Comparison of SB glasses:

Table 3: Comparison of atomic% between SB1 and SB2

| SB glasses | | | | | | |
|------------|------------|-----------|-------------|------------|------------|------------|
| element | at% theor. | | SB1 | | SB2 | |
| | with B | without B | at% EDS | wt% EDS | at% EDS | wt% EDS |
| B | 24.5 | 0.0 | 0.0 ± 0.0 | 0.0 ± 0.0 | 0.0 ± 0.0 | 0.0 ± 0.0 |
| Si | 59.1 | 78.2 | 78.2 ± 78.3 | 72.9 ± 1.1 | 81.4 ± 2.5 | 75.9 ± 2.9 |
| P | 7.2 | 9.6 | 9.6 ± 5.8 | 5.9 ± 0.4 | 2.2 ± 0.9 | 2.3 ± 1.0 |
| Ca | 9.2 | 12.2 | 12.2 ± 16.0 | 21.2 ± 0.9 | 16.4 ± 1.8 | 21.8 ± 2.2 |

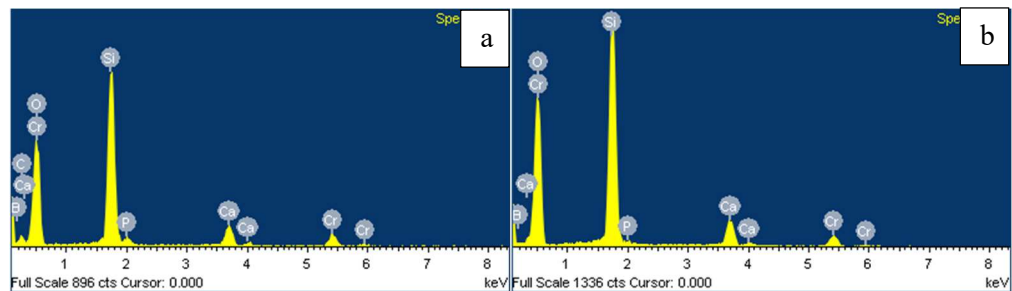


Figure 4.17: EDS spectra of SB1 (a) and SB2 (b)

Comparison of SBCu glasses

Table 4: Comparison of atomic% between SBCu1 and SBCu2

| SBCu glasses | | | | | | |
|--------------|------------|-----------|------------|------------|------------|------------|
| element | at% theor. | | SBCu1 | | SBCu2 | |
| | with B | without B | at% EDS | wt% EDS | at% EDS | wt% EDS |
| B | 23.7 | 0.0 | 0.0 ± 0.0 | 0.0 ± 0.0 | 0.0 ± 0.0 | 0.0 ± 0.0 |
| Si | 57.0 | 74.7 | 77.5 ± 0.4 | 68.6 ± 0.7 | 79.7 ± 1.3 | 70.7 ± 1.9 |
| P | 7.0 | 9.2 | 6.2 ± 0.3 | 6.0 ± 0.3 | 2.5 ± 0.4 | 2.4 ± 0.5 |
| Ca | 8.9 | 11.6 | 9.9 ± 0.7 | 12.6 ± 1.0 | 11.9 ± 0.7 | 15.0 ± 1.0 |
| Cu | 3.4 | 4.5 | 6.4 ± 0.7 | 12.9 ± 1.3 | 5.9 ± 0.2 | 11.9 ± 0.4 |

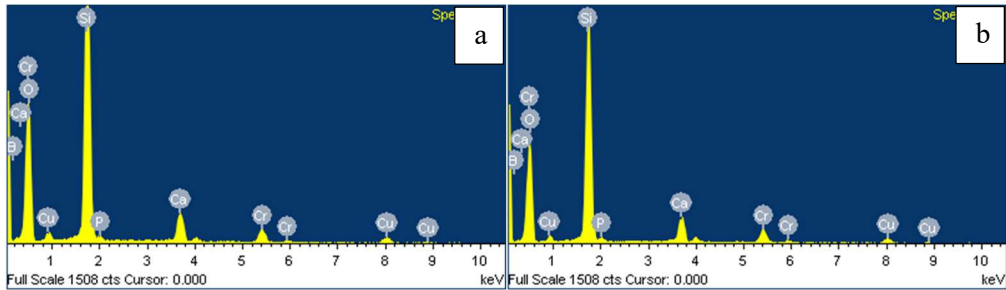


Figure 4.18: EDS spectra of SBCu1 (a) and SBCu2 (b)

4.1.3

4.1.3 X-ray diffraction analysis

The prepared glass powders were studied by x-ray diffraction (XRD) measurements in order to assess their structure. As expected, the XRD pattern (reported in Figure 4.19 and Figure 4.20) shows a typical broad halo between 15° and 30° which is corresponding to the amorphous phase of glass (underlined by the two lines in Figure 4.19) [98][65][99][53][55][100][101][102].

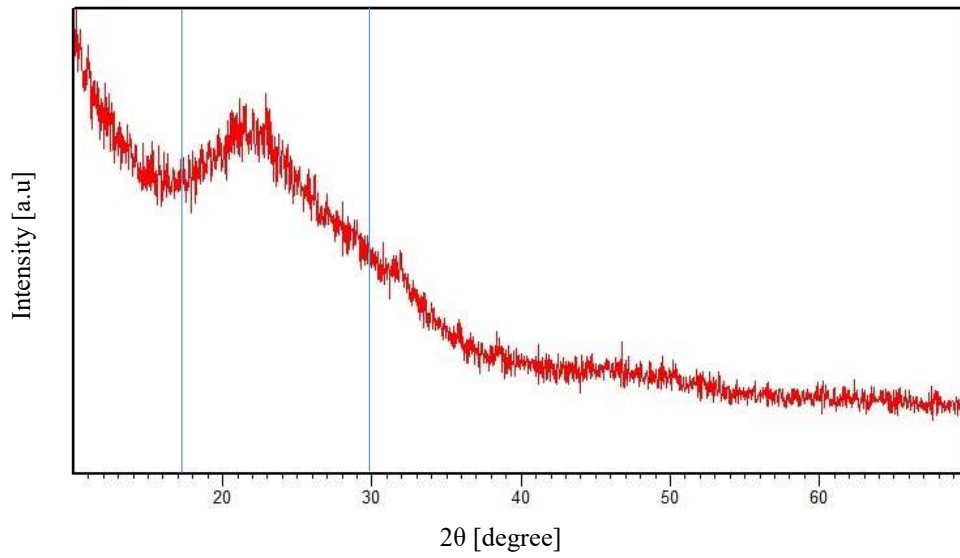


Figure 4.19: XRD spectrum of S1 as example

All XRD patterns are similar with no big difference in pure and doped glasses, in agreement with other experimental works [103] (as shown in Figure 4.20).

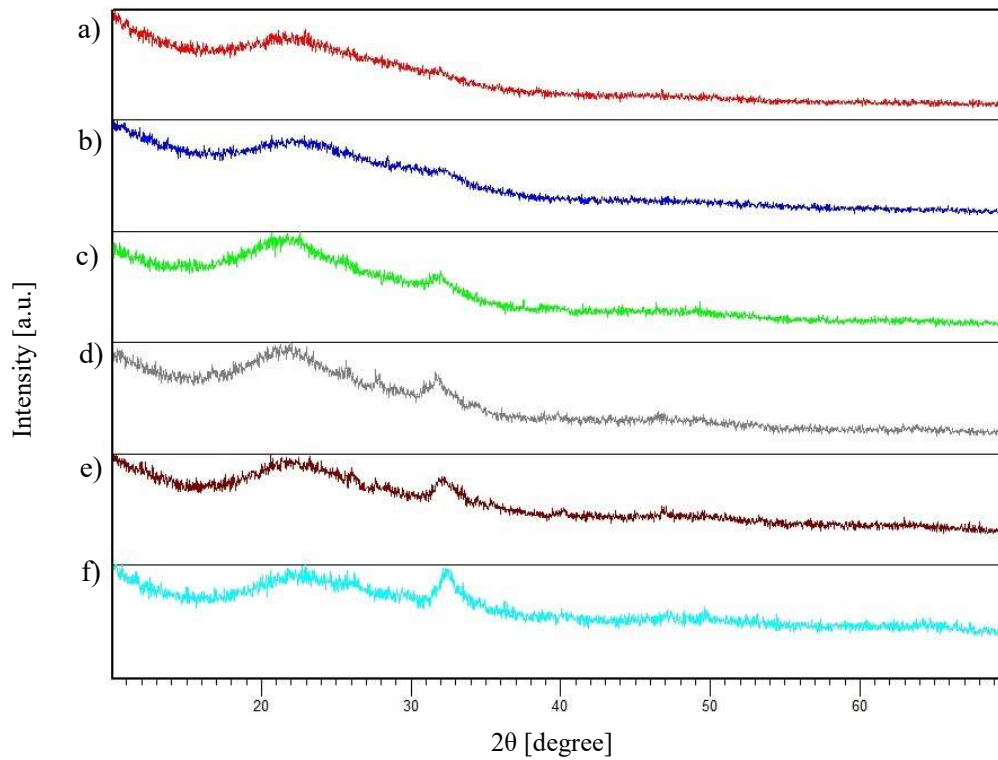


Figure 4.20: XRD spectra comparison of glasses S1 (a), S2 (b), SB1 (c), SB2 (d), SBCu1 (e) and SBCu2 (f)

However, some peaks are present and indicate the existence of a crystalline phase. Indeed, although a very wide diffraction maxima can be observed between 15° and 35°, a sharp maxima around 32° and two smaller peaks at 40° and 50° are visible, as shown in the spectrum reported as example in Figure 4.21.

These peaks can probably attributed to a calcium silicate Ca_2SiO_4 [104], or to hydroxyapatite [48], as calculated using a computer program (X'Pert Highscore) and in agreement with literature results, as shown in Figure 4.21, Figure 4.22, and Figure 4.23. These peaks could be also attributed to boron oxide B_2O_3 [105], but this hypothesis was rejected, because they are present in all XRD spectra, including S glasses with nominal composition of 77 wt% SiO_2 , 14 wt% CaO and 9 wt% P_2O_5 .

Moreover, they are more evident in case of glasses prepared by synthesis 2, in particular in XRD spectra of doped glasses (SB and SBCu glasses), confirming the difficulty to obtain completely amorphous glasses in case of addition of elements such as boron and copper [102].

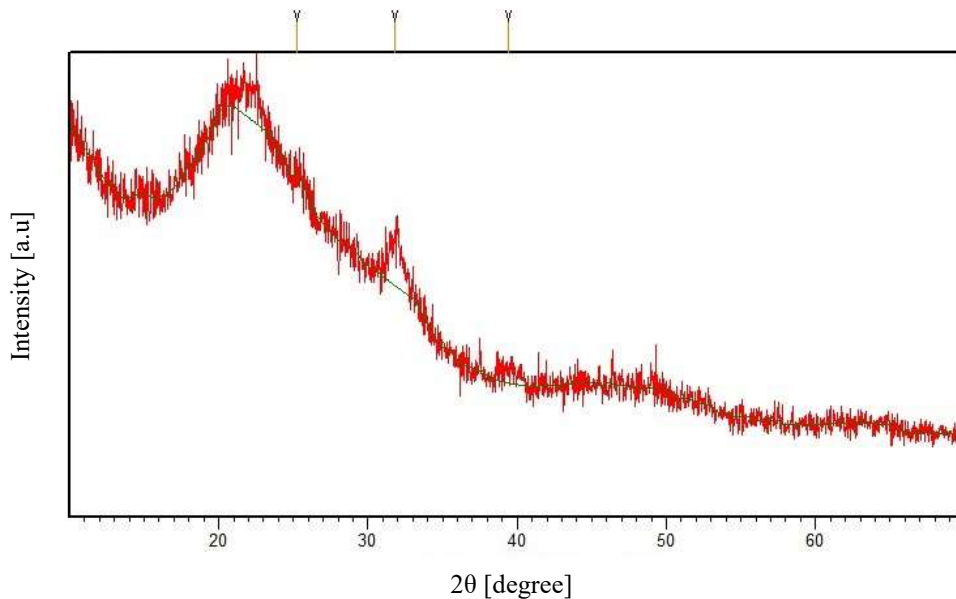


Figure 4.21: trend of peaks in the XRD spectrum of SB1

In Figure 4.22 peaks of calcium silicate that were identified in XRD spectrum of SB1 are reported, showing a good matching between typical peaks of Ca_2SiO_4 and peaks which were measured in SB1.

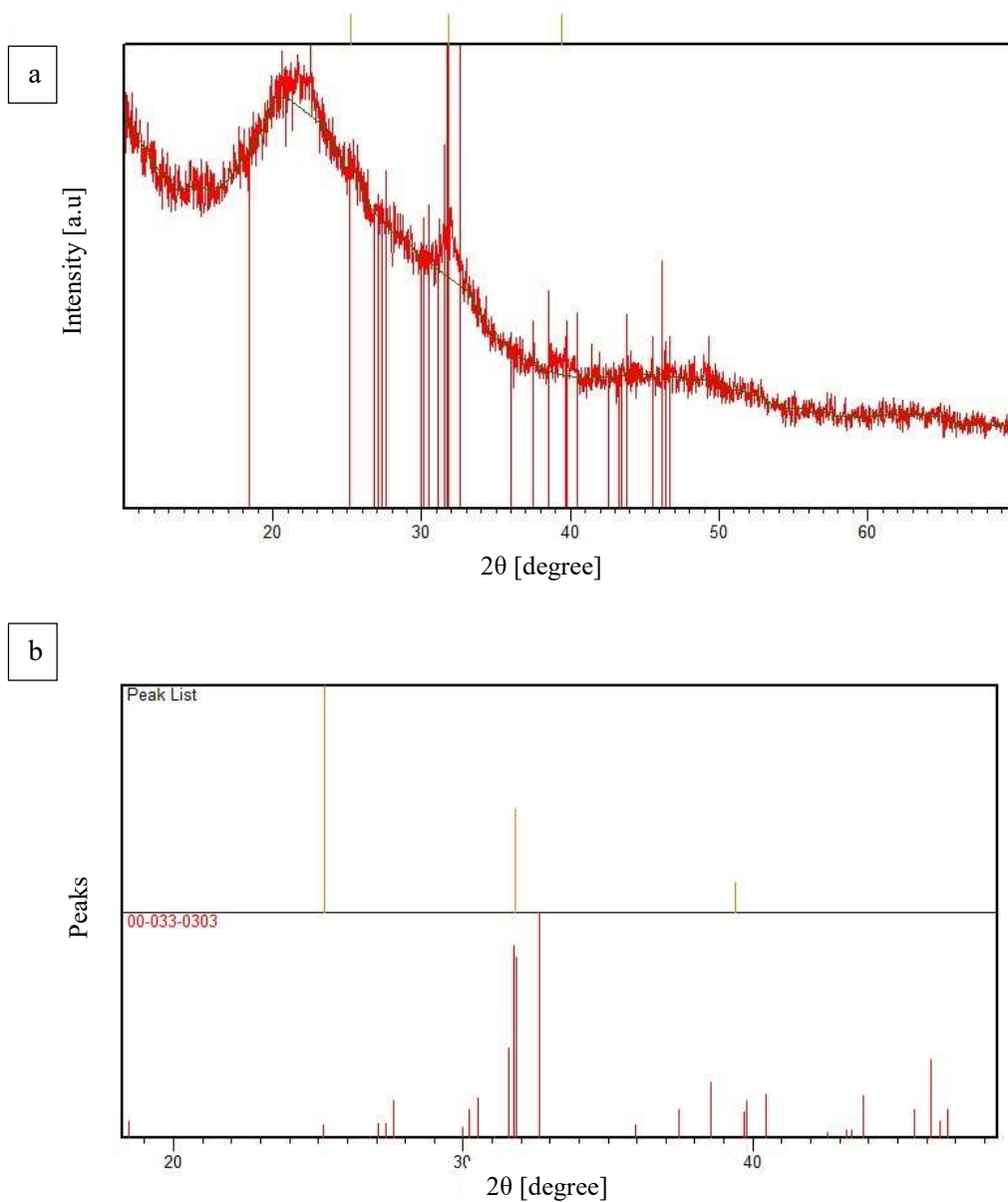


Figure 4.22: peaks of Ca_2SiO_4 in SB1 where a) trend of peaks and b) pattern)

Peaks and related pattern of B_2O_3 and their comparison with peaks present in XRD spectra of SB1 are reported in Figure 4.23.

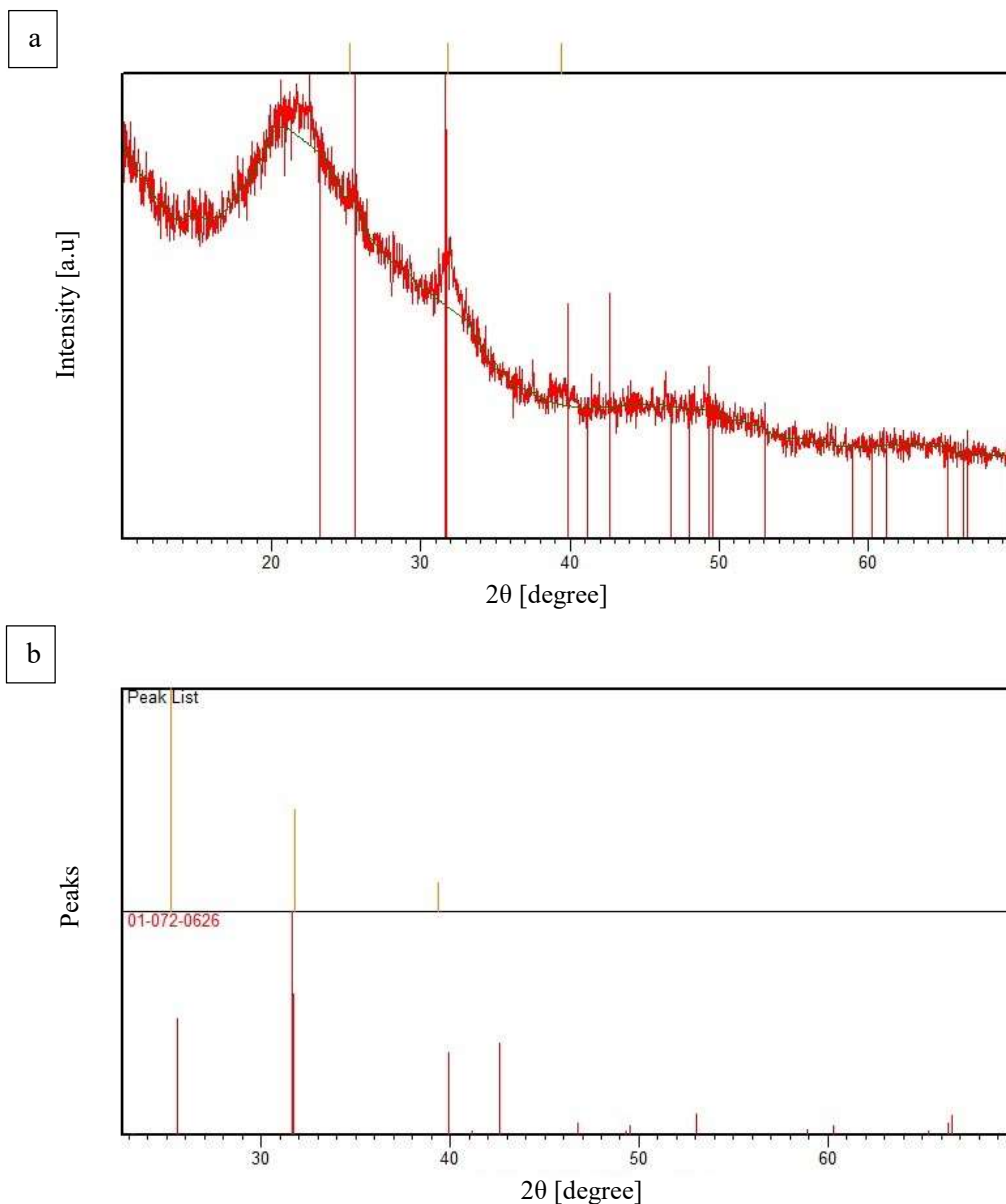


Figure 4.23: peaks of B_2O_3 in SBI where a) trend of peaks and b) pattern

Similar results were reported by *Moorthi et al.* [106], who synthesized BG nanoparticles mixing an acid solution of calcium nitrate and TEOS into a mixture of ethanol:water (1:2 ratio) and a basic solution of diammonium hydrogen orthophosphate and PEG; the pH of the first solution was maintained around 2 by the addition of 1 M citric acid, whereas the pH of the second one was maintained to 10 by adding ammoniated water. After calcination at 700 °C, they obtained semicrystalline particles containing β -tricalcium phosphate $Ca_3(PO_4)_2$ (JCPDS No. 09-0169) and wollastonite $CaSiO_3$ (JCPDS No. 19-0248) phases. *Ahmadi et*

al. [107] have synthesized BG nanoparticles via an acid-catalysed sol-gel method using the same precursors and the same acidifying agent (nitric acid) employed during this master thesis work and discovered into the XRD patterns of their particles some peaks with very low intensity related to different crystalline phases, including CaSiO_3 (JCPDS 42-0547) and pseudowollastonite $\text{Ca}_3(\text{Si}_3\text{O}_9)$ (JCPDS 74-0874).

Taking into consideration the above reported results, the presence of a crystalline phase in the amorphous network of the synthesized glass particles can be related to the calcination step at 600°C . In any case, extended studies on the different synthesis stages should be done in order to understand chemical reactions and nucleation mechanisms on the glassy nature of the synthesized glasses.

4.1.4 BET analysis

The total area of the glasses prepared using synthesis 1 is bigger, as shown in Table 5. Moreover, the glasses containing copper (SBCu1 and SBCu2) have a smaller area. It is worth noticing that BET surface gives a correct value for the entire surface accessible to nitrogen and the available area is strongly dependent on the extent of surface roughness and porosity and the dimensions of the adsorbed molecules [108]. Because glasses produced in both acidic and basic media are made of coalesced nanoparticles, they present a lot of inter-particle interstices.

Table 5: Values of surface areas calculated by BET

| Surface area [m^2/g] | | |
|--|-----------------------------|-----------------------------|
| glasses | synthesis 1 | synthesis 2 |
| S | (S1) | (S2) |
| | 243.7 m^2/g | 192.6 m^2/g |
| SB | (SB1) | (SB2) |
| | 131.8 m^2/g | 68.7 m^2/g |
| SBCu | (SBCu1) | (SBCu2) |
| | 66.5 m^2/g | 55.1 m^2/g |

4.1.5 Acellular bioactivity test

Variations versus soaking time of element concentrations and solution pH, as well as changes in the glass surface are related to the rate of biomineralization of the bioactive glasses after immersion in simulated body fluid (SBF).

In graph in Figure 4.24 are represented the trends of pH values during immersion time of the six glasses in SBF.

It is evident that pH does not vary very much up to 14 days, remaining in the range 7.34–7.56. However, a slight increase in pH value by increasing immersion time can be observed, in agreement with literature results [95][96][109][110][104][107], although this increase seems to be slower if compared to similar glass composition, probably because of the different element percentage, in particular the low amount of phosphorus really incorporated in the glasses that have been synthesized during this master thesis work, and the different particle structure. For example, *Mozafari et al.* [95] have carried out an acellular bioactivity test of mesoporous BG nanoparticles with the composition 64% SiO₂, 5% P₂O₅ and 31% CaO (based on mol%) and have reported that pH increased up to 8 during the first 7 days of immersion and then slowly up to 8.3 until 14 days, confirming that mesoporous glasses have a higher *in vitro* reactivity.

Moreover, pH trends show some fluctuations that can be attributed to ion exchange between the SBF solution and the glass powders or to the different temperature at which pH was measured, although it has been always paid attention to measure the pH maintaining the temperature of the solution in the same range (34°C-36°C).

Variations in pH values have been also recorded by *Simogaki et al.* [111], who prepared monodisperse silica-based spheres containing phosphorus and calcium by the modified Stöber's sol-gel method. They measured a slight pH increase during the two first days of immersion, followed by a slower increase (from 7.7 to 7.8) after 15 days in SBF. After this initial increase, pH decreased between the 15 and 21 days to 7.6. After that, the pH values increase again slowly to reach a value around 7.5 – 7.8 at 30 days of soaking. Indeed, firstly a rapid exchange between Ca²⁺ with H⁺ or H₃O⁺ from SBF occurred, causing hydrolysis of the

silica groups. Consequently, soluble silica is lost in the form of $\text{Si}(\text{OH})_4$ to the solution and creates silanol (Si-OH) groups at the glass solution interface. This process leads to an initial increase in the pH of the solution, as a result of replacement of H^+ ions in the solution by cations as a consequence of the release in Ca^{2+} ions from glass to SBF and the uptake of H^+ present in the SBF by the glass surface. After that, the cation exchange increases the hydroxyl concentration of the solution, which leads to attack of the silica glass network and an increase in Si concentration on glass surface with soaking time. When the third stage of formation of the hydroxyapatite-like layer occurred, condensation and repolymerisation of a SiO_2 -rich layer on the surface exhaust alkalis and alkali-earth cations, causing a gradually decrease in P and Ca concentrations and a new small and slow increase in pH. After that Ca^{2+} and PO_4^{3-} groups migrate to the surface through the SiO_2 -rich layer, forming a $\text{CaO-P}_2\text{O}_5$ -rich film on top of the SiO_2 -rich layer, followed by growth of the amorphous $\text{CaO-P}_2\text{O}_5$ -rich film by incorporation of soluble calcium and phosphates from solution, that results in a change in Ca and P ion levels. Finally, a HA layer is formed on the top of the glass surface thanks to the crystallization of the amorphous $\text{CaO-P}_2\text{O}_5$ film by incorporation of OH^- and CO_3^{2-} anions from the SBF solution [95][40][112][113][114].

It is worth mentioning that glasses containing boron seem to show a flatter trend, characterized by lower pH values, probably due to the buffering effect of boron, showing pH values and trends similar to a previous work of *Mancuso et al.* [48], who supposed that the almost stable measured pH values might be governed by the total sum of both basic and acidic ion concentration present in the glass composition. A quick alkali-mediated sol-gel method, which show some similarities with the one adopted during this master thesis work, was used by *Moonaki et al.* to synthesize BGs from TEOS, TEP and $\text{Ca}(\text{NO}_3)_2$ [47]. In details TEOS was mixed in 2M nitric acid and distilled water to undergo acid hydrolysis for 1 h and after the addition of the other precursors, 1 M NH_3 solution was added until gelation occurred; after that gel was dried at 60 °C for 24 h and a heat treatment at 600 °C was applied for 2 h in a muffle furnace. In order to synthesize boron-doped BGs, different quantities of H_3BO_3 were added to the mixture 30

min after the addition of TEOS. Their results show that pH change was slower for highest B group (21%), especially for the first 3 days. Other studies show that borate glasses attained a constant value in a quite shorter time compared to the silicate glass (~500 h for silicate glass and ~50 h for borate glass) and the final pH value of the borate glass (9.6) was much lower than that of the silicate glass (11.5). The increase in pH is due to the fact that strongly basic NaOH overpowers the weak acidic nature of B(OH)₃ and Si(OH)₄. When all the Na₂O dissolves rapidly, the pH reaches its final value and since B(OH)₃ has stronger acidic nature than Si(OH)₄, the borate glass exhibits lower pH value than the silicate glass.

It is also possible to observe that SBCu glasses show the lowest pH values; this seems to confirm previous literature results with copper-doped bioactive glass [115]. In fact, *Koohkan et al.* have demonstrated that calcium phosphate precipitation can occur at lower pH (less than 8) in case of the 68SiO₂–23CaO–4P₂O₅–CuO (mol%) bioactive glass, which was synthesized during their experimental work.

In conclusion, the pH decrease between the different type of glass follows the ranking S > SB > SBCu. However, it is important to underline that the variation range is very small. Moreover, slight difference in pH values could be attributed to difference in measurement temperature. It is interesting to mention that similar pH values around 7 are usually considered optimal in provision of future *in vitro* cell culture.

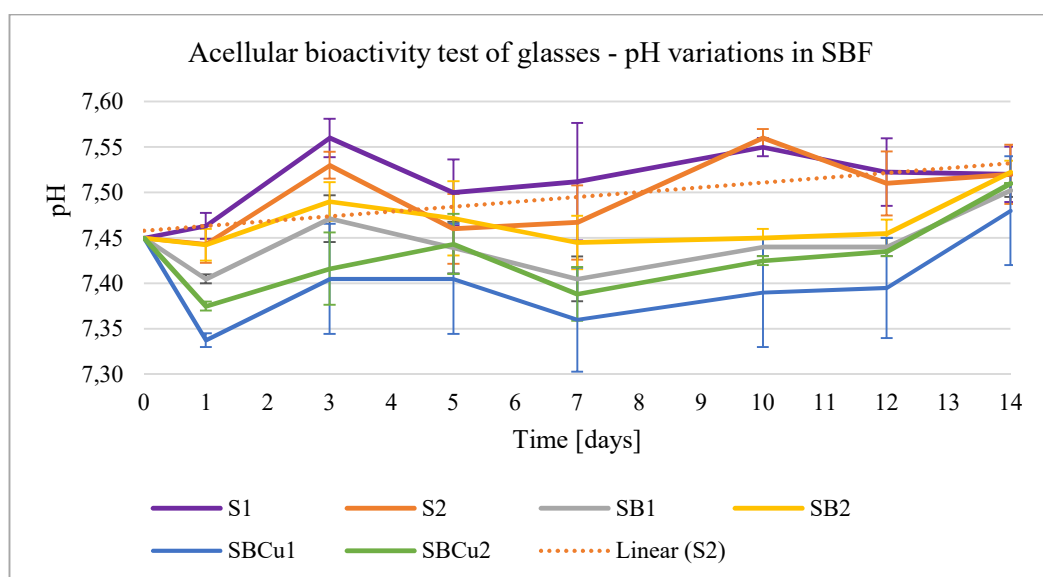


Figure 4.24: pH trend during acellular bioactivity test of glasses

EDS measurements were performed to evaluate the relative concentrations of Ca and P present on the glass surfaces resulting from the immersion time in SBF [87][116]. EDS pattern of S glasses are shown in Figure 4.25

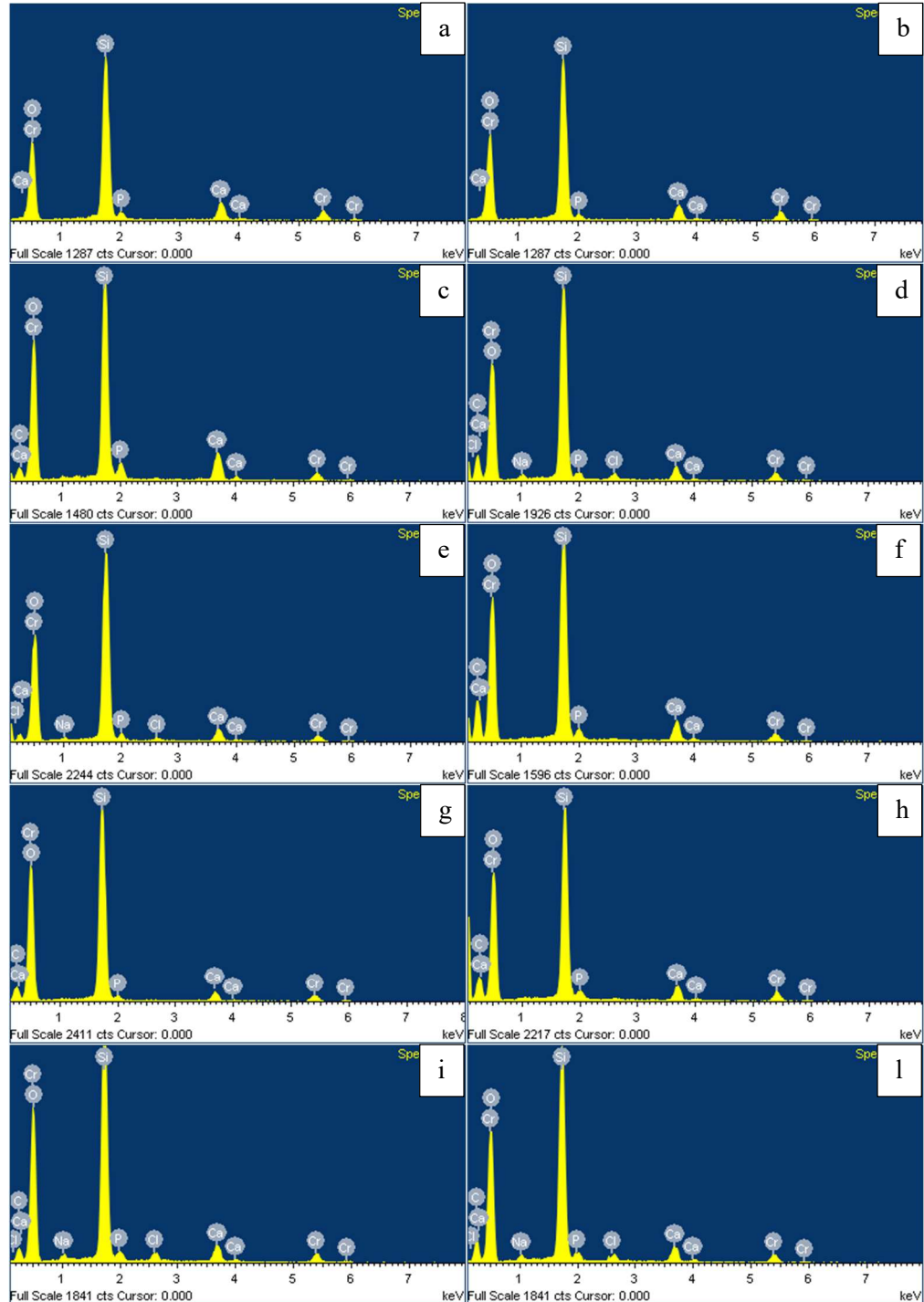


Figure 4.25: EDS spectra of S glasses at different time points in SBF
a) EDS spectra of a zone of S1 0d and b) of S2 0d where 0d = before SBF immersion
c) EDS spectra of a zone of S1 1d and d) of S2 1d where 1d = 1 day in SBF
e) EDS spectra of a zone of S1 3d and f) of S2 3d where 3d = 3 days in SBF
g) EDS spectra of a zone of S1 7d and h) of S2 7d where 7d = 7 days in SBF
i) EDS spectra of a zone of S1 14d and l) of S2 14d where 14d = 14 days in SBF

EDS pattern of SB glasses are shown in Figure 4.26.

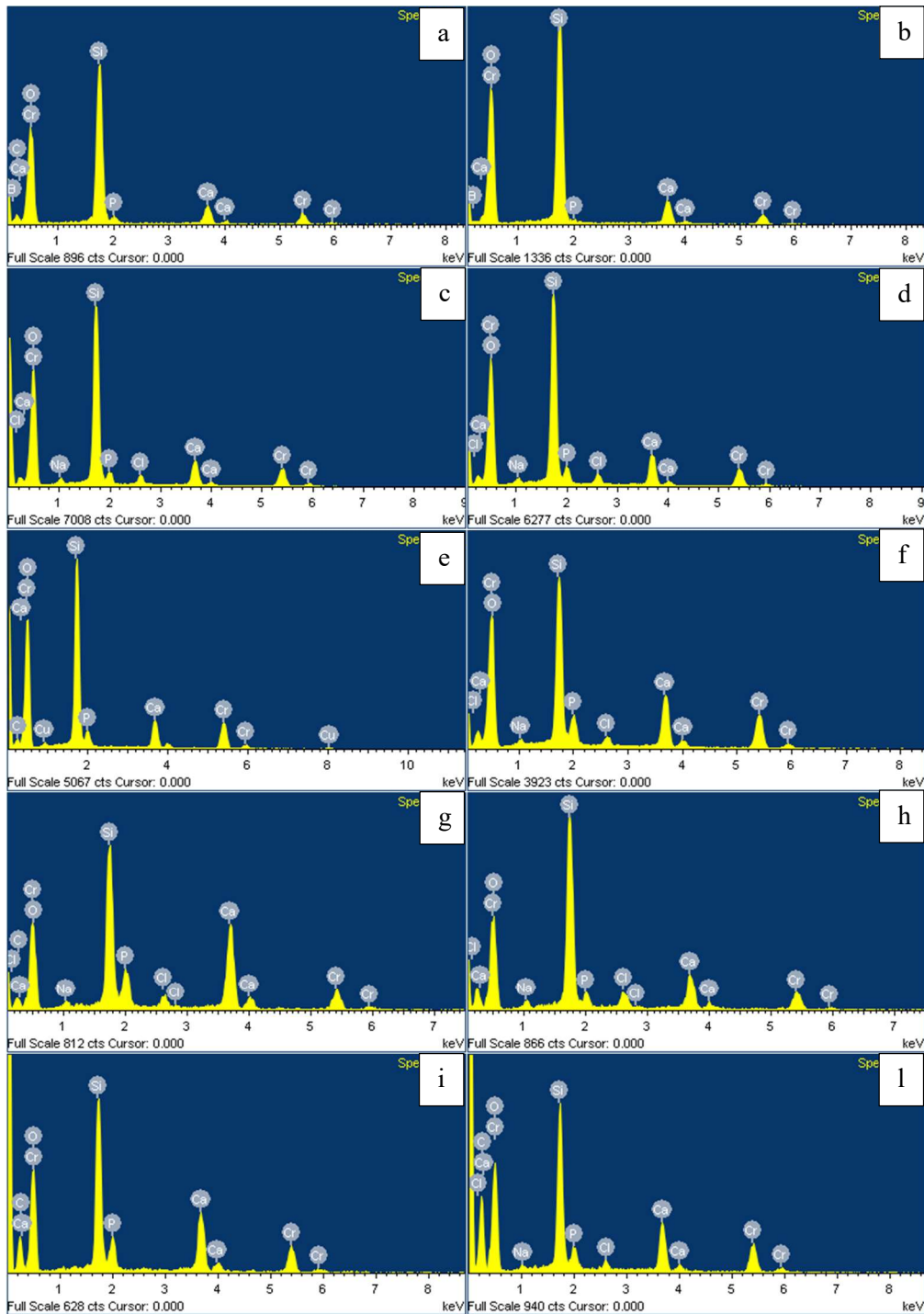


Figure 4.26: EDS spectra of SB glasses at different time points in SBF
 a) EDS spectra of a zone of SB1 0d and b) of SB2 0d
 c) EDS spectra of a zone of SB1 1d and d) of SB2 1d
 e) EDS spectra of a zone of SB1 3d and f) of SB2 3d
 g) EDS spectra of a zone of SB1 7d and h) of SB2 7d
 i) EDS spectra of a zone of SB1 14d and l) of SB2 14d

EDS pattern of SBCu glasses are shown in Figure 4.27.

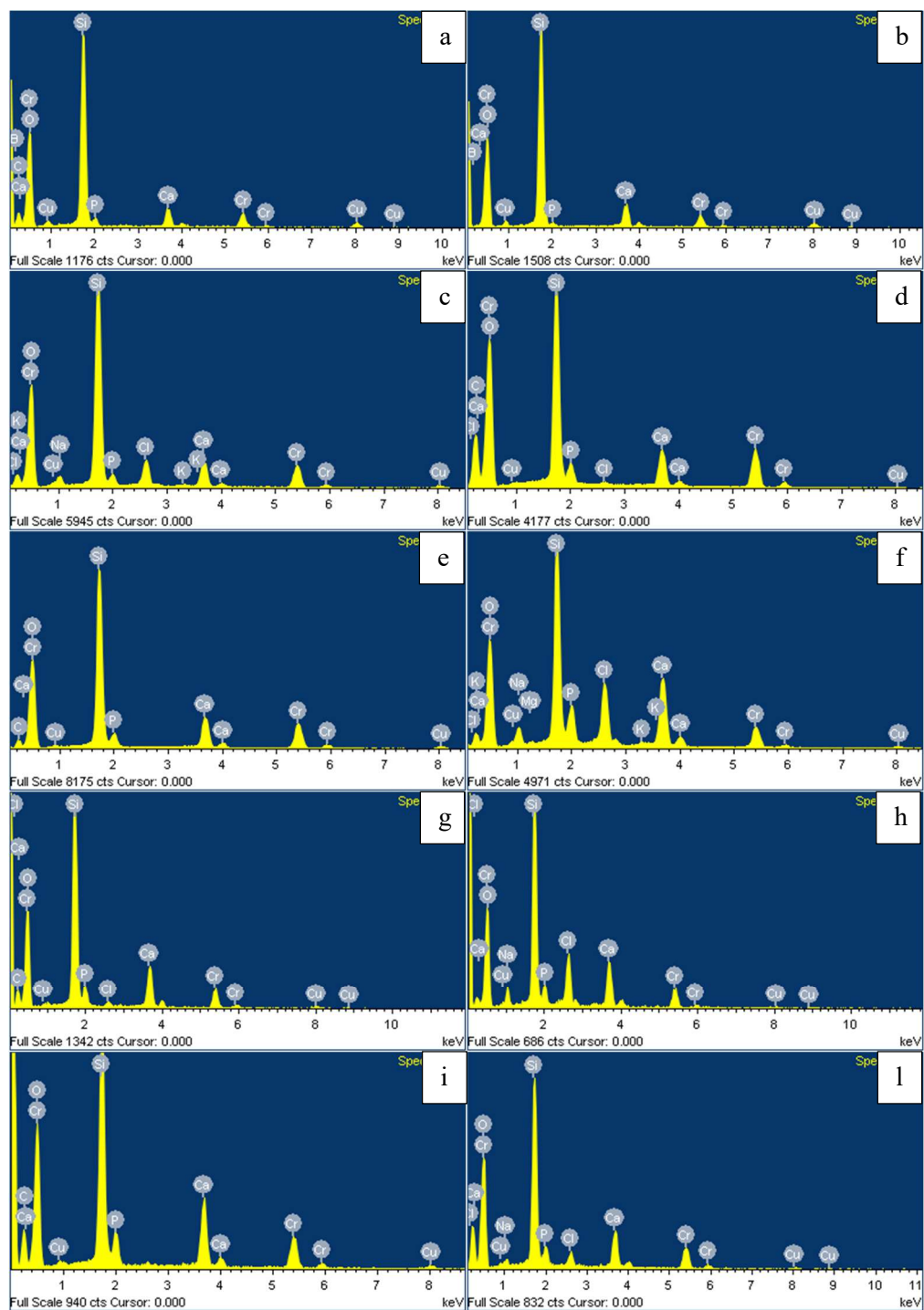


Figure 4.27: EDS spectra of SBCu glasses at different time points in SBF
 a) EDS spectra of a zone of SBCu1 0d and b) of SBCu2 0d
 c) EDS spectra of a zone of SBCu1 1d and d) of SBCu2 1d
 e) EDS spectra of a zone of SBCu1 3d and f) of SBCu2 3d
 g) EDS spectra of a zone of SBCu1 7d and h) of SBCu2 7d
 i) EDS spectra of a zone of SBCu1 14d and l) of SBCu2 14d

The EDS analysis of samples immersed in SBF demonstrated a significant difference in P and Ca element amount compared to the primary EDS pattern (Figure 4.25, Figure 4.26 and Figure 4.27), indicating the increase of P and Ca, due to the formation of a calcium phosphate phase.

The presence of chlorine and sodium is due to the formation of sodium chloride on the nanoparticle surface during the SBF test, that was not possible to eliminate during washing of the powders in distilled water. In all samples, the peak of silicon is still very high after immersion in SBF, because the thickness of the analysis area of the samples is bigger than the thickness of the coating. Moreover, it is possible to notice that the peaks of Ca and P seem to be higher in case of SB and SBCu glasses.

In Figure 4.28 the variation in Ca and P amounts for all six glasses during immersion time are compared.

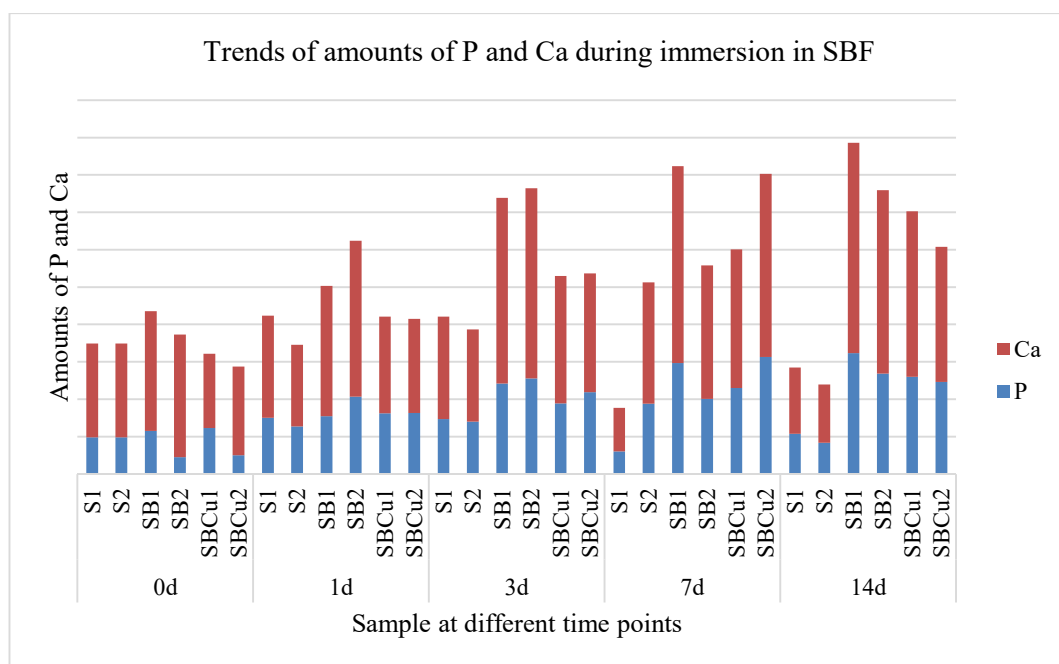


Figure 4.28: P and Ca amounts during immersion of glasses in SBF

EDS results have been plotted in terms of Ca and P concentration versus immersion time in graphs in Figure 4.29 and Figure 4.30, and show a clear increase of phosphorus and calcium contents on the surface of the synthesized glasses during soaking time. Apatite crystals grow, in fact, by consuming calcium and phosphate ions from the SBF solution and those that migrate from the

medium to the surface of the glasses. This increase is evident even after only 1 day.

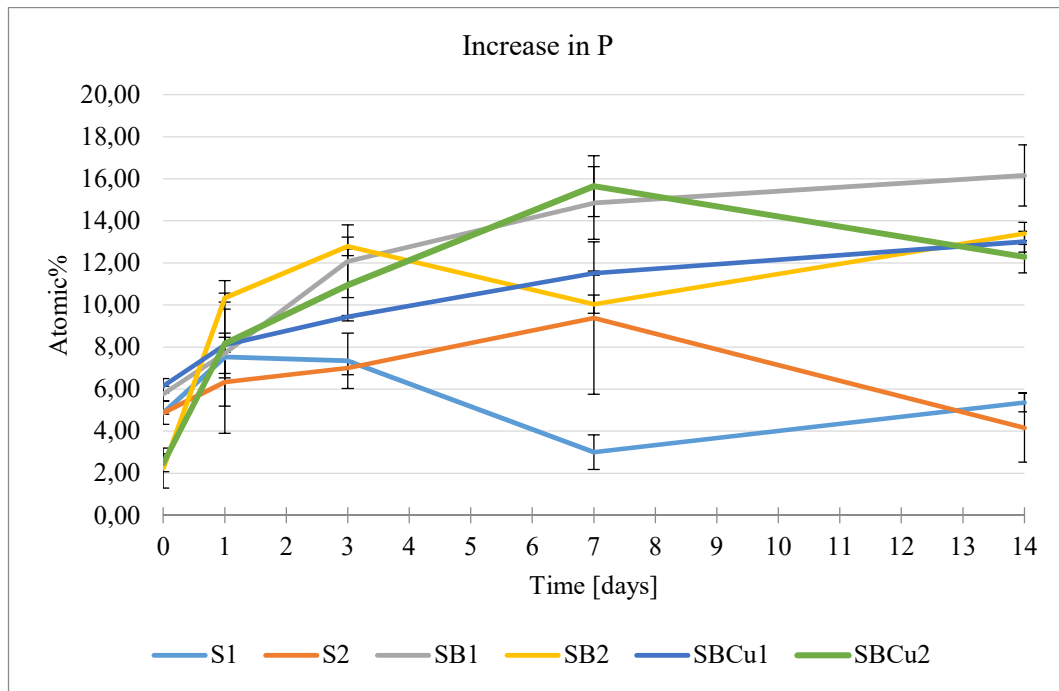


Figure 4.29: trend of P amount during immersion of glasses in SBF

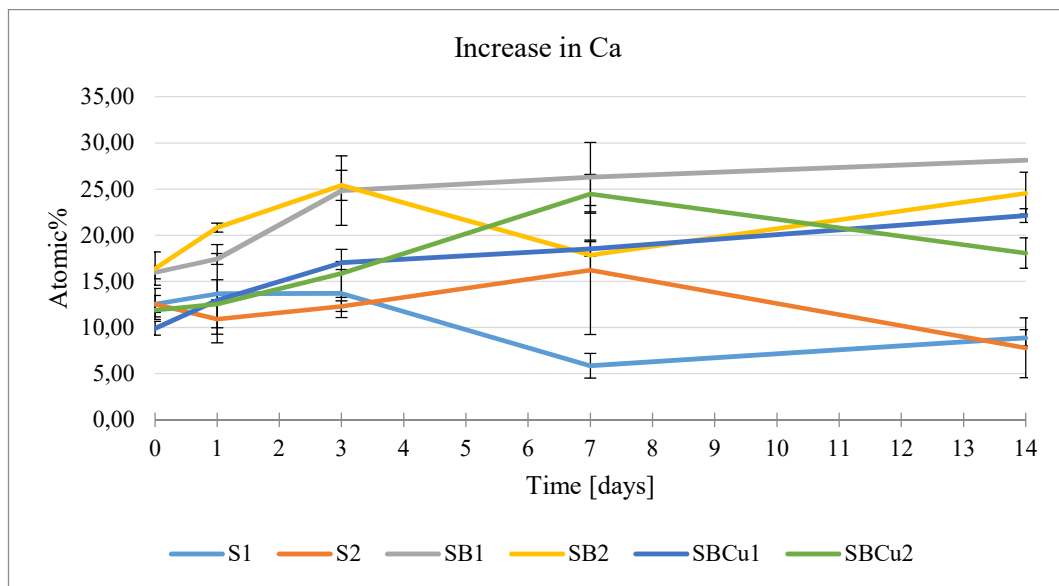


Figure 4.30: trend of Ca amount during immersion of glasses in SBF

Moreover, from these results it seems that SB glasses possess a higher bioactive response, in agreement with literature results that show how the presence of boron ions improve the bioactivity of the glasses [18].

Values of Ca/P atomic ratios determined from the EDS spectra (reported in Table 6) are similar to the ratio value for stoichiometric HA (1.68), confirming the previous observations about the bioactivity of the synthesized glasses [117].

Table 6: Ca/P ratio of glasses during acellular bioactivity test

| Ca/P ratio (atomic%) | | | | |
|----------------------|-----------|-----------|-----------|-----------|
| Glass | 1d | 3d | 7d | 14d |
| S1 | 1.8 ± 0.4 | 1.9 ± 0.1 | 2.0 ± 0.3 | 1.7 ± 0.1 |
| S2 | 1.7 ± 0.1 | 1.8 ± 0.1 | 1.7 ± 0.1 | 1.9 ± 0.1 |
| SB1 | 2.3 ± 0.2 | 1.8 ± 0.1 | 1.8 ± 0.1 | 1.7 ± 0.2 |
| SB2 | 2.0 ± 0.0 | 1.8 ± 0.1 | 1.8 ± 0.1 | 1.8 ± 0.1 |
| SBCu1 | 1.6 ± 0.1 | 1.8 ± 0.0 | 1.6 ± 0.1 | 1.7 ± 0.0 |
| SBCu2 | 1.5 ± 0.0 | 1.4 ± 0.0 | 1.6 ± 0.0 | 1.5 ± 0.0 |

Moreover, there is a copper release, as shown in the following photos (Figure 4.31, Figure 4.32 and Figure 4.33) and EDS results graph in Figure 4.34.



Figure 4.31: SBCu glasses after 1 day in SBF



Figure 4.32: SBCu glasses after 3 days (left) and 7 days (right) in SBF



Figure 4.33: SBCu glasses after 14 days in SBF

The atomic amount of copper in SBCu glasses seems to decrease during immersion time, following a comparable trend for both glasses doped with Cu (see Figure 4.34).

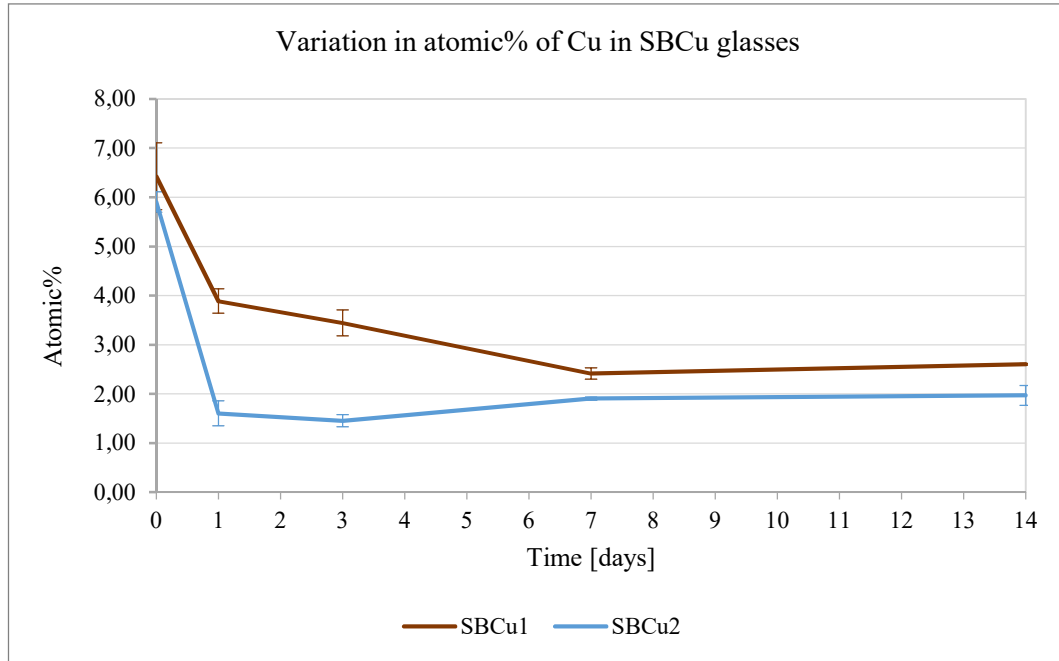


Figure 4.34: Change in Cu amount during immersion in SBF

The X-ray diffraction analysis results of all glasses are compared and shown in , Figure 4.37, Figure 4.38, Figure 4.38, Figure 4.39 and Figure 4.40. The XRD peak assignment followed the pattern calculated using the computer program X'Pert Highscore and is in agreement with literature [118][119]. In order to facilitate the identification of the peaks, the following symbols are used:

- Calcium silicate
- ▲ HA
- NaCl

For a complete and correct analysis of the obtained XRD spectra, it is necessary to mention again that spectra of all glasses before immersion in SBF solution show the presence of the typical peaks of calcium silicate at 25° and 32° (as previously discussed). These peaks correspond or are very near to some of the peaks of hydroxyapatite. Indeed, the peak at 32° can also be assigned to (2 1 1) apatite according to the standard JCPDS (09-0432). Moreover, in some of these spectra,

beside the presence of the initial crystalline phase of calcium silicate and the nucleation of apatite, new peaks attributable to sodium chloride NaCl are observable, in agreement with element peaks which were previously observed in EDS patterns. However, after immersion in SBF, new peaks at 26°, 40°, 46° and 49° appear and can be assigned to HA.

Figure 4.35 show XRD spectra of S1 glass at each analyzed time point.

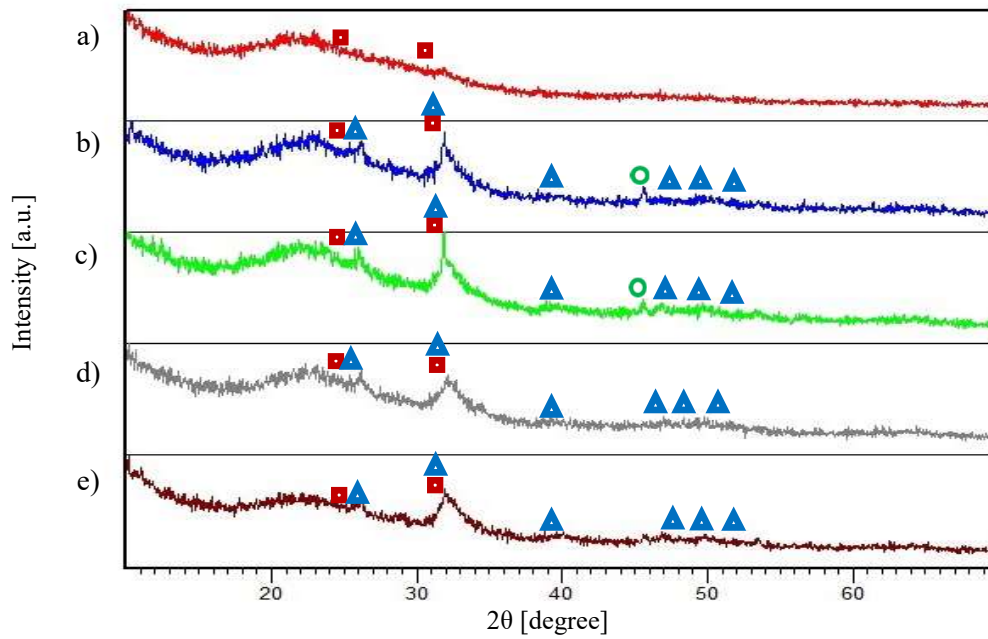


Figure 4.35: Comparison of XRD spectra of S1 where a) S1 0d b) S1 1d c) S1 3d d) S1 7d and e) S1 14d

Figure 4.36 show XRD spectra of S1 glass at each analyzed time point.

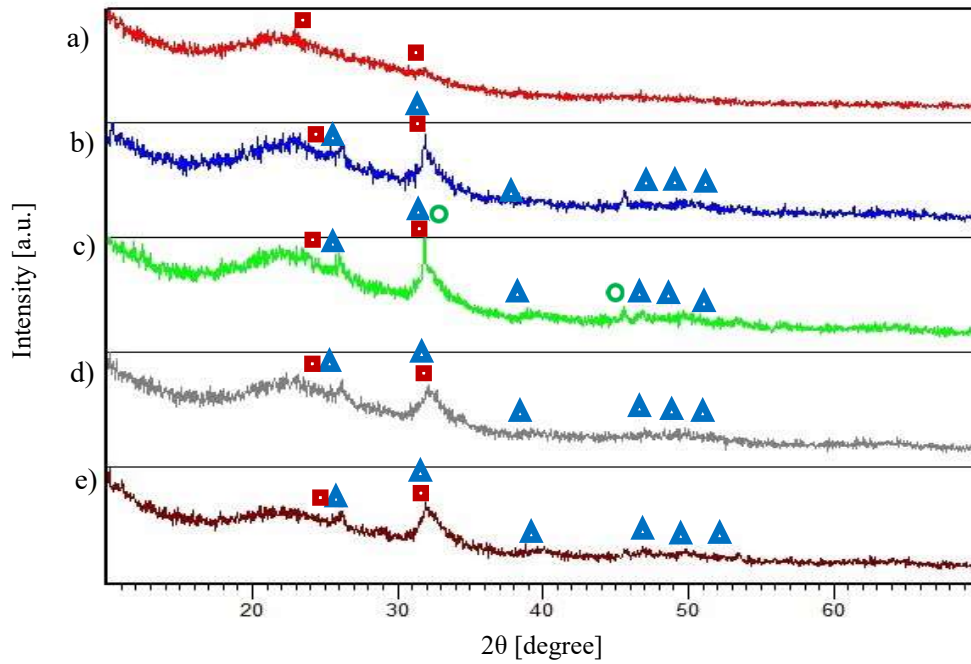


Figure 4.36: Comparison of XRD spectra of S2 where a) S2 0d b) S2 1d c) S2 3d d) S2 7d and e) S2 14

Figure 4.37 show XRD spectra of SB1 glass at each analyzed time point.

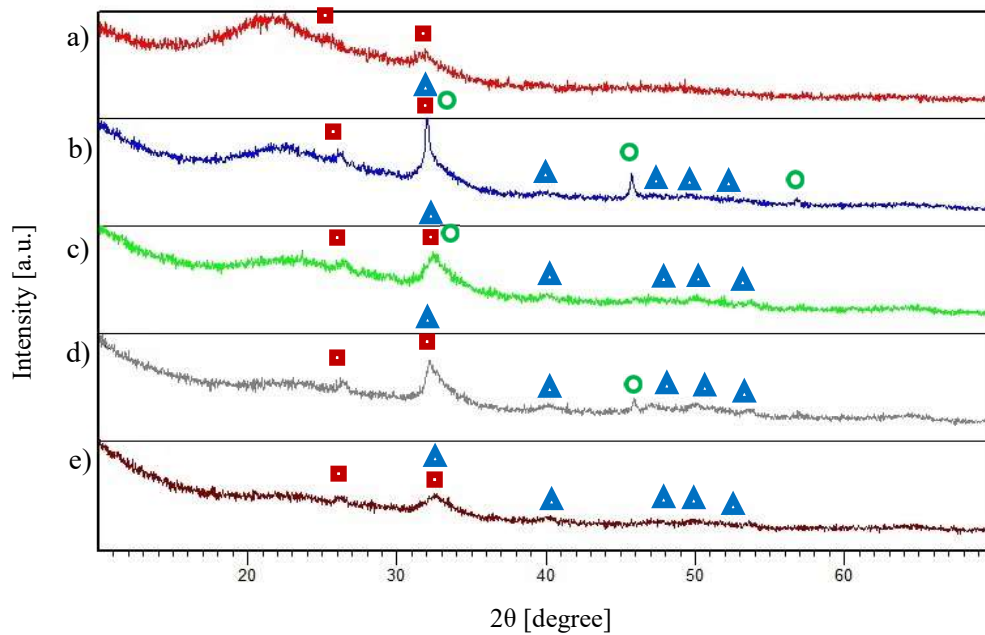


Figure 4.37: Comparison of XRD spectra of SB1 where a) SB1 0d b) SB1 1d c) SB1 3d d) SB1 7d and e) SB1 14d

Figure 4.38 show XRD spectra of SB2 glass at each analyzed time point.

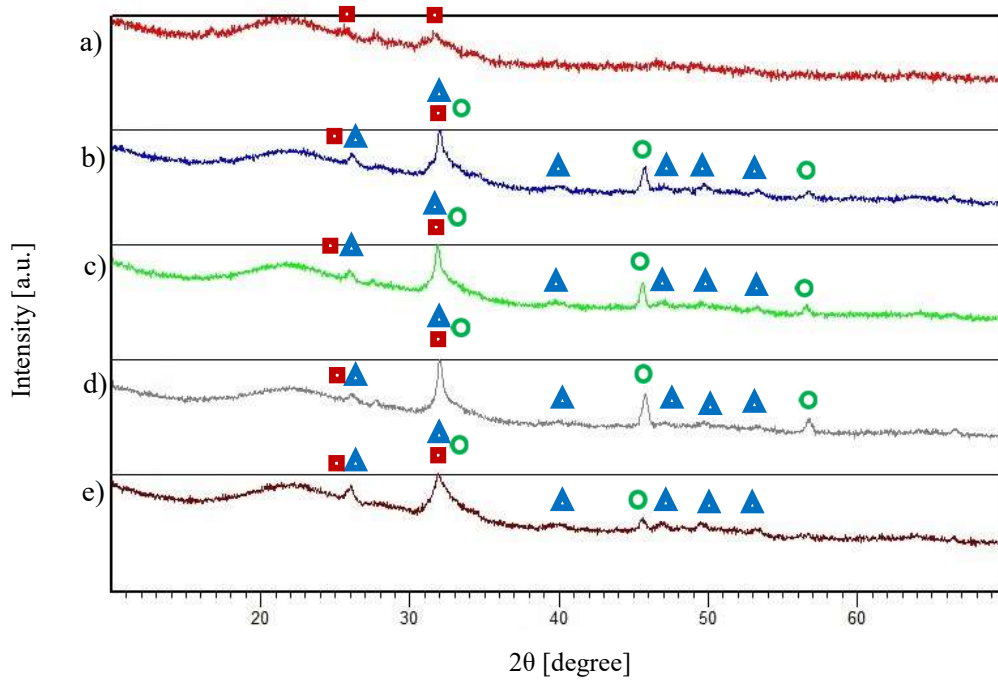


Figure 4.38: Comparison of XRD spectra of SB2 where a) SB2 0d b) SB2 1d c) SB2 3d d) SB2 7d and e) SB2 14d

Figure 4.39 show XRD spectra of SBCu1 glass at each analyzed time point.

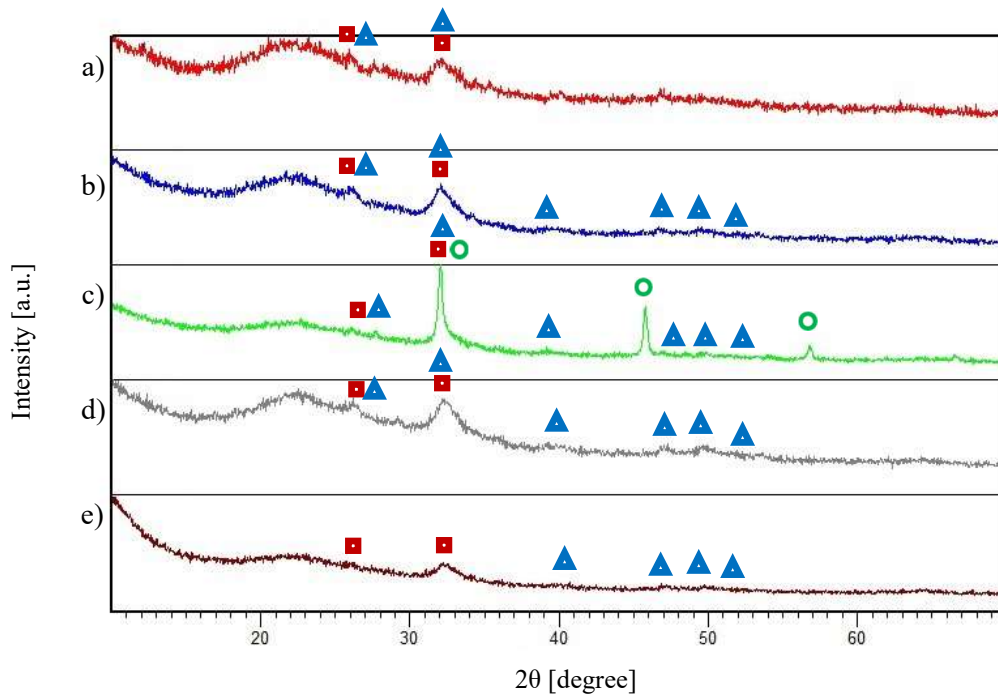


Figure 4.39: Comparison of XRD spectra of SBCu1 where a) SBCu1 0d b) SB2 1d c) SBCu1 3d d) SBCu1 7d and e) SBCu1 14d

Figure 4.40 show XRD spectra of SBCu1 glass at each analyzed time point.

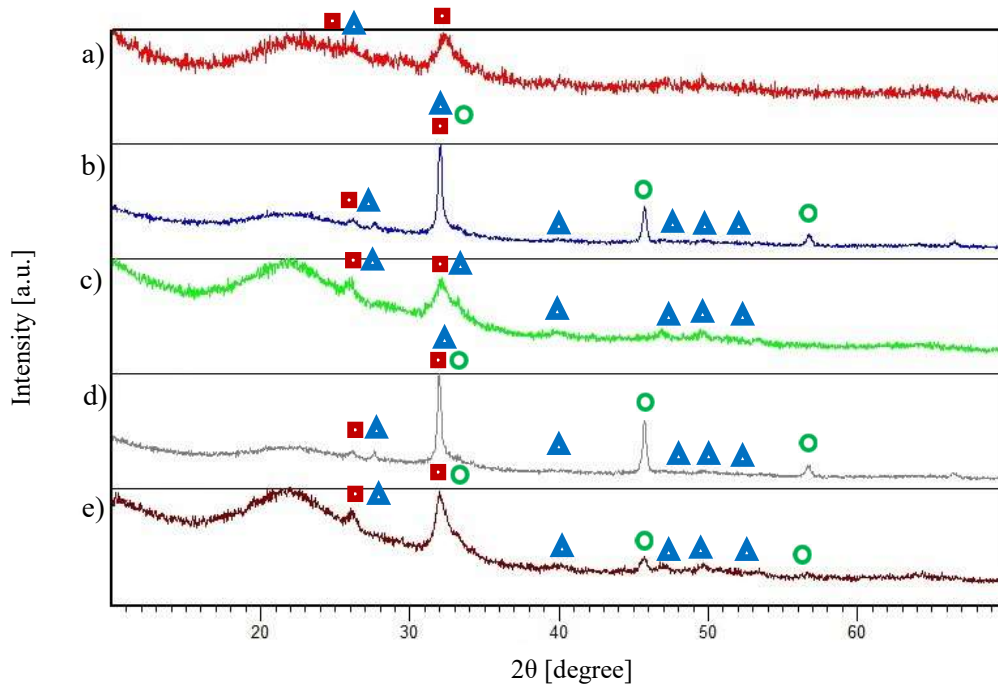


Figure 4.40: Comparison of XRD spectra of SBCu2 where a) SBCu2 0d b) SBCu2 1d c) SB2 3d d) SBCu2 7d and e) SBCu2 14d

The hydroxyapatite peaks that correspond to peaks present in SB1 after 1 day of immersion in SBF are shown Figure 4.41.

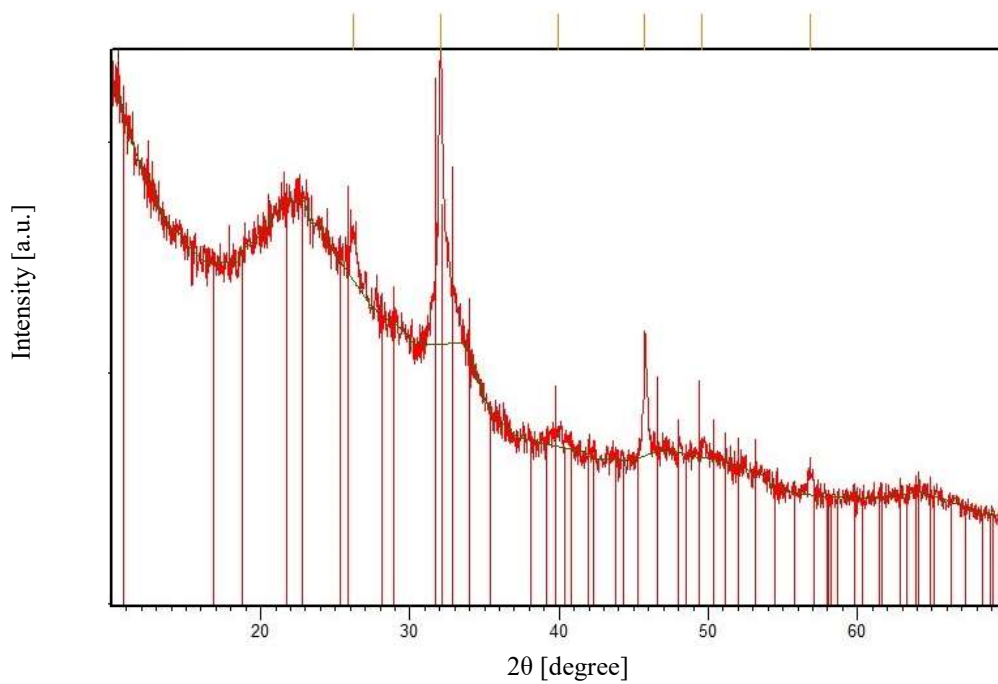


Figure 4.41: Peaks of hydroxyapatite in SB1 1d

Figure 4.42 show the peaks of hydroxyapatite that can be recognized in XRD spectra of SB2 after 1 day of immersion in SBF.

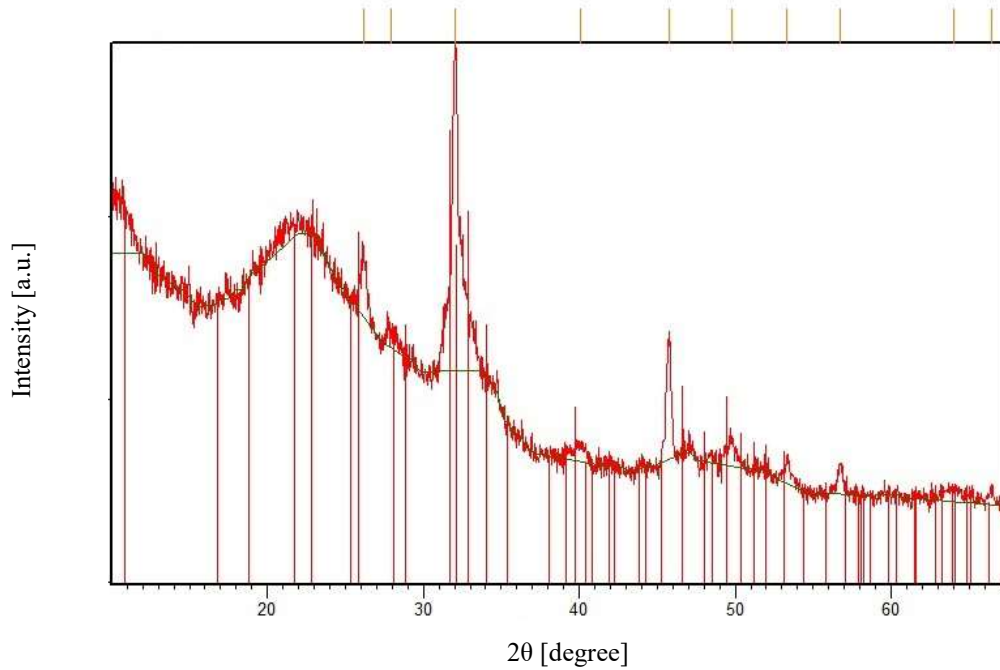


Figure 4.42: Peaks of hydroxyapatite in SB2 1d

Peak list of all SB glasses after 1 day of immersion are compared with peaks of hydroxyapatite (code 01 074 0566) in Figure 4.43.

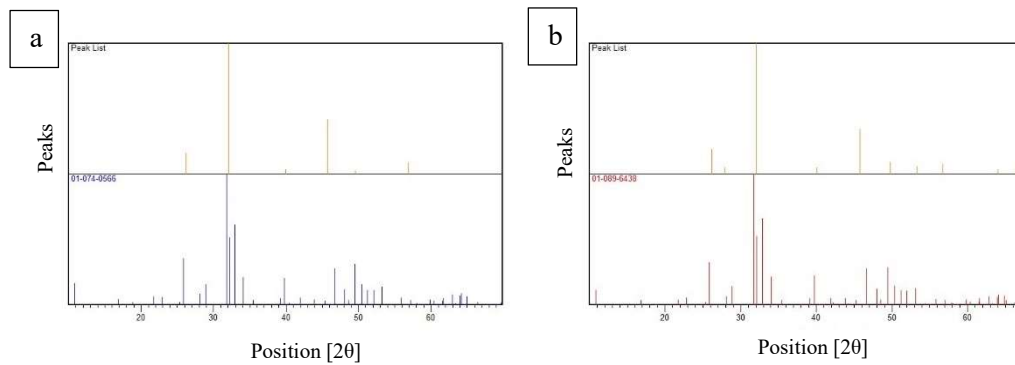


Figure 4.43: Hydroxyapatite peaks vs peaks in a) SB1 1d and b) SB2 1d

Peak list of SBCu glasses after 1 day of immersion are compared with peaks of hydroxyapatite (code 01 074 0566) in Figure 4.44.

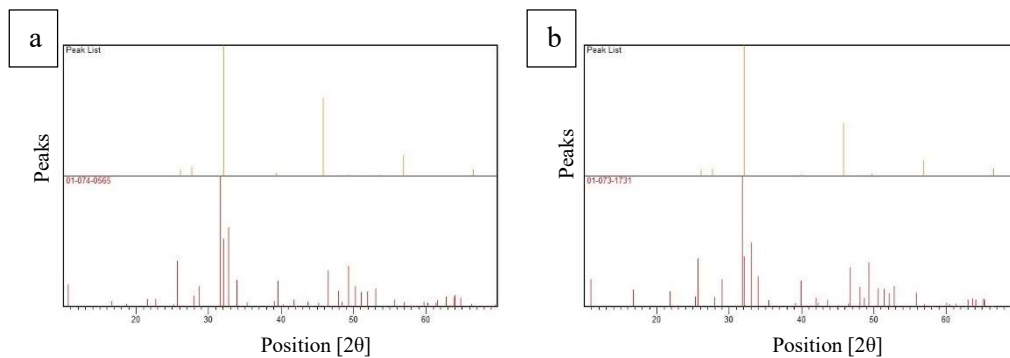


Figure 4.44: Hydroxyapatite peaks vs peaks in a) SBCu1 1d and b) SBCu2 1d

As above mentioned, in Figure 4.45, the typical peaks of NaCl are observable.

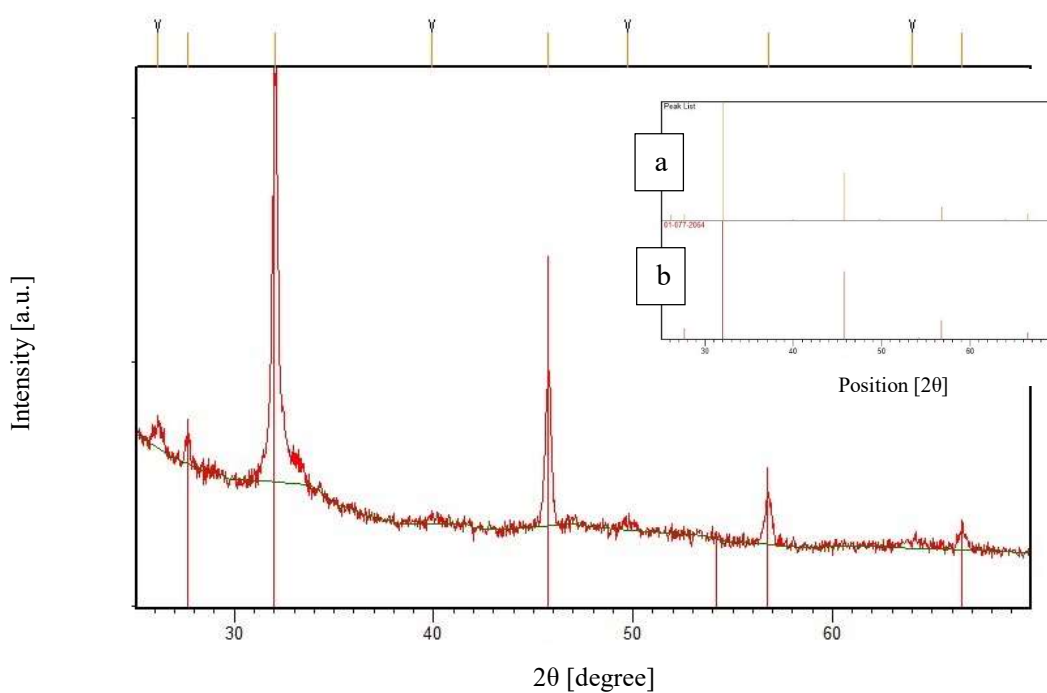


Figure 4.45: Peaks of Ca_2SiO_4 in SBCu2 1d where a) peak list of SBCu1 1d and b) peak list of sodium chloride

SB1 powders immersed until 14 days in SBF is reported in Figure 4.46.

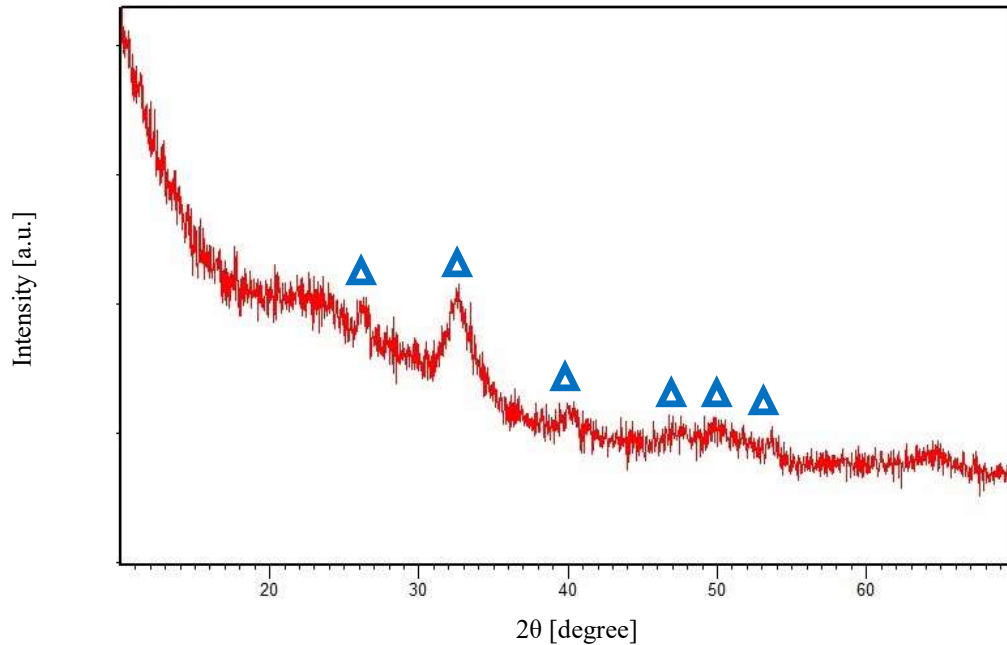


Figure 4.46 XRD spectrum of SB1 14d

The FE-SEM images reveal that the surface of the glass nanoparticles undergoes important changes during the reaction with SBF, confirming the formation of a hydroxyapatite-like layer. For example, in Figure 4.47, Figure 4.48, Figure 4.49, Figure 4.50 and Figure 4.51, it is possible to observe the growth of HA-like nanoparticles on the glass surface after soaking the sample for 14 days.

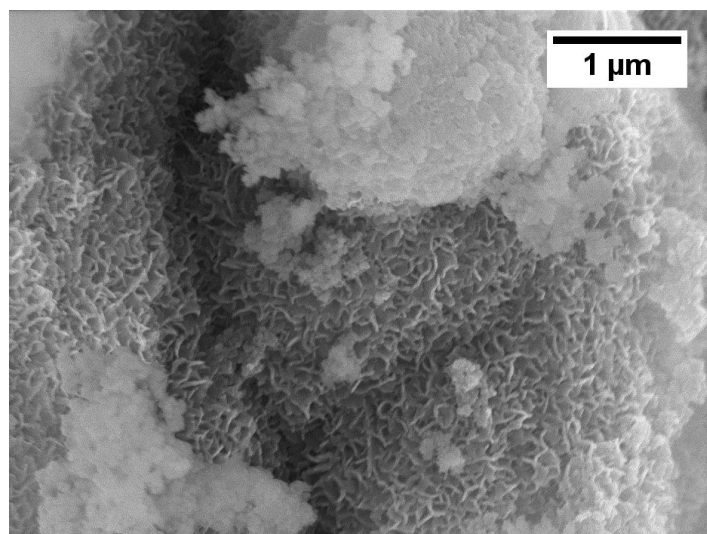


Figure 4.47: SEM micrograph of SB1 after 14 days in SBF (at 50K X)

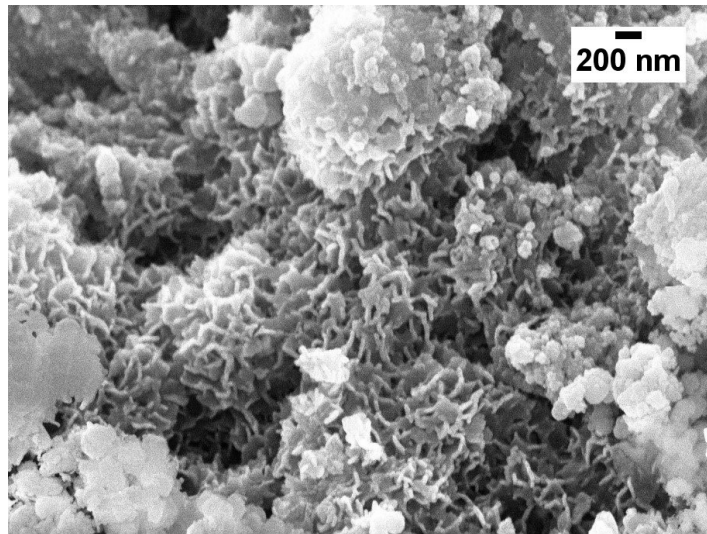


Figure 4.48 SEM micrograph of SB1 after 14 days in SBF (at 50K X)

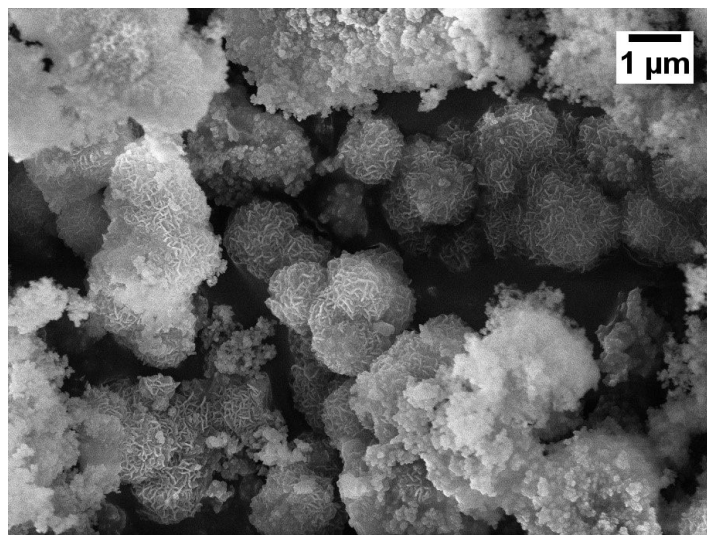


Figure 4.49: SEM micrograph of SB2 after 14 days in SBF (at 20K X)

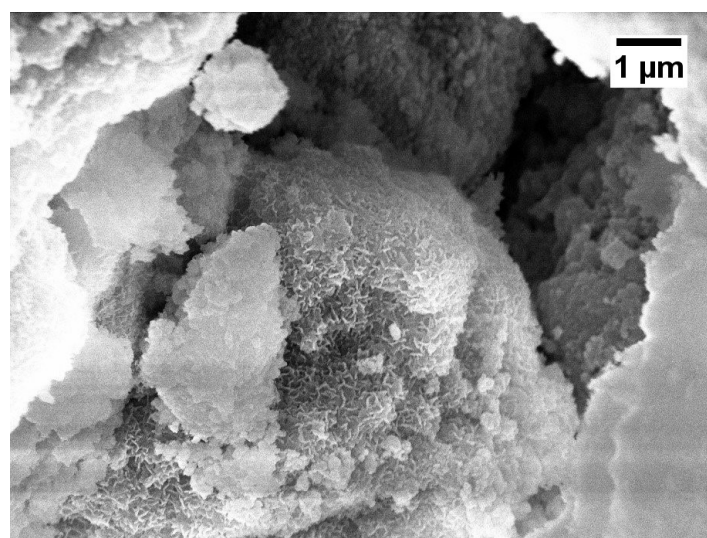


Figure 4.50 SEM micrograph of SBCu1 after 14 days in SBF (at 30K X)

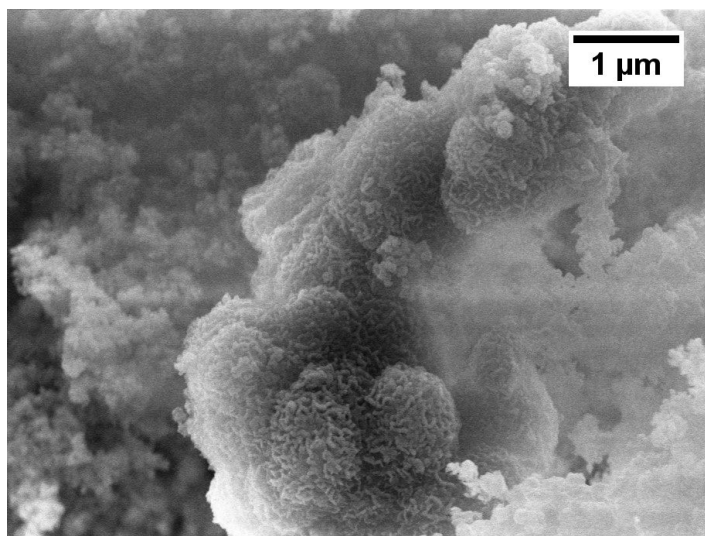


Figure 4.51 SEM micrograph of SBCu2 after 14 days in SBF (at 40K X)

In conclusion, the synthesized glasses are resulted to be bioactive and actual results confirm previous experimental observations that have shown that the addition of boron did not inhibit the calcium solubility in boron-modified glasses of the CaO-P₂O₅-SiO₂ system and that BGs containing boron have a higher bioactivity than pure silicate glasses.

4.2 Optimization of electrospinning solution

4.2.1 Fiber morphology observations

As explained before in chapter “Materials and methods”, the first composite fibers have been electrospun from a solution of PCL in a mixture of acetic acid and formic acid, containing 5% of glass powders (in respect to polymer amount), that have been mixed with the polymer solution thanks to immersion of the final electrospinning solution (PCL+glass) in US bath for 10 min [120][23].

Morphological analysis of these fibers show the presence of big aggregates of glass particles in all electrospun fibers mats (see Figure 4.52, Figure 4.53 and Figure 4.54). Moreover, by looking at these SEM images, it was not possible to notice a relevant difference between fibers obtained from solutions containing glasses prepared by synthesis 1 (S1, SB1 and SBCu1) or by synthesis 2 (S2, SB2 and SBCu2), confirming qualitative observations made during preparation of the different electrospinning solutions.

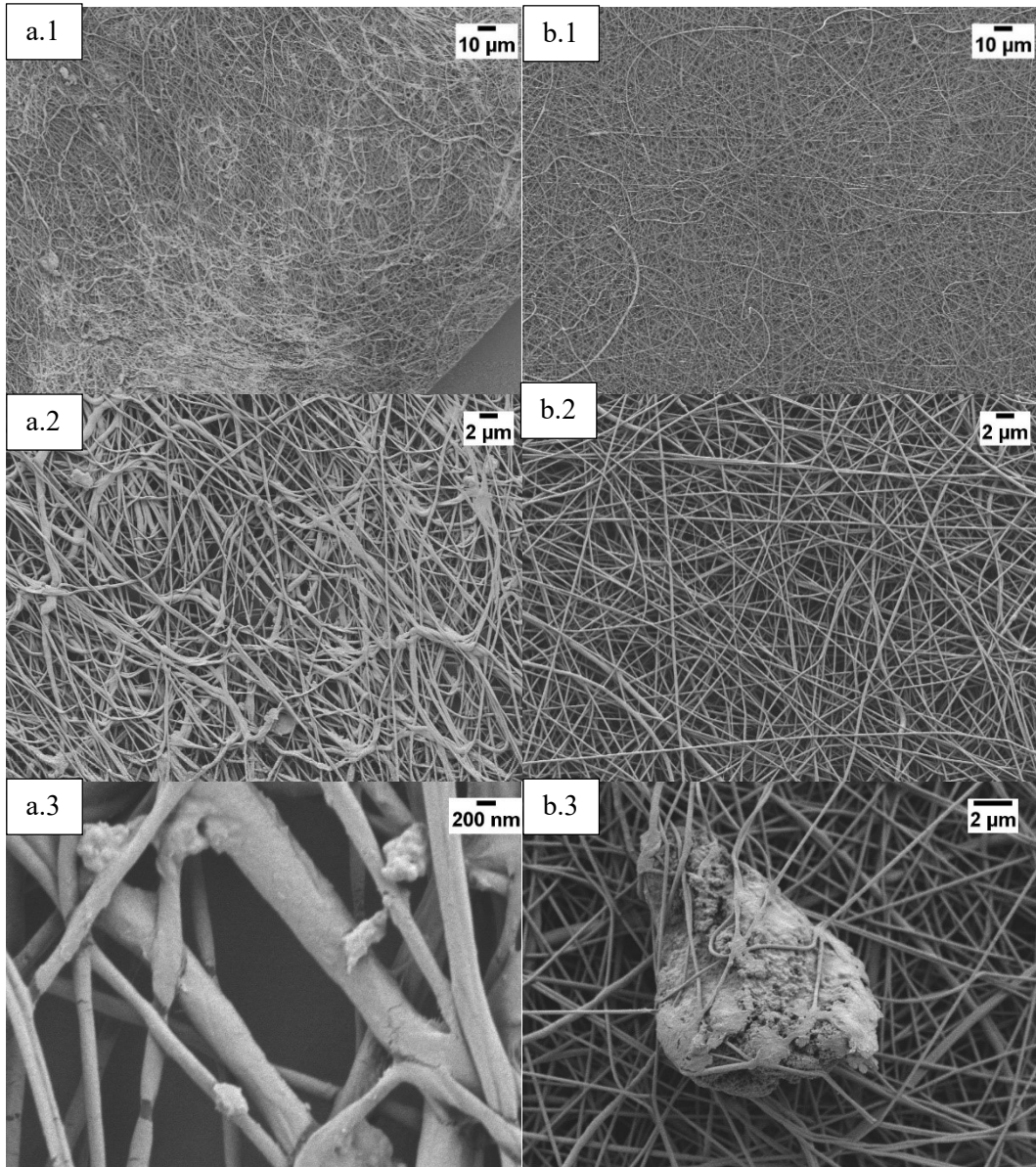


Figure 4.52: SEM micrographs of fibers containing 5% of S1 and S2 PCL/AA/FA/S1(5%) at 1K X (a.1), at 5K X (a.2) and at 45K X (a.3) vs PCL/AA/FA/S2(5%) at 1K X (b.1), at 5K X (b.2) and at 10K X (b.3)

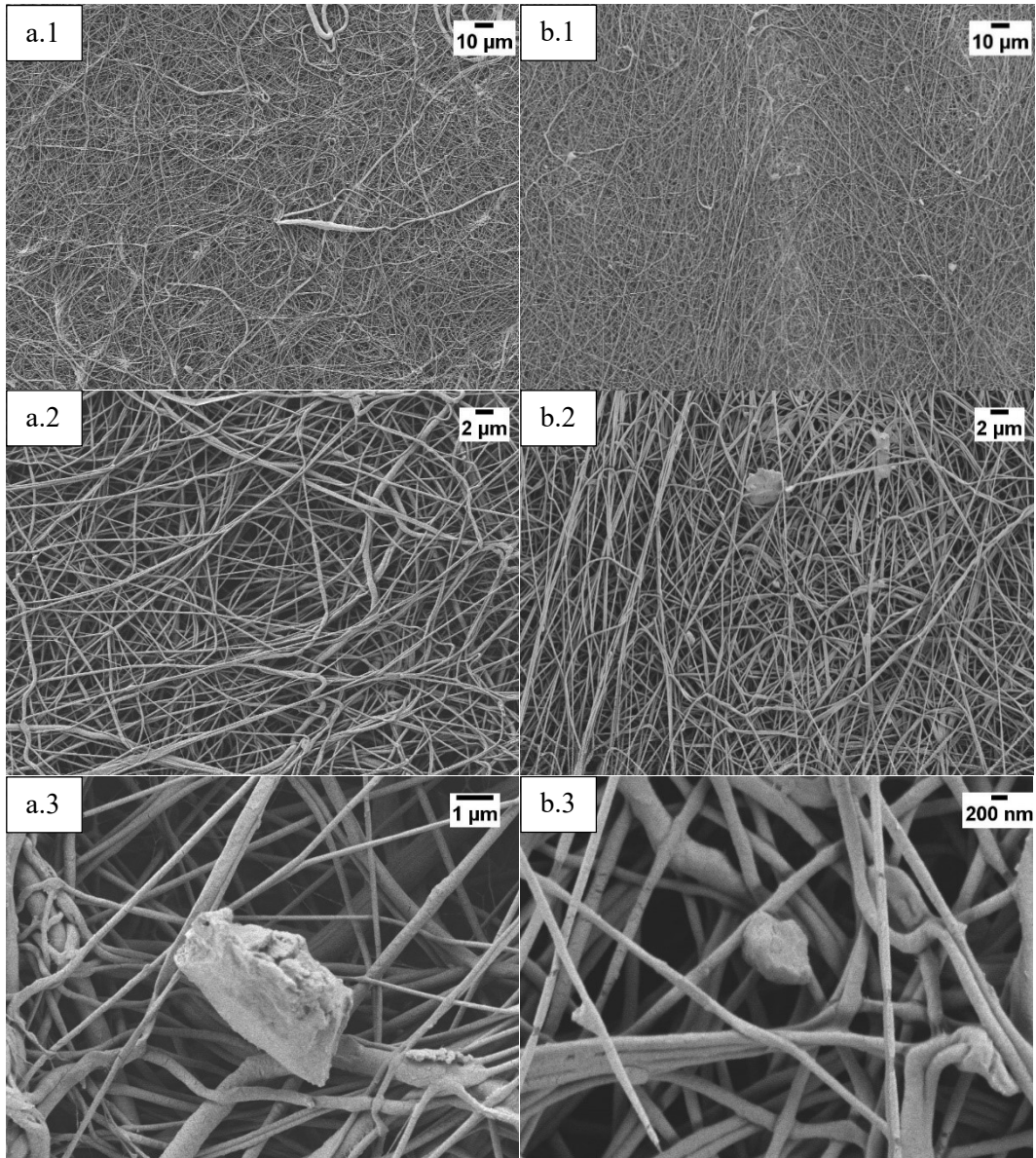


Figure 4.53: SEM micrographs of fibers containing 5% of SB1 and SB2 PCL/AA/FA/SB1(5%) at 1.00 K X (a.1), at 5K X (a.2) and at 20K X (a.3) vs PCL/AA/FA/SB2(5%) at 1K X (b.1), at 5K X (b.2) and at 20K X (b.3)

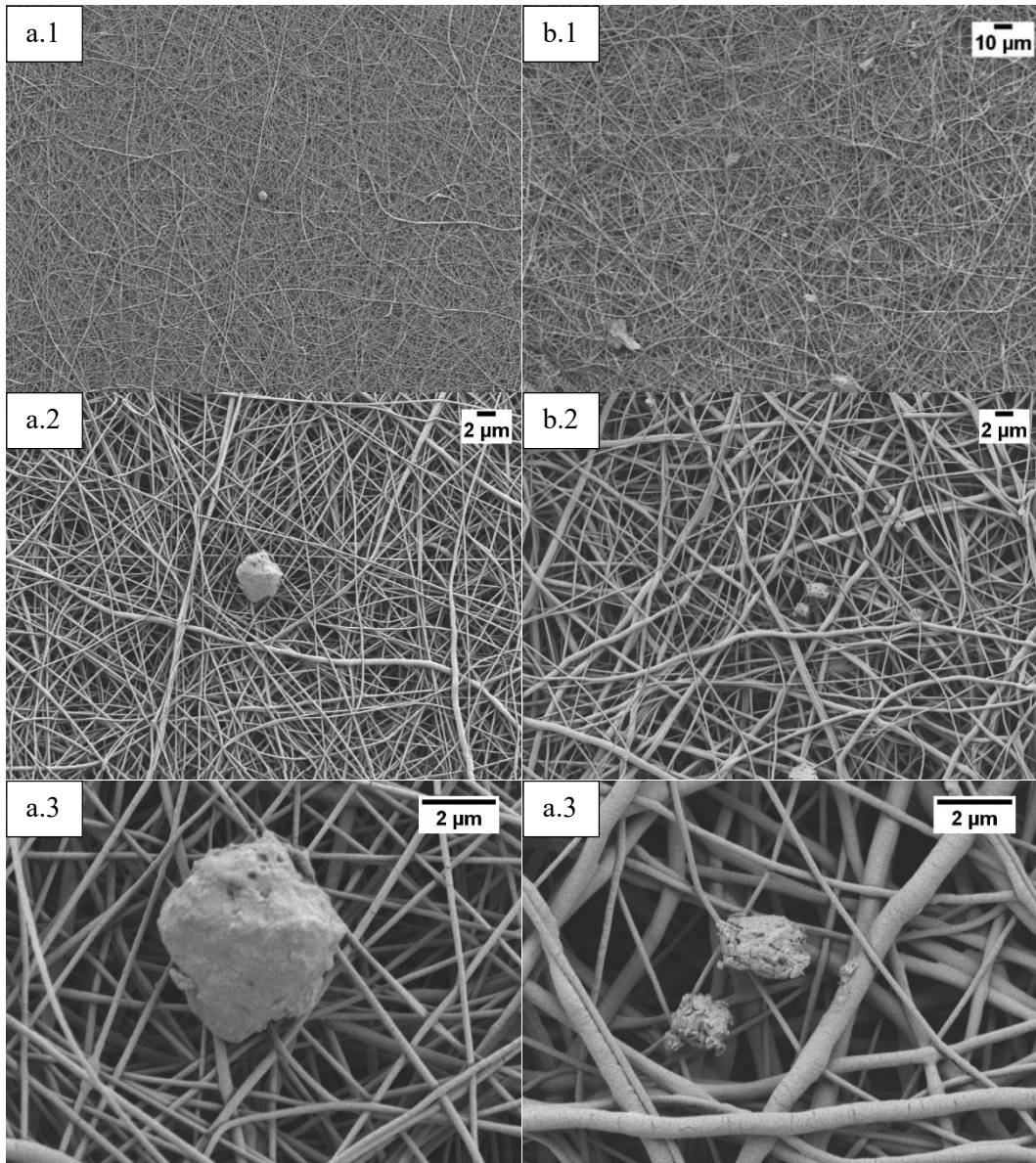


Figure 4.54: SEM micrographs of fibers containing 5% of SBCu1 and SBCu2 PCL/AA/FA/SBCu1(5%) at 1K X (a.1), at 5K X (a.2) and at 20K X (a.3) vs PCL/AA/FA/SBCu2(5%) at 1K X (b.1), at 5K X (b.2) and at 20K X (b.3)

In any case, a first acellular bioactivity test was carried out (until 7 days of immersion in SBF) in order to assess the bioactivity of these composite fibers. These results (Figure 4.55, Figure 4.56, Figure 4.57 and Figure 4.58) show that a concentration of 5% of glass powders was insufficient to obtain bioactive composite fibers with these glasses. As example, some SEM micrographs are reported below. All the reported images refer to the first day of immersion, because, due to the little thickness of the mats, after seven days in SBF most of the samples were broken.

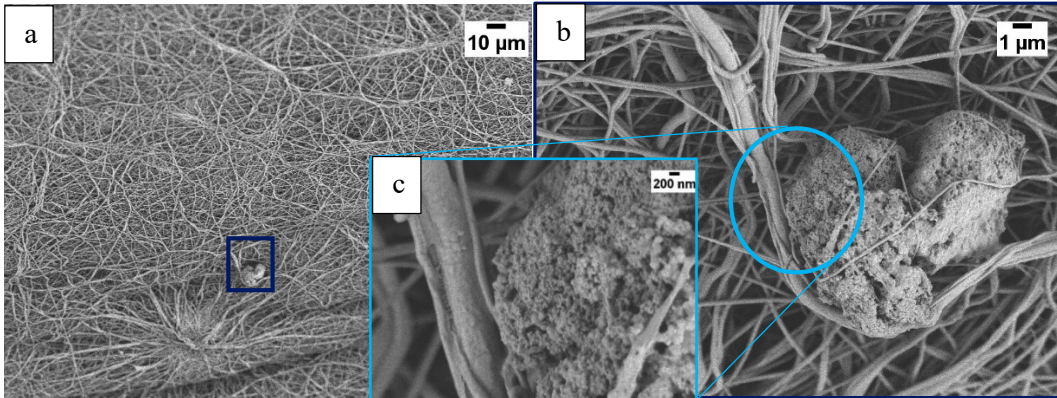


Figure 4.55: PCL/AA/FA/SI(5%) SBF 1d where a) 1K X b) 10K X c) 45k X

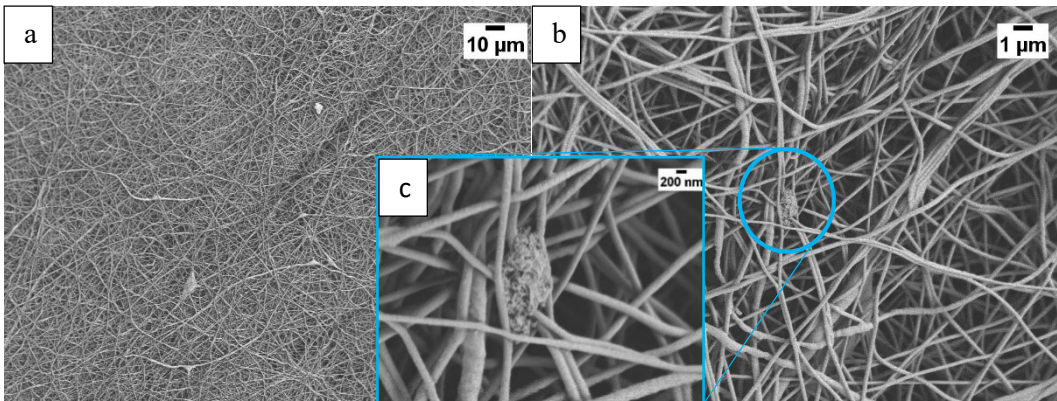


Figure 4.56: PCL/AA/FA/S2(5%) SBF 1d where a) 1K X b) 10K X c) 45K X

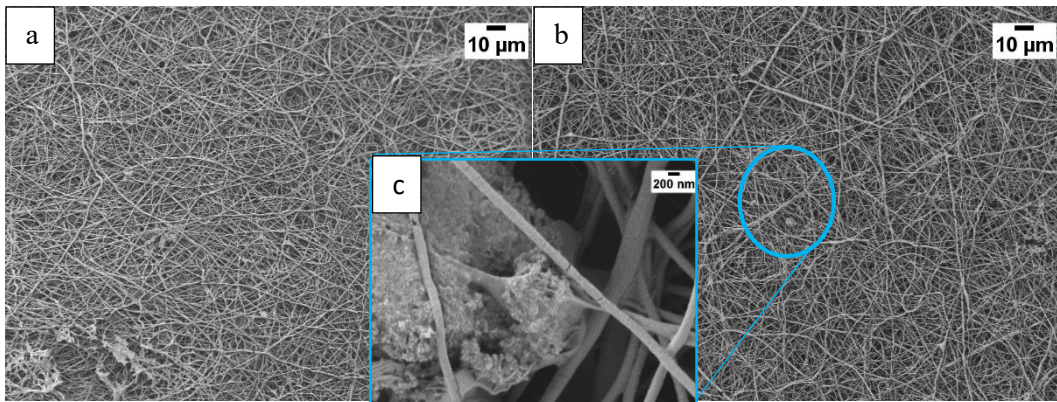


Figure 4.57: PCL/AA/FA/SBCu1(5%) SBF 1d where a) 1K X b) 10K X c) 45K X

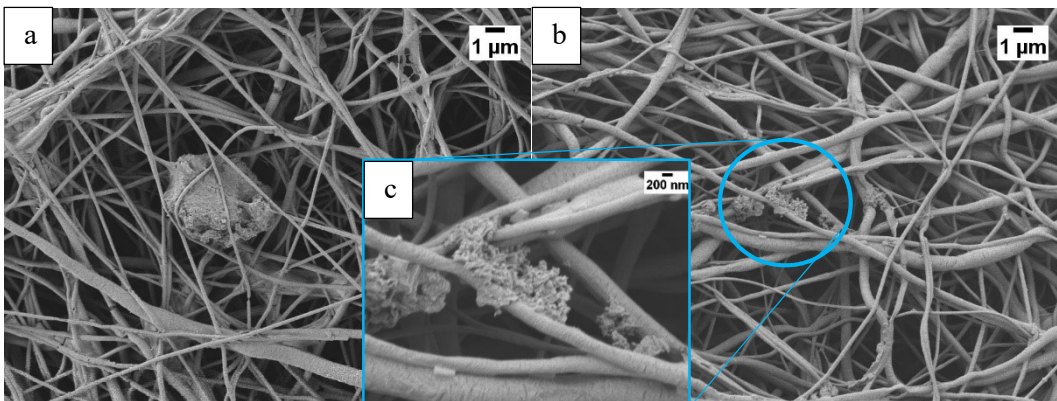


Figure 4.58: PCL/AA/FA/SBCu2(5%) SBF 1d where a) 1K X b) 10K X c) 45K X

At this point, it was observed, that, due to humidity, the aggregation of the glass nanoparticles was increased, so to remove the current aggregation, avoid further aggregation and improve the dispersion of the glass powders in the PCL solution, glasses were conserved in desiccator, pressed with mortar and dried in heater at 60°C overnight before use.

As explained by *Augustine et al.* [82], the formation of agglomerates is related to the high surface energy of the nanoparticles that results in a lacking dispersion in the PCL solution. Consequences of that agglomeration are a reduced electrospinning efficiency, a limited nanoparticle loading capacity and a poor dispersion within the fibers. Therefore, different addition methods have been tried to overcome this agglomeration and disperse the glass particles in the PCL matrix, aiming to obtain a homogenous dispersion (see Figure 4.59). All these trials have been carried out using S1 glass. In fact, glasses obtained through synthesis 1 (S1, SB1 and SBCu1) were initially preferred to glasses prepared through synthesis 2, because the first ones are more packed and it was supposed it could be easier to increase the glass concentration (20% and 30%) in the polymeric solution, in order to improve the bioactivity of the composites.

In details, the following methods of addition were tried:

- a) after glass addition, 10 min of magnetic stirring and 1 min in US bath;
- b) after glass addition, manual mixing for 2 min and 1 min in US bath;
- c) addition of glass powders in 1 ml of the mixture of acetic acid and formic acid, followed by manual mixing and later addition in the polymer solution (glass dispersion method);
- d) method similar to the previous one, but in this case glass powders were mixed with Pluronic (1%w/w) in the mixture of AA and FA [18].

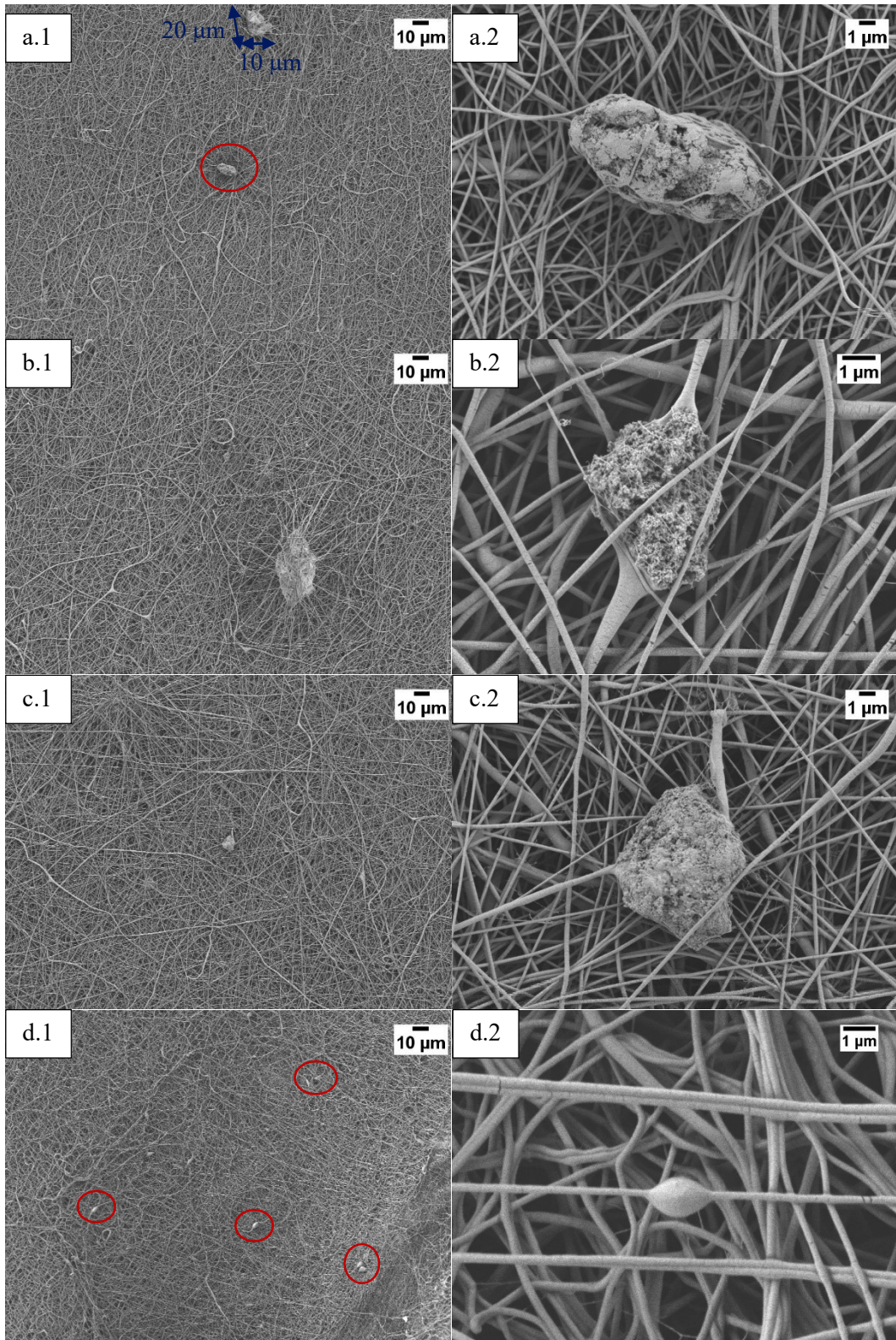


Figure 4.59: Comparison between different methods of glass addition
 SEM micrographs of PCL/AA/SI(5%) prepared adding glass through the previous explained method A (a.1 and a.2), method B (b.1 and b.2), method C (c.1 and c.2) and method D (d.1 and d.2)

Hence, the glass dispersion method was selected. This selection was based on the evaluation of the main features of the various electrospinning solutions and the analysis of the SEM micrographs of the samples obtained with the different methods of glass addition, reported in Figure 4.59. Referring to the characteristics of the prepared electrospinning solutions, viscosity and homogeneity were evaluated.

Moreover, taking into consideration the size of the agglomerates, that were still present in the samples, at this point it was decided to try the system PCL/AA. Indeed, the size of the conglomerates was bigger than the average size of the PCL nanofibers and, according to literature results [18][20], electrospinning a solution of PCL in acetic acid using 11 cm as working distance, an applied voltage of 15 kV and a flowrate of ca. 0.4 cc/h allows to obtain fibers with average size in the micrometric range. SEM micrographs of fibers obtained from solutions of PCL in a mixture of acetic acid and formic acid (20 %w/v) and PCL in acetic acid (15 %w/v) are shown in Figure 4.60 and Figure 4.61. In both cases, glass powders were added thanks to the method of the glass dispersion.

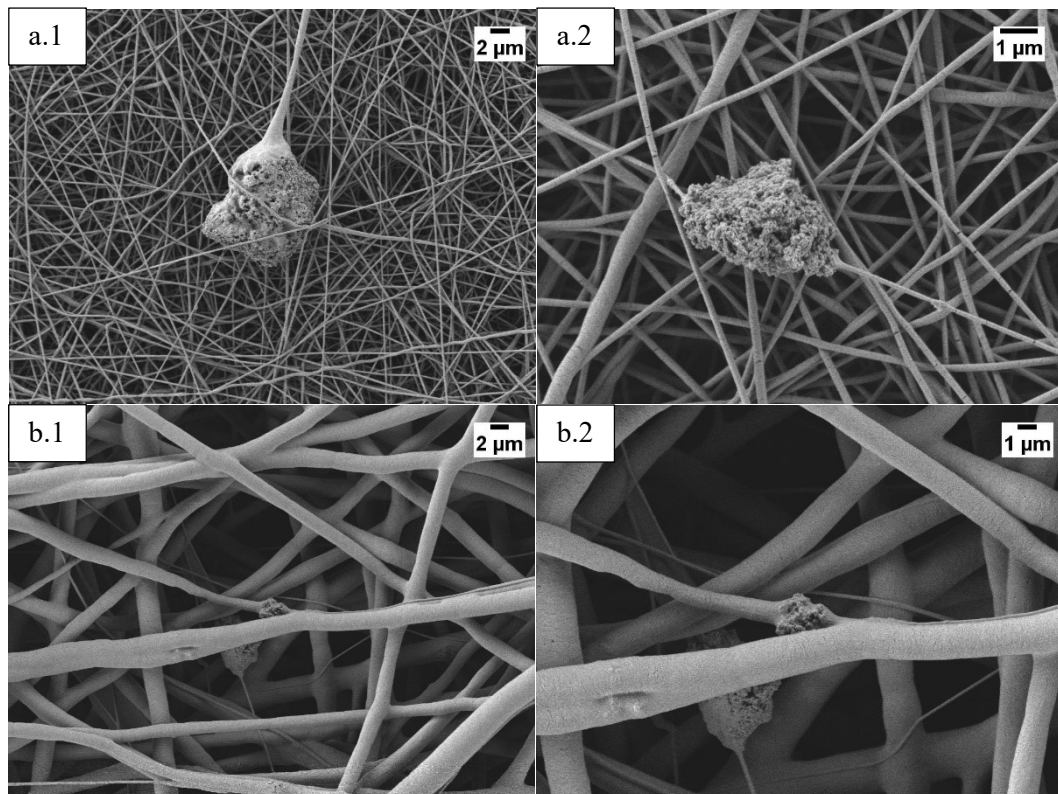


Figure 4.60: Comparison between PCL/AA/FA and PCL/AA systems
SEM micrographs of fibers obtained by PCL in AA/FA at 5.0K X (a.1) and at 20K X (a.2) vs
fibers by PCL in AA at 5K X (b.1) and at 20K X (b.2) in case of addition of 20% SBI

As a result of this comparison, the system with the formic acid was excluded and the system PCL/AA was preferred, because in this case the agglomerated nanoparticles seem to be better link to the PCL fibers, as underlined in Figure 4.61.

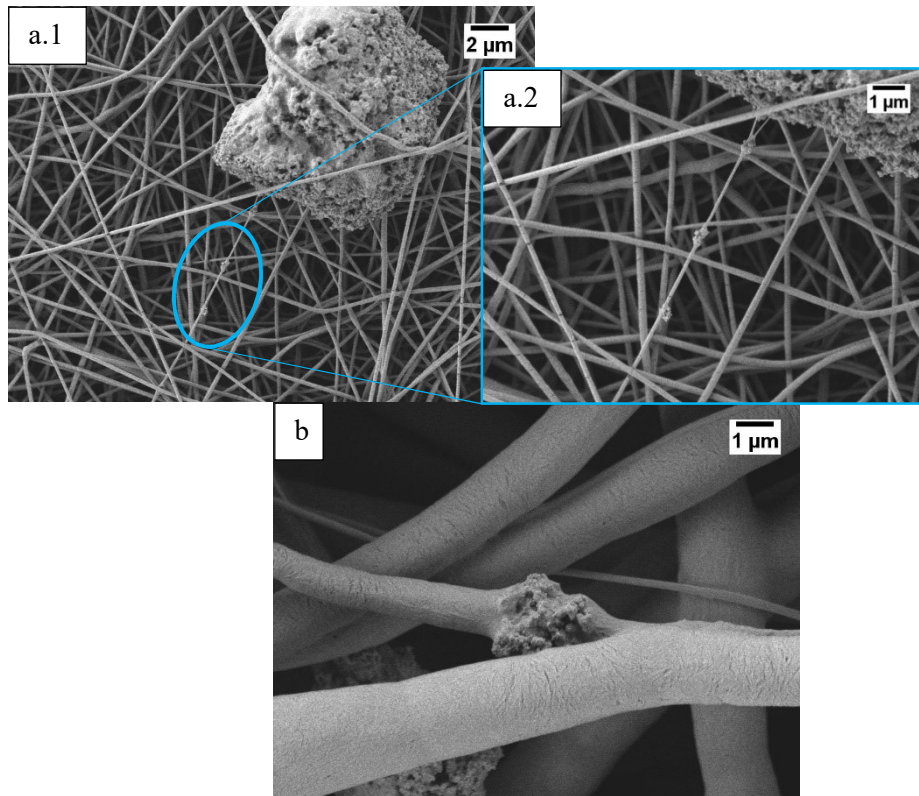


Figure 4.61: Examples of glass incorporation in fibers
SEM micrographs of PCL/AA/FA/SB1(20%) at 10.00 K X (a.1) and details at 20.00 K X (a.2) vs PCL/AA/SB1(20%) at 20.00 K X (b), which corresponds to detail of image b.1 and b.2 of Fig. 60

In the following images (Figure 4.62), it is possible to observe that the increase of glass concentration up to 30% results in many aggregates; anyway they are well linked to the PCL fibers.

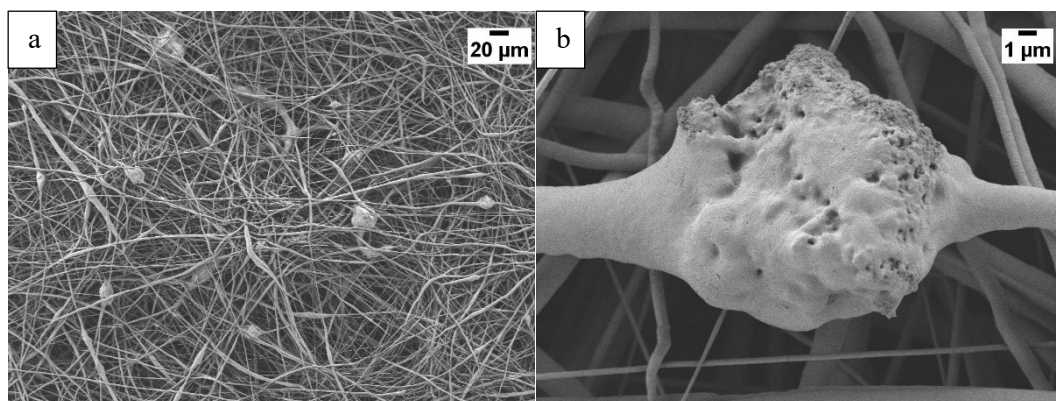


Figure 4.62: SEM micrographs of PCL/AA/FA/SBCu1(30%) at 500.00 K X (a) and at 10.00 K X (b)

However, the glass dispersion method brings about results which are not reproducible, because every time that a new electrospinning solution was prepared, it was not possible to pour all glass dispersion (20% of glass in 1 ml of acetic acid) in the polymer solution, so that different electrospinning solutions with different and unverifiable glass concentration and consequently different solution viscosity and conductivity were obtained. Moreover, as above mentioned, before use, glasses were pressed with the mortar, in order to crumble them as much as possible, and it was observed that, although all these treatments, it was still very difficult to crumble SBCu1 glass (that represents the hardest synthesized glass), so that in the SBCu1 dispersion are still present remarkable big conglomerates and the nanoparticles are still not completely homogeneously dispersed in the PCL matrix. Due to all these observations, it was decided to try to use the glasses prepared through synthesis 2 (S2, SB2 and SBCu2), which were directly added to the PCL solution, making the glass addition being followed by 2 min of manual stirring, 5 min of magnetic stirring and 1 min in US bath.

Due to the voluminous size of these glasses, the concentration of glass was lowered to 10% and a needle with bigger diameter (21 G x 7/8") was used. After assessing the electrospinnability of the PCL/AA system with a 10% of S2, SB2 and SBCu2 glasses, the glass concentration was again increased to 20%.

An attempt was also done with SBCu2 in order to raise the glass concentration up to 30% in respect to polymer amount, but with the increase of nanoparticle content, no significative improvement in quantity of incorporated glass was detected and only the number and size of the micrometric agglomerates increased (in agreement with results previously obtained by *Moura et al.* [82]).

In Figure 4.63 a comparison between fibers containing the theoretical glass concentration of 10%, 20% and 30% is shown.

In order to complete this overview of the optimization process of electrospinning solutions and fiber fabrication, few brief comments on the electrospinning time should be done. Initially all solutions were electrospun for 10 minutes. In fact, it was observed that, in case of PCL/AA/FA system, after 15 minutes, when pulled off, the fiber mats tend to delaminate. For the fabrication of the final samples, the electrospinning time was raised again to 15 minutes because of the small

thickness of the mats. In any case, in order to pull them off without breaking them, as soon as the electrospun mats were fabricated, the samples were immersed for few seconds in a bath of EtOH and then when the solvent started to evaporate the fibers were carefully detached.

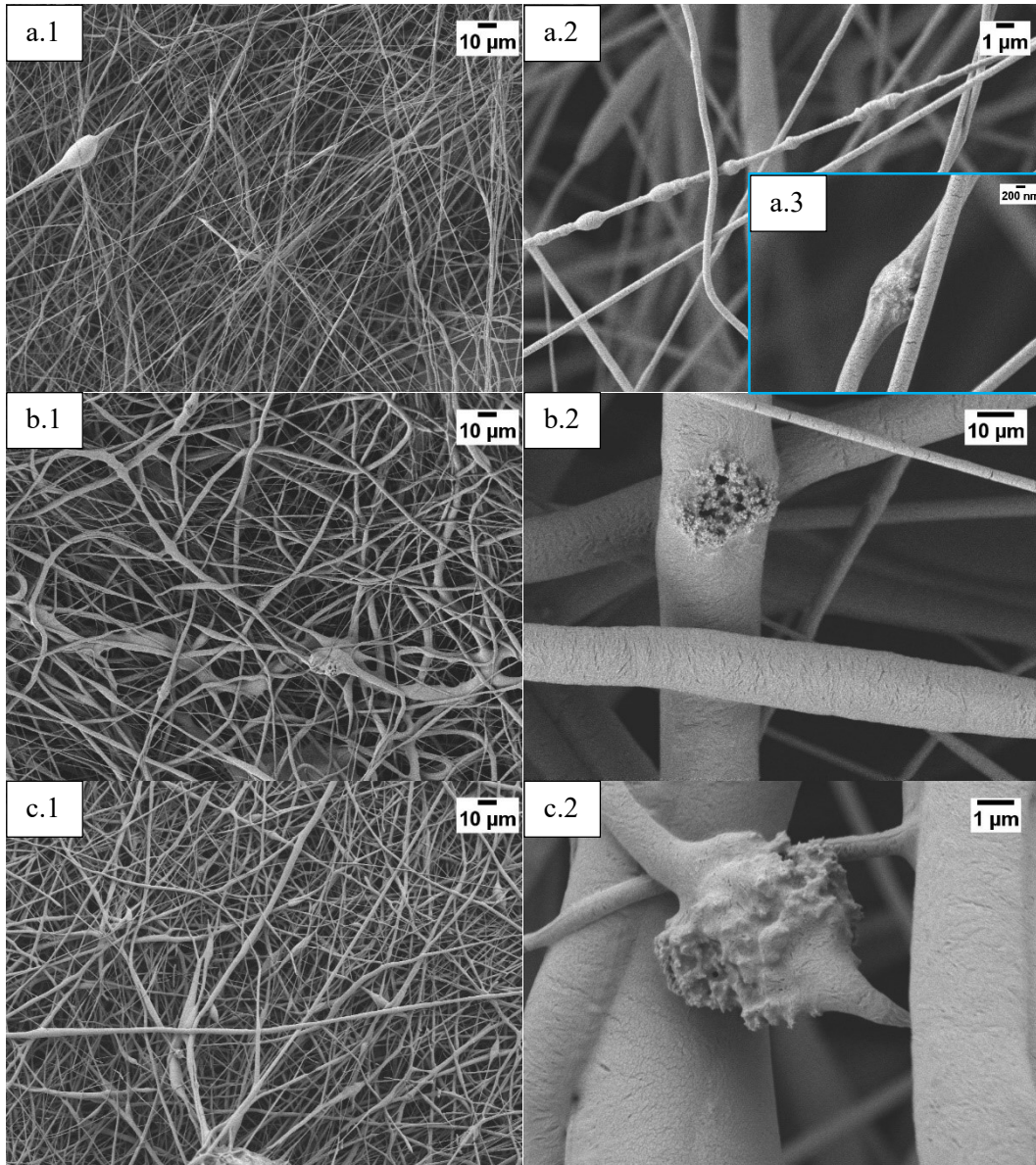


*Figure 4.63: Comparison of fibers containing different concentration of SBCu2
SEM micrographs of PCL/AA/SBCu2(10%) at 1K X (a.1), 20K X (a.2) and at 45K X (a.3)
vs PCL/AA/SBCu2(20%) at 1K X (b.1) and 20K X (b.2)
vs PCL/AA/SBCu2(30%) at 1K X (c.1) and 20K X (c.2)*

To summarize, the sample that have been further completely characterized are:

- PCL/AA/S2(20%), 11 cm, 15 kV and flowrate of 0.39 cc/h (pump selector rate on 2.9)
- PCL/AA/SB2(20%)11 cm, 15 kV and flowrate of 0.39 cc/h (pump selector rate on 2.9)
- PCL/AA/SBCu2(20%), 11 cm, 15 kV, flowrate of 0.68 cc/h (pump selector rate on 5).

4.3 Features of the final mats

4.3.1 Morphological characterization

The final samples have been morphologically characterized by SEM analysis, as shown in Figure 4.64, Figure 4.65 and Figure 4.66, and their diameters have been calculated using software ImageJ.

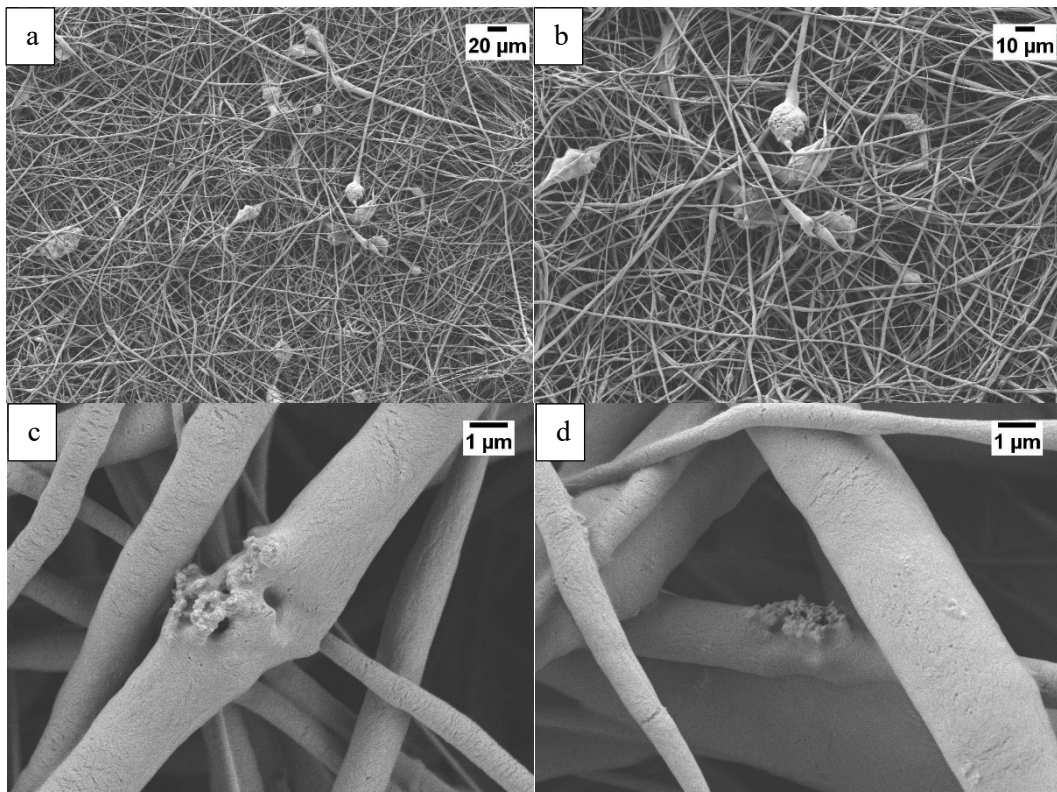


Figure 4.64: SEM micrographs of **PCL/AA/S2(20%)** at 500 X (a), at 1K X (b) and at 20K X (c) and (d)

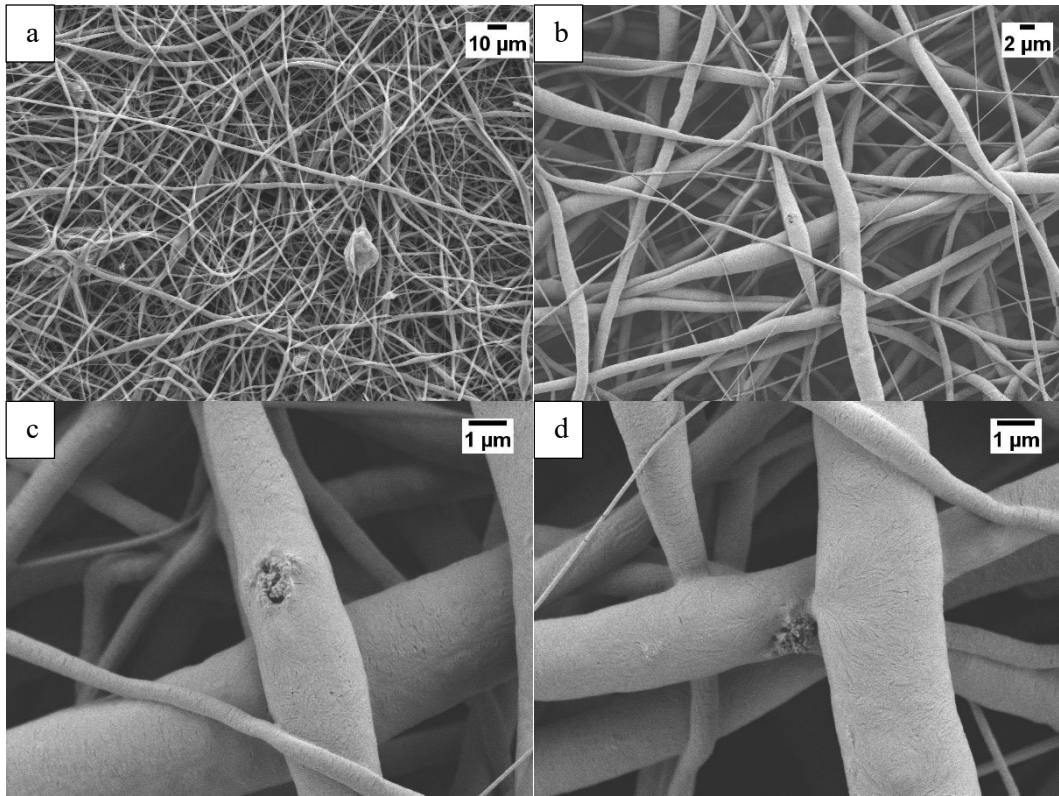


Figure 4.65: SEM micrographs of *PCL/AA/SB2(0%)* at 1K X (a), at 4K X (b), at 20K X (c) and (d)

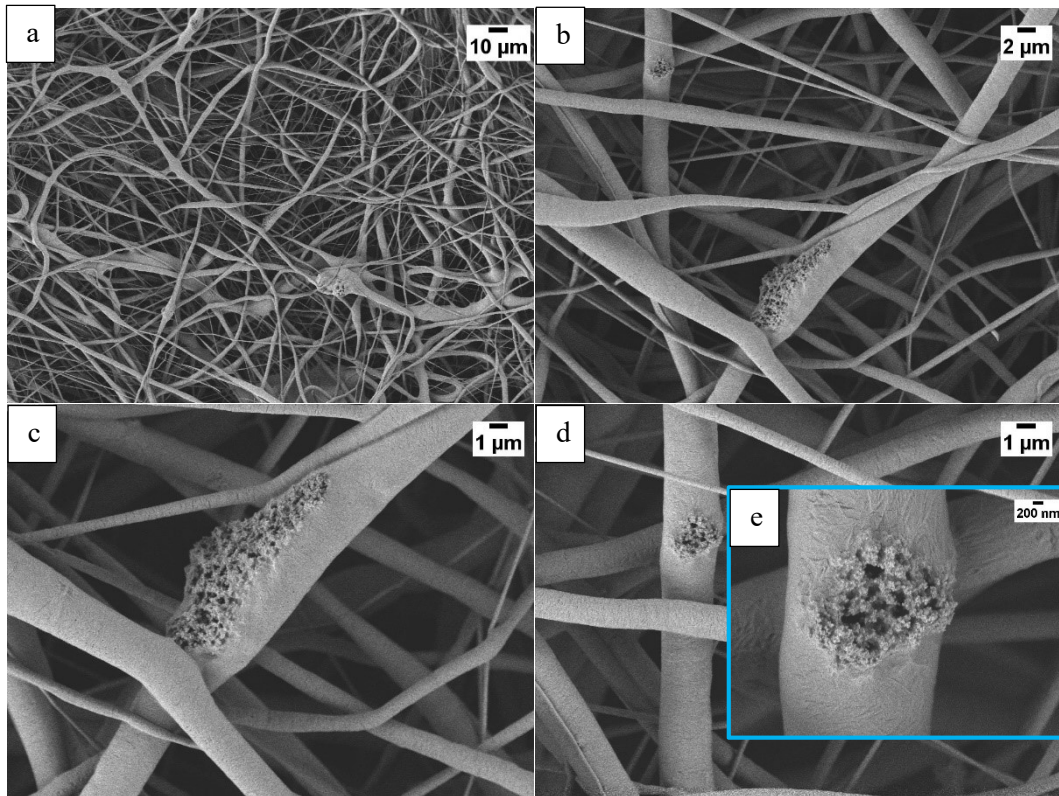


Figure 4.66: SEM micrographs of *PCL/AA/SBCu2(0%)* at 1K X (a), at 5K X (b), at 10K X (c) and (d) and at 45K X (e)

It is observable that a concentration of 20% of glass led to electrospun mats that are very rich of glass, as desired. Although some clusters of particles are still present, glass powders are well incorporated in the fibers and are distributed intra-electrospun nanofibers and in the matrix of the nanofibrous webs [23][18]. Indeed, some superficial particles and a higher roughness in the fiber surface can be observed, which can be caused by the incorporation of smaller nanoparticles in the fibers, in agreement with previous results of *Moura et al.* [82][120][23]. All composite fibers show an average diameter around 1 μm and no remarkable differences in diameter values among the different type of composites was underlined, but a significant diameter increase was observed near to glass agglomerates. This result confirm that the glass particles are not uniformly distributed.

4.3.2 Compositional characterization

Composite fibers were characterized with EDS to verify the glass incorporation inside the polymeric matrix. The Si, Ca and P amounts were clearly detected in the polymeric PCL matrix, as reported by the EDS map and EDS spectra (see Figure 4.67, Figure 4.68 and Figure 4.69). Taking into account the similarities in glass granulometry and fiber morphology, EDS map analysis was performed only in case of PCL/AA/SB2(20%) mat.

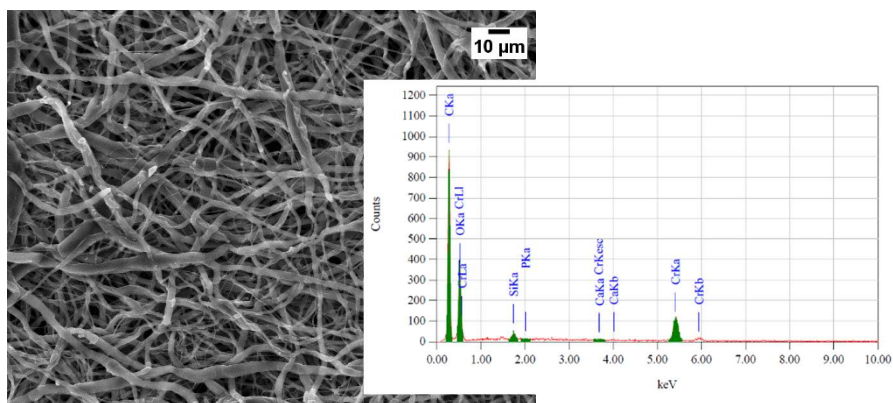


Figure 4.67: SEM micrograph and EDS spectrum of an area of PCL/AA/S2(20%)

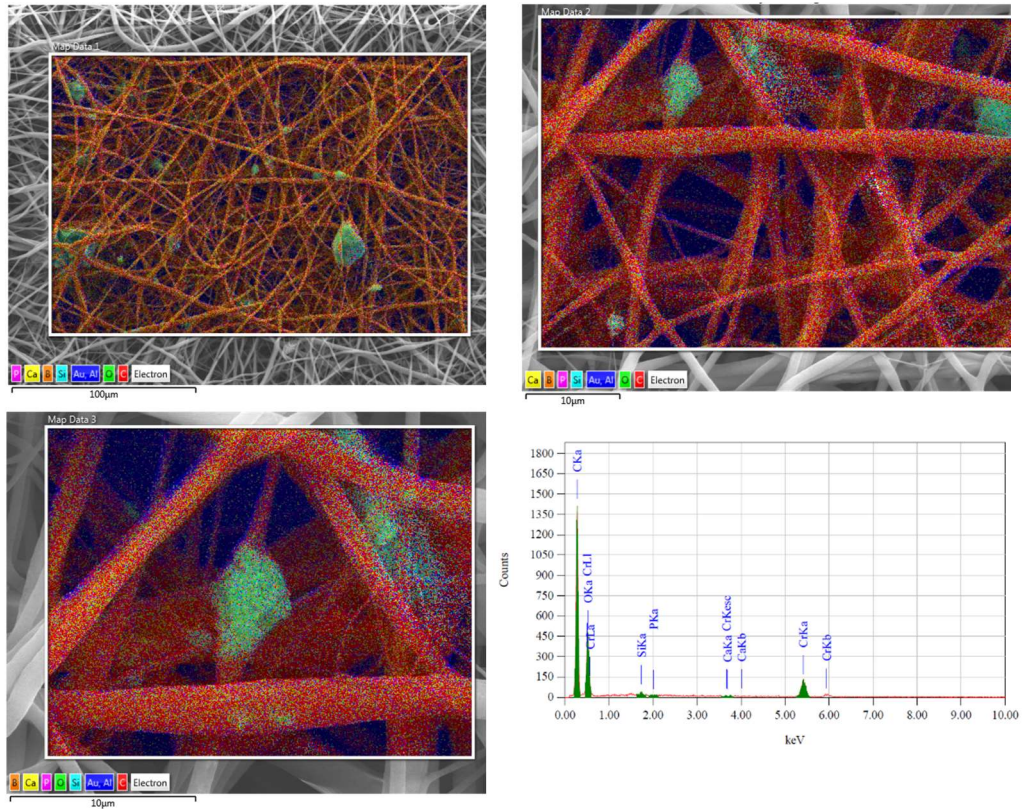


Figure 4.68: EDS map of PCL/AA/SB2(20%) at 1kX (a), 5.00 K X (b) and 10.00 K X (c) and spectrum (d)

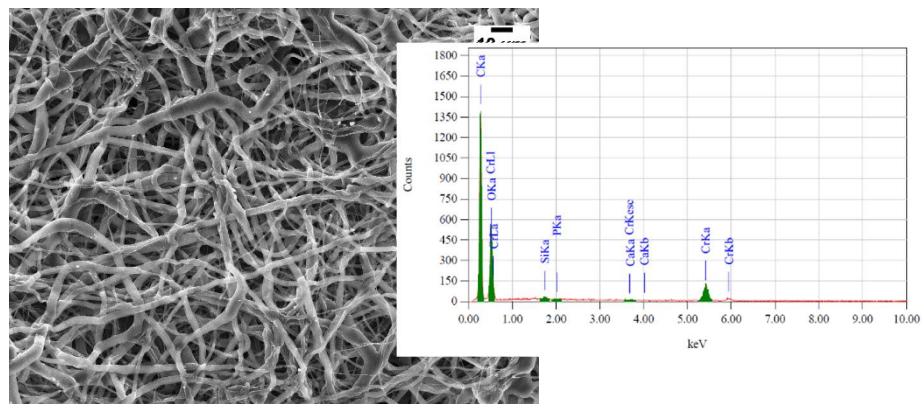


Figure 4.69: SEM micrograph and EDS spectrum of an area of PCL/AA/SBCu2(20%)

4.3.3 Physical-chemical characterization

Both the spectra of the neat PCL fibers and composite fibers (shown in Figure 4.70) are dominated by the main PCL bands: asymmetric and symmetric CH_2 stretching at 2943 cm^{-1} and 2866 cm^{-1} , carbonyl ($\text{C}=\text{O}$) stretching at 1722 cm^{-1} , C-C stretching at 1294 cm^{-1} , asymmetric and symmetric C-O-C stretching at 1240 cm^{-1} and 1165 cm^{-1} , respectively [20][121]. Silicate absorption bands for bioactive glass

nanoparticles are identified by peaks at 1085 cm^{-1} and 800 cm^{-1} , which are assigned to asymmetric stretching mode, symmetric stretching vibration and rocking vibration of Si-O-Si, respectively. Peaks located at 1045 and 1090 cm^{-1} are assigned to P-O bond. However, as it is possible to observe from graphs reported in Figure 4.70, all these bands are masked by the bands assigned to PCL, in agreement with results reported in literature [82]. As previously discussed, the glass distribution was not uniform due to the presence of glass clusters. Therefore, the synthesized composite mats are overall lacking in glass incorporation and, probably, the investigated zone was lacking in glass powders. As a result of this poor glass incorporation, it was not possible to observe the presence of peaks related to chemical bonds of the glasses.

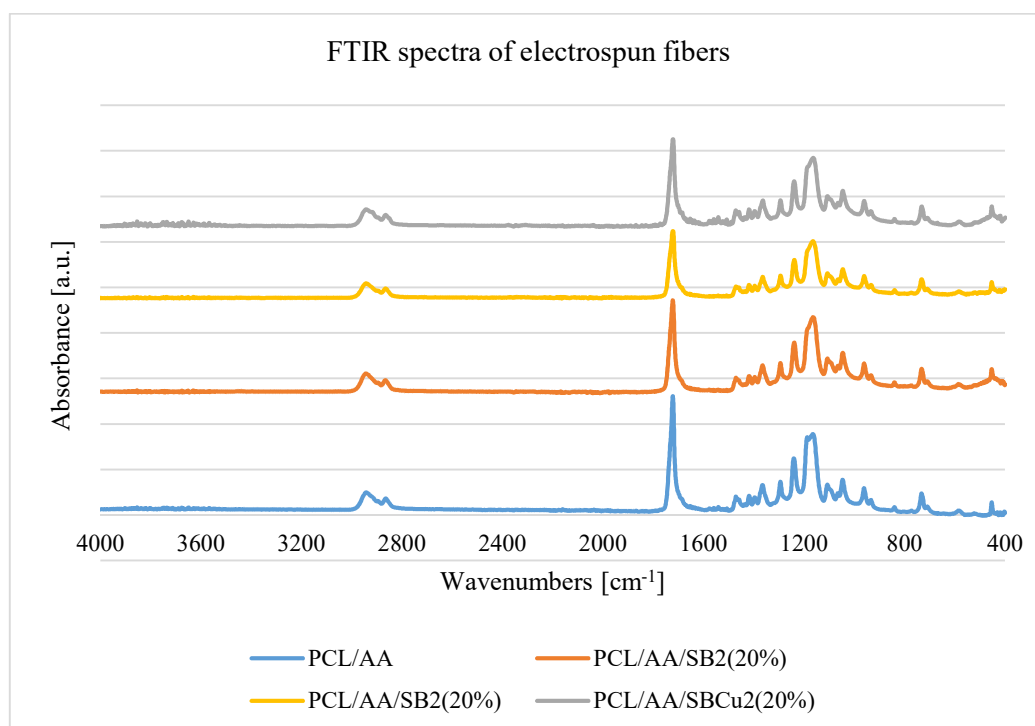


Figure 4.70: FTIR spectra of neat and composite fibers

4.3.4 Water-Contact-Angle measurements

PCL has recognized as a biocompatible polymer suitable for a variety of tissue engineering applications. However, its hydrophobic nature is a hindering factor in some biological applications, preventing permeation of water molecules into the

structure of scaffold and, thus, diminishing attachment, spreading and infiltration of cells in PCL matrix.

The hydrophobic feature of PCL is associated with existence of CH₂ groups along the main polymer chain [122]. Incorporation of bioactive glass particles in PCL matrix can be a reliable strategy to overcome the above mentioned application constraints [123][124][121][125].

The contact angle measurements results are shown in terms of mean value and standard deviation in Figure 4.71.

Keyvan Shirani et al. [126] have reported that pure electrospun polycaprolactone mats develop with water drop a contact angle of 105°, showing a hydrophobic behavior. Analogous results have been published by Zhang et al. [70], who obtained a contact angle of 109° for PCL mats. Even higher values for pure PCL fibers was recorded by Ekaputraby et al. (128°) [127] and by Fujihar et al. (134°) [128], confirming the hydrophobicity of these polymer scaffolds. Liverani et al. [78] fabricated electrospun mats composed by mesoporous calcium containing BGs in a polymer matrix and compared their properties with neat PCL mats, showing that the contact angle value for neat PCL mats was 141±3°, while the value for the composite mats was 144±5°.

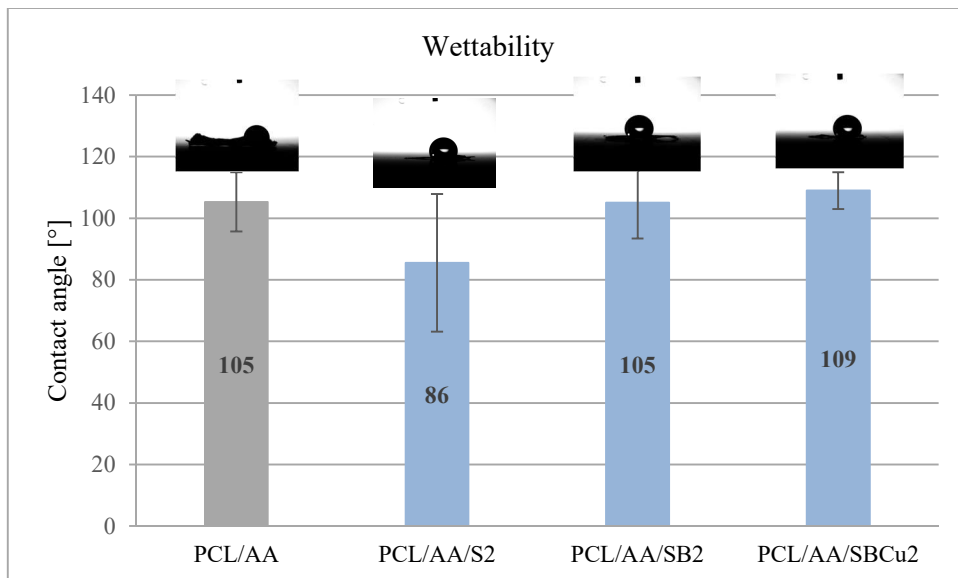


Figure 4.71: Contact angle values of the different electrospun fibers

For each kind of electrospun fiber, the contact angle measurements were performed in three times. The experimental results are represented as mean values with \pm standard deviations (SD).

In agreement with above mentioned literature studies, current results show hydrophobic behavior for both neat PCL and the composite electrospun mats.

Wettability properties depend, in fact, not only on chemical composition of the samples, but also on their roughness and porosity.

The glass nanoparticles are mainly grouped together and are not very homogeneous dispersed in the PCL matrix. Moreover, only the lower central part of the mat is rich of glass nanoparticles. Probably these are the reasons why the composite fibers have still a hydrophobic behaviour.

4.3.5 Acellular bioactivity test

During the acellular bioactivity test, at fixed time point, pH measurements were carried out and the obtained results are shown in Figure 4.72. It is possible to observe that pH trend is almost linear and similar for all investigated samples.

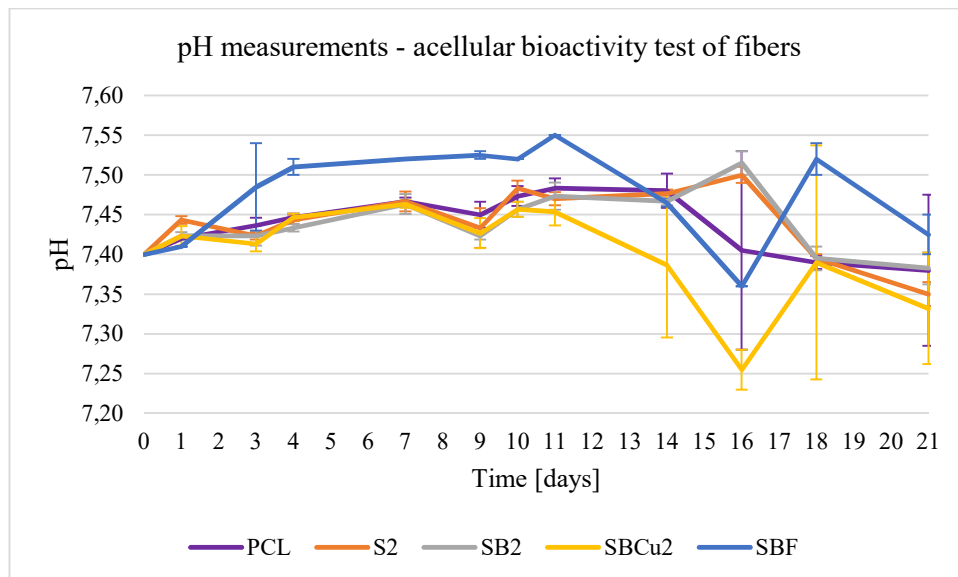


Figure 4.72: pH value trends during acellular bioactivity test of fibers

EDS analysis were performed at each time point on different areas of each samples. From analysis of big areas, it was not possible to extract any useful and

reasonable trend of P and Ca amounts, because the glass nanoparticles are not enough homogeneously dispersed. However, it was observed an increase in phosphorus and calcium, as expected in case of HA nucleation. This increase is more evident looking at EDS analysis of small areas where glass nanoparticles can clearly be seen. SEM micrographs show that until fourteenth days of immersion any precipitates with the typical morphology of HA crystals were grown on fiber surface. However, after 7-14 days of SBF treatment an enrichment of Ca and P was observed on glass particles.

In Figure 4.73 some SEM micrographs of PCL/AA/S2(20%) at different time points of immersion in SBF are shown. Glass nanoparticles are visible but apatite crystals are observable.

In Figure 4.74 and Figure 4.75 EDS pattern of areas of PCL/AA/S2(20%) different time points of immersion in SBF are reported.

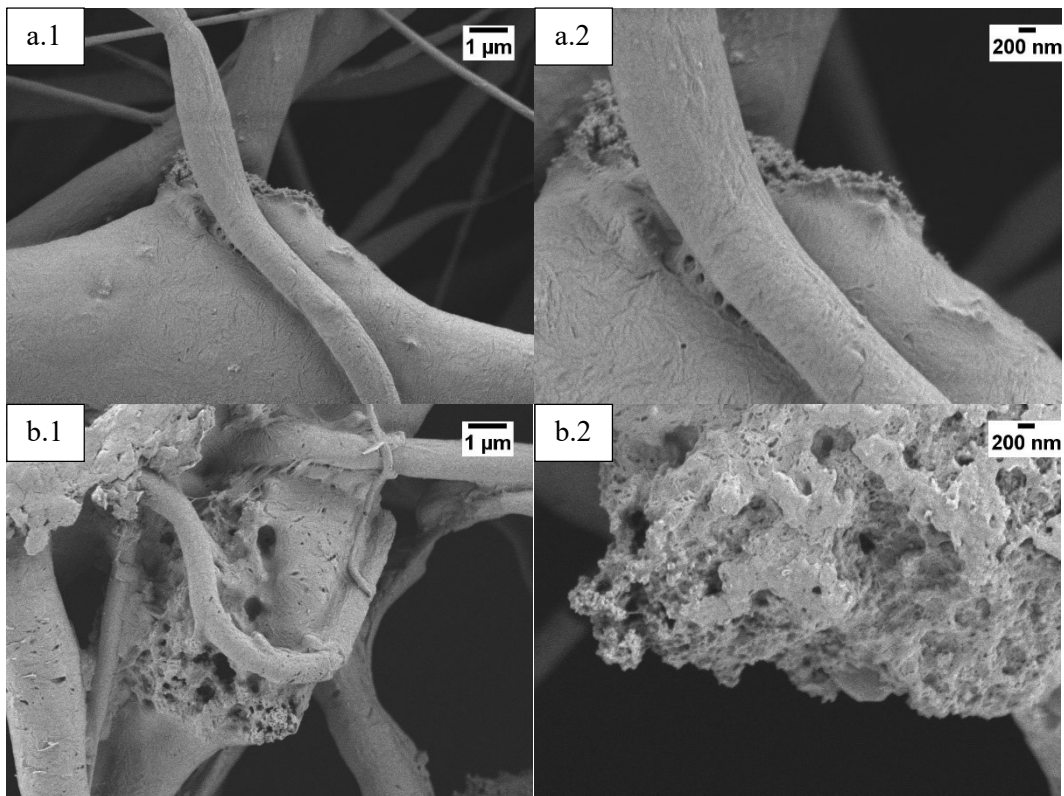


Figure 4.73: SEM micrograph of PCL/AA/S2(20%) at different time points of immersion in SBF where a) after 1 day of immersion in SBF at 20K X (a.1) and at 45K X (a.2); b) after 7 days in SBF at 20K X (b.1) and 45K X (b.2)

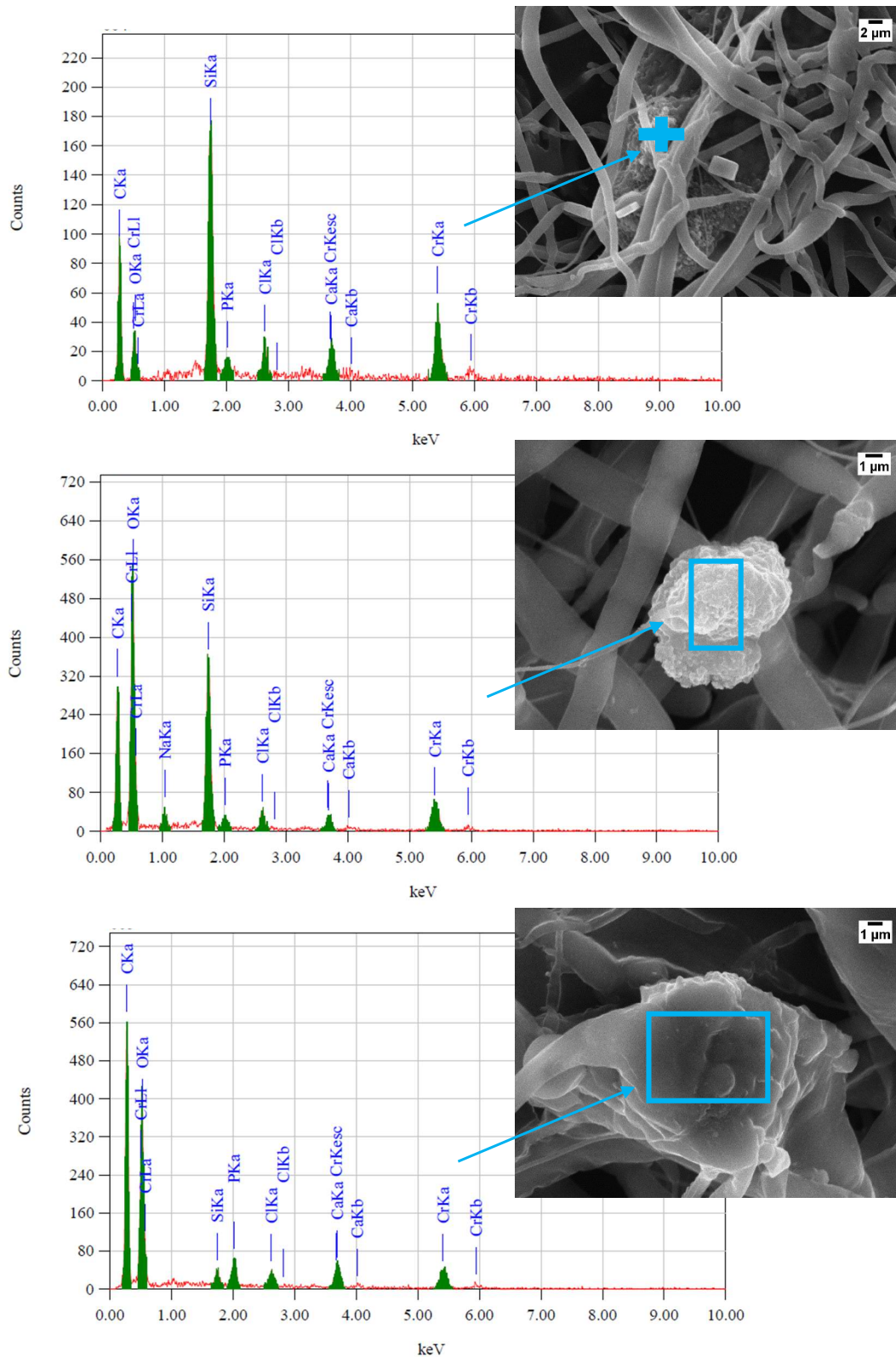


Figure 4.74: SEM micrograph and EDS pattern of glass clusters in PCL/AA/S2(20%) SBF 1d

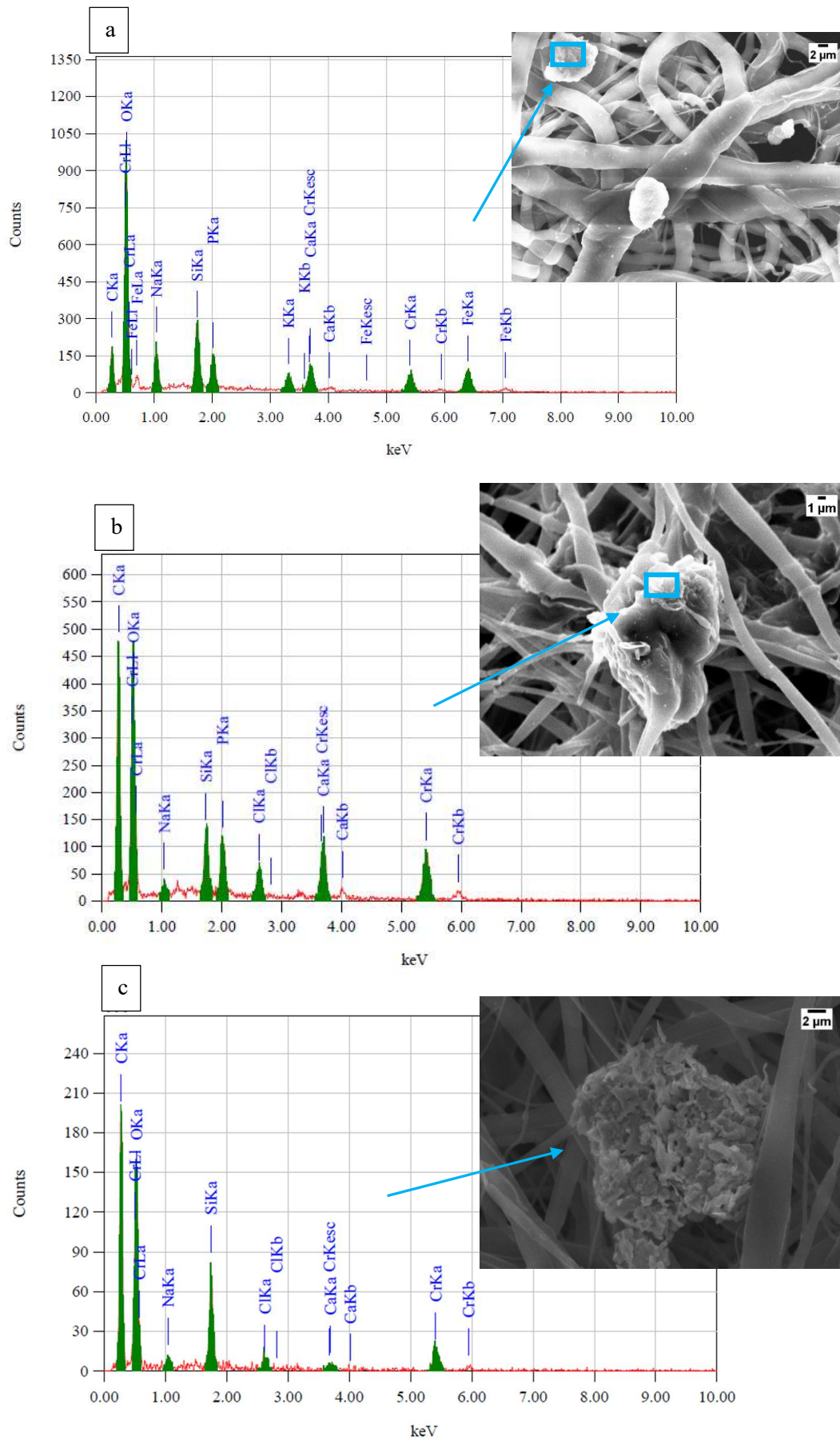


Figure 4.75: SEM micrograph of PCL/AA/S2(20%) SBF 3d(a), SBF 7d (b) and 14d (c)

In Figure 4.76, Figure 4.77 and Figure 4.79 SEM micrographs and EDS pattern of PCL/AA/SB2(20%) at different time points of immersion in SBF are shown.

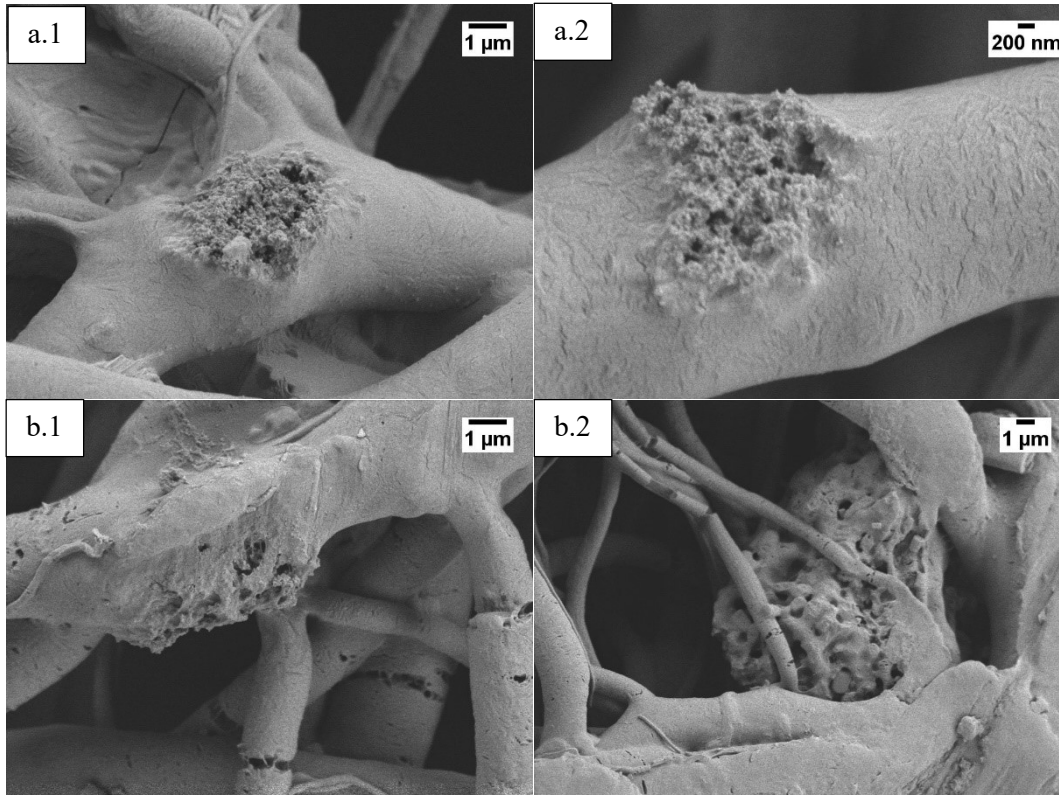


Figure 4.76: SEM micrograph of PCL/AA/SB2(20%) SBF 1d at 20K X (a.1) and 45K X (a.2); after 7 days in SBF at 20K X (b.1) and 45K X (b.2)

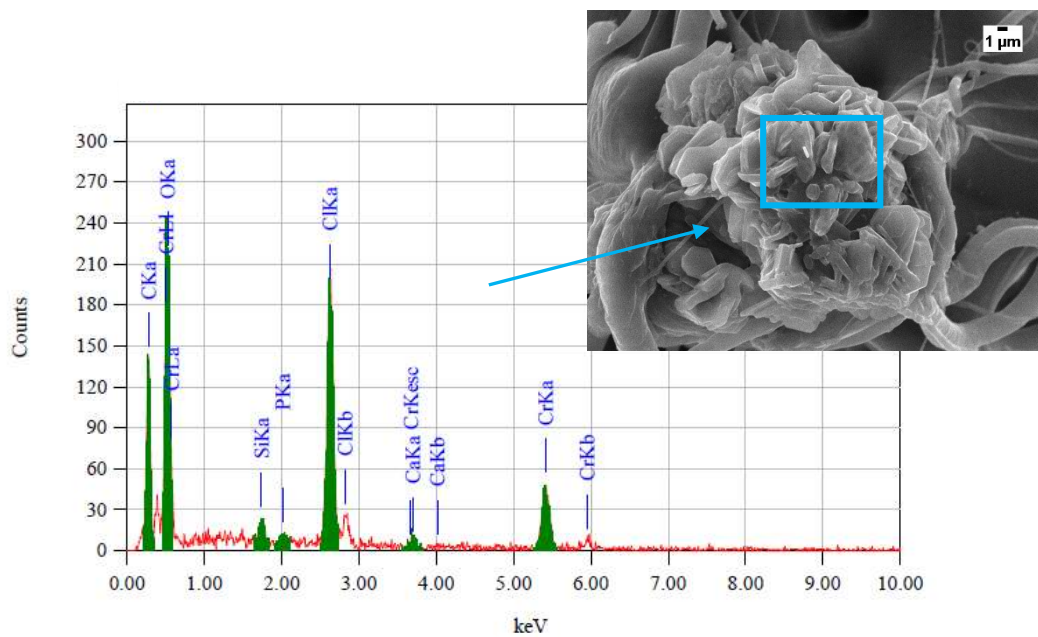


Figure 4.77: SEM micrograph of PCL/AA/S2(20%) SBF 1d

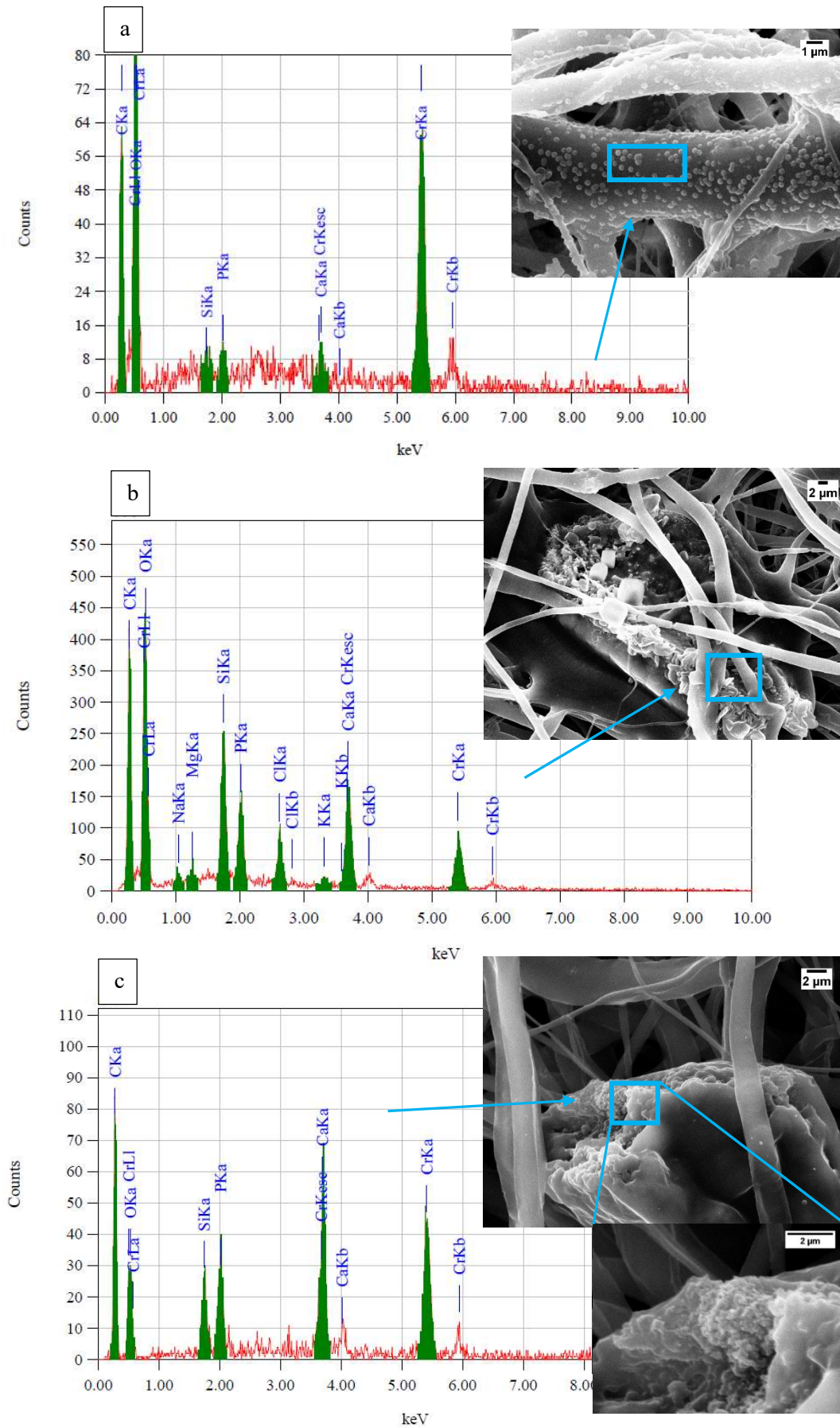


Figure 4.79: SEM micrograph of PCL/AA/SB2(20%) SBF 3d (a), SBF 7d (b) and SBF 14d (c)

In Figure 4.80 SEM micrographs of PCL/AA/SCBu2(20%) at different time points of immersion in SBF are shown.

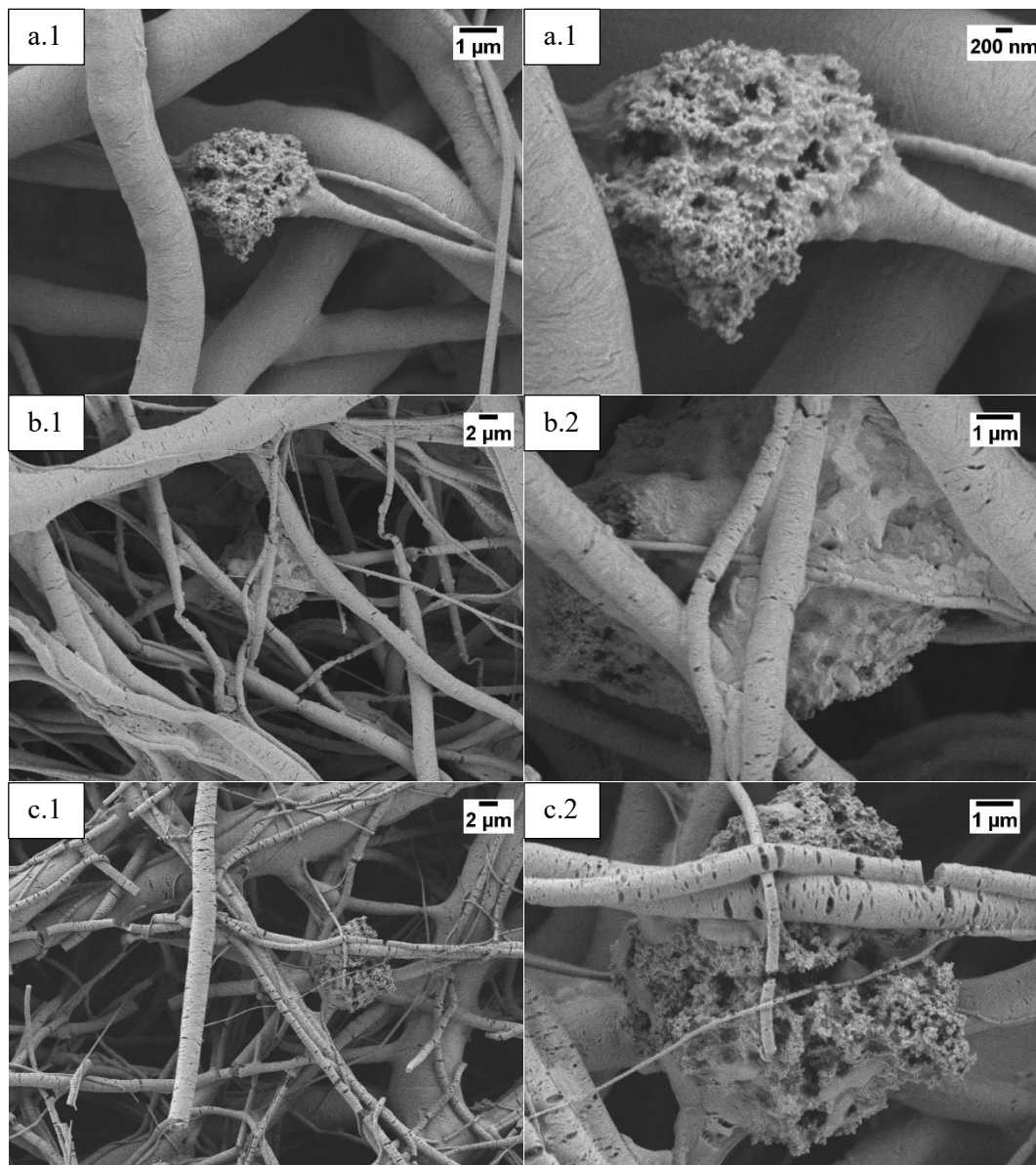


Figure 4.80: SEM micrograph of PCL/AA/SBCu2(20%) immersed in SBF after 1 day in SBF at 20K X (a.1) and 45.00 K X (a.2) after 3 days in SBF at 5K X (b.1) and 20K X (b.2) after 7 days in SBF at 5K X (c.1) and 20K X (c.2)

In Figure 4.81 EDS pattern and related SEM micrograph of different areas of PCL/AA/SBCu2(20%) SBF 1d are shown.

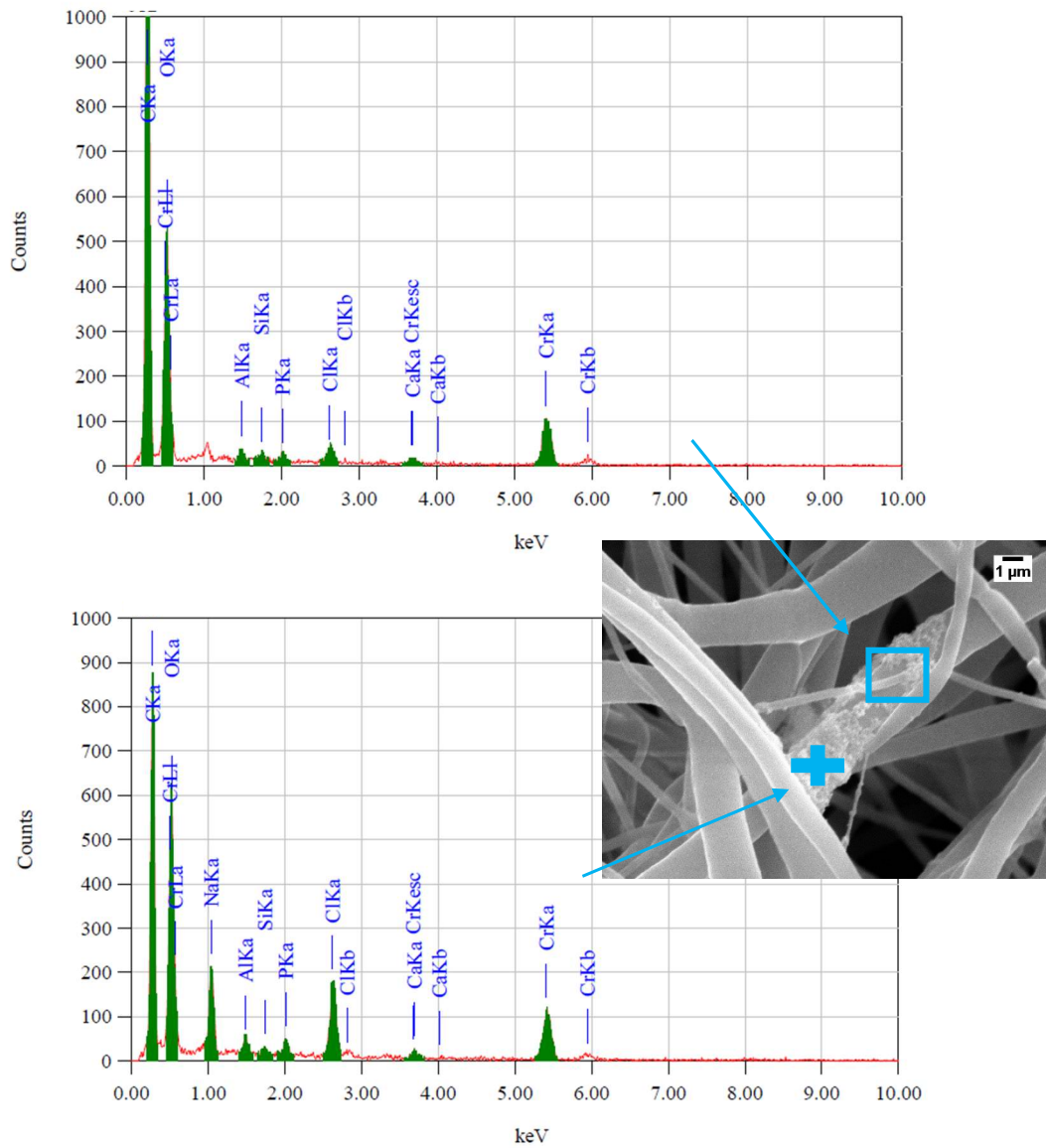


Figure 4.81: SEM micrograph and EDS pattern of PCL/AA/SBCu2(20%) SBF 1d

The aluminium (Al) peak is probably related to a contamination that took place during the preparation of this sample for the acellular bioactivity test.

In Figure 4.82 EDS pattern and related SEM micrograph of a small area of PCL/AA/SBCu2(20%) SBF 3d is shown. From this micrograph it is possible to observe the presence of NaCl, in agreement with EDS pattern.

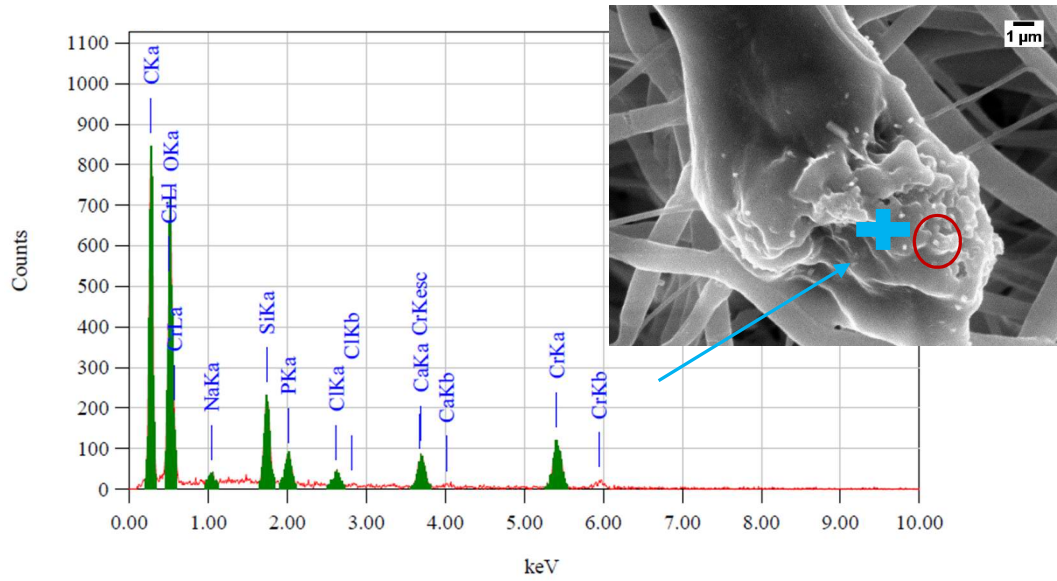


Figure 4.82: SEM micrograph and EDS pattern of PCL/AA/SBCu₂(20%) SBF 3d

In Figure 4.83 EDS pattern and related SEM micrograph of an area of PCL/AA/SBCu₂(20%) SBF 7d are shown.

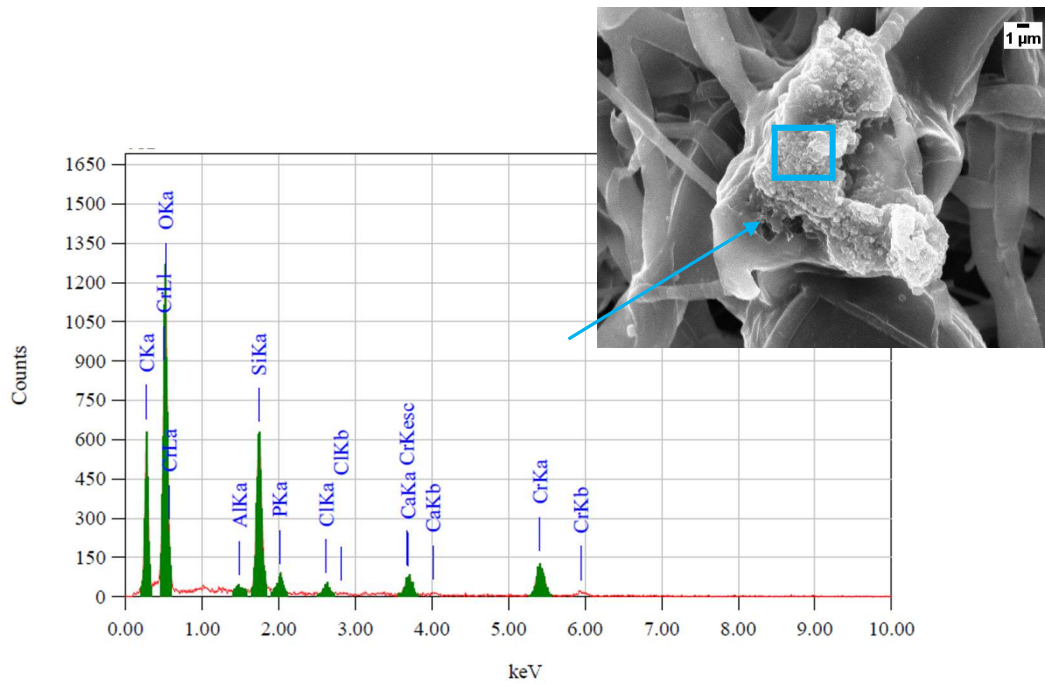


Figure 4.83: SEM micrograph and EDS pattern of PCL/AA/SBCu₂(20%) SBF 7d

In Figure 4.84 EDS pattern and related SEM micrograph of an area of PCL/AA/SBCu2(20%) SBF 14d are shown.

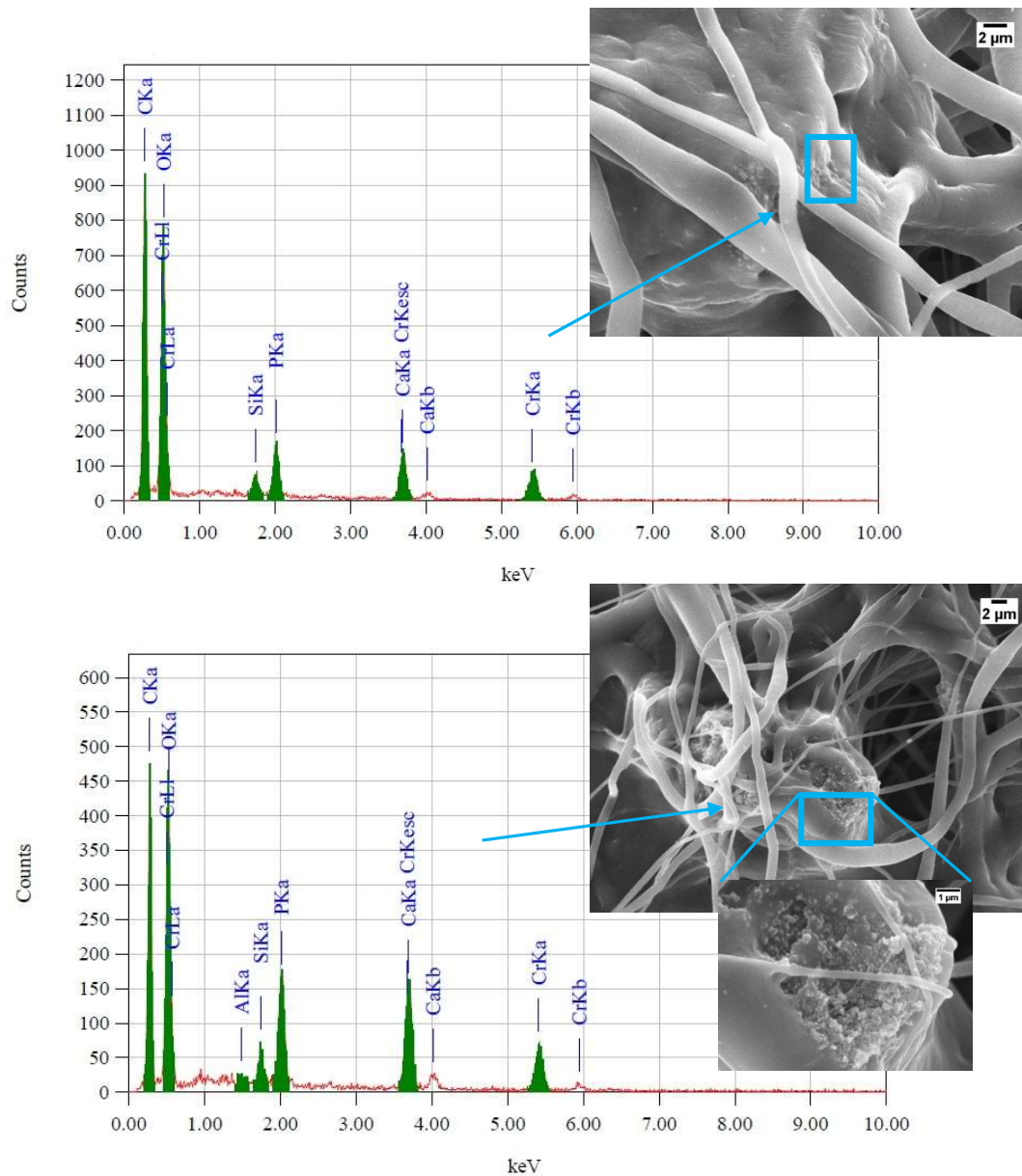


Figure 4.84: SEM micrograph and EDS spectra of PCL/AA/SBCu2(20%) SBF 14d

After 21 days of immersion in SBF solution, it is clear evident the nucleation of hydroxyapatite on the surface of the composite fibers containing S2 and SB2 (as shown in Figure 4.85 and Figure 4.86), whereas it was not possible to detach any HA-like crystals on surface of PCL/AA/SBCu2(20%). This delayed bioactivity could be attributed to different causes: the presence of copper ions in the glass

network [52] or/and the effect of the immersion in acetic acid (as discussed later) or/and the slight difference in porosity and thickness of the composite mats.

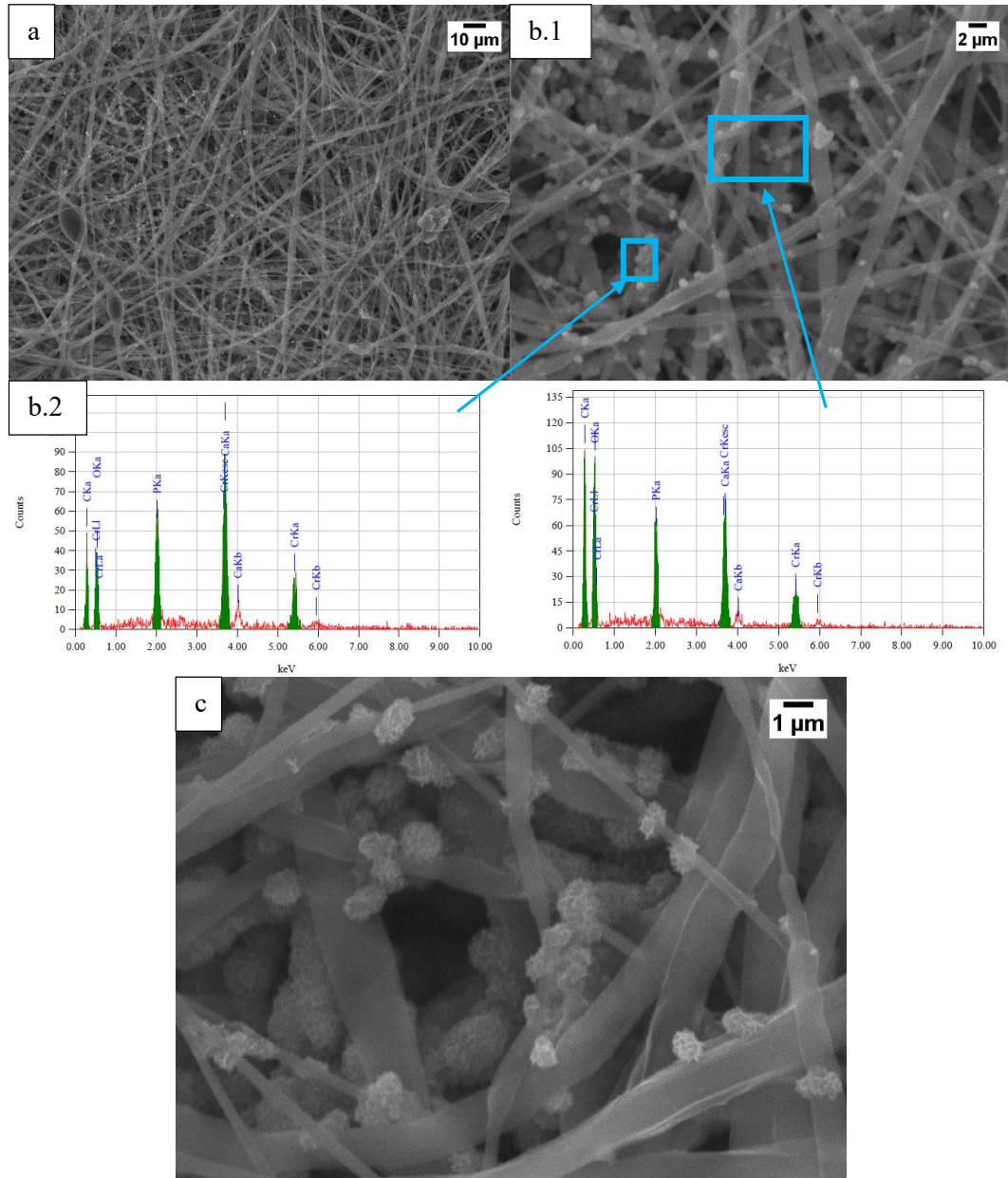


Figure 4.85: SEM micrograph and EDS spectra of PCL/AA/S2(20%) SBF 21d where magnification of SEM micrographs 500 X (a), 2000 X (b.1) 5000 X (c) and the EDS spectra is related to zones of image at 2000 X (b.2)

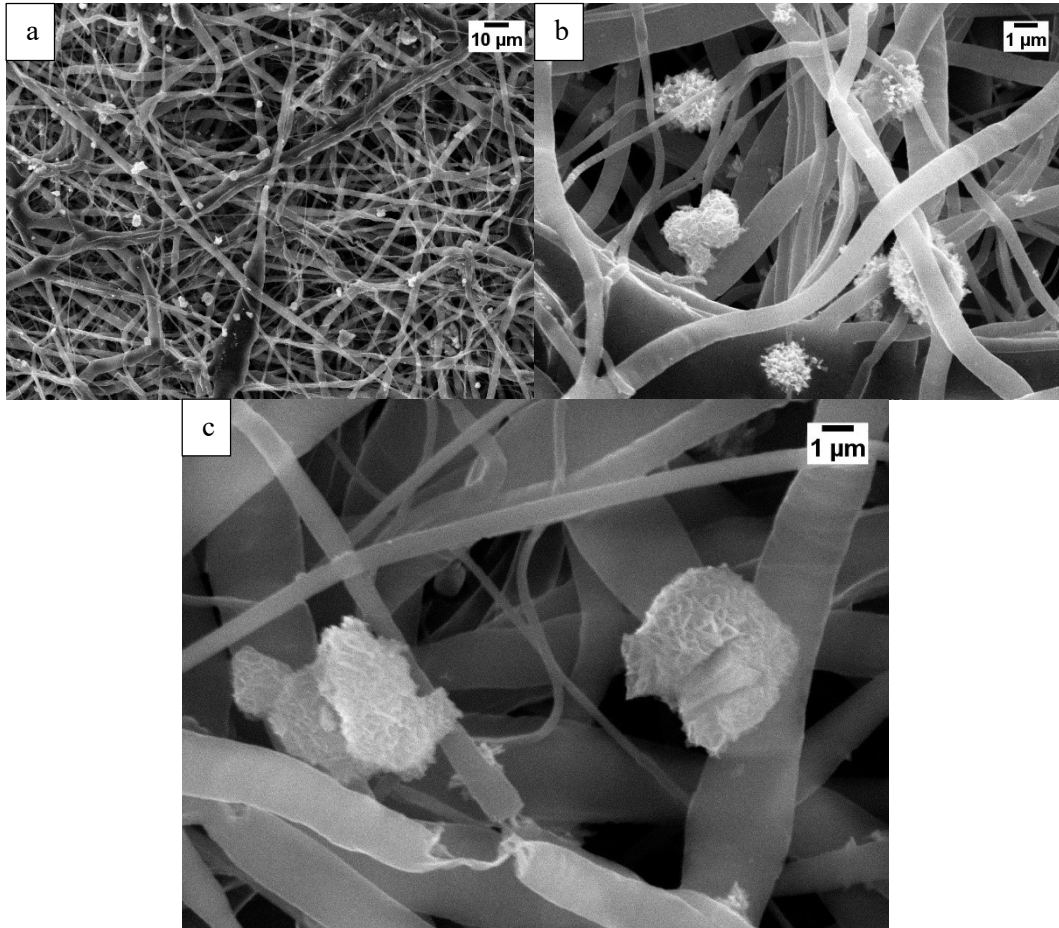


Figure 4.86: SEM micrograph and EDS spectra of PCL/AA/SB2(20%) SBF 21d at 500 X (a), at 3000 X (b) and at 5000 X (c)

EDS pattern and related SEM micrograph of an area of PCL/AA/SBCu₂(20%) SBF 7d are shown in Figure 4.87.

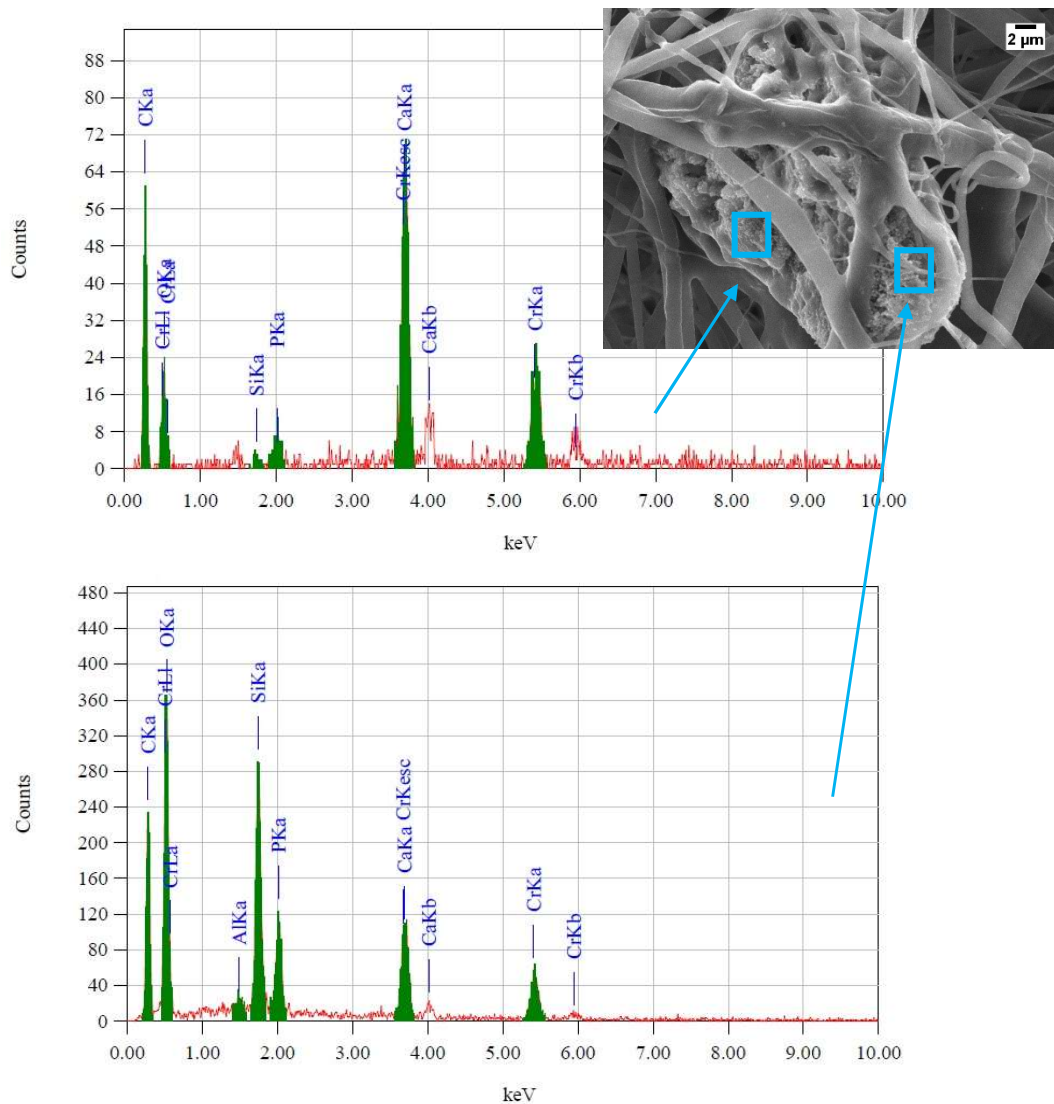


Figure 4.87: SEM micrograph and EDS spectra of PCL/AA/SBCu₂(20%) SBF 21d

4.3.6 Degradation test

In order to establish the behavior of the samples in PBS, pH measurements were carried out. Indeed, if the material degrades by hydrolysis, a decrease in the pH value should be recorded.

The trend of pH for the present test is shown in Figure 4.88.

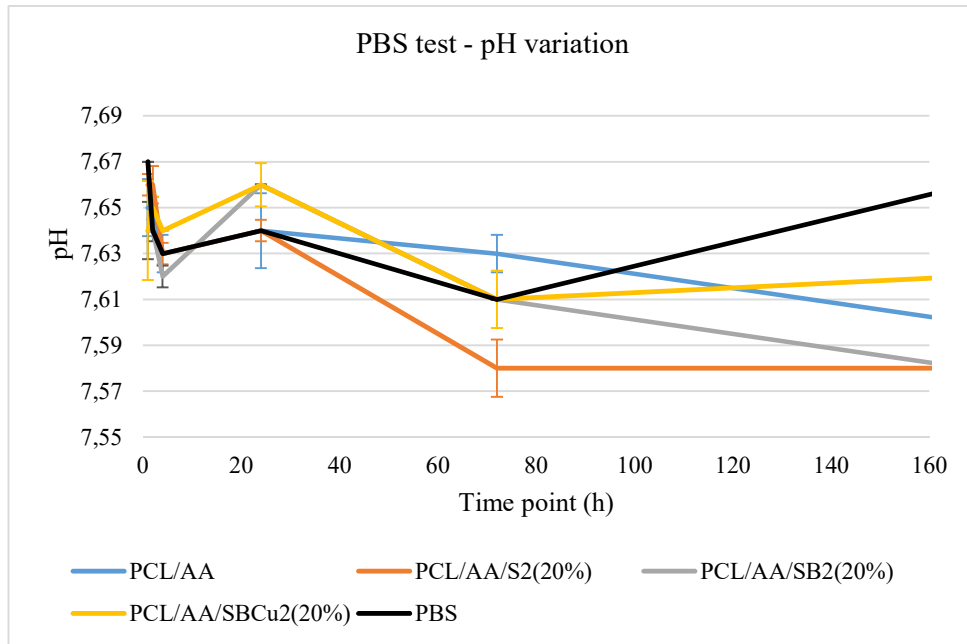


Figure 4.88: PBS pH trend of both neat and composite electrospun mats

From the graph (Figure 4.88), in agreement with pH measurements during immersion in SBF, no huge variations of the samples in terms of pH during immersion time is recorded. Indeed, the trend of all the samples is quite similar to the trend of the control taken as reference.

The FTIR analysis for all the samples evaluated at each time point (reported in Figure 4.89, Figure 4.90 and Figure 4.91) does not show any significant variation.

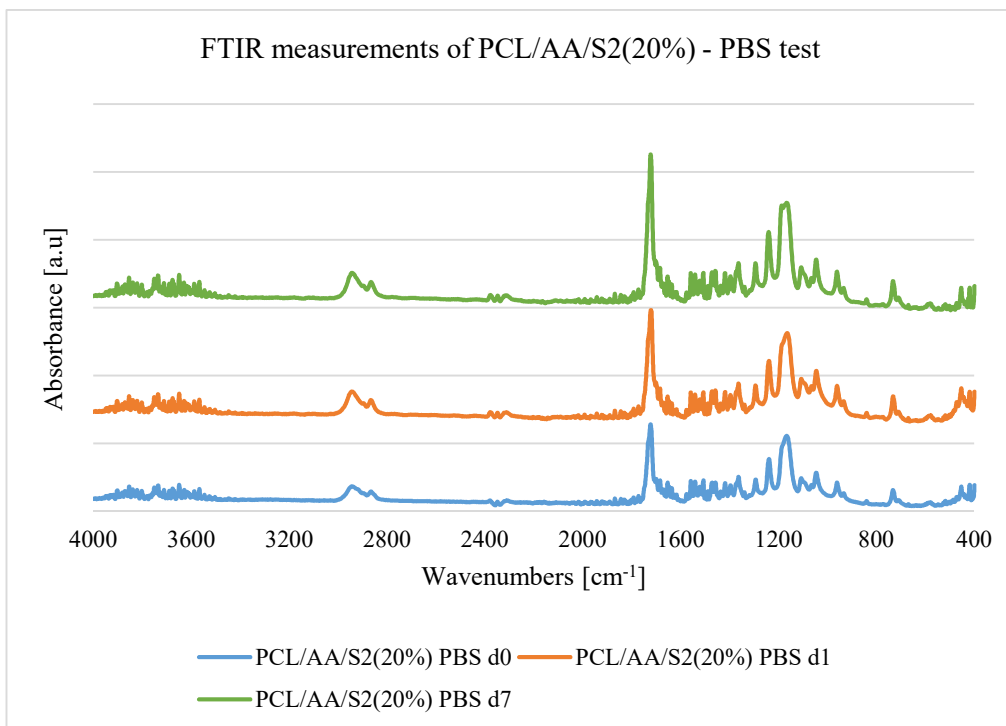


Figure 4.89: Comparison of FTIR results of PCL/AA/S2(20) 0d and 7d

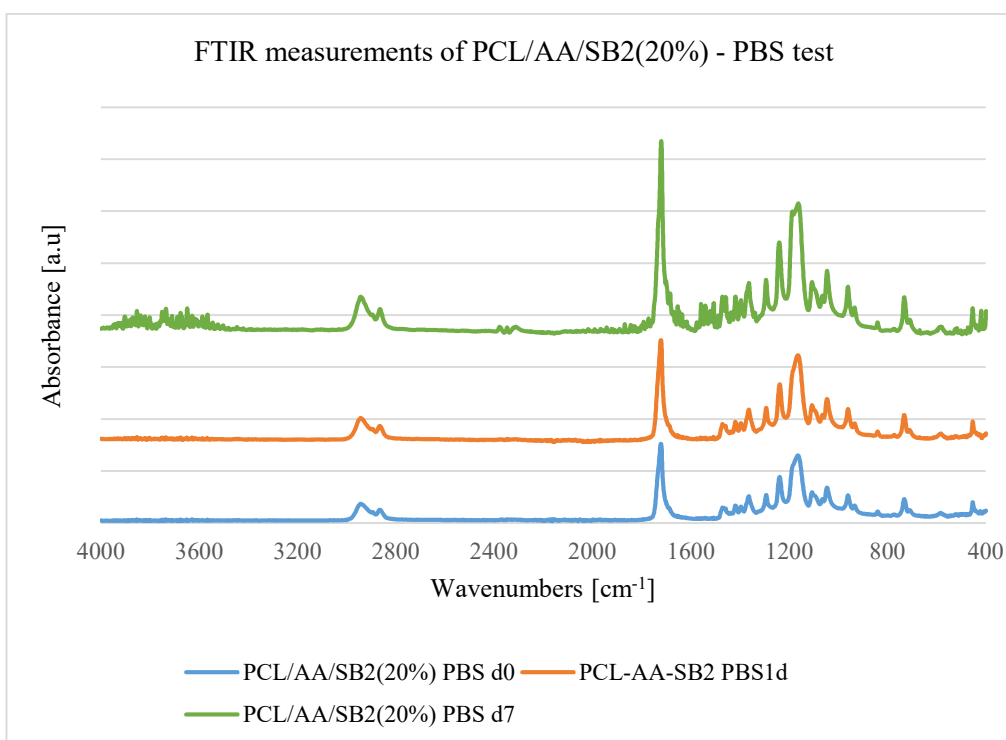


Figure 4.90: Comparison of FTIR results of PCL/AA/SB2(20) 0d and 7d

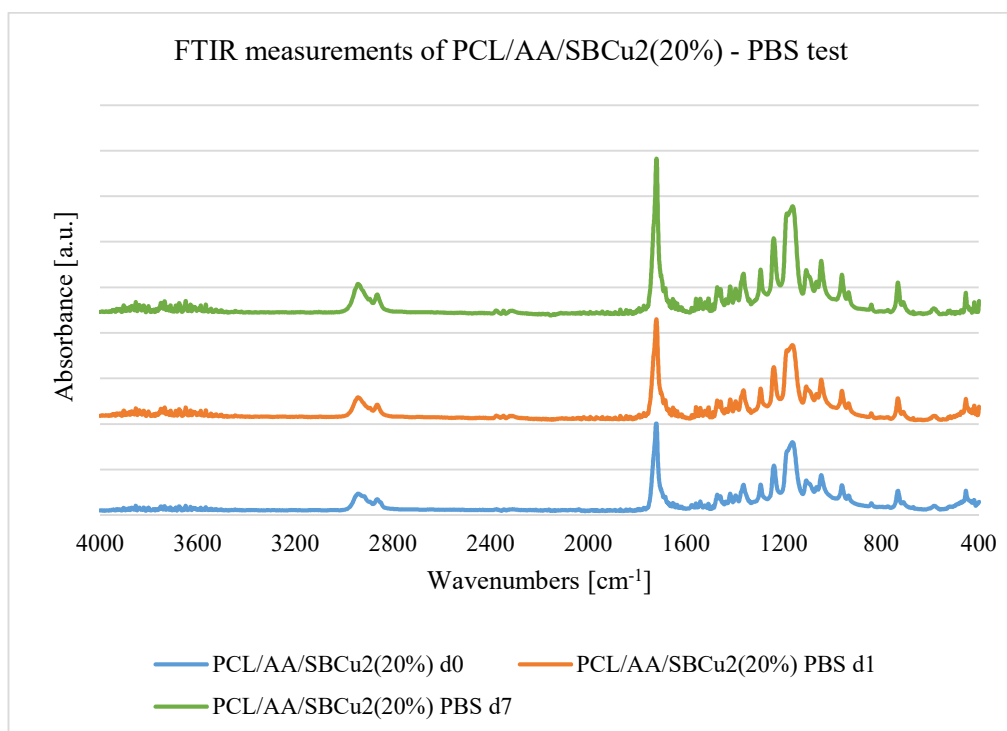


Figure 4.91: Comparison of FTIR results of PCL/AA/S₂(20) 0d and 7d

The morphological analysis was assessed in order to see if degradation occurs. Generally, polymer degradation kinetics is affected by chemical and structural characteristics of the polymer itself. In case of PCL, degradation occurs through a random hydrolytic chain scission of the ester linkage. However, as PCL is a hydrophobic and highly crystalline polyester, it does not allow fast water penetration into its network and, consequently, the rate of its hydrolytic degradation is relatively low and, as shown in Figure 4.92, the extent of degradation of the pure PCL fibers was very trivial, in agreement with literature experimental studies [126][129].

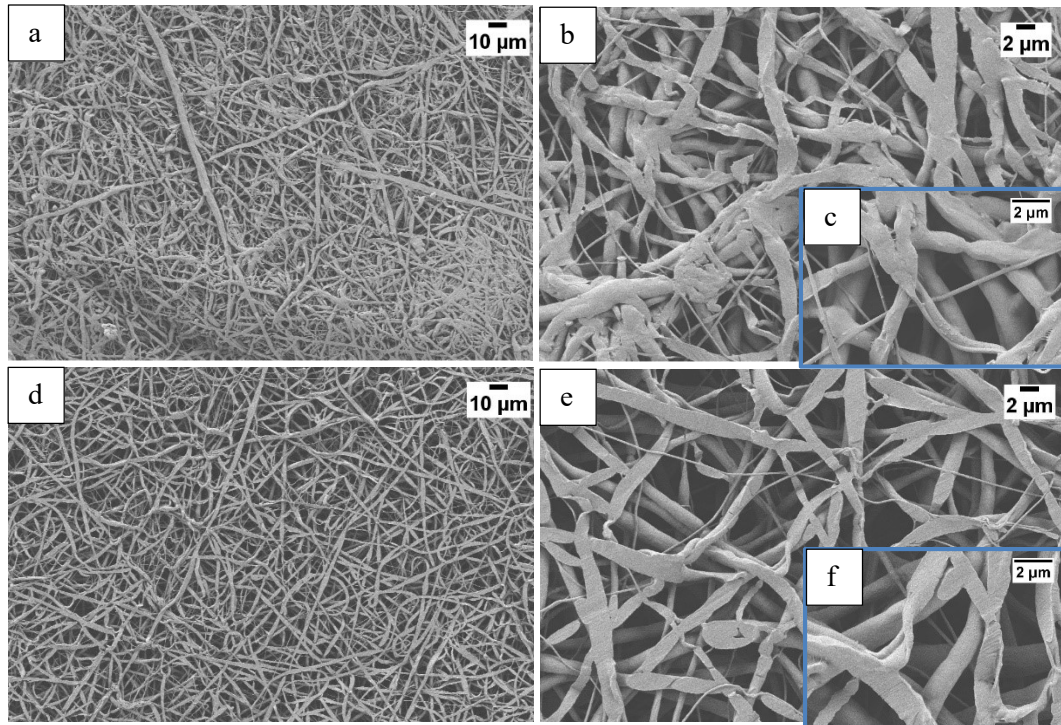


Figure 4.92: SEM micrographs of neat PCL fibers at different time point of immersion in PBS where a) after 1 day at 1000 X, b) after 1 day at 5000 X, c) after 1 day at 20000 X, d) after 7 days at 1000 X, e) after 7 days at 5000 X, c) after 7 days at 20000 X

As expected from acellular bioactivity test results, the morphological analysis (see Figure 4.93, Figure 4.94 and Figure 4.95) confirmed that bulk degradation of the composite fibers took place. Indeed, already before immersion in PBS electrospun fibers show some cracks due to the evaporation of the solvent from the polymer solution during the electrospinning process. By immersion in PBS, glass particles were released from the polymer matrix, leading to an increase in the size of the cracks. Moreover, it is possible to observe that fibers containing Cu-doped glasses seem to be less degraded. This could be attributed to the lower porosity of the fiber mat PCL/AA/SBCu2(20%) or the different glass distribution between the composite mats.

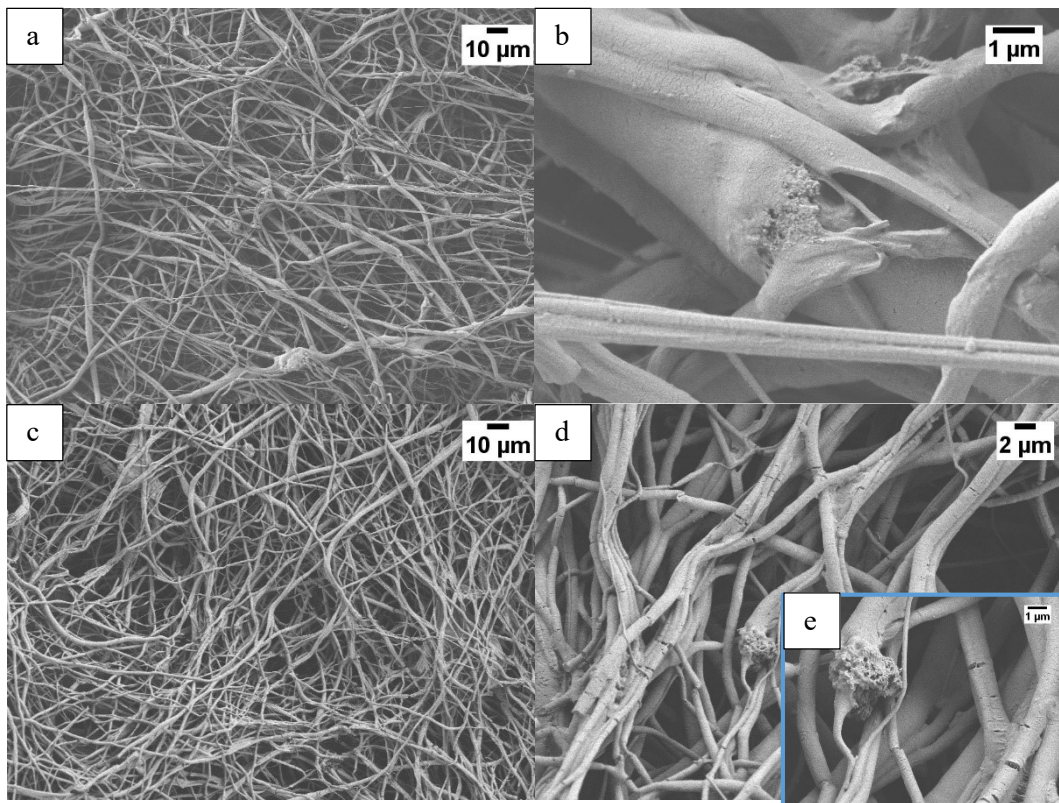


Figure 4.93: SEM micrographs of PCL/AA/S2(20%) at different time point of immersion in PBS where a) after 1 day at 1K X, b) after 1 day at 45K X, c) after 7 days at 1K X, d) after 7 days at 25K X, e) after 7 days at 45K X

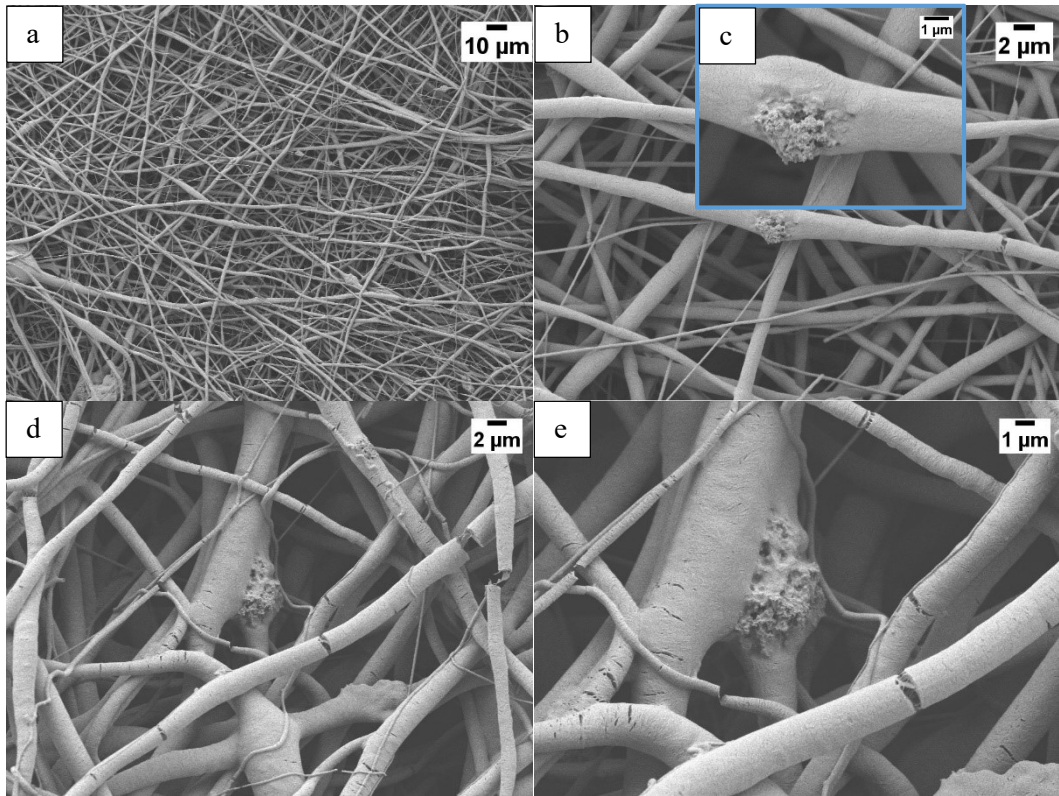


Figure 4.94: SEM micrographs of PCL/AA/SB2(20%) at different time point of immersion in PBS where a) after 1 day at 1K X, b) after 1 day at 20K X c) after 1 day at 45K X, d) after 7 days at 1K X, e) after 7 days at 45K X

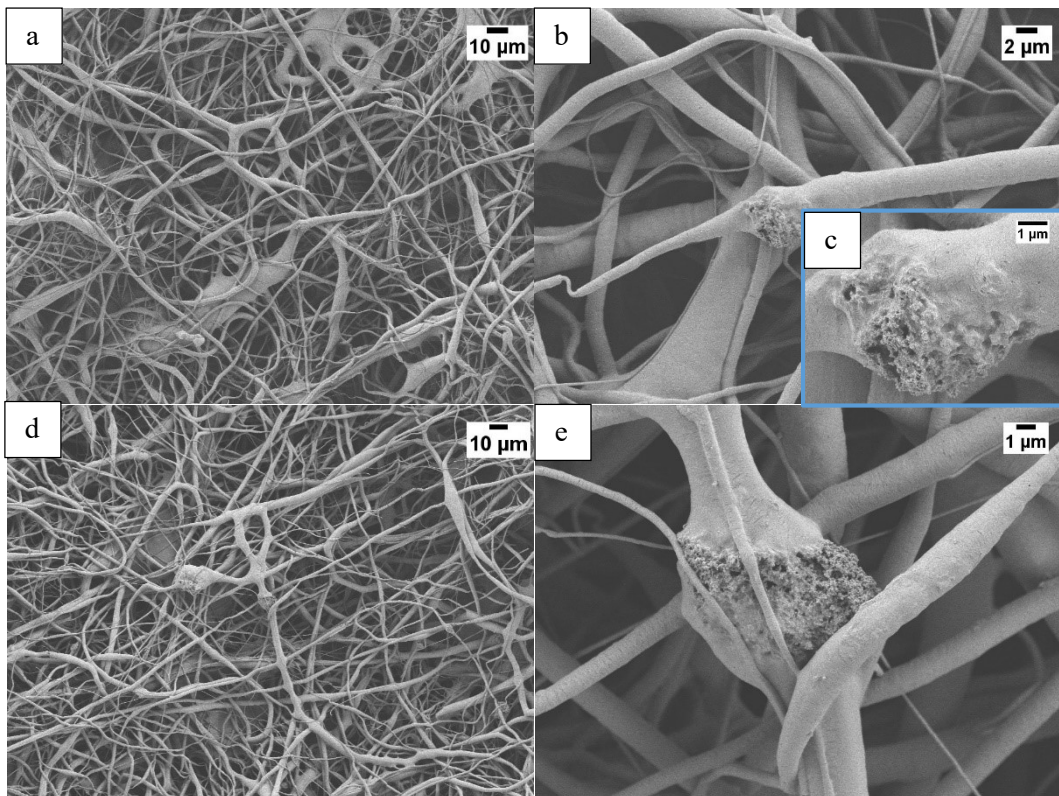


Figure 4.95: SEM micrographs of PCL/AA/SBCu2(20%) at different time point of immersion in PBS where a) after 1 day at 1K X, b) after 1 day at 20K X, c) after 1 day at 45K X d) after 7 days at 1K X, e) after 7 days at 45K X

4.3.7 Mechanical test

It is important to understand the mechanical properties of the composite fibers, since they are essential for the success of the potential application of these samples, in particular in terms of reducing the mismatch between the graft and the host tissue.

Tensile properties were calculated from the stress-strain curves as the mean of five measurements and the average value was reported with standard deviation (\pm SD). In Table 7 the force at break, the tensile displacement strain at break, the ultimate tensile stress (UTS) and the Young's modulus of the neat and composite electrospun fibers are reported.

The stress σ could be calculated dividing the force F that cause the deformation by the area A to which the force was applied. During this master thesis work, the sample area was calculated as $b \times t$ where b is the width of the sample corresponding to the inner width of the frame which was used in order to perform the mechanical test and t is the thickness of the sample. The measured thickness value of the all composite membranes was in the range 0.05 mm – 0.06 mm.

Table 7: Mechanical properties of electrospun fibers

| Sample | Force at break [N] | Tensile strain at break [%] | UTS [MPa] | Young's modulus |
|--------------|--------------------|-----------------------------|---------------|-----------------|
| PCL/AA | 0.3 ± 0.1 | 169.1 ± 98.5 | 3.1 ± 1.2 | 11.9 ± 1.9 |
| PCL/AA/S2 | 0.2 ± 0.0 | 155.5 ± 7.2 | 1.5 ± 0.3 | 4.7 ± 1.5 |
| PCL/AA/SB2 | 0.2 ± 0.1 | 60.0 ± 41.2 | 1.7 ± 0.4 | 11.1 ± 1.6 |
| PCL/AA/SBCu2 | 0.2 ± 0.0 | 70.5 ± 20.9 | 1.0 ± 0.1 | 4.1 ± 0.8 |

As reported in the literature for both sample types, namely composite and neat polymeric fibers, two linear trends in the stress–strain curve could be observed: the first one is a linear elastic Hookean response due to the load application and the second one, a non-linear plastic behavior, could be related to the fiber alignment before the sample fracture [78][129], as shown in Figure 4.96.

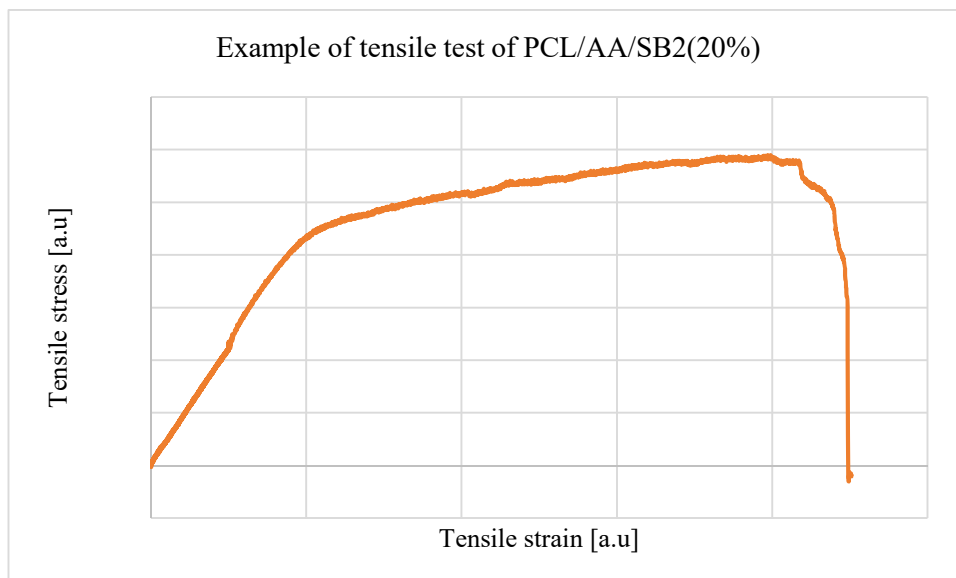


Figure 4.96: Example of tensile stress – tensile stress curve

Mechanical properties of the neat PCL fibers agreed with previous experimental studies [78][127] and were compared with the ones calculated for the composite fibers, in order to evaluate the effect of the glass addition.

As expected from any composite in which a rigid phase has been added to a polymer matrix [23][72][82][120], the present results show that the addition of the BG nanoparticles restricted the elongation of the PCL matrix, limiting its plastic deformation. Therefore, the measured tensile strain reduction limited the plastic deformation of the fibers and so their elongation at break decreased.

Regarding the tensile stress, it is possible to observe a decrease in the UTS values in case of composite fibers. The current results are probably influenced by the nonhomogeneous distribution of nanoparticles in the PCL matrix due to their agglomeration, which caused stress concentration regions, leading to a drop in the UTS value, in agreement with experimental results which are available in literature [82][130][131][132].

The addition of an inorganic filler should improve theoretically the mechanical properties and, usually, the addition of inorganic filler increases the Young's modulus of polymers [16][72][133][132][134][133]. The Young's modulus or elastic modulus E of the fibers represents the stiffness of the samples and is generally described as the quantity that measures an object or substance's resistance to be deformed elastically (i.e., non-permanently) when it is submitted

to a mechanical stress. The current results did not show an increase in E value. As above mentioned, the reason might be the poor interaction of BG particles with the polymer and the agglomeration of glass particles, as previously attained by *Tansaz et al.* [133] and/or the slight increase in the inhomogeneity in the distribution of the average fiber diameter and the presence of roughness on the surface of the electrospun mats, according to previous results of *Liliana et al.* [20]. The effect of the addition of BG particles on mechanical properties must be coupled with the reduction in the average fiber diameter, The mechanical behaviour of the composites tightly depends on the homogeneity of the dispersion of glass particles in the fibres and on the interaction at the interface between the polymer and the BG particles, which can lead to the [134]. In conclusion, the introduction of another phase can lead to the formation of a weak point in the material at the interface between the two phases and the presence of clusters can cause local stress concentration, lowering the mechanical properties.

The differences between the Young's modulus of the composite scaffolds might originate from the different glass dispersion, fiber orientation and porosity [135].

4.3.8 Stability test

A list of abbreviations is here reported:

- S2/AA: S2 glass after immersion in acetic acid for 1 h,
- SB2/AA: SB2 glass after immersion in acetic acid for 1 h,
- SBCu2/AA: SBCu2 glass after immersion in acetic acid for 1 h.

In Figure 4.97, some photos of dried glass powders after immersion in acetic acid are shown.

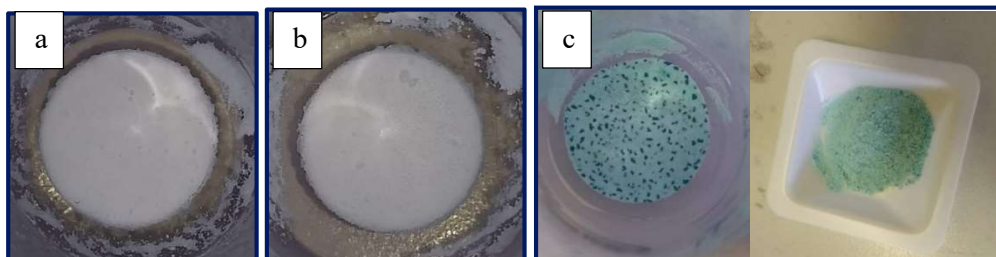


Figure 4.97: S2 (a), SB2 (b) and SBCu2 (c) after 1 hour of immersion in AA

It was observed that there was a change in coloration of the acetic acid in which SBCu2 glass was immersed and, consequently, it is obviously to supposed that a release of copper ions took place. However, this fact did not seem to affect the bioactivity of the glass, as discussed later in this same paragraph.

As shown in Figure 4.98, even though immersion in acetic acid, glasses S2, SB2 and SBCu2 maintain their morphology and, as expected, these micrographs confirm the presence of big agglomerates, that have to be destroy using mortar prior addition of glass into PCL solution.

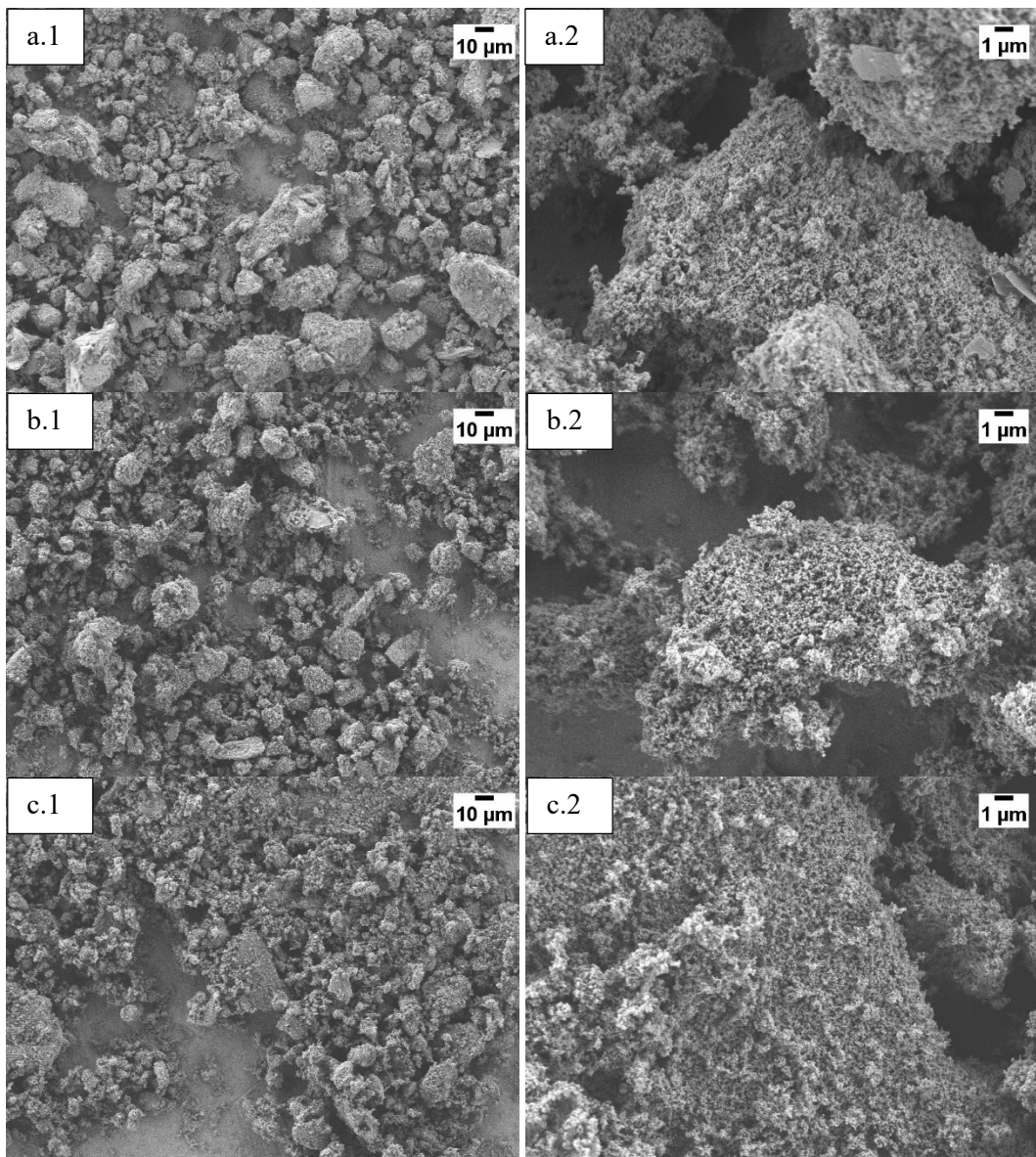


Figure 4.98: SEM micrographs of glasses of synthesis 2 after immersion in AA where a.1) S2/AA at 1K X, a.2) S2/AA and at 5K X, b.2) SB2/AA at 1K X, b.2) SB2/AA at 5K X, c.1) SBCu2/AA at 1K X and c.2) SBCu2/AA at 10K X

An acellular bioactivity test was carried out, soaking the samples in SBF until 14 days. The obtained results were compared with the ones related to original glasses (meaning ‘glasses before immersion in acetic acid’).

Variations in pH values during the acellular bioactivity test (reported in graph in Figure 4.99) did not show relevant dissimilarity with pH trend of original glasses.

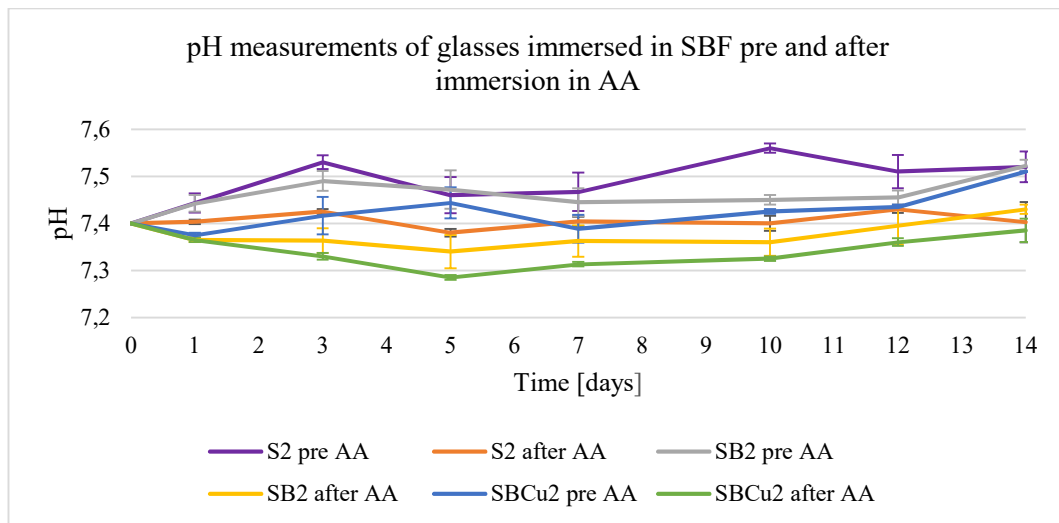


Figure 4.99: pH trend during acellular bioactivity test of all glasses soaked in AA

Analogously to original glasses, EDS spectra show an increase in the peaks of P and Ca (see Figure 4.100, Figure 4.101 and Figure 4.102). As written in the paragraph 4.1.5, peaks of Na and Cl are related to the formation of sodium chloride on the surface of the BG particles during immersion in SBF.

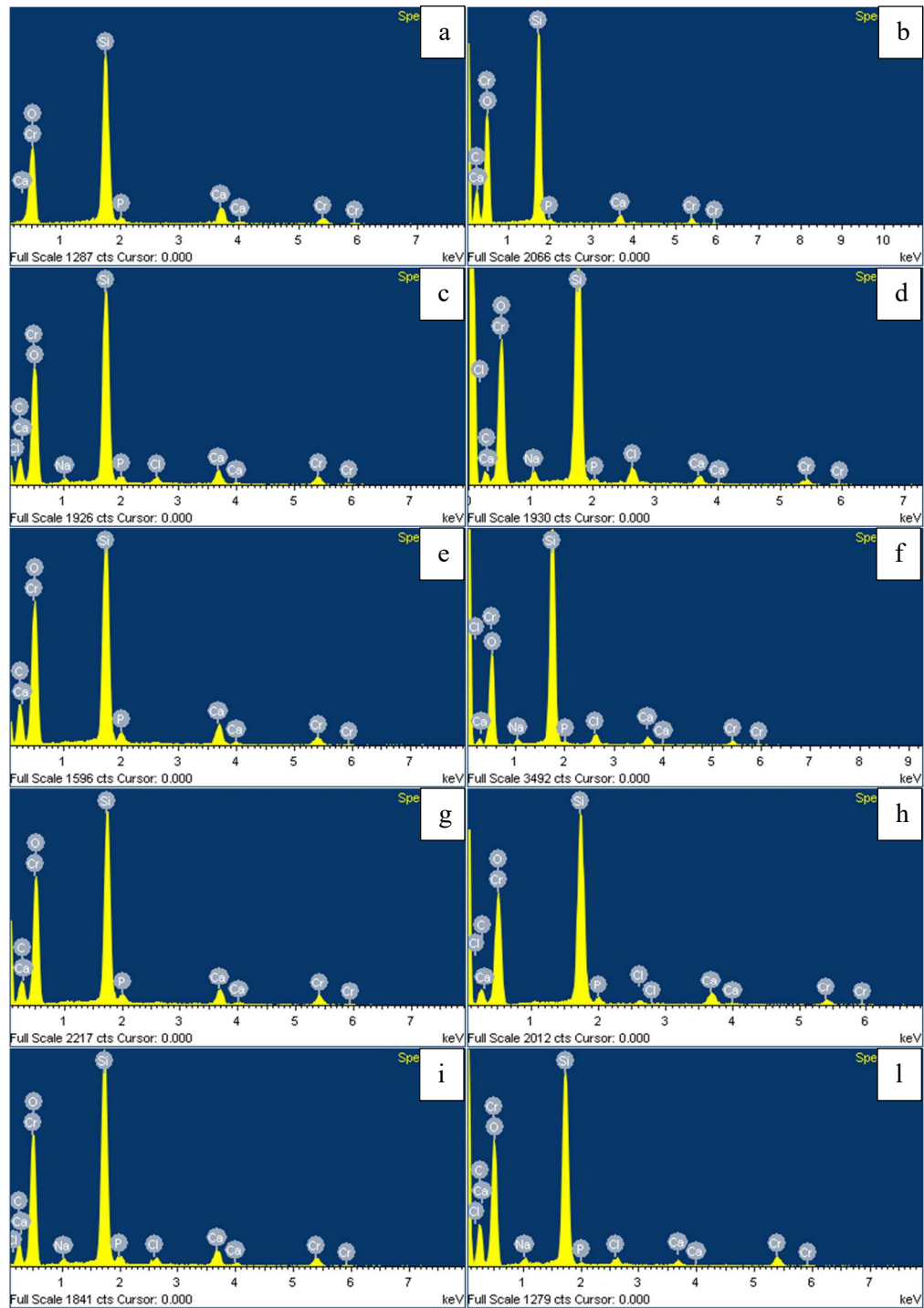


Figure 4.100: EDS spectra of S2 glasses at different time points in SBF

- a) EDS spectra of a zone of S2 0d and b) of S2/AA 0d
- c) EDS spectra of a zone of S2 1d and d) of S2/AA 1d
- e) EDS spectra of a zone of S2 3d and f) of S2/AA 3d
- g) EDS spectra of a zone of S2 7d and h) of S2/AA 7d
- i) EDS spectra of a zone of S2 14d and l) of S2/AA 14d

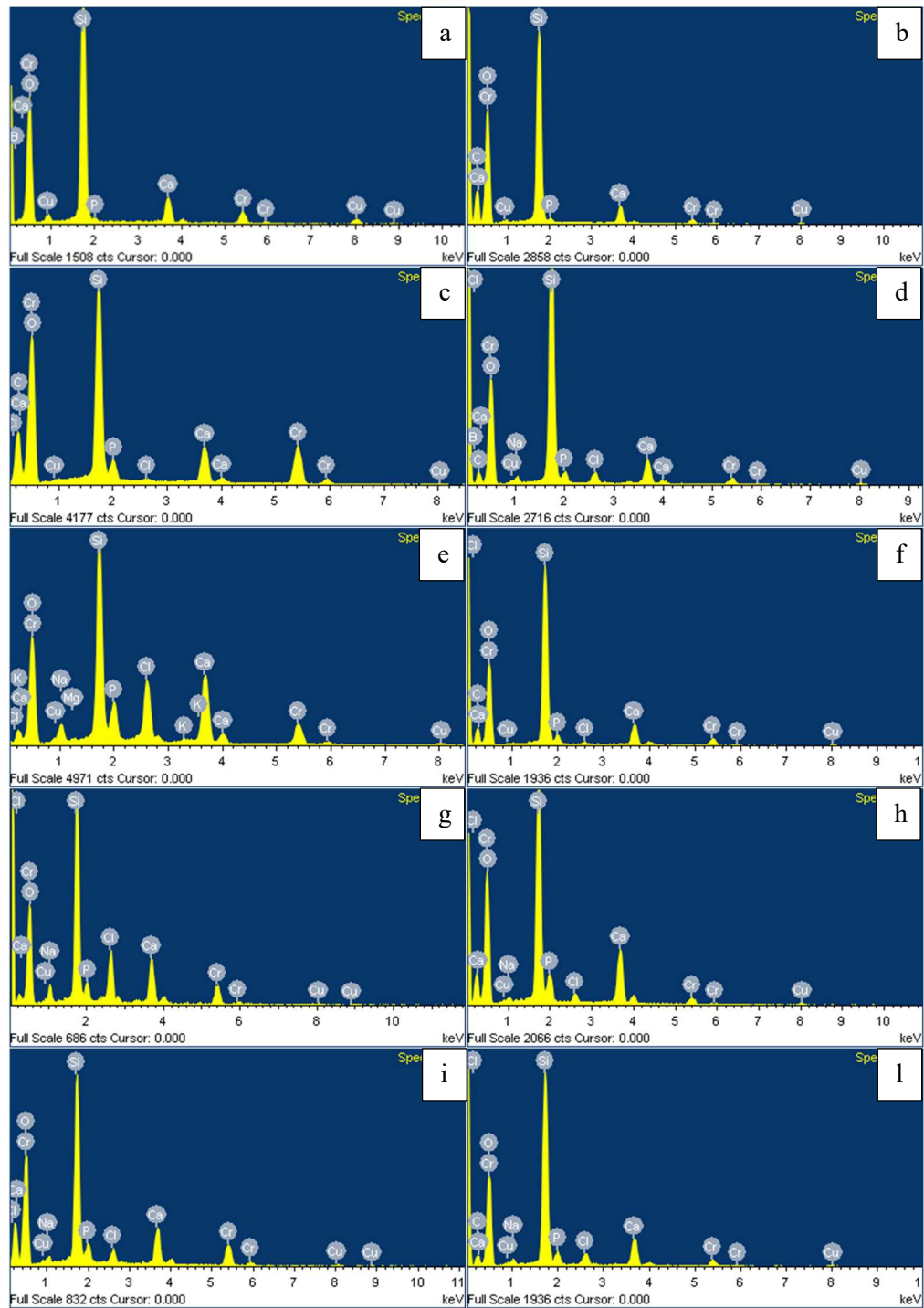


Figure 4.102: EDS spectra of SBCu2 glasses at different time points in SBF

- a) EDS spectra of a zone of SBCu2 0d and b) of SBCu2/AA 0d
- c) EDS spectra of a zone of SBCu2 1d and d) of SBCu2/AA 1d
- e) EDS spectra of a zone of SBCu2 3d and f) of SBCu2/AA 3d
- g) EDS spectra of a zone of SBCu2 7d and h) of SBCu2/AA 7d
- i) EDS spectra of a zone of SBCu2 14d and l) of SBCu2/AA 14d

P amount of glasses immersed in acetic acid during the acellular bioactivity test were plotted versus time. Comparing these trends with results obtained original glasses, it is evident an increase in P and Ca amount, with values and trend which are similar to the ones recorded for glasses before immersion in acetic acid.

Figure 4.103 shows the trend of P amount for both S2 and S2/AA during immersion in SBF.

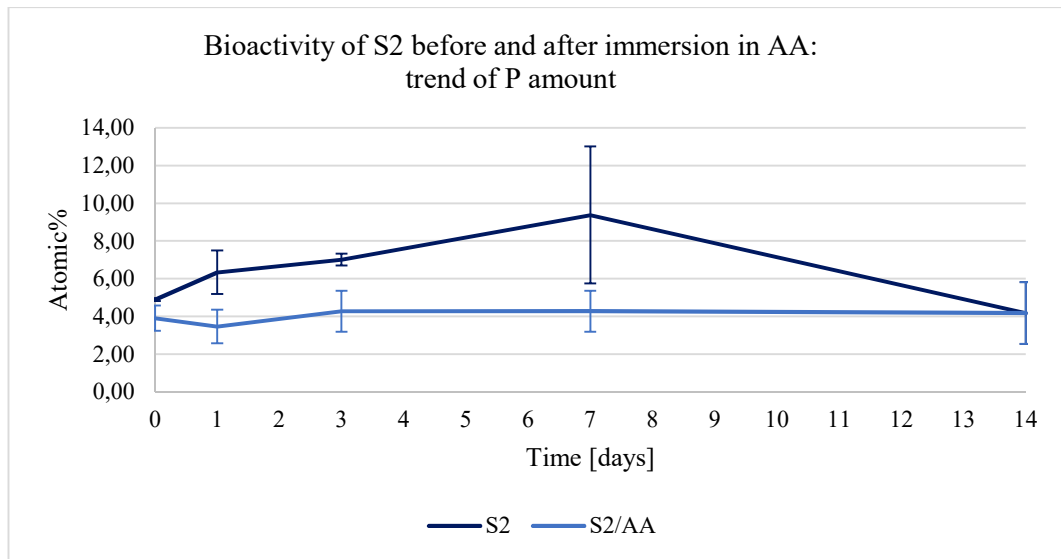


Figure 4.103: P amount in S2 and S2/AA after immersion in SBF

Figure 4.104 shows the trend of P amount for both SB2 and SB2/AA during immersion in SBF.

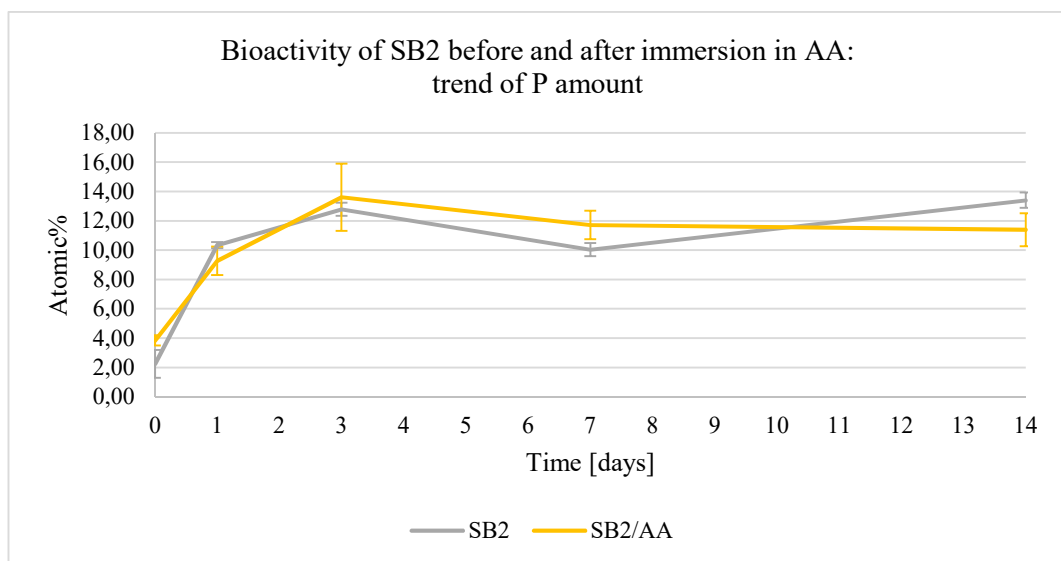


Figure 4.104: P amount in SB2 and SB2/AA after immersion in SBF

Figure 4.105 shows the trend of P amount for both SBCu2 and SBCu2/AA during immersion in SBF.

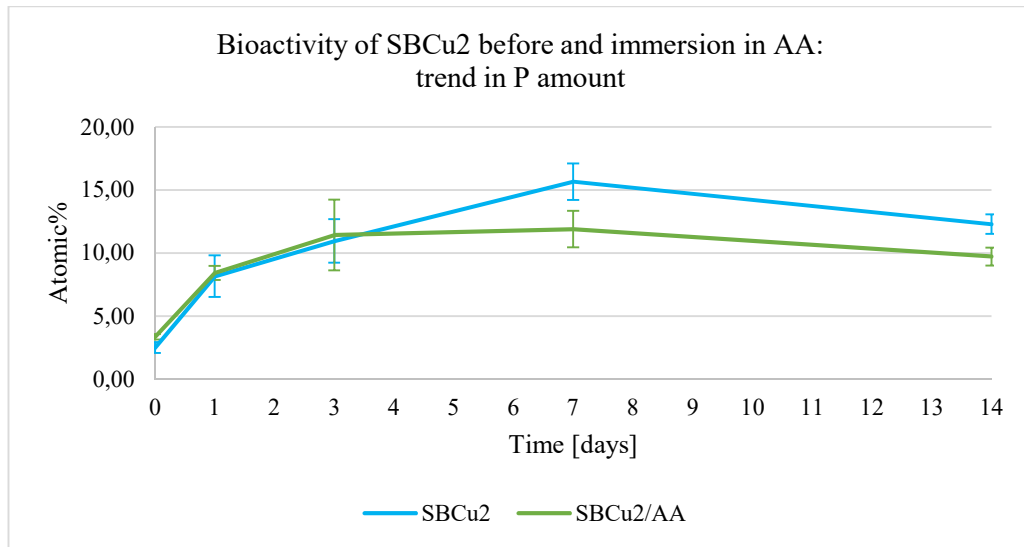


Figure 4.105: P amount in SB2 and SB2/AA after immersion in SBF

Ca amount of glasses immersed in acetic acid during the acellular bioactivity test were plotted versus time. No significant difference between trends of the glasses before and after soaking in AA was observed. Only SBCu2 seems to show a very slight decrease that could have caused the delayed bioactivity of the composite fiber PCL/AA/SBCu2(20%).

Figure 4.106 shows the trend of Ca amount for both S2 and S2/AA during immersion in SBF.

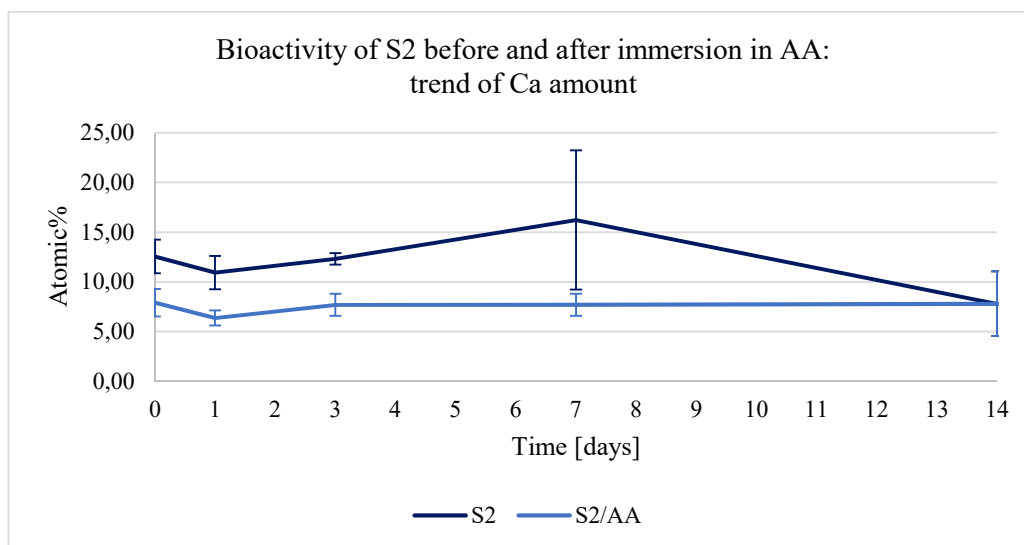


Figure 4.106: Ca amount in S2 and S2/AA after immersion in SBF

Figure 4.107 shows the trend of Ca amount for both SB2 and SB2/AA during immersion in SBF.

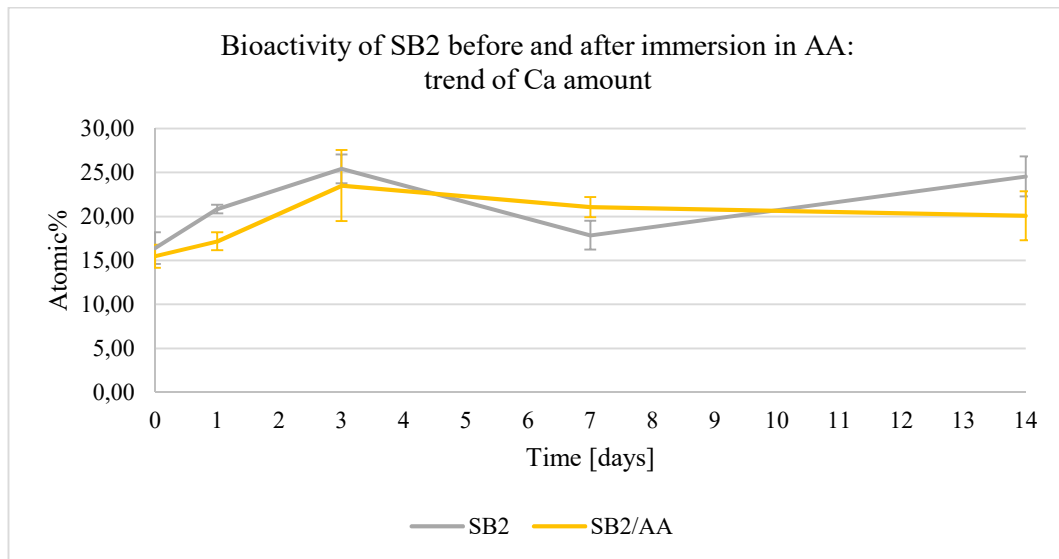


Figure 4.107: Ca amount in SB2 and SB2/AA after immersion in SBF

Figure 4.108 shows the trend of Ca amount for both SBCu2 and SBCu2/AA during immersion in SBF.

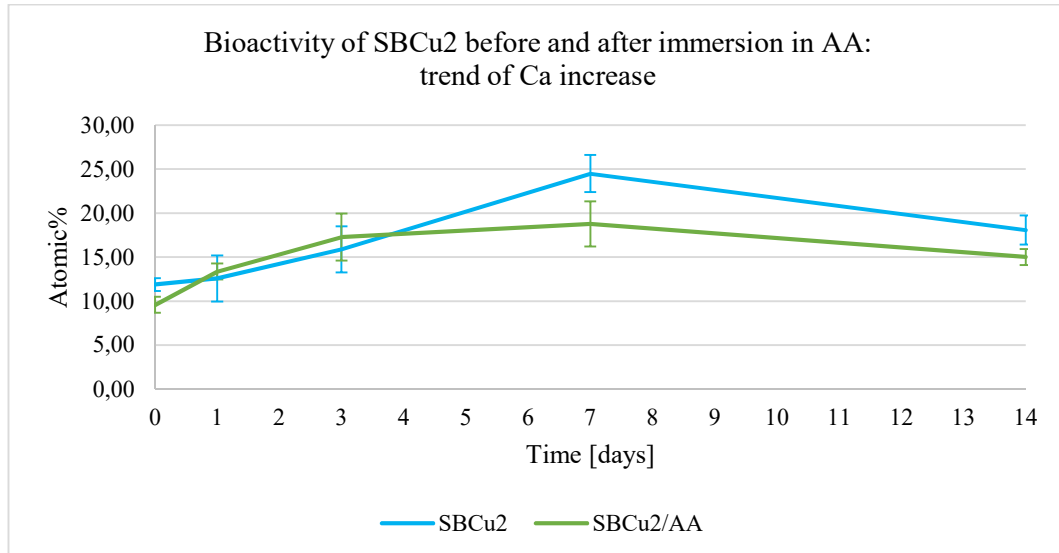


Figure 4.108: Ca amount in SBCu2 and SBCu2/AA after immersion in SBF

Values of Ca and P ratio (reported in Table 8) are coherent with the above reported P and Ca trends and with Ca/P values of the glasses before immersion in AA (shown in paragraph 3.3.4. As above mentioned, these values are similar to the stoichiometric ratio of HA. Lastly, it should be pointed out that the ratio values

are lower in case of SBCu2, in agreement with the delay in bioactivity observed in the electrospun fibers containing SBCu2 glass, commonly named as PCL/AA/SBCu2(20%).

Table 8: Ca/P ratio of glasses immersed in AA during acellular bioactivity test

| Ca/P ratio (atomic%) | | | | |
|----------------------|-----------|-----------|-----------|-----------|
| Glass | 1d | 3d | 7d | 14d |
| S2/AA | 1.9 ± 0.3 | 1.6 ± 0.1 | 1.6 ± 0.1 | 1.9 ± 0.2 |
| SB2/AA | 1.9 ± 0.1 | 1.7 ± 0.0 | 1.8 ± 0.1 | 1.8 ± 0.1 |
| SBCu2/AA | 1.6 ± 0.0 | 1.6 ± 0.2 | 1.6 ± 0.1 | 1.5 ± 0.1 |

Analogously to analysis performed on original glasses, x-ray diffraction analysis was carried out on the glasses/AA before and after immersion in SBF and XRD spectra were analyzed using the same computer program (X'Pert Highscore) used for analysis of XRD spectra of original glasses.

These spectra confirm the formation of an HA-like layer on the surface of the tested glasses, even after immersion in AA for 1 hour. Besides apatite nucleation, in few samples, the presence of sodium chloride was also detected, as previously obtained in case of original glasses.

In order to facilitate the identification of the peaks, the following symbols are used:

-  Calcium silicate
-  HA
-  NaCl
-  Copper acetate

In Figure 4.109 the XRD spectra of S2/AA is compared with XRD spectra of S2/AA after immersion in SBF solution until 14 days.

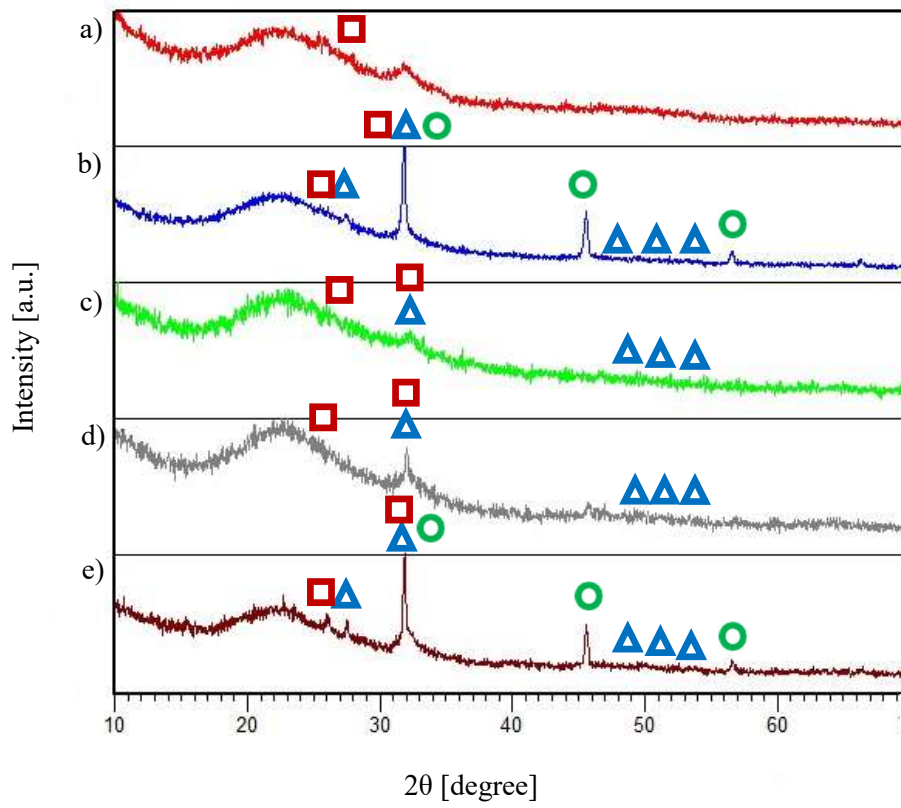


Figure 4.109: XRD spectra of S2/AA before and after immersion in SBF where a) S2/AA 0d b) S2/AA 1d c) S2/AA 3d d) S2/AA 7d and e) S2/AA 14d

In Figure 4.110 the spectra of S2/AA after 14 days in immersion in SBF is reported. The presence of the majority of apatite peaks is clearly evident.

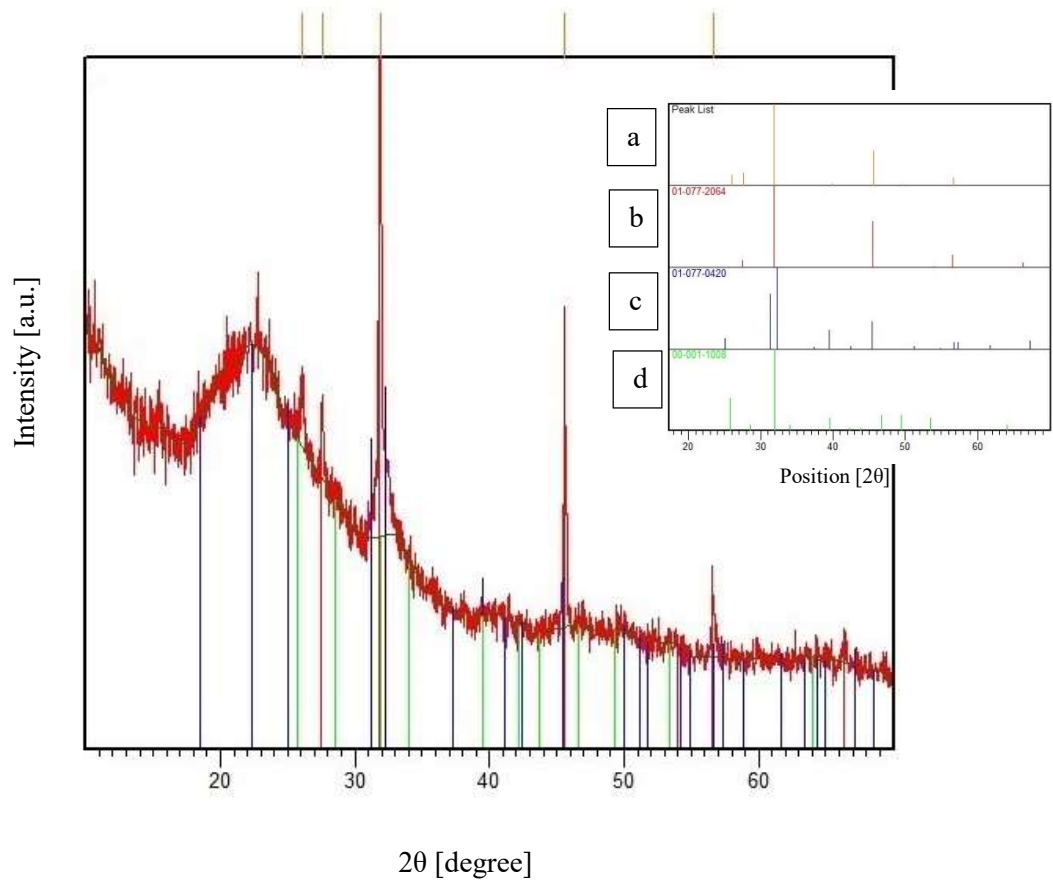


Figure 4.110: XRD spectrum of S2/AA after 14 days in SBF and related peaks lists where a) sample b) NaCl c) Ca₂SiO₄ and d) HA

A comparison of XRD spectra of SB2/AA at each different time point is shown in Figure 4.111.

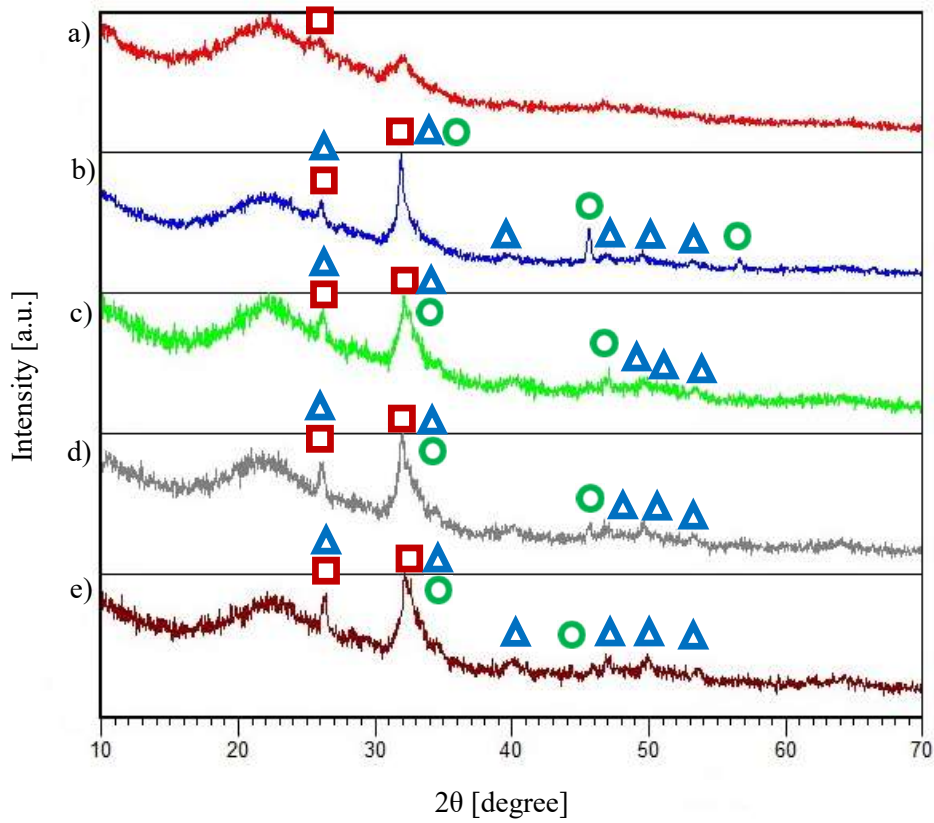


Figure 4.111: XRD spectra of SB2/AA before and after immersion in SBF where a) SB2/AA 0d b) SB2/AA 1d c) SB2/AA 3d d) SB2/AA 7d and e) SB2/AA 14d

Analogously to analysis carried out on S2/AA, in Figure 4.112 the spectra and peaks list comparison of SB2/AA after 14 days in immersion in SBF are reported.

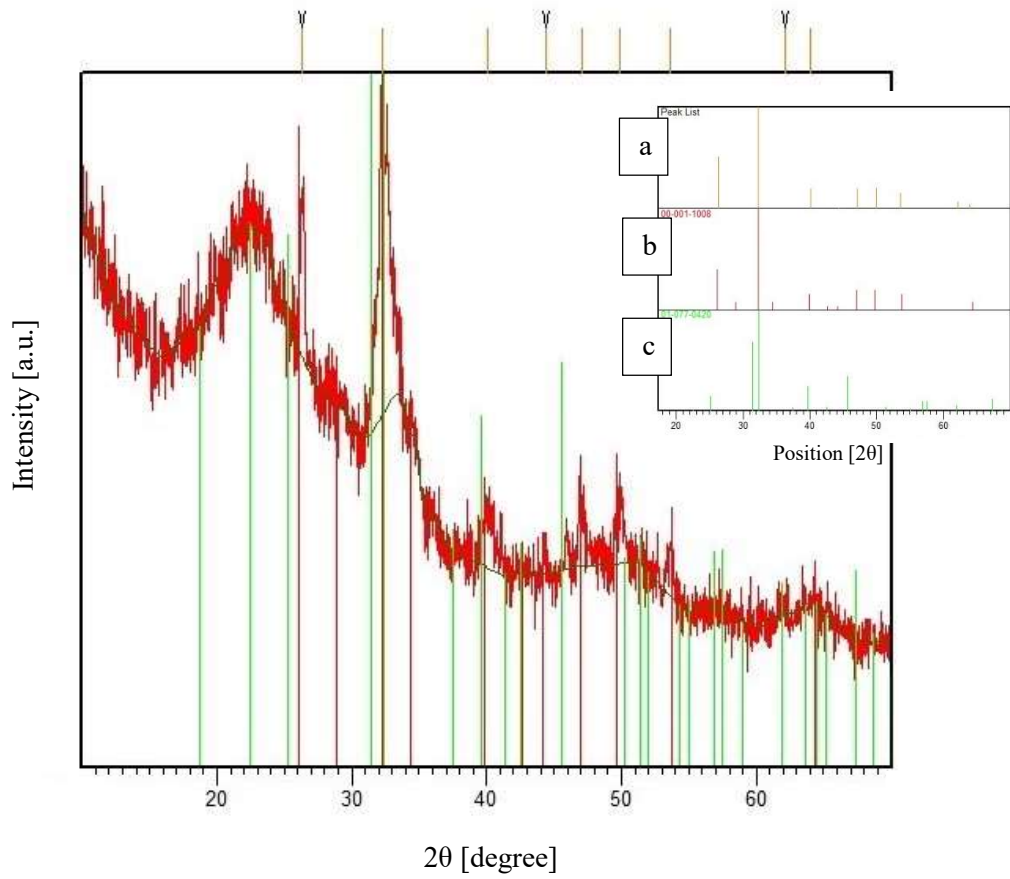


Figure 4.112: XRD spectrum of SB2/AA 14d and related peaks lists where a) sample b) Ca₂SiO₄ and c) HA

A comparison of XRD spectra of SBCu2/AA at each different time point and the XRD spectra at d14 is shown in Figure 4.113 and Figure 4.115.

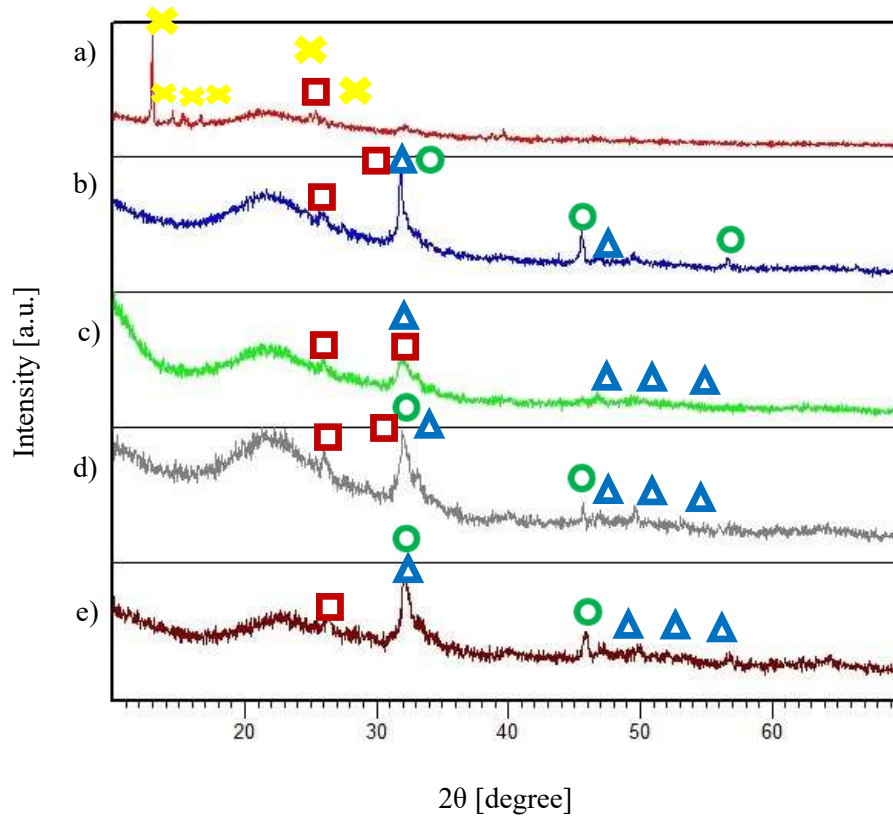


Figure 4.113: XRD spectra of SBCu2/AA before and after immersion in SBF where a) SBCu2/AA 0d b) SBCu2/AA 1d c) SBCu2/AA 3d d) SBCu2/AA 7d and e) SBCu2/AA 14d

In Figure 4.113 the XRD spectrum of SBCu2/AA after 1 day of immersion in SBF is shown. In this spectrum the typical peaks of the copper acetate are observable. However, after 1 day of immersion in SBF these peaks were not seen anymore. It was supposed that during soaking in AA the precipitation of copper acetate and its deposition on the BG particle surface took place, followed by its dissolution in the aqueous environment of SBF during the acellular bioactivity test.

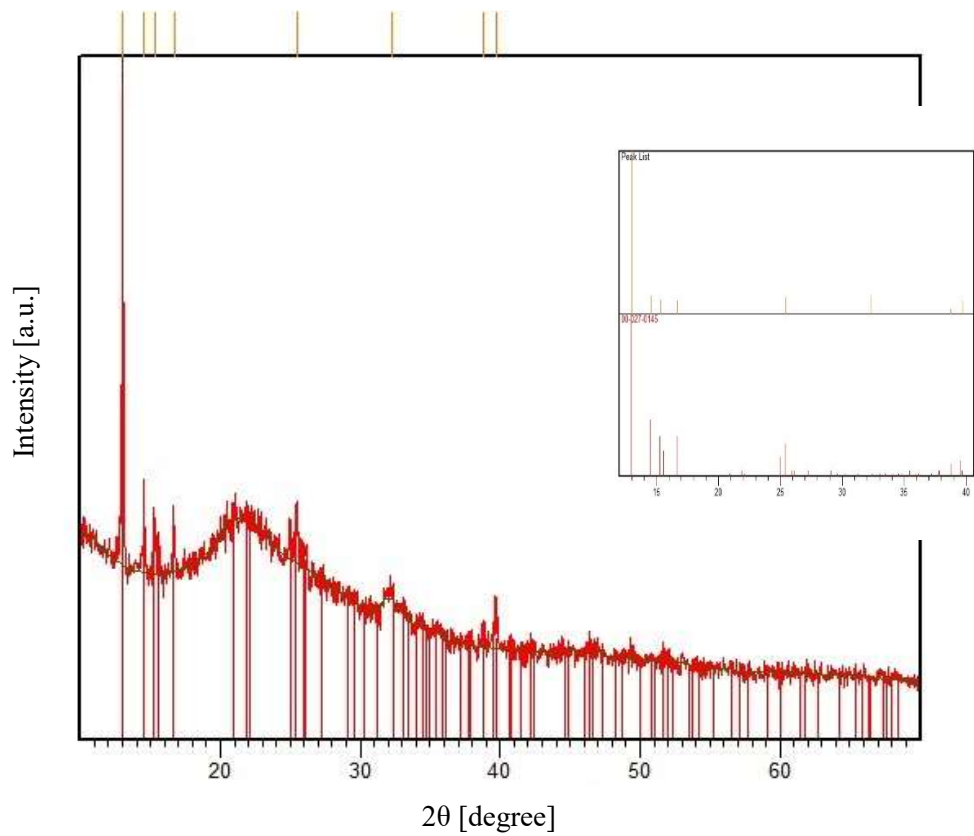
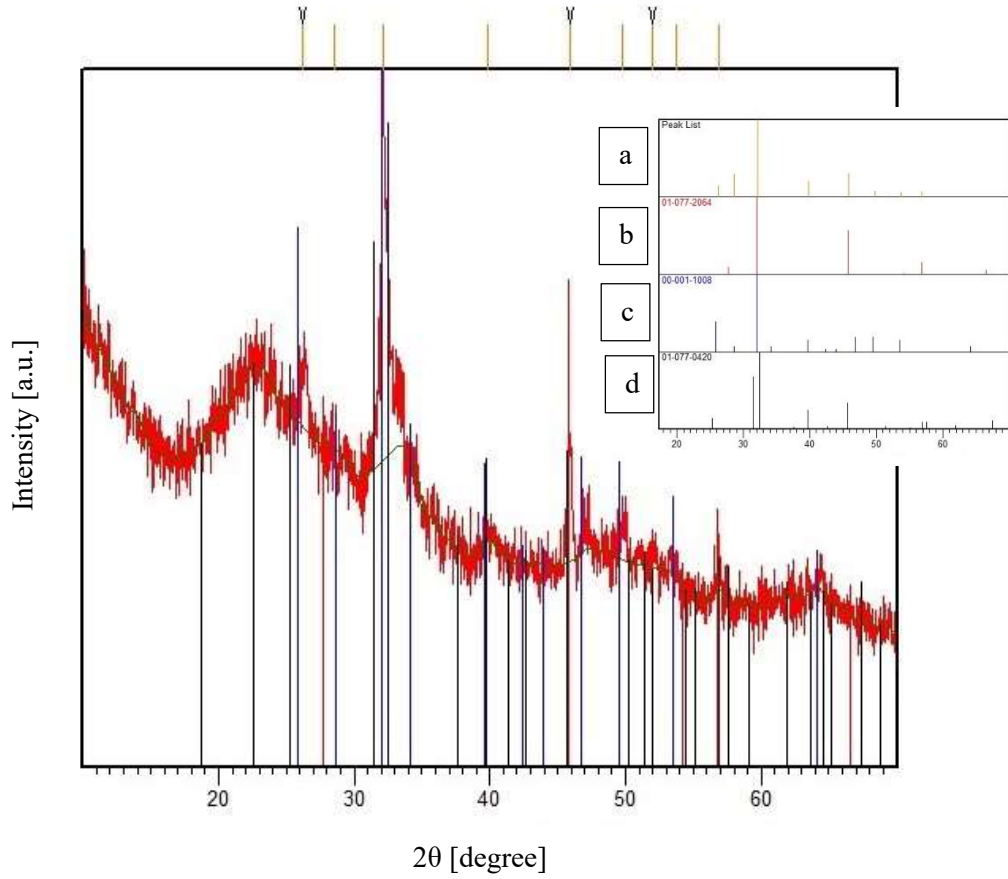


Figure 4.114: XRD spectrum of SBCu₂/AA SBF 1d with peaks of copper acetate

In Figure 4.115 the XRD spectrum of SBCu2/AA after 14 days of immersion in SBF is shown.



FE-SEM images were recorded on samples immersed in SBF, in order to evaluate the after growth of an HA-like layer on the surface of the glass nanoparticles, even after immersion in acetic acid. As shown in Figure 4.117, the presence of HA-like crystals was detected.

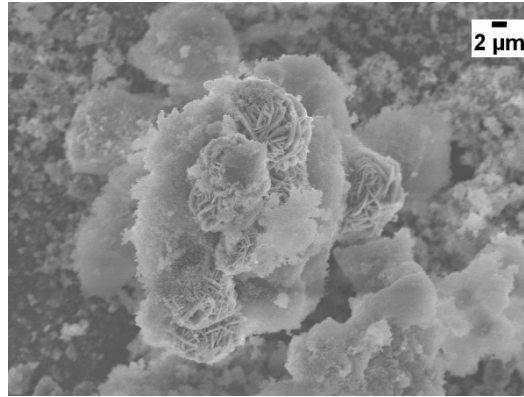


Figure 4.116: SEM micrograph of S2/AA SBF 1d (at 4K X)

Although the composite mats PCL/AA/SBCu2(20%) showed a delay in bioactivity, it is evident from Figure 4.117 that the surface of SBCu2 glass is covered with apatite crystals after 14 days in SBF, confirming that bioactive behaviour of SBCu2 was not hindered.

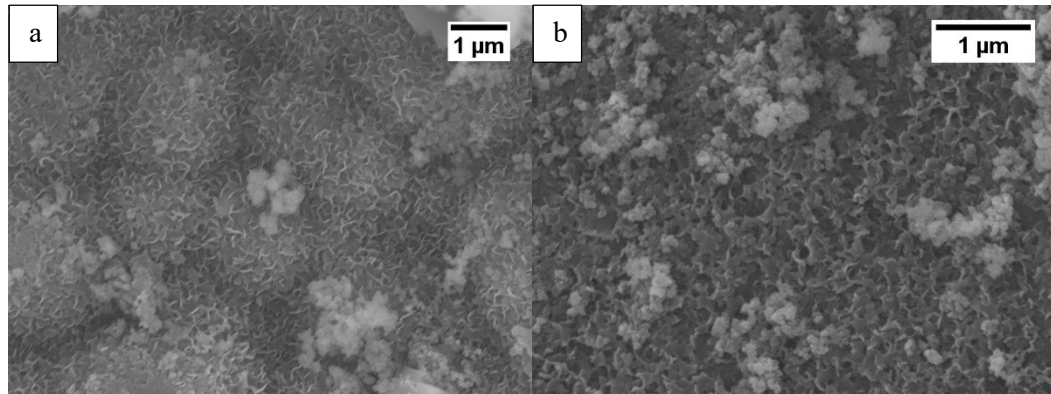


Figure 4.117: SEM micrograph of SBCu2/AA in SBF 14d at 30K X (a) and at 50.K X (b)

All these results confirm that the bioactivity of the glasses was not inhibited by acetic acid during the preparation of the electrospinning solutions.

4.3.9 Biological assay

The results from WST-8 assay are summarized in the Figure 4.118. In particular, it is possible to observe that for what concerns the evaluation of cells adhesion and viability after one day from the seeding, there are not differences between the control sample of neat PCL electrospun fibers and the composite fibers. The composite sample with SBCu2 glass particles showed the lowest value of absorbance at this timepoint. After 7 days from the seeding, even though the average value of absorbance for the control sample was higher respect to all the composites, it is possible to observe a relevant increase in the absorbance of all the composite samples, confirming that the presence of the glass particles did not inhibit cell proliferation.

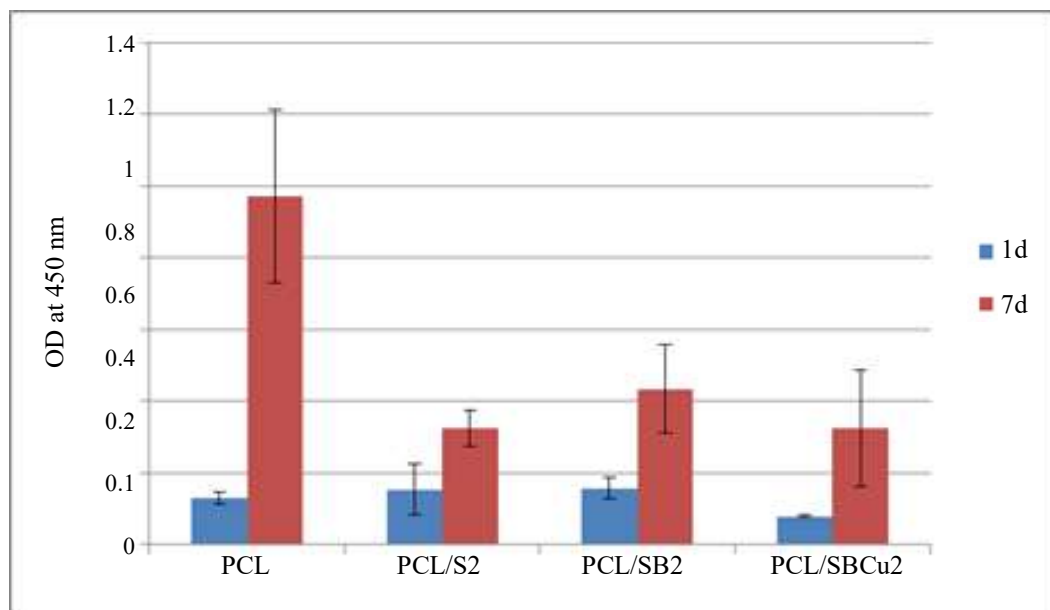


Figure 4.118: Biological assay results for both neat and composite electrospun mats

In fluorescence images of all samples after seven days (reported in Figure 4.119), the presence of vital cells on both pure PCL and composite fibers is clearly evident, confirming the composites were non toxic and cells were allowed to grow on them. These results are very promising considering the potential TE applications of the electrospun composite mats, synthesized during this master thesis work.

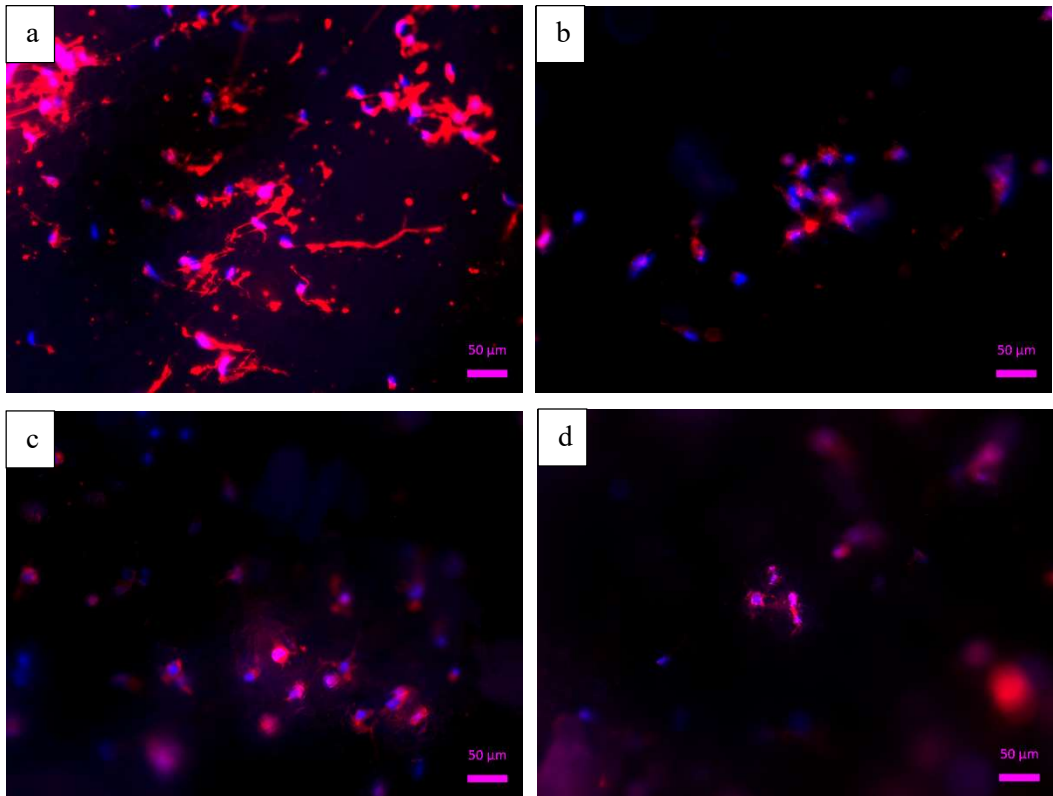


Figure 4.119: Fluorescence microscopy images
where a) PCL/AA b) PCL/AA/S2(20%) c) PCL/AA/SB2(20%) d) PCL/AA/SBCu2(20%)

5 Conclusion and future works

The aim of this master thesis project was the synthesis and characterization of composite fibrous scaffolds containing new synthesized glass powders. Indeed, the development of composite fibers is attractive for several applications related to the fabrication of scaffolds for tissue engineering. Composites of bioactive glasses and polymers are ones of the most promising materials in tissue engineering field.

Composite electrospun fibers can be obtained by the incorporation of bioactive glass nanoparticles inside a polymeric mat thanks to the electrospinning technique. This approach has been already widely investigated in the literature, especially for the development of composite electrospun scaffolds for bone tissue engineering. Although the development of optimal scaffolds is still a challenge in tissue engineering, the electrospinning technique is simple and versatile and allow to fabricate scaffolds characterized by morphological features similar to the ECM. In the current literature, a majority of polymers that have been successfully electrospun into ultrafine fibers are synthetic. Among them, PCL was selected because of its biocompatibility, biodegradability, ability to be processed by electrospinning, in particular with benign solvents, and considering its FDA approval for clinical use.

Limiting the use of harsh solvents is highly beneficial in terms of avoiding the presence of toxic solvent residuals inside the mats which could limit their applications in the biomedical field, lab worker safety and environmental impact. Moreover, using benign solvents, in future, it could be possible to incorporate proteins, such as collagen and other sensitive biomolecules, preventing denaturation.

The synthesis of bioactive glasses doped with boron and copper was successfully achieved by both synthesis methods. It is worth noticing that the chemical composition of the actual synthesized glasses is innovative and these glasses have a lot of potential applications in the tissue engineering field thanks to the

incorporation of boron and copper ions, which have been proven to have osteogenic and angiogenic effect, and antibacterial properties, respectively.

The effort to synthesize glass particles with average size in the nanometric range was done, because according to literature results, it is easier to insert nanoparticles in fibers with diameters varying from micro to nano scale, but because of their nano-sized dimension the obtained particles have been resulted very aggregated, hindering the achievement of a homogenous dispersion of the glass powders in the PCL matrix.

Clearly, an important challenge in the fabrication of composites is the ability to obtain as completed as possible dispersion of the primary particles and to maintain this dispersion throughout the lifetime of the composite. During this experimental work, a lots of different addition methods were tried in order to prevent the formation of glass aggregates. It was possible to limit it but presence of glass clusters in the polymer mat was not completely avoided. Therefore, aggregation should be reduced before composite fabrication. In future, surface modification of the nanoparticles, such as adsorption of surfactants or polyelectrolytes as well as surface grafting techniques, could be tried. Alternatively, synthesis process could be modified. In the latter approach, to prevent glass particles agglomeration, the following strategies could be adopted:

- calcium methoxyethoxide could be uses as calcium source instead of calcium nitrate, because calcium would be directly involved in the inorganic polymerization process and thus inserted inside the silica network;
- the sol-gel process, and more particularly NH_4OH addition, could be carry out under ultrasonic treatment (in addition the mechanical stirring);
- glass particles could be freeze-dried before annealing treatment;
- lactic acid could be added during sol-gel process (according to recent results, morphology, size and distribution of bioactive glass nanoparticles can be controlled by addition of LA during synthesis);
- surfactants (like CTAB), additives and other organic species acting as shape-forming agents or as steric barriers could be added during glass synthesis, to improve the dispersity of particles.

However, the results of this master thesis work highlight the potential applications of the obtained mats as scaffolds for tissue engineering applications, in particular in case of incorporation of SB2 glass. In fact, the glass powders were bioactive and their incorporation in the PCL fibers was able to induce the HA precipitation on the polymer fibers after 21 days. However, in order to optimize the bioactive behavior of the composite mats, the glass dispersion in the PCL network should be improved.

A preliminary study on cell viability was carried out, but further detailed studies focused on cell viability with other cell lines could be done, in order to complete the characterization of the composite nanofibers for the intended applications.

Recently, some natural biopolymer fibers (including silk, fibrinogen and collagen) have also been successfully electrospun. Compared to synthetic polymers, natural biopolymers have good biocompatibility; however, their processability is, in general, pretty poor. Therefore, the synthesis of composite fibrous mats by combination of blends of PCL and natural polymers, and the glasses synthesized during this master thesis work, could also be tried.

6 Bibliography

- [1] S. Zhao *et al.*, “Wound dressings composed of copper-doped borate bioactive glass micro fibers stimulate angiogenesis and heal full-thickness skin defects in a rodent model,” *Biomaterials*, vol. 53, 2015.
- [2] F. Baino, S. Fiorilli, and C. Vitale-brovarone, “Bioactive glass-based materials with hierarchical porosity for medical applications: Review of recent advances,” *Acta Biomater.*, vol. 42, pp. 18–32, 2016.
- [3] F. J. O. Brien, “Biomaterials & scaffolds for tissue engineering,” *Mater. Today*, vol. 14, no. 3, pp. 88–95, 2011.
- [4] J. P. Vacanti and R. Langer, “Tissue engineering: the design and fabrication of living replacement devices for surgical reconstruction and transplantation,” *Mol. medicine*, vol. 354, pp. 32–34, 1999.
- [5] B. Pei, W. Wang, Y. Fan, X. Wang, F. Watari, and X. Li, “Fiber-reinforced scaffolds in soft tissue engineering,” *Regen. Biomater.*, pp. 257–268, 2017.
- [6] R. Sridhar, S. Sundarajan, J. Reddy, R. Ravichandran, and S. Ramakrishna, “Electrospun inorganic and polymer composite nanofibers for biomedical applications,” *J. Biomater. Sci. Polym. Ed.*, vol. 5063, 2013.
- [7] L. Gerhardt and A. R. Boccaccini, “Bioactive Glass and Glass-Ceramic Scaffolds for Bone Tissue Engineering,” *Materials (Basel)*, vol. 3, pp. 3867–3910, 2010.
- [8] M. Wang, “Developing bioactive composite materials for tissue replacement,” *Biomaterials*, vol. 24, no. October 2002, pp. 2133–2151, 2003.
- [9] E. M. F. Lemos, S. M. Carvalho, P. S. O. Patrício, C. L. Donnici, and M. M. Pereira, “Comparison of the Effect of Sol-Gel and Coprecipitation Routes on the Properties and Behavior of Nanocomposite Chitosan-Bioactive Glass Membranes for Bone Tissue Engineering,” vol. 2015, 2015.
- [10] Q. Fu, E. Saiz, M. N. Rahaman, and A. P. Tomsia, “Bioactive glass scaffolds for bone tissue engineering: state of the art and future perspectives,” *Mater. Sci. Eng. C*, vol. 31, no. 7, pp. 1245–1256, 2011.
- [11] K. Rezwani, Q. Z. Chen, J. J. Blaker, and A. R. Boccaccini, “Biodegradable and bioactive porous polymer/inorganic composite scaffolds for bone tissue engineering,” *SEAIQ. (South East Asia Iron Steel Institute)*, vol. 27, pp. 3413–3431, 2006.
- [12] X. Wang, J. Chang, and C. Wu, “Bioactive inorganic/organic nanocomposites for wound healing,” *Appl. Mater. Today*, vol. 11, pp. 308–319, 2018.
- [13] A. R. Boccaccini, M. Erol, W. J. Stark, D. Mohn, Z. Hong, and J. F. Mano, “Polymer/bioactive glass nanocomposites for biomedical applications: A review,” *Compos. Sci. Technol.*, vol. 70, no. 13, pp. 1764–1776, 2010.
- [14] B. A. Allo, A. S. Rizkalla, and K. Mequanint, “Synthesis and Electrospinning of ϵ -Polycaprolactone-Bioactive Glass Hybrid Biomaterials via a Sol-Gel Process,” *Langmuir*, vol. 26, no. 13, pp. 18340–18348, 2010.
- [15] Q. Chen, J. A. Roether, and A. R. Boccaccini, “Tissue Engineering Scaffolds from Bioactive Glass and Composite Materials,” in *Topics in Tissue Engineering*, 2008,

p. 27.

- [16] S. L. GrØndahl and K. S. Jack, "Composite materials for bone repair," in *Biomedical composites*, p. 126.
- [17] H. Zhou, J. G. Lawrence, and S. B. Bhaduri, "Fabrication aspects of PLA-CaP/PLGA-CaP composites for orthopedic applications: A review," *Acta Biomater.*, vol. 8, no. 6, pp. 1999–2016, 2012.
- [18] O. Access, W. C. Lepry, S. Smith, L. Liverani, A. R. Boccaccini, and S. N. Nazhat, "Acellular Bioactivity of Sol-Gel Derived Borate Glass-Polycaprolactone Electrospun Scaffolds," *Biomed. Glas.*, vol. 2, no. May, pp. 88–98, 2016.
- [19] P. Wutticharoenmongkol, N. Sanchavanakit, P. Pavasant, and P. Supaphol, "Preparation and characterization of novel bone scaffolds based on electrospun polycaprolactone fibers filled with nanoparticles," *Macromol. Biosci.*, vol. 6, no. 1, pp. 70–77, 2006.
- [20] L. Liverani and A. Boccaccini, "Versatile Production of Poly(Epsilon-Caprolactone) Fibers by Electrospinning Using Benign Solvents," *Nanomaterials*, vol. 6, no. 4, p. 75, 2016.
- [21] L. Gerhardt *et al.*, "The pro-angiogenic properties of multi-functional bioactive glass composite scaffolds," *Biomaterials*, vol. 32, pp. 4096–4108, 2011.
- [22] K. Noh, H. Lee, U. Shin, and H. Kim, "Composite nano fiber of bioactive glass nano filler incorporated poly (lactic acid) for bone regeneration," *Mater. Lett.*, vol. 64, no. 7, pp. 802–805, 2010.
- [23] M. Otadi and D. Mohebbi-kalhari, "Evaluate of Different Bioactive Glass on Mechanical Properties of Nanocomposites Prepared Using Electrospinning Method," *Procedia Mater. Sci.*, vol. 11, no. 2013, pp. 196–201, 2015.
- [24] H. Kim, E. Lee, I. Jun, H. Kim, and J. C. Knowles, "Degradation and Drug Release of Phosphate Glass/Polycaprolactone Biological Composites for Hard-Tissue Regeneration," *Wiley Period.*, pp. 34–41, 2005.
- [25] K. Zheng and A. R. Boccaccini, "Sol-gel processing of bioactive glass nanoparticles: A review," *Adv. Colloid Interface Sci.*, vol. 249, pp. 363–373, 2017.
- [26] C. Wanpeng and L. L. Hench, "Bioactive Materials," *Bioact. Mater.*, vol. 8842, no. 95, pp. 493–507, 1996.
- [27] A. M. Deliormanlı and M. Yildirim, "Sol-gel synthesis of 13-93 bioactive glass powders containing therapeutic agents," vol. 52, pp. 9–19, 2016.
- [28] F. Bairo, "Bioactive Glasses: Where Are We and Where Are We Going?," *J. Funct. Biomater.*, vol. 9, no. 25, pp. 1–26, 2018.
- [29] D. Qiu, R. A. Martin, J. C. Knowles, M. E. Smith, and R. J. Newport, "A comparative study of the structure of sodium borophosphates made by sol-gel and melt-quench methods," *J. Non. Cryst. Solids*, vol. 356, no. 9–10, pp. 490–494, 2010.
- [30] C. Vichery and J. Nedelec, "Bioactive Glass Nanoparticles: From Synthesis to Materials Design for Biomedical Applications," 2016.
- [31] F. E. Ciraldo, L. Liverani, and A. R. Boccaccini, "Synthesis and Characterization

- of Silver-Doped Mesoporous Bioactive Glass and Its Applications in Conjunction with Electrospinning,” *Materials (Basel)*, vol. 11, no. 692, pp. 1–16, 2018.
- [32] B. H. Kim, H. Kim, and J. C. Knowles, “Production and Potential of Bioactive Glass Nanofibers as a Next-Generation Biomaterial,” *Adv. Funct. Mater.*, vol. 16, pp. 1529–1535, 2006.
- [33] X. Chen, B. Lei, Y. Wang, and N. Zhao, “Morphological control and in vitro bioactivity of nanoscale bioactive glasses,” *J. Non. Cryst. Solids*, vol. 355, no. 13, pp. 791–796, 2009.
- [34] M. M. Pereira, J. R. Jones, L. L. Hench, M. M. Pereira, J. R. Jones, and L. L. Hench, “Bioactive glass and hybrid scaffolds prepared by sol–gel method for bone tissue engineering,” *Adv. Appl. Ceram.*, vol. 6753, 2013.
- [35] D. Bellucci *et al.*, “Processing and characterization of innovative scaffolds for bone tissue engineering,” pp. 1397–1409, 2012.
- [36] D. Kim, J. Lee, S. Jun, and H. Kim, “Sol–gel-derived bioactive glass nanoparticle incorporated glass ionomer cement with or without chitosan for enhanced mechanical and biomineralization properties,” *Dent. Mater.*, vol. 33, no. 7, pp. 805–817, 2017.
- [37] A. Lopez-Noriega *et al.*, “Ordered Mesoporous Bioactive Glasses for Bone Tissue Regeneration,” *Chem. Mater.*, vol. 18, no. 18, pp. 3137–3144, 2006.
- [38] A. A. R. de Oliveira, D. A. de Souza, S. M. de Carvalho, and M. de M. Mansur, Herman Sander and Pereira, “Synthesis, characterization and cytocompatibility of spherical bioactive glass nanoparticles for potential hard tissue engineering applications,” *Biomed. Mater.*, vol. 8, no. 025011, pp. 1748–6041, 2013.
- [39] X. Yan *et al.*, “The in-vitro bioactivity of mesoporous bioactive glasses,” *Biomaterials*, vol. 27, pp. 3396–3403, 2006.
- [40] A. M. El-kady and M. M. Farag, “Bioactive Glass Nanoparticles as a New Delivery System for Sustained 5-Fluorouracil Release: Characterization and Evaluation of Drug Release Mechanism,” vol. 2015, 2015.
- [41] H. Yun, S. Kim, S. Lee, and I. Song, “Synthesis of high surface area mesoporous bioactive glass nanospheres,” *Mater. Lett.*, vol. 64, no. 16, pp. 1850–1853, 2010.
- [42] P. Taylor, “‘Cotton candy’ that heals? Borate glass nanofibers look promising,” *Bulletin*, pp. 2–6.
- [43] N. Gupta, D. Santhiya, S. Murugavel, A. Kumar, and A. Aditya, “Effects of transition metal ion dopants (Ag, Cu and Fe) on the structural, mechanical and antibacterial properties of bioactive glass,” *Colloids Surfaces A*, vol. 538, no. August 2017, pp. 393–403, 2018.
- [44] C. Wu, R. Miron, A. Sculean, S. Kaskel, T. Doert, and R. Schulze, “Proliferation, differentiation and gene expression of osteoblasts in boron-containing associated with dexamethasone deliver from mesoporous bioactive glass scaffolds,” *Biomaterials*, vol. 32, pp. 7068–7078, 2011.
- [45] S. P. S, S. Datta, T. Adarsh, P. Diwan, and K. Annapurna, “Effect of boron oxide addition on structural, thermal, in vitro bioactivity and antibacterial properties of bioactive glasses in the base S53P4 composition,” *J. Non. Cryst. Solids*, vol. 498, no. May, pp. 204–215, 2018.

- [46] X. Lu, L. Deng, P. Kuo, M. Ren, I. Buterbaugh, and J. Du, "Effects of boron oxide substitution on the structure and bioactivity of SrO-containing bioactive glasses," *J. Mater. Sci.*, vol. 52, no. 15, pp. 8793–8811, 2017.
- [47] R. Moonesi, A. Z. Alshemary, Z. Evis, D. Keskin, and K. Altunba, "Structural and biological assessment of boron doped bioactive glass nanoparticles for dental tissue applications," vol. 44, no. October 2017, pp. 9854–9864, 2018.
- [48] E. Mancuso, O. Bretcanu, M. Marshall, and K. W. Dalgarno, "Sensitivity of novel silicate and borate-based glass structures on in vitro bioactivity and degradation behaviour," *Ceram. Int.*, vol. 43, no. April, pp. 12651–12657, 2017.
- [49] R. Gustavo *et al.*, "Preparation and characterization of boron-based bioglass by sol-gel process," *J. Sol-Gel Sci. Technol.*, pp. 181–191, 2018.
- [50] C. Gérard, L. Bordeleau, J. Barralet, and C. J. Doillon, "The stimulation of angiogenesis and collagen deposition by copper," *Biomaterials*, vol. 31, pp. 824–831, 2010.
- [51] X. Wang *et al.*, "Biocomposites of copper-containing mesoporous bioactive glass and nanofibrillated cellulose: Biocompatibility and angiogenic promotion in chronic wound healing application," *Acta Biomater.*, vol. 46, pp. 286–298, 2016.
- [52] J. Bejarano, P. Caviedes, and H. Palza, "Sol-gel synthesis and in vitro bioactivity of copper and zinc-doped silicate bioactive glasses and glass-ceramics," *Biomed. Mater.*, vol. 10, pp. 1–13, 2015.
- [53] J. Li *et al.*, "Preparation of copper-containing bioactive glass/eggshell membrane nanocomposites for improving angiogenesis, antibacterial activity and wound healing," *Acta Biomater.*, vol. 36, pp. 254–266, 2016.
- [54] F. Martin *et al.*, "Copper-dependent activation of hypoxia-inducible factor (HIF)-1: implications for ceruloplasmin regulation," *Blood*, vol. 105, no. 12, pp. 4613–4620, 2005.
- [55] E. Mancuso, O. A. Bretcanu, M. Marshall, M. A. Birch, A. W. Mccaskie, and K. W. Dalgarno, "Novel bioglasses for bone tissue repair and regeneration: Effect of glass design on sintering ability, ion release and biocompatibility," *Mater. Des.*, vol. 129, no. January, pp. 239–248, 2017.
- [56] Y. Lin, W. Xiao, B. S. Bal, and M. N. Rahaman, "Effect of copper-doped silicate 13–93 bioactive glass scaffolds on the response of MC3T3-E1 cells in vitro and on bone regeneration and angiogenesis in rat calvarial defects in vivo," *Mater. Sci. Eng. C*, vol. 67, pp. 440–452, 2016.
- [57] S. Ö. Gönen, M. E. Taygun, and S. Küçükbayrak, "Fabrication of bioactive glass containing nanocomposite fiber mats for bone tissue engineering applications," *Compos. Struct.*, vol. 138, pp. 96–106, 2016.
- [58] H. Palza, B. Escobar, J. Bejarano, D. Bravo, M. Diaz-dosque, and J. Perez, "Designing antimicrobial bioactive glass materials with embedded metal ions synthesized by the sol – gel method," *Mater. Sci. Eng. C*, vol. 33, no. 7, pp. 3795–3801, 2013.
- [59] K. T. Noh, H. Y. Lee, U. S. Shin, and H. W. Kim, "Composite nanofiber of bioactive glass nanofiller incorporated poly(lactic acid) for bone regeneration," *Mater. Lett.*, vol. 64, no. 7, pp. 802–805, 2010.

- [60] A. E. Danks, S. R. Hall, and Z. Schnepp, "The evolution of 'sol-gel' chemistry as a technique for materials synthesis," *Mater. Horizons*, vol. 3, pp. 91–112, 2016.
- [61] G. J. Owens *et al.*, "Sol-gel based materials for biomedical applications," *Prog. Mater. Sci.*, vol. 77, pp. 1–79, 2016.
- [62] F. Baino, E. Fiume, M. Miola, and E. Verné, "Bioactive sol-gel glasses: Processing, properties, and applications," *Appl. Ceram. Technol.*, vol. 15, no. January, pp. 841–860, 2018.
- [63] L. P. Singh *et al.*, "Sol-Gel processing of silica nanoparticles and their applications," *Adv. Colloid Interface Sci.*, vol. 214, pp. 17–37, 2014.
- [64] E. Muzzi, "Il processo sol-gel per la sintesi del vetro: dalle nanoparticelle al bulk," Politecnico di Torino, 2018.
- [65] W. Xia and J. Chang, "Preparation and characterization of nano-bioactive-glasses (NBG) by a quick alkali-mediated sol-gel method," *Mater. Lett.*, vol. 61, no. 3, pp. 3251–3253, 2007.
- [66] D. Nagao, H. Osuzu, A. Yamada, E. Mine, and Y. Kobayashi, "Particle formation in the hydrolysis of tetraethyl orthosilicate in pH buffer solution," *J. Colloid Interface Sci.*, vol. 279, pp. 143–149, 2004.
- [67] F. Sharifianjazi, N. Parvin, and M. Tahriri, "Synthesis and characteristics of sol-gel bioactive SiO₂-P₂O₅-CaO-Ag₂O glasses," *J. Non. Cryst. Solids*, vol. 476, no. August, pp. 108–113, 2017.
- [68] F. Tescione, "Sintesi Sol-Gel e Caratterizzazione di Materiali Ibridi e Nanocompositi," Università degli Studi di Napoli "Federico II" D, 2009.
- [69] D. I. Braghirolli, D. Steffens, and P. Pranke, "Electrospinning for regenerative medicine: a review of the main topics," *Drug Discov. Today*, vol. 19, no. 6, pp. 743–753, 2014.
- [70] Y. Zhang, H. Ouyang, C. T. Lim, S. Ramakrishna, and Z. Huang, "Electrospinning of Gelatin Fibers and Gelatin/PCL Composite Fibrous Scaffolds," *Wiley Intersci.*, pp. 156–165, 2004.
- [71] H. S. Yoo, T. G. Kim, and T. G. Park, "Surface-functionalized electrospun nano fibers for tissue engineering and drug delivery," *Adv. Drug Deliv. Rev.*, vol. 61, no. 12, pp. 1033–1042, 2009.
- [72] M. S. Kang, J. H. Kim, R. K. Singh, J. H. Jang, and H. W. Kim, "Therapeutic-designed electrospun bone scaffolds: Mesoporous bioactive nanocarriers in hollow fiber composites to sequentially deliver dual growth factors," *Acta Biomater.*, vol. 16, no. 1, pp. 103–116, 2015.
- [73] J. F. Cooley, "Apparatus for electrically dispersing fluids," US692631, 1902.
- [74] W. J. Morton, "Method of dispersing fluid," US 70569.
- [75] T. Jiang, E. J. Carbone, and K. W. Lo, "Electrospinning of polymer nanofibers for tissue regeneration," *Prog. Polym. Sci.*, vol. 46, pp. 1–24, 2015.
- [76] S. Thenmozhi, N. Dharmaraj, K. Kadirvelu, and H. Yong, "Electrospun nanofibers: New generation materials for advanced applications," *Mater. Sci. Eng. B*, vol. 217, pp. 36–48, 2017.

- [77] Q. P. Pham, U. Sharma, D. Ph, A. G. Mikos, and D. Ph, "Electrospinning of Polymeric Nanofibers for Tissue Engineering Applications : A Review," vol. 12, no. 5, 2006.
- [78] L. Liverani, E. Boccardi, and A. Maria, "Incorporation of Calcium Containing Mesoporous (MCM-41-Type) Particles in Electrospun PCL Fibers by Using Benign Solvents," pp. 1–16, 2017.
- [79] A. Haider, S. Haider, and I. Kang, "REVIEW A comprehensive review summarizing the effect of electrospinning parameters and potential applications of nanofibers in biomedical and biotechnology," *Arab. J. Chem.*, vol. 11, no. 8, pp. 1165–1188, 2018.
- [80] C. Teck, "Nanofiber technology: current status and emerging developments," *Prog. Polym. Sci.*, vol. 70, pp. 1–17, 2017.
- [81] L. Liverani *et al.*, "Incorporation of bioactive glass nanoparticles in electrospun PCL/chitosan fibers by using benign solvents," *Bioact. Mater.*, vol. 3, no. 1, pp. 55–63, 2018.
- [82] D. Moura *et al.*, "Development of a bioactive glass-polymer composite for wound healing applications," *Mater. Sci. Eng. C*, vol. 76, pp. 224–232, 2017.
- [83] J. Li *et al.*, "Effect of Voltage and Flow Rate Electrospinning Parameters on Polyacrylonitrile Electrospun Fibers Effect of Voltage and Flow Rate Electrospinning Parameters on Polyacrylonitrile Electrospun Fibers," 2018.
- [84] S. Zargham, S. Bazgir, A. Tavakoli, A. S. Rashidi, and R. Damerchely, "The Effect of Flow Rate on Morphology and Deposition Area of Electrospun Nylon 6 Nanofiber," vol. 7, no. 4, pp. 42–49, 2012.
- [85] J. J. Stanger, D. Jacobs, J. Stanger, N. Tucker, K. Kirwan, and S. Coles, "Effect of Charge Density on the Taylor Cone in Electrospinning Effect of Charge Density on the Taylor Cone in Electrospinning," 2009.
- [86] L. Van Der Schueren, B. De Schoenmaker, Ö. I. Kalaoglu, and K. De Clerck, "An alternative solvent system for the steady state electrospinning of polycaprolactone," *Eur. Polym. J.*, vol. 47, no. 6, pp. 1256–1263, 2011.
- [87] Z. Hong, A. Liu, L. Chen, X. Chen, and X. Jing, "Preparation of bioactive glass ceramic nanoparticles by combination of sol–gel and coprecipitation method," *J. Non. Cryst. Solids*, vol. 355, no. 6, pp. 368–372, 2009.
- [88] R.-S. Mikhail, S. Brunauer, and E. E. Bodor, "Investigations of a Complete Pore Structure Analysis I. Analysis of Micropores," *J. Colloid Interface Sci.*, vol. 3, 1968.
- [89] D. Dollimore, P. Spooner, and A. Turner, "The BET method of analysis of gas absorption data and its relevance to the calculation of surface areas," *Surf. Technol.*, vol. 4, pp. 121–160, 1976.
- [90] K. Tadashi and H. Takadama, "How useful is SBF in predicting in vivo bone bioactivity?," *Biomaterials*, vol. 27, pp. 2907–2915, 2006.
- [91] L. Liverani, M. S. Killian, and A. R. Boccaccini, "Fibronectin Functionalized Electrospun Fibers by Using Benign Solvents: Best Way to Achieve Effective Functionalization," *Front. Bioeng. Biotechnol.*, vol. 7, no. April, pp. 1–12, 2019.

- [92] G. M. Luz and F. Mano, "Preparation and characterization of bioactive glass nanoparticles prepared by sol-gel for biomedical applications," *Nanotechnology*, vol. 22, no. 494014, pp. 1–11, 2011.
- [93] B. Lei, X. Chen, Y. Wang, and N. Zhao, "Synthesis and in vitro bioactivity of novel mesoporous hollow bioactive glass microspheres," *Mater. Lett.*, vol. 63, no. 20, pp. 1719–1721, 2009.
- [94] A. M. El-kady, A. F. Ali, and M. M. Farag, "Development, characterization, and in vitro bioactivity studies of sol-gel bioactive glass/poly (L-lactide) nanocomposite scaffolds," *Mater. Sci. Eng. C*, vol. 30, no. 1, pp. 120–131, 2010.
- [95] M. Mozafari, F. Moztarzadeh, and M. Tahriri, "Investigation of the physico-chemical reactivity of a mesoporous bioactive SiO₂-CaO-P₂O₅ glass in simulated body fluid," *J. Non. Cryst. Solids*, vol. 356, no. 28–30, pp. 1470–1478, 2010.
- [96] S. Zhao, Y. Li, and D. Li, "Synthesis and in vitro bioactivity of CaO-SiO₂-P₂O₅ mesoporous microspheres," *Microporous Mesoporous Mater.*, vol. 135, pp. 67–73, 2010.
- [97] M. Bengisu, E. Ylmaz, H. Farzad, and S. T. Reis, "Borate, lithium borate, and borophosphate powders by sol-gel precipitation," *J. Sol-Gel Sci. Technol.*, vol. 45, pp. 237–243, 2008.
- [98] X. Wang, Y. Zhang, C. Lin, and W. Zhong, "Sol-gel derived terbium-containing mesoporous bioactive glasses nanospheres: In vitro hydroxyapatite formation and drug delivery," *Colloids Surfaces B Biointerfaces*, vol. 160, pp. 406–415, 2017.
- [99] A. Bonici, G. Lusvardi, G. Malavasi, L. Menabue, and A. Piva, "Synthesis and characterization of bioactive glasses functionalized with Cu nanoparticles and organic molecules," *Ecros*, vol. 32, pp. 2777–2783, 2012.
- [100] M. Prabhu, K. Kavitha, and P. Manivasakan, "Synthesis, characterization and biological response of magnesium- substituted nanobioactive glass particles for biomedical applications," *Ceram. Int.*, vol. 39, no. 2, pp. 1683–1694, 2013.
- [101] A. M. El-kady, A. F. Ali, R. A. Rizk, and M. M. Ahmed, "Synthesis, characterization and microbiological response of silver doped bioactive glass nanoparticles," *Ceram. Int.*, vol. 38, no. 1, pp. 177–188, 2012.
- [102] D. G. Soraru *et al.*, "Sol-gel synthesis of SiBOC glasses," *J. Non. Cryst. Solids*, vol. 224, pp. 173–183, 1998.
- [103] Q. Nawaz *et al.*, "Synthesis and characterization of manganese containing mesoporous bioactive glass nanoparticles for biomedical applications," *J. Mater. Sci. Mater. Med.*, vol. 5, pp. 29–64, 2018.
- [104] A. Martinez, I. Izquierdo-Barba, and M. Vallet-Regi, "Bioactivity of a CaO-SiO₂ Binary Glasses System," *Chem. Mater.*, vol. 12, no. 14, pp. 3080–3088, 2000.
- [105] N. C. B. O, F. H. Elbatal, M. A. Ouis, and H. A. Elbatal, "Comparative studies on the bioactivity of some borate glasses and glass-ceramics from the two systems: Na₂O-CaO-B₂O₃ and NaF-CaF₂-B₂O₃," *Ceramics*, vol. 42, pp. 8247–8256, 2016.
- [106] A. Moorthi, P. R. Parihar, S. Saravanan, M. Vairamani, and N. Selvamurugan, "Effects of silica and calcium levels in nanobioglass ceramic particles on

- osteoblast proliferation,” *Mater. Sci. Eng. C*, vol. 43, pp. 458–464, 2014.
- [107] S. M. Ahmadi, A. Behnamghader, A. Asefnejaad, and B. Group, “Sol-gel synthesis, characterization and in vitro evaluation of SiO₂–CaO–P₂O₅ Bioactive glass nanoparticles with various CaO/P₂O₅ ratios,” vol. 12, no. 3, pp. 847–860, 2017.
- [108] K. S. W. Sing, *Assessment of Surface Area by Gas Adsorption*, 2nd ed. Elsevier Ltd., 2014.
- [109] A. Bari *et al.*, “Copper-containing mesoporous bioactive glass nanoparticles as multifunctional agent for bone regeneration,” *Acta Biomater.*, vol. 55, pp. 493–504, 2017.
- [110] A. M. Abdelghany and H. Kamal, “Spectroscopic investigation of synergetic bioactivity behavior of some ternary borate glasses containing fluoride anions,” *Ceram. Int.*, vol. 40, pp. 8003–8011, 2014.
- [111] T. Shimogaki and H. Tokoro, “Large-scale synthesis of monodisperse microporous silica nanoparticles by gradual injection of reactants,” *J. Sol-Gel Sci. Technol.*, vol. 74, pp. 109–113, 2015.
- [112] J. Chen, L. Zeng, X. Chen, T. Liao, and J. Zheng, “Preparation and characterization of bioactive glass tablets and evaluation of bioactivity and cytotoxicity in vitro,” *Bioact. Mater.*, vol. 3, pp. 315–321, 2018.
- [113] S. Najem, H. Oudadesse, and B. Lefeuvre, “New sol-gel process allowing nano bioactive glasses manufacturing with particle size control,” pp. 1–17.
- [114] H. C. Li, D. G. Wang, J. H. Hu, and C. Z. Chen, “Effect of the partial substitution of K₂O, MgO, B₂O₃ for CaO on crystallization, structure and properties of Na₂O–CaO–SiO₂–P₂O₅ system glass-ceramics,” *Mater. Lett.*, vol. 106, pp. 373–376, 2013.
- [115] R. Koohkan, T. Hooshmand, M. Tahriri, and D. Mohebbi-kalhari, “Synthesis, characterization and in vitro bioactivity of mesoporous copper silicate bioactive glasses,” *Ceram. Int.*, vol. 44, no. 2, pp. 2390–2399, 2018.
- [116] A. Balamurugan, G. Sockalingum, J. Michel, J. Fauré, and V. Banchet, “Synthesis and characterisation of sol gel derived bioactive glass for biomedical applications,” *Mater. Lett.*, vol. 60, pp. 3752–3757, 2006.
- [117] L. Ji, W. Wang, D. Jin, S. Zhou, and X. Song, “In vitro bioactivity and mechanical properties of bioactive glass nanoparticles/polycaprolactone composites,” *Mater. Sci. Eng. C*, vol. 46, pp. 1–9, 2015.
- [118] M. Mac, E. Spiecker, and A. R. Boccaccini, “Bioactive glass type 45S5) nanoparticles: in vitro reactivity on nanoscale and biocompatibility,” *J. Nanoparticle Res.*, vol. June, pp. 14–966, 2012.
- [119] H. Pirayesh, J. A. Nychka, and M. Behavior, “Sol–Gel Synthesis of Bioactive Glass-Ceramic 45S5 and its in vitro Dissolution and Mineralization Behavior,” *J. Am. Chem. Soc.*, vol. 96, no. 5, pp. 1643–650, 2013.
- [120] M. Kouhi, M. Morshed, J. Varshosaz, and M. H. Fathi, “Poly (ϵ -caprolactone) incorporated bioactive glass nanoparticles and simvastatin nanocomposite nanofibers: Preparation, characterization and in vitro drug release for bone regeneration applications,” *Chem. Eng. J.*, vol. 228, pp. 1057–1065, 2013.

- [121] X. Li, J. Shi, X. Dong, L. Zhang, and H. Zeng, "A mesoporous bioactive glass / polycaprolactone composite scaffold and its bioactivity behavior," *J. Biomed. Mater. Res. Part A*, pp. 84–91, 2007.
- [122] M. Fadaie, E. Mirzaei, B. Geramizadeh, and Z. Asvar, "Incorporation of nano fibrillated chitosan into electrospun PCL nano fibers makes scaffolds with enhanced mechanical and biological properties," *Carbohydr. Polym.*, vol. 199, no. May, pp. 628–640, 2018.
- [123] S. K. Misra *et al.*, "Comparison of nanoscale and microscale bioactive glass on the properties of P(3HB)/Bioglass composites," *Biomaterials*, vol. 29, pp. 1750–1761, 2008.
- [124] S. I. Roohani-esfahani, S. Nouri-khorasani, Z. F. Lu, R. C. Appleyard, and H. Zreiqat, "Effects of bioactive glass nanoparticles on the mechanical and biological behavior of composite coated scaffolds," *Acta Biomater.*, vol. 7, pp. 1307–1318, 2011.
- [125] B. J. Shi, N. M. Alves, and J. F. Mano, "Thermally Responsive Biomineralization on Biodegradable Substrates," *Adv. Funct. Mater.*, vol. 17, pp. 3312–3318, 2007.
- [126] K. Shirani, M. S. Nourbakhsh, and M. Rafienia, "Electrospun polycaprolactone/gelatin/bioactive glass nanoscaffold for bone tissue engineering," *Int. J. Polym. Mater. Polym. Biomater.*, vol. 0, no. 0, pp. 1–9, 2018.
- [127] A. K. Ekaputra, Y. Zhou, S. M. Cool, and D. W. Huttmacher, "Composite Electrospun Scaffolds for Engineering Tubular Bone Grafts," *Tissue Eng. Part A*, vol. 15, no. 12, pp. 3779–3788, 2009.
- [128] K. Fujihara, M. Kotaki, and S. Ramakrishna, "Guided bone regeneration membrane made of polycaprolactone/calcium carbonate composite nano-fibers," *Biomaterials*, vol. 26, pp. 4139–4147, 2005.
- [129] J. Dulnik, P. Denis, and P. Sajkiewicz, "Biodegradation of bicomponent PCL/gelatin and PCL/collagen nano fibers electrospun from alternative solvent system," *Polym. Degrad. Stab.*, vol. 130, pp. 10–21, 2016.
- [130] H. Tong, M. Wang, Z. Li, and W. W. Lu, "Electrospinning, characterization and in vitro biological evaluation of nanocomposite fibers containing carbonated hydroxyapatite nanoparticles," *Biomed. Mater.*, vol. 5, pp. 1–13, 2010.
- [131] C. Chan, J. Wu, J. Li, and Y. Cheung, "Polypropylene/calcium carbonate nanocomposites," *Polymer (Guildf.)*, vol. 43, pp. 2981–2992, 2002.
- [132] J. Jo *et al.*, "In Vitro/In Vivo Biocompatibility and Mechanical Properties of Bioactive Glass Nanofiber and Poly (ε-caprolactone) Composite Materials," *J. Biomed. Mater. Res. Part B Appl. Biomater.*, pp. 213–220, 2009.
- [133] S. Tansaz, L. Liverani, L. Vester, and A. R. Boccaccini, "Soy protein meets bioactive glass: Electrospun composite fibers for tissue engineering applications," *Mater. Lett.*, vol. 199, pp. 143–146, 2017.
- [134] F. Serio, M. Miola, E. Verné, D. Pisignano, and A. R. Boccaccini, "Electrospun Filaments Embedding Bioactive Glass Particles with Ion Release and Enhanced Mineralization," *Nanomaterials*, vol. 9, no. 182, pp. 1–15, 2019.
- [135] F. Croisier *et al.*, "Mechanical testing of electrospun PCL fibers," *Acta Biomater.*, vol. 8, pp. 218–224, 2012.